A PETROGRAPHIC AND GEOCHEMICAL STUDY OF SELECTED PERIDOTITIC AND PYROXENITIC XENOLITHS FROM THREE KIMBERLITE LOCALITIES IN THE LAC DE GRAS REGION, NORTHWEST TERRITORIES, CANADA.

Patricia Mary Doyle

Department of Geological Sciences

University of Cape Town, RSA

November 2002

Dissertation submitted to the University of Cape Town in fulfilment of the requirements for the degree of Master of Science.

Declaration

I hereby declare that all the work
presented in this dissertation is my own,
except where otherwise stated in the text.

Signed by candidate

Signature Removed

Patricia Mary Doyle

November 2002

ACKNOWLEDGEMENTS

To Those who Initiated and Backed this Project.....

To my supervisors, Anton le Roex and John Gurney - Thank you so much for the time you invested in discussions and reading drafts!! I really appreciate both the encouragement, and the constructive criticism you have given. I wish you all the very best in your future endeavours.

In advance I wish to thank my anonymous markers for their precious time. I eagerly await your constructive comments on this work.

The National Research Foundation and BHP are gratefully acknowledged for their financial assistance during the duration of this project.

To my Varsity Colleges.....

To Michele Grégoire, Jodie Miller, John Labreque, and Andrew Menzies - a huge thank you for your time, input, ideas and constructive comments!! You definitely broadened my outlook!! I am sure that you will all succeed where ever you go, and whatever you chooses to do! Go and rock the world!!!

Dave Reid - Thank you for being willing to help sort out computer problems at the drop of the hat!! This could not have been printed without your intervention! Russell Bailie, Kalle Westerlund and Eva Anckar - thank you for helping obtain references and other odds and ends in the last month - you are all stars! And to Roxy for being in the department at all hours of the night - it was good to have company!

Dave Wilson and Ivan Wilson - Thank you for your help in preparing samples, finding things in the department, and always being willing to help with a smile!

And a big thank you to Mike Baumgartner!! Thank you for introducing me to kimberlites and mantle rocks at the end of my second year. And thank you for showing me how to do stats-categorised plots!! It may seem small, but without that hint, this project would have taken a LOT longer!!

Last but not least... to the occupants of Room 606, Russell Bailie, Bernadette Azzie and our resident Canadians, John Labreque and Muy Nugo. Thank you so much for the memorable times, the chilli plant, the drip catchers and your enthusiasm for collecting rocks on field trips - WOW!! It has been a privilege to have shared an office with such a diverse and talented group. I wish you all the best in your future endeavours - the world round!!!

To my Friends and Family.....

My family, digs mates Pete & Chris, and my friends, Sarah G, Sarah C, Becky, Kirstan, Cheryl, Shacky and numerous others are thanked for their prayer, encouragement and understanding. Especially during the last month of preparation! May God continue to guide and bless you!!

And the greatest thanks of all... I praise God for holding me fast to the end. May all praise, honour and glory go to The Ancient of Days.

ABSTRACT

Eighty-five peridotitic and pyroxenitic xenoliths from the Arnie, Pigeon and Misery kimberlites in the Lac de Gras region, Northwest Territories, Canada were selected for inclusion in this study. The three kimberlites are situated within a 40 km radius of one another on the BHP property, and all are diamond-bearing. The Misery kimberlite is presently being mined, and the Pigeon kimberlite is part of the future BHP-Dia Met Ekati mining plan.

A petrographic study of the xenoliths using both transmitted light microscopy and binocular microscopy was followed by major and trace element analysis. Major element compositions of individual minerals were determined using a wavelength dispersive electron microprobe, and trace element abundances were determined using laser ablation ICP-MS. Pressures and temperatures of equilibration were then determined using garnet-olivine, garnet-orthopyroxene and trace element geothermobarometers (T_{Ni}, P_{Cr}).

The petrographic study was limited by the small sample size (0.5-1.5 cm) in comparison to the large grain size (0.05-1 cm). Rock types were determined using mineral associations within the xenolith in conjunction with mineral compositions. Xenoliths containing garnet were preferentially selected for geothermobarometric and mineral compositional studies. The peridotite suite consisted of both garnet-harzburgites and garnet-lherzolites, whereas the pyroxenitic suite consisted of garnet-clinopyroxenites and garnet-websterites.

Peridotite xenoliths were dominant at all three kimberlite localities, but the Misery kimberlite entrained a higher proportion of eclogitic and websteritic xenoliths relative to peridotite xenoliths than the Pigeon and Arnie kimberlites. Spinel exsolution from ortho- and clinopyroxene in both peridotitic and pyroxenitic xenoliths from the Misery and Arnie kimberlites is indicative of partial re-equilibration of these xenoliths from a region of high pressure and temperature to lower pressure and temperature. Such dynamic processes and small scale heterogeneity suggest a complex history for the lithosphere beneath the Slave province.

The major element study showed that the pyroxenitic minerals are more Fe-rich and Cr_2O_3-poor than the peridotitic minerals. The harzburgitic xenoliths were divided into two sub-groups based on CaO and Cr_2O_3 content in garnet, namely a high-Ca group with similar major element compositions to the lherzolitic xenoliths, but with similar trace element compositions to the second group, the low-Ca

harzburgites. In general the low-Ca harzburgitic minerals are more Mg-rich than the lherzolitic minerals.

Trace element studies focused on garnet and clinopyroxene as these are the main repositories for trace elements in the mantle. The lherzolitic and pyroxenitic garnets have chondrite-normalised LREE-depleted patterns, whereas the harzburgitic garnets have sinusoidal and MREE-enriched patterns in addition to the LREE-depleted pattern. Various models have been proposed in the literature for the formation of the MREE-enriched pattern, but none for the sinusoidal pattern. This study shows that if majorite had a sinusoidal REE pattern and it exsolved into pyrope and orthopyroxene during decompression re-equilibration, the pyrope would retain the sinusoidal REE pattern of the majorite. However, if pyrope and clinopyroxene are the exsolution products, the pyrope has a LREE-depleted pattern, as seen in the lherzolitic garnets.

Major and trace element geothermobarometry reveal that the peridotitic xenoliths define a 40 $mW.m^{-2}$ geotherm. Major element geothermobarometry indicates that although there are geochemical similarities between the low-Ca garnets in harzburgites and peridotitic garnets included in diamond, not all low-Ca harzburgites have pressures and temperatures of equilibration in the diamond stability field. Those low-Ca harzburgitic xenoliths with <6 wt% Cr_2O_3 in garnet (ARN008, ARN026) have shallow pressures and temperatures of equilibration. In contrast, the low-Ca and high-Ca harzburgitic xenoliths with >8 wt% Cr_2O_3 (e.g. ARN002, PGN312) have pressures and temperatures of equilibration within the diamond stability field. Xenoliths with 6-8 wt% Cr_2O_3 straddle the graphite-diamond stability field.

Numerous studies of the Slave craton have recognised layering within the underlying lithospheric mantle. Single mineral trace element abundances and geothermobarometry (T_{Ni}) support this concept with the lherzolites having higher pressures and temperatures of equilibration and more enriched compositions than the harzburgites. However, major element geothermobarometry using coexisting mineral pairs for a larger number of samples shows that the harzburgites and lherzolites are inter-layered with depth, rather than separated into two distinct layers.

TABLE OF CONTENTS

LIST OF FIGURES

LIST OF TABLES

1 . INTRODUCTION

1 .1 OVERVIEW OF MANTLE STUDIES

"Everything happening at the surface of the Earth, including such diverse phenomena as the building of mountain ranges, the formation of ocean basins, volcanic activity, and even changes in sedimentation (with their attendant rise or decline of faunal and floral populations) is a response to events taking place within the upper mantle..." J.B. Dawson (1981)

Mantle dynamics have intrigued scientists for well over 2500 years (Bergman, 1987). The Greek philosophers such as Aristotle, Anaxagoras, Democritus and Anaximenes believed that surface phenomena, such as earthquakes, were linked to processes occurring within the mantle. Early hypotheses explaining the cause of earthquakes included: the decent of ether into the Earth's interior, or the ascent of water from the interior, or alternatively by "volcanic eruptions due to the inflammation of moving wind imprisoned within the interior" (see Geikie, 1897; review by Bergman, 1987). Theories of mantle processes and their effects on Earth processes have changed dramatically since that time.

Daly (1914) and Barrell (1914) were among the first to recognise the existence of a less rigid asthenospheric mantle beneath a more rigid lithospheric mantle. Wegner's theory of plate tectonics further explained many processes influenced by mantle processes, such as earthquakes and volcanism at convergent plate margins.

As instrumentation and resolution become more refined, the understanding of the mantle and the processes driven by the dynamic mantle will become better understood. Geophysical investigations such as the Southern African Kaapvaal project and the Canadian LITHOPROBE project have revealed some of the structural complexities within the upper mantle. Particularly the seismic profile SNORCLE Corridor 1 (Clowes, 1997 in Helmstaedt and Harrap, 1999).

The isolated nature of the mantle makes direct study of the upper mantle difficult. Tectonic emplacement of Alpine peridotite and ophiolite sequences provide insight into the mantle beneath oceanic provinces, as do volcanic rocks from hot spots and other oceanic volcanism. To obtain an understanding of the upper mantle beneath the cratonic regions, one has to rely on out-of situ fragments of the mantle derived from ascending mafic and ultramafic magmas such as basalts and kimberlites.

Petrographic and geochemical analysis of these mantle xenoliths provide insight into the mode of formation, and the processes affecting the mantle.

Petrographic studies of mantle xenoliths reveal the existence of different rock suites, namely peridotites, pyroxenites, eclogites and megacrysts. These attest to the heterogeneous, and complex nature of the upper mantle. Whereas many mantle xenoliths have attained textural equilibrium, others have recrystallization and exsolution features which are transient (Field and Haggerty, 1995). These reflect dynamic processes occurring within the mantle.

The relative depletion or fertility of different rock suites in major elements such as Na, Ca, Al and Fe suggests different processes affecting the mantle. Mantle xenoliths depleted in these elements are likely to be the residues of partial melting events (Nixon and Davies, 1987). Correspondingly, xenoliths enriched in these lower temperature melting elements may represent the crystallisation product of partial melting, or the enrichment of those elements due to metasomatic processes. Major element analyses are therefore used to infer different modes of formation of different rock suites. Stable and radiogenic isotopes may also be used to determine the mode and age of formation of portions of the mantle (review by Menzies and Hawkesworth, 1987).

Trace element studies of the minerals within xenoliths are further used to constrain the different processes affecting the mantle. Whereas modal metasomatism may be detected by the presence of metasomatic clinopyroxene, phlogopite, K-richterite, and/or amphibole; cryptic metasomatism may be detected in enrichment in incompatible trace element contents in minerals (Harte, 1987).

Coexisting minerals within equilibrium assemblages are useful for obtaining pressures and temperatures of equilibration. Assuming that the rocks have not moved stratigraphically since the time of equilibration, nor re-equilibrated during entrainment in the kimberlite, cross-sections of the continental lithosphere may be constructed (Boyd and Gurney, 1986; Kopylova et al., 1999a).

Kimberlites are one of the few melts that originate from sufficient depth to sample the deep lithosphere beneath the craton. Based on majoritic garnet inclusions in diamond (Moore and Gurney, 1985), Ringwood et al. (1992) suggest a depth of origin for kimberlite of 400-650 km, from an area corresponding to the seismic transition zone. Therefore the volumetrically small kimberlite intrusions (carrot-shaped pipes, dykes, and sills) play an important role in mantle studies due to the xenoliths they entrain. The kimberlite is itself described as a "volatile-rich, potassic, ultrabasic igneous" rock (Clement et al., 1984) and provides a mantle signature for further study. The mantle xenoliths entrained within three kimberlite from the Northwest Territories, Canada, are the focus of this study.

1 .2 RECENT XENOLITH STUDIES FROM CANADA

Numerous spinel lherzolites, websterites, wehrlites and clinopyroxenites have been described from basaltic rocks of the Canadian Cordillera, an area extending over 200km * 50km from the Alaska-Yukon border, through British Columbia and into the Snake River Plains (USA), (Mitchell, 1987). Xenoliths from an alnöite in Île Bizard (Quebec) and from lamprophyres from Ontario and Labrador have also been described. Yet by 1987, xenoliths from only one kimberlite province had been described, namely xenoliths from the Somerset Island kimberlite province (review by Mitchell, 1987). This kimberlite province contained both garnet and spinel lherzolites, and was first briefly described by Mitchell (1976).

Numerous research projects have been initiated as a result of the recent kimberlite discoveries in the Slave craton (Carlson et al., 1999). These include geophysical, kimberlite, mantle xenolith and diamond studies. All of which lead to a better understanding of the lithosphere beneath the Slave craton.

To name but a few of the recent studies: Boyd and Canil (1997) have studied xenoliths from the Grizzly kimberlite, located within the central Lac de Gras region. Kopylova and associates have investigated the emplacement, kimberlite and mantle xenoliths of the Jericho kimberlite, ~150 km north of Lac de Gras (Kopylova et al., 1996, 1998, 1999, 2001; Kopylova and Russell, 2000). Pearson et al. (1999) and Doyle et al. (1999) have worked on mantle xenoliths and diamonds from the Tli Kwi Cho kimberlite complex to the south of Lac de Gras. Griffin et al. (1999a) have mapped the mantle beneath Lac de Gras and the surrounding region using garnet and chromite xenocrysts. Many of these authors recognise a layering within the lithosphere beneath the Slave craton (Pearson et al., 1999; Griffin et al., 1999a; Kopylova and Russell, 2000), as discussed further in chapter 9.

1 .3 AIMS OF THIS STUDY

The aims of this study are :

1) To characterise the mantle xenoliths from three kimberlites in the Lac de Gras region, Canada in terms of petrography, major and trace element content.
2) To determine the xenolith geotherm for the Lac de Gras region using both major element and trace element geothermobarometers, and furthermore, to compare the results of both methods.
3) To use petrographic and geochemical signatures of xenoliths to suggest processes having affected the mantle beneath the Lac de Gras region of the Northwest territories, Canada.

2. GEOLOGICAL SETTING

2.1 OVERVIEW

Physiographic Setting

The xenoliths in this study are derived from three kimberlites located within the Northwest Territories (NWT), one of the thirteen political provinces of Canada (figure 2.1). The Northwest Territories is a large province (1 171 918 km^2) that straddles the Arctic circle, and can be divided into two broad geographical regions. The north has Arctic and sub-Arctic winters and is characterized by tundra, a rocky expanse where the cold climate has stunted vegetation growth. The south is more temperate with mild summers and cold winters. Much of the land is low lying with numerous lakes, the land having been sculptured by past glaciations (Doyle et al., 1999).

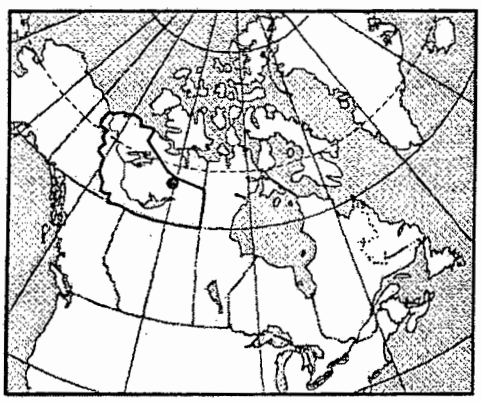

Figure 2.1 Geographical Location of study samples
(modified from Kjarsgaard et al., 1999)
Dot - Sample locality
Outline - The Northwest Territories (NWT)

Broad Geological Domains within Canada

About two-fifths of Canada is composed of exposed Archean crust (figure 2.2). G.M. Stott (1997) noted that "almost a quarter of all exposed Archean crust in the world lies in the Superior province of North America". The Superior province is the largest of the Archean provinces in Canada, and forms the core of the Canadian shield which consists of a number of smaller cratonic nuclei, namely: the Hearne, Rea and Slave Province (Stott, 1997).

These Archean nuclei are cemented together by Proterozoic orogenic belts. The easterly Proterozoic orogenic belt is itself bound to the east by a Paleozoic orogenic belt, as shown in figure 2.2 (Carlson et al., 1999). Paleozoic rocks are also found in the center of the Canadian Shield adjacent to Hudson Bay. The western margin of the Canadian Shield is not well defined as Phanerozoic rocks cover much of the western portion of Canada. These Phanerozoic rocks are in turn bound to the west by a Mezozoic orogenic belt.

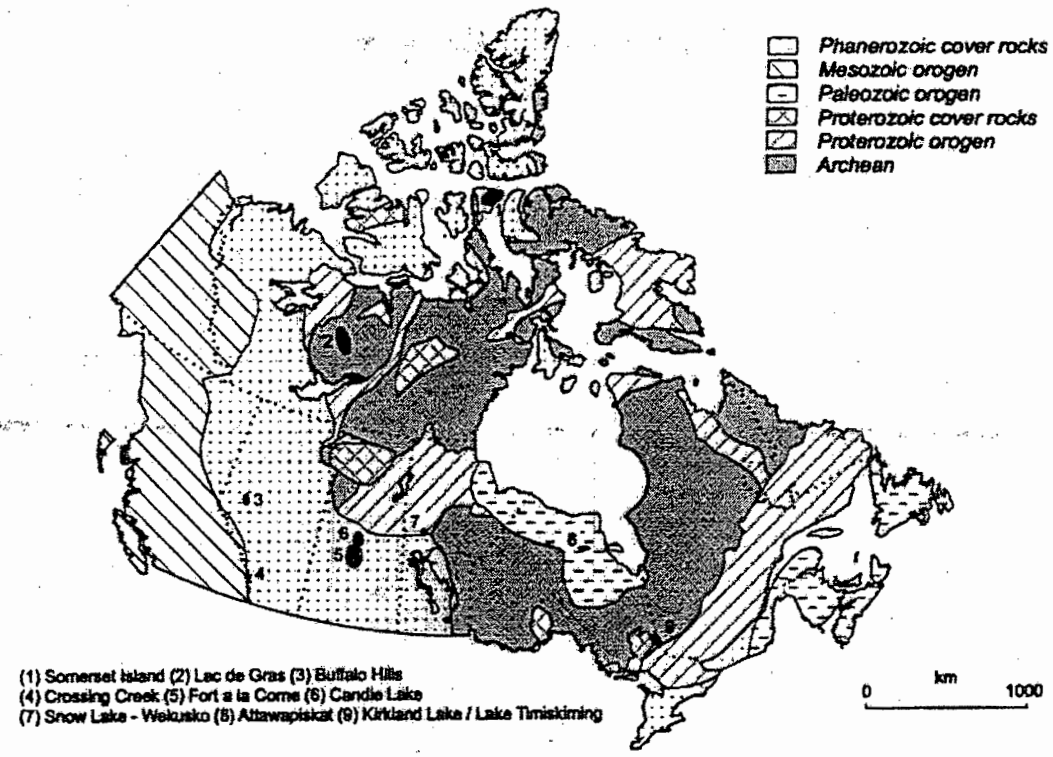

Figure 2.2 Broad geological domains within Canada and known kimberlite provinces. The Slave craton is one of the smaller cratonic nuclei that compose the Canadian Shield (Carlson et al., 1999; modified from Kjarsgaard, 1996).

Geological provinces of the Slave Craton

The Slave craton may be divided into three main domains, namely: the Anton terrane, the Hackett River terrane and the Contwoyto terrane, figure 2.3 (Carlson et al., 1999). It consists predominantly of granites, migmatite gneisses and metasedimentary schists in a granite-turbidite-greenstone terrane (2.7-2.6 Ga) with inliers of older gneiss-granite (4.0-2.8 Ga) (review by King and Helmstaedt, 1997). The Anton terrane, believed to be the oldest terrane, consists of migmatites, quartzo-feldspathic gneisses and deformed granites, and is bound to the east by a thrust belt. The easterly portion of the craton may be divided into the northern Hackett River terrane, and the central Contwoyto terrane (Griffin et al., 1999a). The Hackett River terrane is composed of volcanic rocks and their associated subvolcanic plutons. It is bounded to the east by the back-arc sediments of the Beechy Lake domain (Kusky, 1989; King et al., 1992). The Contwyoto terrane consists of turbidites with Fe-formations and tectonic slivers of mafic volcanics (Kusky, 1991).

The Slave craton is bound to the south by the MacDonald fault, juxtaposing Proterozoic rocks of the Churchill province with the Archean rocks of the Slave craton (figure 2.3). It is bound to the north by the sea, and to both the east and west by Proterozoic belts. To the east it is bound by the Thelon orogen and to the west by the Wopmay orogenic belt (Griffin et al., 1999a).

Many authors propose a plate-tectonic model for the formation of the Slave Craton in which the younger, eastern portion of late Archean island arc complexes (magmatic arcs and accretionary prisms) accreted onto the older, Anton terrane (review by King and Helmstaedt, 1997, and references therein). Thrust sheets of oceanic affinity to the east of the Anton terrane (Kusky, 1991), and the complex structures in the mantle beneath the Northwest Territories as revealed by geophysical investigations such as the LITHOPROBE project would support such a theory. Several eastward-dipping imbricated reflectors reaching depths of 100 km (figure 2.4) within the LITHOPROBE SNORKLE Corridor 1 profile (Clowes, 1997 in Helmstaedt and Harrap, 1999) would further suggest tectonic underplating of the lithosphere and westward accretion of continental fragments onto the Anton terrane (Helmstaedt and Harrap, 1999).

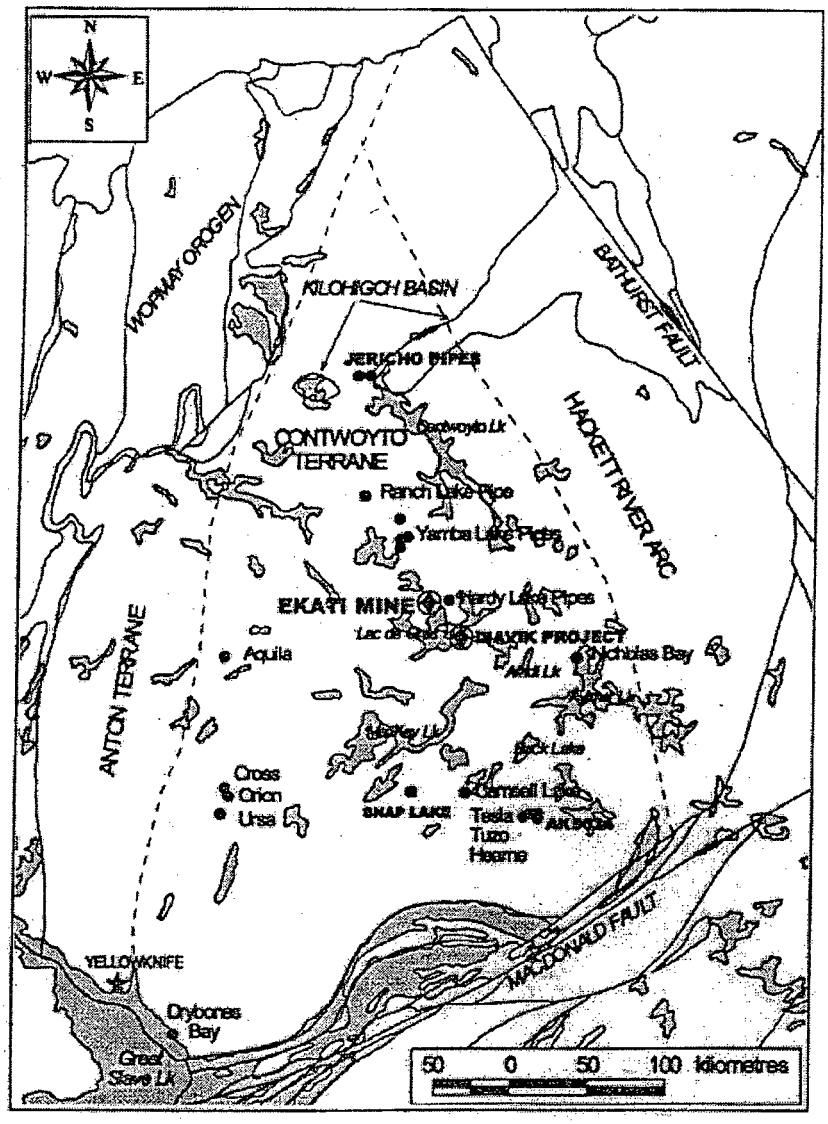

Figure 2.3. The Slave craton may be divided into three dominant terranes, namely the Anton terrane, the Hackett River terrane and the Contwoyto terrane. Dashed lines define approximate boundaries for these terranes (Carlson et al., 1999). The Misery kimberlite forms part of the operational Ekati Mine located in the Lac de Gras region in the central portion of the craton.

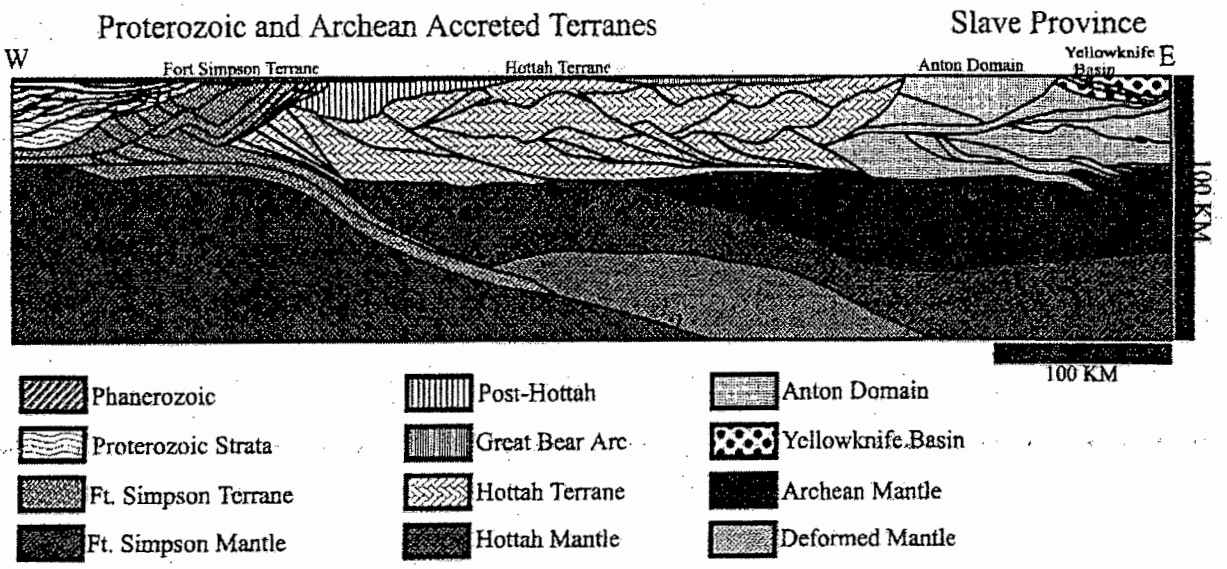

Figure 2.4 An interpretation of the seismic profile of the LITHOPROBE SNORKLE Corridor 1 (Clowes, 1997 in Helmstaedt and Harrap, 1999). Numerous eastward dipping reflectors can be seen, some are evident to depths of >100 km. These features suggest a tectonic nucleation of the Slave craton.

Dyke swarms

Numerous diabase dykes intrude the rocks of the Slave craton. The Lac de Gras, Mackenzie and Contwyoto dyke swarms are of interest due to the position of the Misery kimberlite in relation to these dykes (figure 2.5). The Contwyoto dyke swarm trends at 045°, and the individual dykes are between 20-40m wide (Kjarsgaard and Wyllie, 1993). These dykes were emplaced around 2.03 Ga (U-Pb baddeleyite ages, LeCheminant and O' Breemen, pers comm. in Kjarsgaard and Wyllie, 1993). The individual dykes of the Lac de Gras dyke swarm are between 35-60m wide, and generally trend along a bearing of 010° (Kjarsgaard et al., 1994). They were emplaced at 2.03-2.02 Ga (LeCheminant et al., 1995). According to field relations, they are younger than the Contwoyto dyke swarm. The Mackenzie diabase dykes trend 330°-340°, and individually may be up to 100m wide. Field relations reveal that they are younger than the Lac de Gras and Contwyoto dykes (Kjarsgaard and Wyllie, 1993). These dykes have been dated to be 1.72 Ga (LeCheminant and Heaman, 1989) and extend over 2300 km (Griffin et al., 1999a).

A northerly source for both the Lac de Gras and Mackenzie dyke swarm has been suggested. The source for the north-to-south divergent Lac de Gras dyke swarm is suggested to be below the Kiohogok Basin in the north (figure 2.3), (Griffin et al., 1999a). A plume head with a focus west of Victoria Island has been suggested to explain the radiating pattern of the Mackenzie dykes (Fahrig, 1987). This would be in agreement with the fact that the Mackenzie dykes are intruded vertically in the northern part of the craton, whereas in the south they appear to have been injected horizontally (Ernst and

Baragar, 1992). The plume activity in the north associated with these dyke swarms may have destroyed portions of the mantle root beneath the northern portion of the Slave craton. The horizontal injection of the magma through the crust in the southerly portion of the Slave craton would not have affected the mantle root to the same degree, thereby preserving the diamonds in the southern portion of the mantle root (Helmstaedt and Gurney, 1995).

2.2 RECENT KIMBERLITE DISCOVERIES

Since the discovery of the Point Lake kimberlite in 1991 (Carlson et al., 1999), exploration activities within Canada have greatly increased. Numerous kimberlitic provinces have now been identified (figure 2.2), many of which are diamond bearing e.g. in the Lac de Gras region (NWT), Saskatehewan, Ontario, Quebec, and those in the Buffalo Hills province.

On 14 October 1998 the Ekati Diamond mine operated by BHP Diamonds Inc. came into operation (Kjarsgaard et al., 1999). This mining project is a joint venture between BHP Diamonds Inc., and Dia Met Minerals Ltd. (Carlson et al., 1999). Diamet has since been bought out by BHP Diamonds Inc. Presently this mine recovers diamonds from two of the kimberlites from the Lac de Gras province, namely the Panda and Misery kimberlites. A further six kimberlites form part of the proposed mining plan, namely the Koala, Fox, Pigeon, Beartooth, Sable and Koala North kimberlites (Dia Met Annual Report, 1999-2000).

Now more than 200 kimberlite pipes have been found in the Slave Province alone, the majority of which are concentrated in the central portion of the craton (Carlson et al., 1999). Few pipes exceed 20 hectares in size (Carlson et al., 1999). Rb-Sr dating of selected kimberlites, and pollen and spore studies from kimberlite-derived mudstone suggest that there is more than one phase of kimberlite emplacement in the Slave craton (Northern Miner, 1993). Emplacement ages of kimberlites in the Central Slave craton range from 47 to 84 Ma based on Rb-Sr phlogopite and U-Pb perovskite respectively (Davis and Kjarsgaard, 1997; Carlson et al. 1999). The emplacement ages of those kimberlites in the northern portion of the craton are 172 Ma, whereas those in the southern portion are older, 539 Ma (Carlson et al. 1999). South-eastern kimberlites are dominated by hypabyssal facies kimberlite, whereas those in the north by tuffisitic kimberlite breccia and hypabyssal kimberlite. Kimberlites in the central, Lac de Gras region have a basaltic kimberlite affinity and are generally volcanoclastic in nature (Carlson et al., 1999).

2.3 HOST KIMBERLITE PIPES

Geological setting

The three kimberlite localities in this study lie within a 40 km radius of one another within the Lac de Gras region near the geographic center of the Slave craton. The Pigeon kimberlite is the most northerly locality, the Arnie kimberlite lies about 20km east-south-east of the Pigeon kimberlite, with the Misery kimberlite being the most southerly locality (figure 2.5).

The Arnie kimberlite intrudes metagreywackes consisting of massive psammitic beds and graded psammite-pelite sequences (Kjarsgaard and Wyllie, 1993). The Pigeon kimberlite intrudes a hornblende-biotite tonalite body (Kjarsgaard et al., 1994), whereas the Misery kimberlite intrudes an area of structural weakness within a two-mica granite body. The Misery kimberlite lies on one of the Contwoyto dyke swarm lineaments, about 2 km away from a three-way intersection between dykes of the Contwyoto, Lac de Gras and Mackenzie dyke swarms (figure 2.5).

Diamond-bearing capacity

All three kimberlites in this study are diamond-bearing (J.J. Gurney, pers. comm. 2000). Both the Pigeon and Misery kimberlites form part of the Ekati diamond mine plan, and will be mined by open cast methods. Diamonds from the Misery kimberlite are presently being mined, whereas those from Pigeon form part of the future mining plan (Dia Met Annual Report, 1999-2000).

The Pigeon kimberlite consists of both a crater and a hypabyssal facies (Dia Met Annual Report, 1998-1999). The diamond grade and valuation results for the "1998 Summer RC Drilling program" reveal the diamond grade and quality are better for the crater facies than the hypabyssal facies. The average diamond grade for the crater facies sample was 0.51 carats/tonne at $71 per carat, whereas that for the hypabyssal facies is lower at 0.39 ct/tonne and $39/ct (Dia Met Annual Report, 1998-1999). The 1996 feasibility study on the Misery kimberlite revealed an average grade of 4.26 ct/tonne at $26/ct (Dia Met Annual Report, 1997-1998).

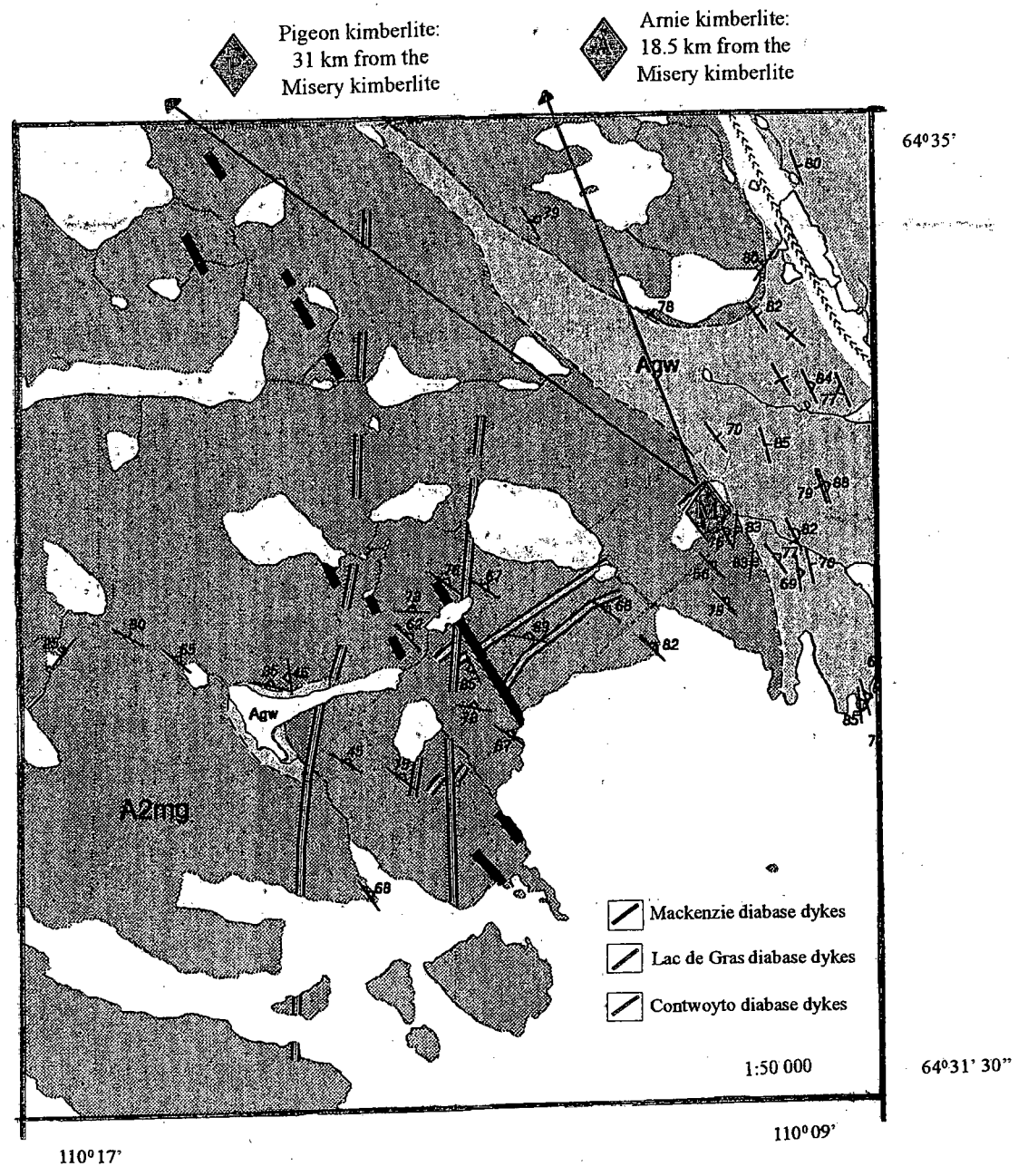

Figure 2.5 The relative positions of the three kimberlite localities from which the xenoliths in this study were obtained. The kimberlites are located in the central portion of the Slave craton in the Lac de Gras region (figure 2.3). The position the Pigeon and Arnie kimberlites are shown in relation to the Misery kimberlite (direction and distance from the Misery kimberlite indicated by arrow). The Misery kimberlite is located in close proximity to the intersection of three dyke swarms.
Geological map: Kjarsgaard and Wyllie (1993)

3 . SAMPLE PREPARATION AND ANALYSIS

3 .1 SAMPLE SELECTION AND PREPARATION

Small fragments of over 1925 mantle xenoliths from the three kimberlite pipes Arnie, Misery and Pigeon were collected by BHP and Mineral Services personnel, and made available for study at the University of Cape Town (UCT). The samples were retrieved after preliminary crushing during an exploration program, and are therefore all less than 1.5 cm in longest dimension. On close inspection, the majority of the samples were monomineralic (1360), 320 were bi-mineralic, and about 245 contained three phases or more.

Peridotitic and pyroxenitic xenolith fragments that contained two or more mineral phases were selectively mounted in epoxy for further study. Eclogitic fragments were explicitly not selected for study by prior arrangement with BHP, who have allocated a study of the eclogitic population from the kimberlites in the Lac de Gras region to an independent researcher.

Thirty-seven samples from the Arnie kimberlite, forty-three samples from the Pigeon kimberlite and fifty-five samples from the Misery kimberlite were selected and mounted in epoxy and polished for further study. From this subgroup, samples that contained garnet and clinopyroxene, and garnet-orthopyroxene-olivine mineral assemblages were preferentially chosen for analysis. This sample selection allows for:

a) the examination of the peridotitic and pyroxenitic component of the mantle beneath the Lac de Gras region of the NWT, using both major and trace elements. Garnet and clinopyroxene are the two main repositories for trace elements, and are therefore of interest in trace element studies.
b) the calculation of a xenolith geotherm for the area. Samples with garnet-orthopyroxene-olivine mineral assemblages are particularly useful for such geothermobarometric calculations.

It was noted that the samples from Misery exhibited some exsolution features, not common in the xenoliths from the Pigeon and Arnie kimberlites. For this reason, thin sections were made of five of the Misery epoxy disks. These five epoxy disks were re-polished for laser ablation ICP-MS trace element analysis.

Mounting the samples in epoxy has a few disadvantages, as distinguishing between strained and unstrained minerals is difficult, and exsolution textures are difficult to detect.

The advantages however out-weigh the disadvantages:

1) The colours of minerals are vivid and can be clearly noted (figure 3.1). Previous studies have noted a correlation between garnet colour and mineral chemistry (Sobolev et al., 1973; Dawson and Stephens, 1975). Garnet colour is a useful aid for the classification of samples into different rock types, and has application for diamond exploration programs.
2) The 3-dimensional nature of the samples is readily apparent. This is particularly noticeable during textural analysis based on a 2-dimensional textural scheme (figure 4.4).
3) The samples are thick enough to easily obtain full trace element analyses using laser ablation techniques without ablating through the mineral.

Samples from the Arnie kimberlite

Scale bar: 2cm. Plane-polarised light.

Samples from the Pigeon kimberlite

Scale bar: 2cm. Plane-polarised light.

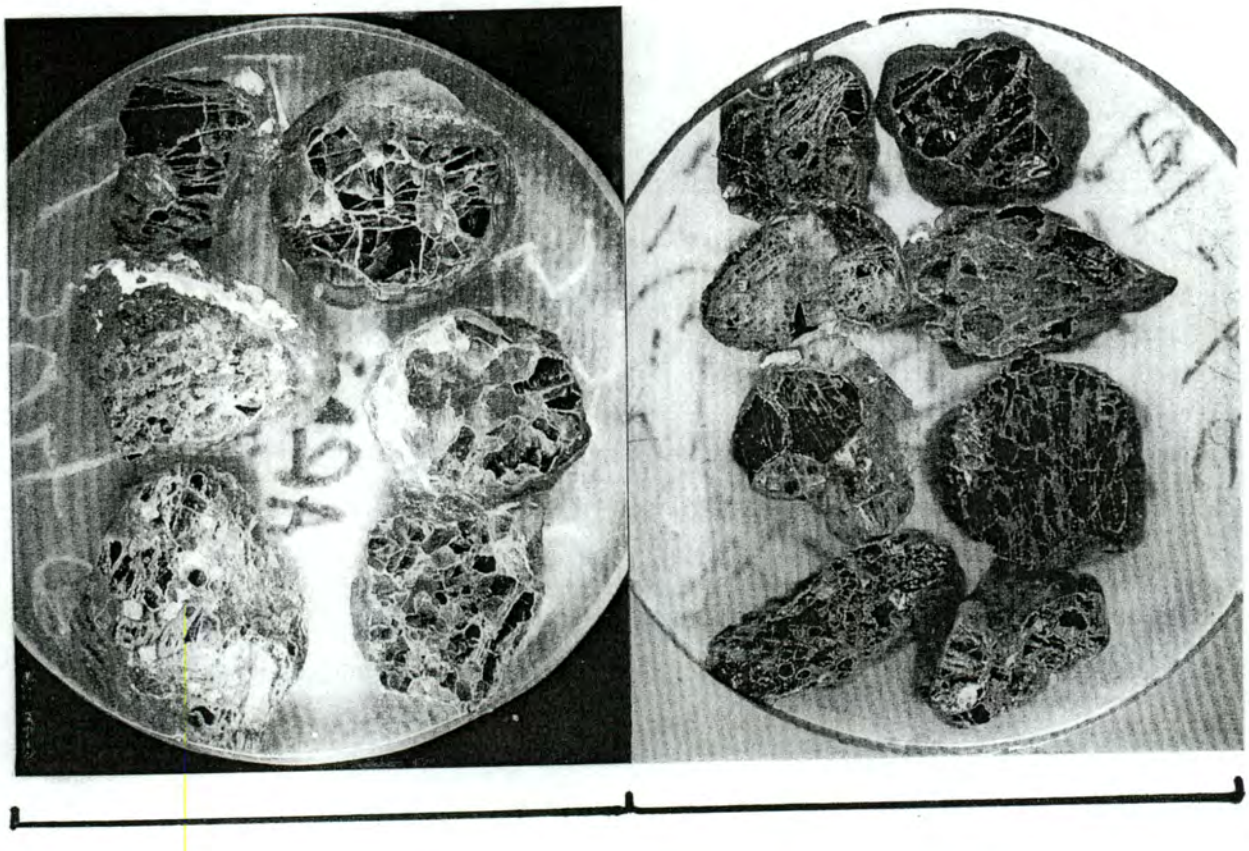

Figure 3.1 Samples mounted in epoxy show vivid colours. The xenoliths from the Arnie kimberlite are chromite-rich, whereas those from the Pigeon kimberlite have a higher proportion of clinopyroxene.

3 .2 ANALYTICAL TECHNIQUES

Major element analysis

Equipment Utilised

The major element analyses were undertaken on the wavelength dispersive Cameca/Camebax electron microprobe in the Department of Geological Sciences at the University of Cape Town (UCT). As the samples are non-conductive, they needed to be coated with a thin (~25nm) layer of carbon to ensure the flow of electrons off the sample to earth, thereby preventing an electron charge build-up on the sample. The samples were coated with a 'peacock-blue'-thin layer of carbon using a Cressington carbon coater located in the Department of Geological Sciences, UCT.

Method and Operating Conditions

An electron beam was accelerated to a set voltage (15kV) and focused onto the sample, striking it at 90°. The atoms of the sample under the beam become excited, generating characteristic x-rays. The intensity of these x-rays are measured using four wavelength dispersive spectrometers. Corrections for matrix effects were made by the P.A.P. computer software. Count data are then quantified by comparing the counts with data from known standards.

Navigation using the high magnification probe ocular was difficult as transmitted light could not be used with samples mounted in epoxy. Navigation of samples mounted in epoxy was therefore undertaken using sound pitch and intensity related to the abundance of SiO_2 and Al_2O_3 in the mineral under the electron beam.

A minimum of two or three analyses with totals within the range 98.5 to 101.0 weight % (wt%) were obtained per mineral analysed. To test homogeneity, both rim and core analyses were obtained, particularly for the garnet grains. Analyses of homogeneous minerals were averaged. When differences between analyses were noted, more analyses were obtained to verify if the difference was due to analytical error, alteration or if the variability was systematic and had a spatial relation. In most cases, the anomalous analyses could be discounted due to variable operating conditions or due to analysis of an altered region within the mineral. Where variations appeared to be natural (e.g. garnet in ARN026), they appeared to be random, showing no systematic variation with distance from grain boundary to core.

Table 3.1 A summary of the operating conditions.

Accelerating Potential	15 kV	
Beam Current	40 nA	
Beam Size	1-2 μm	
Analysing Crystals	1) TLAP	Mg, Na
	2) TLAP	Si, Al
	3) LIF	Fe, Mn, Ni
	4) PET	Ca, Ti, Cr
Peak Count Times	Orthopyroxene - Al_2O_3	40 seconds
	Orthopyroxene - Na_2O	60 seconds
	All other oxides	10 seconds

Lower Limit of Detection

The lower limit of detection is defined by the relationship: $LLD = (6/m)*(R/T)^{1/2}$

where: $R = R_B + R_P$ (and R_B ,R_P are Background and Peak *counts per second* respectively)
$T = T_B + T_P$ (and T_B ,T_P are Background and Peak *counting times* respectively)
$m = (R_P-R_B)$/concentration (in wt%)

Table 3.2 Lower limits of detection (in wt%) for the various oxides based on counting statistics ♦.

Oxide	Olivine	Pyroxene	Garnet	Mica	Chromite
SiO_2	0.04	0.04	0.04	0.04	0.04
TiO_2	0.04	0.04	0.04	0.04	0.05
Al_2O_3	0.03	0.01	0.05	0.05	0.04
Cr_2O_3	0.04	0.04	0.06	0.04	0.05
FeO	0.08	0.08	0.08	0.08	0.08
MnO	0.06	0.06	0.09	0.05	0.07
MgO	0.04	0.04	0.04	0.04	0.04
CaO	0.03	0.05	0.09	0.03	0.02
Na_2O	-	0.01	0.01	0.03	-
K_2O	-	-	-	0.03	-
NiO	0.10	-	-	-	-

Standard Deviation

2σ (in wt%) defines the error in concentration according to the following formula:
$2\sigma = 2 * \text{concentration (wt\%)} * (R_B/T_B + R_P/T_P)^{1/2} / (R_P - R_B)$ (abbreviations as above)

Table 3.3 Standard deviation (wt%) for the various oxides based on counting statistics ♦.

Oxide	Olivine	Pyroxene	Garnet	Mica	Chromite
SiO_2	0.28	0.28	0.27	0.28	0.04
TiO_2	0.04	0.04	0.04	0.10	0.34
Al_2O_3	0.03	0.02	0.19	0.14	0.04
Cr_2O_3	0.05	0.08	0.09	0.05	0.08
FeO	0.35	0.21	0.31	0.20	0.46
MnO	0.06	0.07	0.12	0.06	0.09
MgO	0.25	0.14	0.15	0.16	0.16
CaO	0.06	0.18	0.12	0.02	0.03
Na_2O	-	0.01	0.02	0.03	-
K_2O	-	-	0.03	0.13	-
NiO	0.08	-	-	-	-

♦ Lower limits of detection and standard deviations adapted (Baumgartner, 1994).

Trace element analysis

Equipment Utilised

The precision, low detection limits and the fact that a large number of elements can be measured simultaneously by ICP-MS techniques makes the analysis of trace elements by this technique fast and efficient. There are several advantages to using laser ablation ICP-MS (LA-ICP-MS) techniques rather than solution ICP-MS techniques: mineral compositions may be obtained from individual minerals; fresh, unaltered grains may be selected for analysis; and within-grain compositional variation may be studied.

Trace element compositions for individual minerals were obtained using the Perkin Elmer Elan 6000 Inductively Coupled Plasma-Mass Spectrometer (ICP-MS), coupled to a CETAC LSX-200 UV Laser. This equipment is housed in the Department of Geological Sciences, UCT. After major element analysis by the electron microprobe, the carbon coating on the samples needed to be removed. No further sample preparation was necessary before analysis by LA-ICP-MS.

Method and Operating Conditions

Solid samples were ablated using a pulsed laser. The very fine ablated solid particles are introduced to an Argon plasma by a stream of argon gas. This Ar plasma, which reaches temperatures between 6000 and 8000K at atmospheric pressure and is an efficient source of positively charged analyte ions ionises the sample particles. The ions are then taken into an area of high vacuum where they are focused by an ion lens system and separated by mass/charge ratios by a quadruple mass spectrometer. They are then detected and measured by a detector (commonly an electron multiplier). The operating conditions used are detailed in table 3.4 below.

Table 3.4 Operating conditions for the LA-ICP-MS

Laser power	5.0 mJ per pulse
Pulse repetition rate	4 Hz
Diameter of laser beam	Spot 4: +/- 100 μm
	Spot 5: +/- 200 μm

Analytical calibration is achieved by external standardisation using natural and artificial reference materials. A re-standardisation was undertaken every hour. Two standards were used during the analysis of the samples, namely NIST610 and NIST612 (Perkins et al., 1997). NIST610 and NIST612 are artificial silicate glasses produced by the United States National Institute of Standard Technology. To ensure the standardisation was correct, and that operating conditions were comparable between analytical runs on different days, two reference standards were used. MON-32 and MON-34 were used

as the reference standard for garnet and JJG1424 for pyroxene. These analyses are included in Appendix 3.

A single analysis consisted of three replicates of a hundred readings each. The time for one analysis was typically two minutes. A minimum of three analyses were obtained per mineral in any particular sample. To account for instrumental drift and different ablation characteristics between the standard and the sample, an internal standardisation is required. Ca and Si abundances obtained by electron microprobe analysis are often used for this purpose. Si was used in preference to Ca in this study as the very low CaO contents (1-4 wt%) in many of the harzburgites analysed made normalisation by Ca unsuitable. Analyses from homogeneous minerals were averaged if found to be within error of each other.

Lower Limit of Detection

The lower limit of detection (LLD) was calculated using the relationship:

LLD = 6/m * Std deviation on background

Where: m = (Peak *counts per second* - Background *counts per second*) / concentration (in ppm)

and Std deviation was the standard deviation computed on 3 consecutive "blank" analyses (analysis of pure Argon gas). Each analysis consisted of three replicates of a hundred readings each.

A summary of the results are detailed in table 3.5 below. The laser spot size 5 is larger (+/- 200 μm) than that of spot 4 (+/- 100 μm), the lower limit of detection of spot size 5 is therefore lower than that for spot size 4 (table 3.5). Spot size 5 was used where possible, but due to the small size of the samples, and the fractured nature of many of the mineral grains, spot size 4 was used more regularly than spot size 5.

Possible Sources of Error

During the ablation process there is a danger that the mineral grain is breached, in which case the laser continues to ablate an underlying mineral. Care was taken to avoid this complication by choosing fresh grains that had considerable depth. A real-time graphical representation of the isotope intensities during the analysis was examined in order to note large variations in Si, Ca, Sr and Ba. Any sudden changes in Si and Ca concentration would indicate that the laser had started ablating a second mineral. Concentrations of Sr and Ba were monitored as large peaks (orders of magnitude difference) infer alteration and/or fluid interaction along microscopic fractures in a grain have taken place. Analyses with high Sr and Ba peaks were discarded as only the primary trace element content of minerals were sought.

Table 3.5 Lower limits of detection (LLD) for the trace elements analysed based on counting statistics.

LLD - Spot size 4	
Element	LLD (ppm)
Sc	3.77
Ti	25.62
V	32.07
Co	1.81
Ni	3.29
Rb	0.74
Sr	0.37
Y	0.71
Zr	0.21
Nb	0.22
Ba	1.61
La	0.43
Ce	0.13
Nd	0.21
Sm	0.26
Eu	0.54
Gd	0.41
Dy	0.50
Er	0.47
Yb	0.26
Hf	0.47
Ta	0.05
Th	0.29
U	0.17

LLD - Spot size 5	
Element	LLD (ppm)
Sc	0.33
Ti	1.8
V	2.7
Co	0.16
Ni	0.87
Rb	0.055
Sr	0.031
Y	0.064
Zr	0.020
Nb	0.022
Ba	0.14
La	0.044
Ce	0.012
Nd	0.021
Sm	0.027
Eu	0.051
Gd	0.048
Dy	0.056
Er	0.054
Yb	0.029
Hf	0.052
Ta	0.005
Th	0.029
U	0.013

4. PETROGRAPHY

4.1 INTRODUCTION

Petrographic investigations form the basis of any xenolith study. Mineral associations within xenoliths, and textural features are first order observations that allow one to define different rock types and the state of equilibrium of the mantle sampled by a kimberlite. Secondary mineral growth, and alteration products allow one to infer processes occurring within the mantle and upon emplacement. These may include: interaction with metasomatic fluids within the mantle, and kimberlitic fluids during entrainment, and alteration by deuteric fluids in the secondary environment.

The eighty-five xenoliths in this study have been divided into three rock types, namely harzburgites, lherzolites and pyroxenites. The small sample size (0.5-1.5 cm) in comparison to the large grain size (0.05-1 cm) of the xenoliths places limitations on petrographic analysis. Rock types were therefore defined both on the mineral associations within the xenolith, and on petrographic and geochemical similarities to samples that displayed a fuller mineral compliment.

A textural study of the samples was undertaken to determine the state of equilibrium of the xenoliths. Mineral equilibration is a necessity for geothermobarometric calculations, samples with evidence of exsolution or recrystallization are not suitable for geothermobarometric calculations. These disequilibrium features are transient, and have important implications for the interpretation of dynamic processes occurring within the mantle.

This petrographic study reveals minor mineralogical and textural differences between the xenoliths from the three different kimberlite localities. This has implications for small scale mantle heterogeneity beneath the Slave province, as will be discussed toward the end of this chapter.

4.2 MANTLE XENOLITH CLASSIFICATION SCHEMES

Xenolith Nomenclature

Based on primary mineral associations, mafic and ultramafic xenoliths may be divided into four broad categories, namely peridotites, pyroxenites, eclogites and megacrysts. Peridotites are olivine (ol) bearing, and may contain orthopyroxene and/or clinopyroxene, whereas pyroxenites are orthopyroxene (opx) and/or clinopyroxene (cpx) bearing rocks that may contain olivine. Eclogites are rocks

consisting of pyrope-almandine garnet and omphacitic clinopyroxene, with accessory minerals such as kyanite, ilmenite, rutile, sulphides, amphibole and on the rare occasion, diamond (Carswell, 1990). Megacrysts are larger than 2 cm in longest dimension. They are commonly monomineralic, but may form coarse intergrowths (Gurney et al., 1979).

Only the IUGS nomenclature for peridotitic and pyroxenitic xenoliths will be discussed further as neither eclogites nor megacrysts were included in this project. According to the IUGS classification scheme (Streckeisen, 1980), peridotites are ultramafic rocks consisting predominantly of olivine (>40%) and may contain the ferromagnesian minerals orthopyroxene, clinopyroxene or garnet. Peridotitic xenoliths may further be subdivided according to the modal percentage the minerals olivine, orthopyroxene and clinopyroxene present. Dunite refers to xenoliths with >90% olivine, harzburgites contain <5% clinopyroxene and wehrlites contain <5% orthopyroxene, as shown in figure 4.1. Lherzolites are those peridotitic xenoliths that contain >40% olivine, >5% clinopyroxene and >5% orthopyroxene. Pyroxenites are olivine-poor ultramafic xenoliths (<40% olivine). Pyroxenites may also be subdivided according to the modal percentage of the minerals present. Orthopyroxenites contain >90% orthopyroxene, likewise, clinopyroxenites contain >90% clinopyroxene. Websterites consist predominantly of clinopyroxene or orthopyroxene, with less than 5% olivine. Those xenoliths with >5% olivine are qualified by the term "olivine-pyroxenite" depending on the dominant pyroxene, as shown in figure 4.1.

Notably, the Al-phase is not included in the IUGS classification scheme. The Al-phase varies with depth from plagioclase (0 to ~40 km depth) to spinel (~30-75 km depth) to garnet (below ~100 km), depths derived from White (1997) and Boyd et al. (1999).

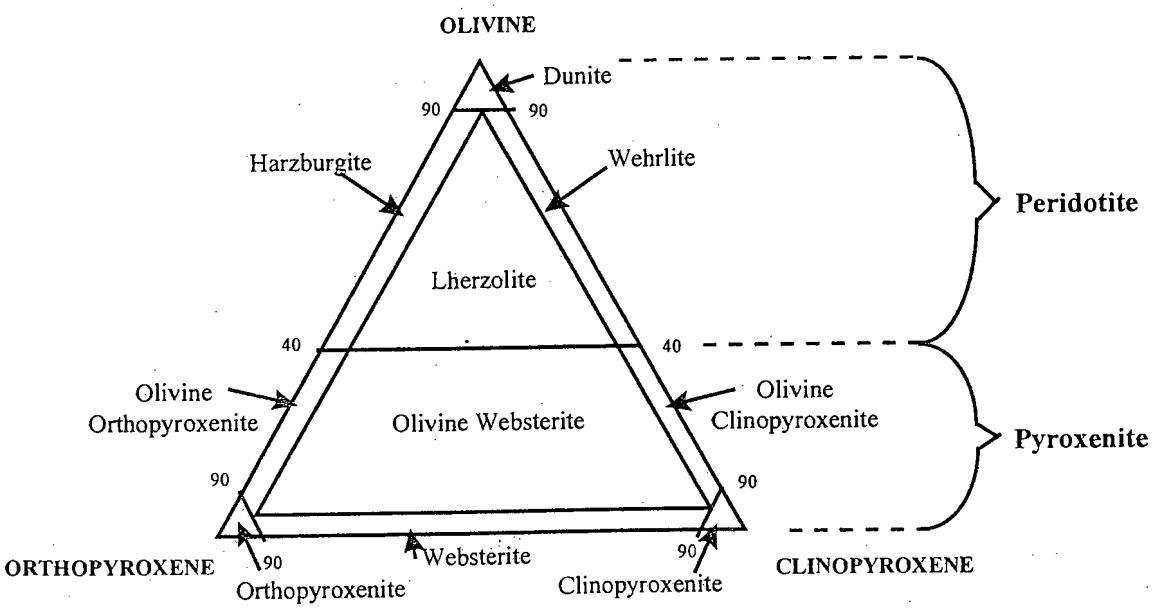

Figure 4.1 Xenolith nomenclature according to the IUGS classification scheme (Streckeisen, 1980)

Xenolith nomenclature of kimberlite-derived mantle xenoliths does not strictly follow the IUGS classification scheme as described above. Harzburgites are regarded as those xenoliths that contain no clinopyroxene (Dawson, 1981), and those xenoliths containing even one grain of clinopyroxene are termed lherzolites. This convention has been adopted by this study.

The small size (<1.5 cm) of the samples in this study relative to the large grain size (0.05-0.5 cm) placed limits on the petrographic analysis. Hence a further simplification of the IUGS classification was applied. The clinopyroxene-bearing fragments that contained olivine were termed lherzolites, whereas those that were olivine-free were termed pyroxenitic. This contrasts with the IUGS classification which terms xenoliths with <40% olivine as pyroxenitic. Using this simplified classification scheme the xenoliths could be divided into two main suites as shown in figure 4.2.

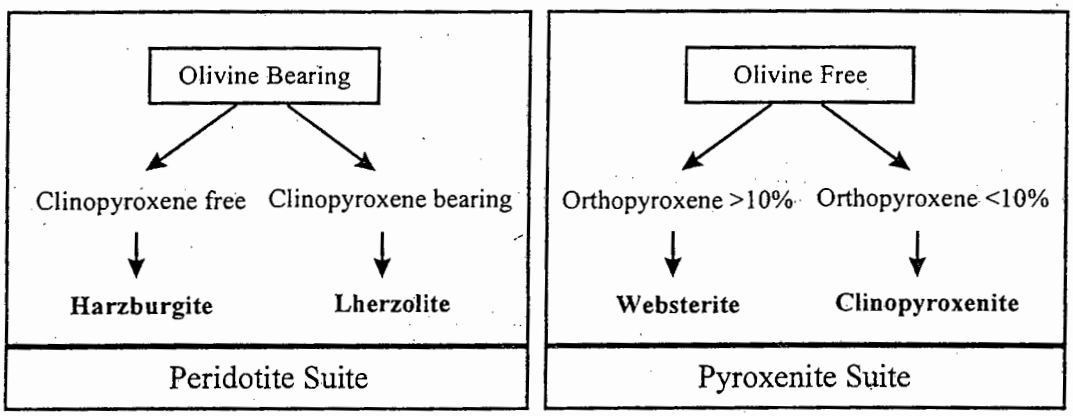

Figure 4.2 Classification of the samples into two main petrographic suites (full explanation in text).

Even application of this scheme was difficult as a number of the xenolith fragments consist of portions of only two grains (e.g. ARN023 and ARN024). Being only fragments of a larger rock, classification purely based on the modal mineralogy is likely to be inconsistent with the whole rock mineral assemblage for these xenolith fragments. The xenolith fragments within this study were therefore placed into two petrographic groups using a combination of the following criteria: mineral assemblage, garnet colour and CaO and Cr_2O_3 content in garnet.

The method employed was as follows: The principle diagnosis of a sample's petrographic suite was based on mineral assemblage. But in particularly coarse-grained samples, where it is apparent that the entire mineral assemblage is not present, garnet colour was used to help distinguish the xenoliths into petrographic suites. Past studies have shown that garnet colour and chemistry (particularly CaO and Cr_2O_3 content in garnet) are related to different parageneses (Sobolev et al., 1973; Dawson and Stephens, 1975). Most xenolith fragments with three or more phases could be distinguished using these methods. The CaO and Cr_2O_3 content in garnet (Gurney, 1984) was used to verify the classification based on garnet colour, and help classify the bimodal xenolith fragments into the different petrographic suites.

Textural Classification

Boyd and Nixon (1972) described two main types of textures in the kimberlite hosted peridotites namely, little deformed (granular) peridotites and strongly deformed (sheared) peridotites. All the peridotite xenoliths in this study are of the granular variety.

Various textural classifications have been proposed (e.g. Mercier and Nicolas, 1975; Basu, 1977) and a correlation between texture and composition has been observed in spinel lherzolites, for example Francis (1978). A standardised textural classification scheme for peridotitic xenoliths was proposed by Harte (1977), in collaboration with numerous scientists. The classification is based on the textural features of the olivine within the sample, as shown in table 4.1.

The samples in this study are difficult to classify using the classification scheme by Harte (1977) for the following reasons:

- The xenoliths are all small (<1.5cm), and may not be representative of the overall textural pattern of the larger rock body.
- Many xenoliths lack olivine entirely.
- Many xenoliths that contained olivine did not contain it in significant amounts. Many of the xenoliths consist of >80% garnet, allowance for which does not feature in the classification scheme by Harte (1977).

This study has therefore used the classification scheme by Harte (1977) where possible, with the addition of the term *"poikilitic"* to describe an unusual texture noted in many of the xenoliths. Xenoliths with a poikilitic texture have one mineral grain that completely encloses smaller grains of other minerals. Whereas garnet is the most common host phase, large clinopyroxene, orthopyroxene and olivine grains can completely enclose smaller grains of other minerals, as shown in figure 4.3. The mineral inclusions are generally sub-rounded and of a similar size to each other. Samples such as MIS426 and PGN329 reveal that the poikilitic texture may not be a texture representative of a whole rock, but rather a localised texture within coarser grained rocks (figure 4.4). In sample MIS426, rounded inclusions of olivine, orthopyroxene, clinopyroxene and chromite are enclosed by a single garnet grain surrounded by a kelyphite rim, whereas larger grained clinopyroxene and altered olivine occur outside the kelyphite rim. Likewise, half of sample PGN329 may be considered poikilitic, whereas the other half is coarse grained (figure 4.4). On closer inspection one notices that the small, rounded garnet in the poikilitic portion is joined to a larger grain beneath the epoxy surface. This shows one of the advantages of mounting xenoliths in epoxy in preference to thin section.

Table 4.1 Adapted textural classification scheme

Textural nomenclature	Classification according to Harte (1977)	Adaptation of classification to this study
Coarse	A rock lacking porphyroclasts and which is predominantly formed by mineral grains greater than 2mm in average dimension.	As for Harte, 1977.
Porphyroclastic	A rock containing porphyroclasts, and in which the proportion of **olivine** occurring as **porphyroclasts** to that in the finer grained matrix is greater than 10%. *(**Porphyroclast** - A relatively large, strained mineral grain surrounded by markedly smaller mineral grains.)*	As for Harte, 1977. Although 100% certainty of strain in the larger olivine grains cannot be assured without the aid of thin section microscopy, the presence of recrystallized olivine has been used to determine samples of this textural type.
Mosaic Porphyroclastic	A rock containing porphyroclasts, and in which 90% of the olivine occurs in small grains with a mosaic texture.	No samples in this study have this texture.
Granuloblastic	A rock without, or with very few (<5%) porphyroclasts, and in which the grains of each mineral show a small size range and a granuloblastic texture. The average grain size of this texture is less than 2 mm.	As for Harte, 1977.
Poikilitic	Not in Harte 1977 scheme	One mineral completely encloses smaller grains of other minerals (also noted by Nielson et al., 1977).

Figure 4.3 Various poikilitic textures noted in this study: (figure on following page)

a) Poikilitic-garnet texture - Garnet encloses orthopyroxene and chromite grains. Chromite needles exsolving from the orthopyroxene and chromite grains on the perimeter of the orthopyroxene grains indicates a change environment and the state of equilibrium of the minerals.
b) Poikilitic-orthopyroxene texture - Garnet grains within orthopyroxene host.
c) Poikilitic-olivine - Clinopyroxene grains within poikilitic olivine host.
d) Poikilitic clinopyroxene texture - Garnet and olivine grains within clinopyroxene host.

a) Sample ARN019

Scale bar: 7 mm. Plane-polarised light.

b) Sample PGN308

Scale bar: 5 mm. Plane-polarised light.

c) Sample ARN033

Scale bar: 6 mm. Plane-polarised light.

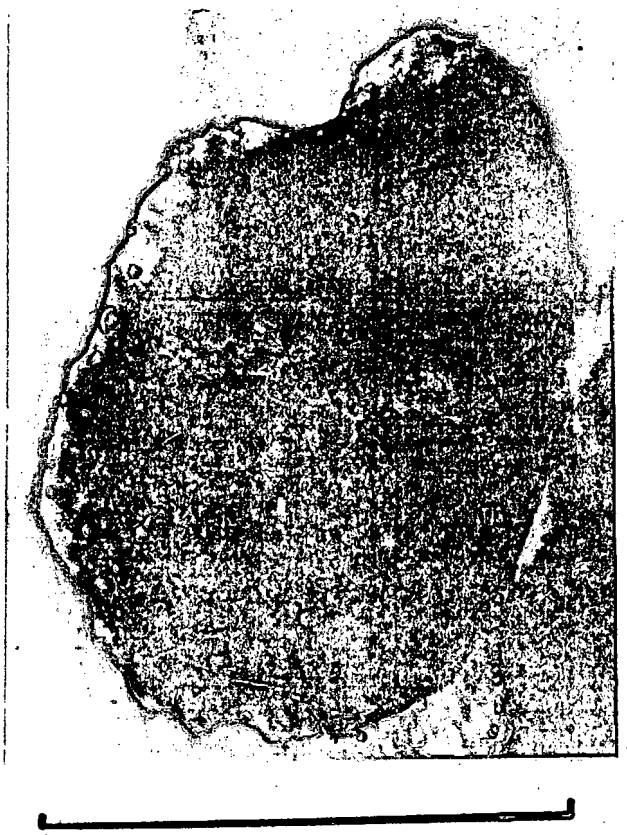

d) Sample PGN336

Scale bar: 4 mm. Plane-polarised light.

Figure 4.3 Various poikilitic textures noted in this study: (caption on previous page)

a) Sample PGN329
Scale bar: 7 mm. Plane-polarised light.

b) Sample MIS426
Scale bar: 4 mm. Plane-polarised light.

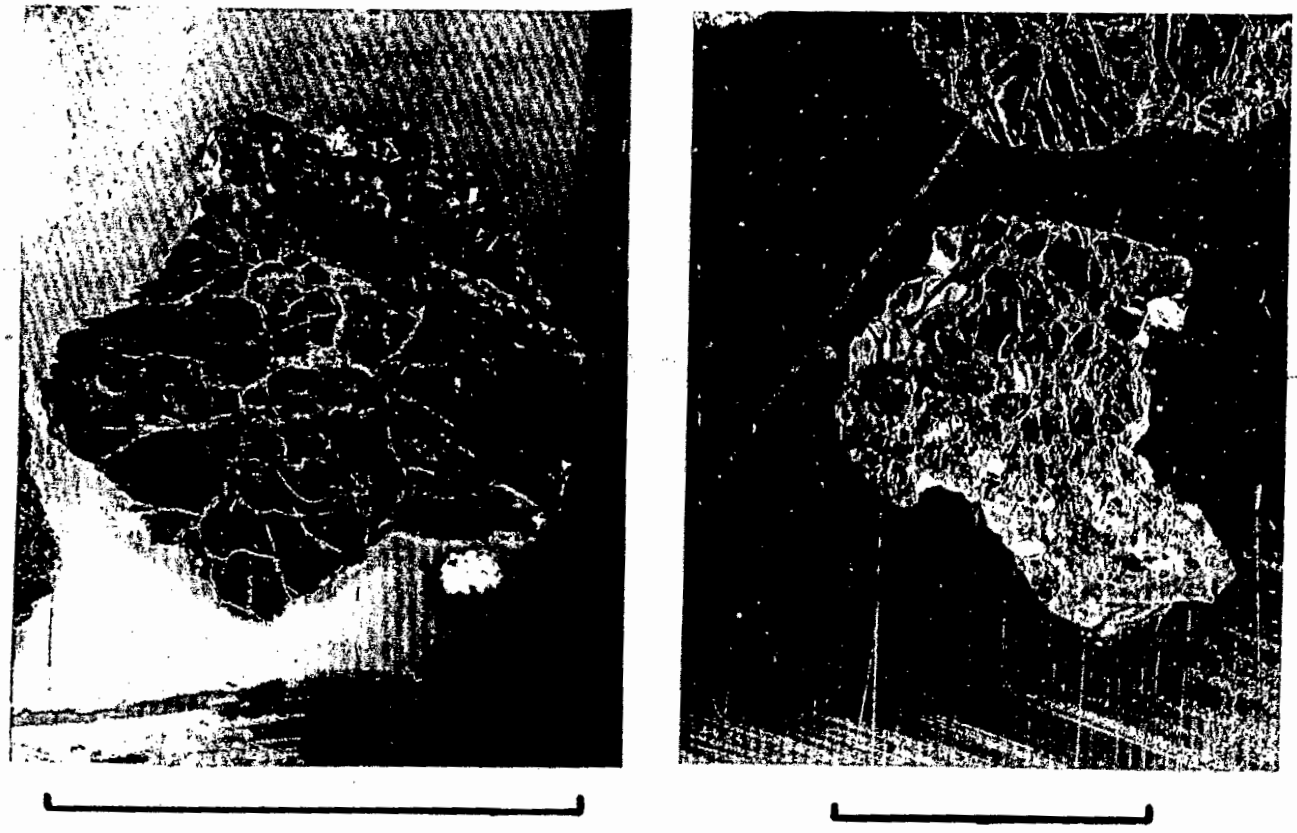

Figure 4.4 It is likely that the poikilitic texture may a small textural feature within a large rock body.

a) A two dimensional section of PGN329 would exhibit two textural features: about half of the xenolith is coarse grained, and on the surface the other portion appears to have a poikilitic texture. The small garnets surrounded by orthopyroxene resemble the orthopyroxene-hosted poikilitic texture of sample PGN308 (figure 4.3). On closer inspection, and utilising the depth perspective provided by the epoxy mounts, one notes that the small garnet grains are connected to larger grains in three dimensional space.
b) The large (>2 mm) olivine and clinopyroxene grains on the perimeter of MIS426 indicate that the larger rock mass may be coarse grained, and the poikilitic garnet is a small scale feature.

4 .3 PETROGRAPHIC DESCRIPTIONS

Harzburgitic suite

Mineral assemblages

The harzburgitic suite constitutes about two-thirds of the samples in this study, and all contain garnet. The large number of garnet-harzburgites is due to physical sample selection rather than a reflection of the random mantle sampling that occurs during kimberlite emplacement. Xenoliths with garnet-olivine-orthopyroxene mineral assemblages were preferentially selected for geothermobarometric calculations, as described in chapter 3. Many of the harzburgites contain primary chromite, particularly those from the Arnie kimberlite pipe. In some xenoliths the chromite occurs as anhedral grains within

the mineral assemblage, e.g. ARN007 and ARN025. In other cases, the chromite is in close spatial relation to orthopyroxene, and appears to have exsolved from the adjacent orthopyroxene, e.g. ARN002 and MIS417. This process is especially evident in ARN019, where chromite grains are noted on the rim of an orthopyroxene grain from which chromite needles were in the process of exsolving (figure 4.3). Smaller (<<0.5mm), euhedral Cr-spinel grains are common within the alteration rims of garnet grains and regions of fluid interaction, e.g. ARN007. These are believed to be part of alteration processes, and are therefore secondary in nature. The olivine is cloudy in many of the harzburgitic xenoliths. The cloudy nature may be attributed to secondary alteration processes, as it is especially apparent in xenoliths with a poikilitic texture in which the host garnet is highly fractured (e.g. PGN341).

Textures noted within the Harzburgitic suite

The samples in the harzburgite suite exhibit three different textures, namely: granuloblastic (fine grained), coarse equant and poikilitic. The poikilitic texture is the most common texture noted amongst the harzburgitic xenoliths (table 4.2).

Poikilitic textured xenoliths generally have large host crystals (5-10mm) enclosing small (0.5*0.5mm to 1*1mm) grains of other minerals, commonly olivine and/or orthopyroxene (figure 4.3). The inclusions are generally rounded to sub-rounded in shape. Very little alteration is noted between the host grain and the enclosed minerals. Garnet-hosted poikilitic textures, where large garnet grains enclose smaller grains of olivine, pyroxene and/or chromite are more common than orthopyroxene-, or olivine-hosted poikilitic textured xenoliths. The outer rim of dominantly garnet xenoliths, if preserved after crushing, has a thick kelyphite rim (~1mm), e.g. ARN008 and ARN025. The garnets in the garnet hosted poikilitic textured xenoliths are usually fractured along one prominent direction.

Those xenoliths with a coarse equant texture (>2mm grain size) contain minerals characterised by both curvi-linear grain boundaries, with approximately 120° grain intersection (e.g. ARN005), and straight grain boundaries (e.g. PGN337, figure 4.4). Most of the garnets feature a orange-brown kelyphite rim, and are fractured. The majority of the xenoliths are extremely fresh (e.g. ARN005), whereas others have been highly altered (e.g. ARN027). ARN026 is a remarkably fresh xenolith that exhibits only a few fractures and no kelyphite rim. The xenoliths with a granuloblastic texture (<2mm average grain size) also have straight grain boundaries and 120° grain intersections indicating textural equilibrium. Some xenoliths are fresh (e.g. ARN006), whereas others are extremely altered (e.g. ARN021).

Table 4.2 Table of mineral assemblages and texture of the Harzburgite suite xenoliths.

Kimberlite Locality	Sample Number	Rock Type	Mineral Assemblage	Texture (host mineral)	Exsolution Features
Arnie	ARN002	Harzburgite (low-Ca)*	gt-opx-ol-spinel	Coarse equant	
Arnie	ARN003	Harzburgite (high-Ca)*	gt-opx-ol-spinel	Coarse equant	
Arnie	ARN004	Harzburgite (high-Ca)	gt-opx-ol	Poikilitic (gt)	
Arnie	ARN005	Harzburgite (high-Ca)	gt-opx-ol	Coarse equant	
Arnie	ARN006	Harzburgite (high-Ca)	gt-opx-ol-spinel	Granuloblastic	
Arnie	ARN007	Harzburgite (low-Ca)	gt-opx-ol-spinel	Poikilitic (gt)	
Arnie	ARN008	Harzburgite (low-Ca)	gt-opx-ol	Poikilitic (gt)	
Arnie	ARN009	Harzburgite (high-Ca)	gt-opx-spinel	Poikilitic (gt)	
Arnie	ARN010	Harzburgite (low-Ca)	gt-opx	Poikilitic (gt)	
Arnie	ARN011	Harzburgite (low-Ca)	gt-opx-ol-spinel	Granuloblastic	
Arnie	ARN012	Harzburgite (low-Ca)	gt-opx-spinel	Poikilitic (gt)	
Arnie	ARN013	Harzburgite (high-Ca)	gt-opx-ol	Granuloblastic	
Arnie	ARN014	Harzburgite (high-Ca)	gt-opx-ol	Granuloblastic	
Arnie	ARN017	Harzburgite (low-Ca)	gt-opx-ol-spinel	Poikilitic (gt)	
Arnie	ARN018	Harzburgite (high-Ca)	gt-opx-ol	Granuloblastic	
Arnie	ARN019	Harzburgite (low-Ca)	gt-opx-spinel	Poikilitic (gt)	Spinel exsolution in opx
Arnie	ARN021	Harzburgite (low-Ca)	gt-opx-ol	Granuloblastic	
Arnie	ARN022	Harzburgite (high-Ca)	gt-opx-ol	Coarse equant	
Arnie	ARN025	Harzburgite (low-Ca)	gt-opx-ol-spinel	Coarse equant	
Arnie	ARN026	Harzburgite (low-Ca)	gt-opx-ol	Coarse equant	
Arnie	ARN027	Harzburgite (low-Ca)	gt-opx-ol-spinel	Coarse equant	
Arnie	ARN029	Harzburgite (high-Ca)	gt-opx-ol	Poikilitic (gt)	
Misery	MIS401	Harzburgite (low-Ca)	gt-opx	Poikilitic (gt)	
Misery	MIS408	Harzburgite (low-Ca)	gt-opx-ol	Coarse equant	
Misery	MIS411	Harzburgite (low-Ca)	gt-opx-ol	Poikilitic (gt)	
Misery	MIS412	Harzburgite (high-Ca)	gt-opx	Poikilitic (gt)	
Misery	MIS413	Harzburgite (high-Ca)	gt-opx-ol	Granuloblastic	
Misery	MIS417	Harzburgite (high-Ca)	gt-opx-ol-spinel	Poikilitic (gt)	Spinel exsolution in oyx
Misery	MIS420	Harzburgite (high-Ca)	gt-opx	Granuloblastic	
Misery	MIS430	Harzburgite (high-Ca)	gt-opx-ol	Coarse equant	
Misery	MIS434	Harzburgite (high-Ca)	gt-opx-ol	Coarse equant	
Misery	MIS463	Harzburgite (low-Ca)	gt-opx-ol	Poikilitic (ol)	
Pigeon	PGN301	Harzburgite (low-Ca)	gt-opx-ol	Coarse equant	
Pigeon	PGN303	Harzburgite (low-Ca)	gt-opx-ol	Poikilitic (gt)	
Pigeon	PGN312	Harzburgite (high-Ca)	gt-opx-ol	Coarse equant	
Pigeon	PGN313	Harzburgite (high-Ca)	gt-opx-ol	Coarse equant	
Pigeon	PGN314	Harzburgite (low-Ca)	gt-opx-ol	Coarse equant	
Pigeon	PGN315	Harzburgite (high-Ca)	gt-ol	Poikilitic (gt)	
Pigeon	PGN317	Harzburgite (low-Ca)	gt-opx-ol	Poikilitic (gt)	
Pigeon	PGN318	Harzburgite (low-Ca)	gt-opx	Poikilitic (gt)	
Pigeon	PGN340	Harzburgite (low-Ca)	gt-opx-ol-spinel	Coarse equant	
Pigeon	PGN341	Harzburgite (low-Ca)	gt-opx-ol	Poikilitic (gt)	
Pigeon	PGN342	Harzburgite (low-Ca)	gt-ol	Poikilitic (gt)	
Pigeon	PGN343	Harzburgite (low-Ca)	gt-opx-ol-spinel	Poikilitic (gt)	

* low-Ca and high-Ca refers to the harzburgitic sub-groups defined by the CaO content in garnet (Chapter 5)

- Gt = Garnet
- Cpx = Clinopyroxene
- Opx = Orthopyroxene
- Ol = Olivine

a) Sample ARN005
Scale bar: 7 mm. Plane-polarised light.

b) Sample PGN337
Scale bar: 7 mm. Plane-polarised light.

c) Sample ARN006
Scale bar: 6 mm. Plane-polarised light.

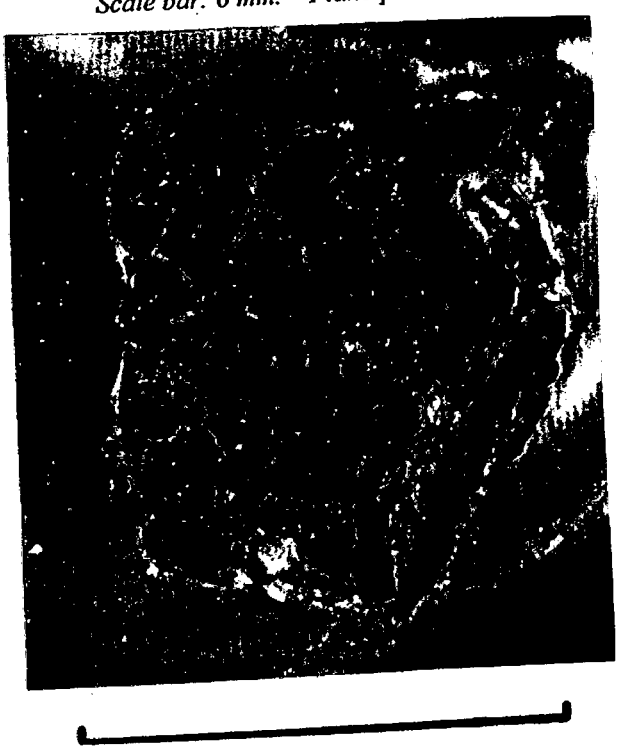

d) Sample PGN307
Scale bar: 7 mm. Plane-polarised light.

Figure 4.5 Textures noted within the peridotitic xenoliths

a) Coarse equant - Curvy-linear grain boundaries with 120° grain intersections in coarse equant xenolith.
b) Coarse equant - Straight grain boundaries with 120° grain intersections in coarse equant xenolith.
c) Granuloblastic - Average grain size <2 mm in size. Textural equilibrium has been achieved.
d) Porphyroclastic - Olivine has been recrystallized, forming olivine porphyroclasts in matrix of smaller olivine neoblasts.

Lherzolite Suite

Mineral assemblages

The lherzolite suite constitutes about a third of the sample population. Xenoliths that are not strictly lherzolitic (i.e. lack one or more of the minerals olivine, orthopyroxene or clinopyroxene) have been included in this suite due to petrographic (texture or mineral colour) and/or chemical similarity to lherzolitic fragments. Only six xenoliths in this study do not contain garnet, namely ARN032, ARN033, ARN034, ARN035, ARN036 and ARN037. Four lherzolitic xenoliths contain primary Cr-spinel, all of which come from the Misery kimberlite locality (MIS409, MIS426, MIS431, MIS433). One xenolith from the Pigeon kimberlite contains exsolved Cr-spinel (PGN333). The olivine in many of the lherzolite xenoliths is cloudy due to secondary alteration processes (e.g. PGN310). Two xenoliths contained phlogopite, one is garnet-bearing (PGN338), the other is not (ARN033). The phlogopite in sample ARN033 was noticed before sample preparation but was unfortunately removed during sample preparation.

Textures noted in the Lherzolite suite

The lherzolitic xenoliths exhibit a variety of textures, namely: coarse equant, poikilitic and porphyroclastic. The coarse equant texture is the most dominant texture noted, followed by the poikilitic texture. Those xenoliths with a coarse equant texture are texturally indistinct from those of the harzburgite suite. Spinel exsolution has occurred from the clinopyroxene grain in one of the coarse equant samples, namely MIS431. The poikilitic texture is not as dominant in the lherzolite suite as in the harzburgite suite. In contrast to the harzburgite suite, where garnet is typically the host phase in poikilitic textured xenoliths, within the lherzolite suite orthopyroxene and clinopyroxene are common host phases in the lherzolite suite (e.g. PGN311 and PGN336). The orthopyroxene in the orthopyroxene-hosted poikilitic textured xenoliths (PGN308, PGN309, PGN311) is honey yellow and encloses red, sub-rounded garnets that are all less than 2 mm in size. Clinopyroxene grains are only enclosed by garnet in three poikilitic textured xenoliths, namely PGN323, PGN333 and MIS409. PGN329 shows an intermediate texture between the poikilitic texture and the coarse equant texture (figure 4.4).

Two samples (PGN306 and PGN316) have a porphyroclastic texture, in which a small portion of the olivine has been recrystallized. These may indeed be true porphyroclastic textured xenoliths, but as the xenoliths are mounted in epoxy, one cannot verify if the larger olivines are strained. The garnets in these xenoliths are rounded, fractured and have a large kelyphite rims (0.5-1mm). Sample PGN324 also has a porphyroclastic-like appearance: the olivine shows a small amount of recrystallization, and

the clinopyroxene and olivine are small (0.5 mm) in comparison to the sub-rounded garnet grains (>2 mm).

Table 4.3 Table of mineral assemblages and texture of the Lherzolite suite xenoliths. Abbreviations as for Table 4.2.

Kimberlite Locality	Sample Number	Rock Type	Mineral Assemblage	Texture (host mineral)	Other Exsolution Features
Arnie	ARN023	Lherzolite	gt-ol	Poikilitic (ol)	
Arnie	ARN024	Lherzolite	gt-ol	Poikilitic (ol)	
Arnie	ARN030	Lherzolite	gt-ol	Poikilitic (gt)	
Arnie	ARN032	Lherzolite	gt-opx-cpx-ol	Poikilitic (ol)	
Arnie	ARN033	Lherzolite	cpx-ol-phlogopite	Poikilitic (ol)	
Arnie	ARN034	Lherzolite	cpx-ol	Poikilitic (ol)	
Arnie	ARN035	Lherzolite	cpx-ol	Poikilitic (ol)	
Arnie	ARN036	Lherzolite	cpx-ol	Poikilitic (ol)	
Arnie	ARN037	Lherzolite	opx-cpx-ol	Poikilitic (ol)	
Misery	MIS409	Lherzolite	gt-opx-cpx-spinel	Poikilitic (gt)	
Misery	MIS419	Lherzolite	gt-opx-cpx	Coarse equant	
Misery	MIS426	Lherzolite	gt-opx-cpx-ol-spinel	Coarse equant (near poikilitic)	
Misery	MIS431	Lherzolite	gt-opx-cpx-ol-spinel	Coarse equant	Spinel exsolution in pyroxene
Misery	MIS433	Lherzolite	gt-opx-cpx-ol-spinel	Coarse equant	
Pigeon	PGN306	Lherzolite	gt-opx-ol	Poikilitic (gt)	
Pigeon	PGN307	Lherzolite	gt-opx-ol	Porphyroclastic	
Pigeon	PGN308	Lherzolite	gt-opx	Poikilitic (opx)	
Pigeon	PGN309	Lherzolite	gt-opx	Poikilitic (opx)	
Pigeon	PGN310	Lherzolite	gt-opx-cpx-ol	Coarse equant	
Pigeon	PGN311	Lherzolite	gt-opx	Poikilitic (opx)	
Pigeon	PGN316	Lherzolite	gt-opx-ol	Porphyroclastic	
Pigeon	PGN321	Lherzolite	gt-cpx	Coarse equant	
Pigeon	PGN323	Lherzolite	gt-cpx	Poikilitic (gt)	
Pigeon	PGN324	Lherzolite	gt-cpx-ol	Porphyroclastic	
Pigeon	PGN325	Lherzolite	gt-opx-cpx	Coarse equant	
Pigeon	PGN329	Lherzolite	gt-opx-cpx	Coarse equant	
Pigeon	PGN333	Lherzolite	gt-cpx-ol-spinel	Poikilitic (gt)	
Pigeon	PGN336	Lherzolite	gt-cpx-ol	Poikilitic (cpx)	
Pigeon	PGN337	Lherzolite	gt-opx-cpx	Coarse equant	
Pigeon	PGN338	Lherzolite	gt-opx-cpx-phlogopite	Coarse equant	
Pigeon	PGN339	Lherzolite	gt-cpx-ol	Coarse equant	

Pyroxenite suite

Mineral assemblages

This suite consists of two websterites (garnet-orthopyroxene-clinopyroxene bearing xenoliths) and eight garnet-clinopyroxenites. One of the clinopyroxenites does contain orthopyroxene (10%), yet it is texturally and chemically distinct from the two websterites (>10% orthopyroxene), and has therefore been described with the clinopyroxenites. The colour of the garnet of the pyroxenitic xenoliths are

distinct from that of the olivine-free lherzolite suite xenoliths: the garnets are orange, whereas those in the lherzolite suite are red.

Oxide exsolution has occurred within the pyroxene and garnet of several xenoliths from the Misery kimberlite. Spinel has exsolved from the pyroxene in samples MIS451 and MIS454. Whereas macroscopic needles of rutile were noted within the garnet of both MIS438 and MIS454, as shown in figure 4.6d.

Textures noted in the Pyroxenite suite

The two garnet websterites (MIS438 and MIS439) are fine grained, with well equilibrated, 120° grain intersections. The garnets are ringed with a thin kelyphite rim (figure 4.6a). Due to the fine grained (<2mm) nature of these rocks and their even mineral distribution, these xenoliths are believed to be representative of the larger rock package from which they originate. The fine grained nature of these garnet-orthopyroxene-clinopyroxene xenoliths texturally discriminates them from the coarse grained and poikilitic garnet-orthopyroxene-clinopyroxene assemblages of the lherzolite suite. The fine grained websterites are also chemically different to those garnet-orthopyroxene-clinopyroxene assemblages included in the lherzolite suite, as will be shown in Chapter 5.

The garnet-clinopyroxenite that contains 10% orthopyroxene (MIS428) is texturally different to the fine-grained garnet-websterites. Large (>2mm) clinopyroxene grains exhibit both spinel and garnet exsolution lamellae that are orientated in the same direction. It also features fine grained orthopyroxene and garnet along the clinopyroxene grain boundaries forming a necklace texture, as shown in figure 4.6b.

Two of the clinopyroxenites have a poikilitic texture where clinopyroxene completely encloses small (1*1mm), rounded garnet grains (PGN319 and MIS454). The remaining five clinopyroxenites have a coarse equant texture (ARN028, ARN031, MIS454, PGN320 and PGN322). They have straight grain boundaries and 120° grain intersections. The two xenoliths from the Arnie kimberlite feature smaller (< 1 by 1 mm) garnet grains located at triple junction between three larger (2mm) clinopyroxene grains (figure 4.6c) suggesting that these xenoliths have undergone recrystallization. The garnets from PGN320 and PGN322 are almost completely altered, whereas the Cr-diopside is fresh. In contrast to the kelyphite rims of other garnets, the alteration around the garnets in PGN320 and PGN322 is grey and spongy.

Table 4.4 Table of mineral assemblages and texture of the Pyroxenite suite xenoliths. Abbreviations as for Table 4.2.

Kimberlite Locality	Sample Number	Rock Type	Mineral Assemblage	Texture (host mineral)	Other Exsolution Features
Arnie	ARN028	Clinopyroxenite	gt-cpx	Coarse equant	
Arnie	ARN031	Clinopyroxenite	gt-cpx	Coarse equant	
Misery	MIS428	Clinopyroxenite	gt-opx-cpx	Coarse equant with necklace texture	Spinel and garnet exsolution from clinopyroxene
Misery	MIS451	Clinopyroxenite	gt-cpx	Poikilitic (cpx)	Spinel exsolution in pyroxene
Misery	MIS454	Clinopyroxenite	gt-cpx	Coarse equant	Spinel exsolution in pyroxene, Oxide needles in garnet
Pigeon	PGN319	Clinopyroxenite	gt-cpx	Poikilitic (cpx)	
Pigeon	PGN320	Clinopyroxenite	gt-cpx	Coarse equant	
Pigeon	PGN322	Clinopyroxenite	gt-cpx	Coarse equant	
Misery	MIS438	Websterite	gt-opx-cpx	Granuloblastic	Needles in garnet
Misery	MIS439	Websterite	gt-opx-cpx	Granuloblastic	

Figure 4.6 Textures of the pyroxenite suite. (figure on following page)

a) Granoblastic texture of the pyroxenite suite websterites.
b) Necklace texture of garnet and orthopyroxene on grain boundaries of large clinopyroxene grains. Spinel and garnet exsolution within clinopyroxene grains.
c) Recrystallization textures: Fine grained garnets at intersection of three clinopyroxene grain.
d) Macroscopic rutile needles in MIS451, also noted in MIS438 and MIS454.

a) Sample MIS438

Scale line: 5 mm. Plane-polarised light.

b) Sample MIS428

Scale line: 4.5 mm. Plane-polarised light.

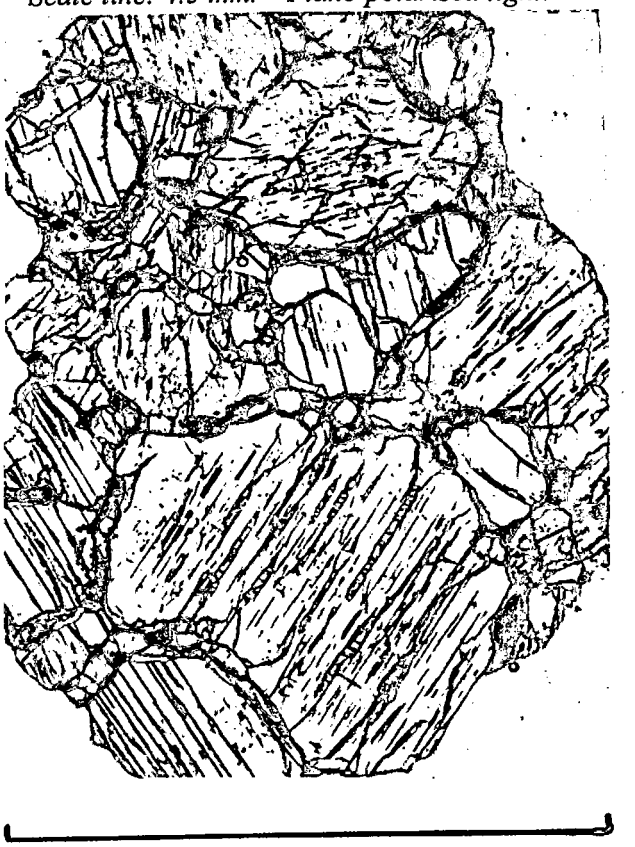

c) Sample ARN028

Scale line: 5 mm. Plane-polarised light.

d) Sample MIS451

Scale line: 0.25 mm. Plane-polarised light.

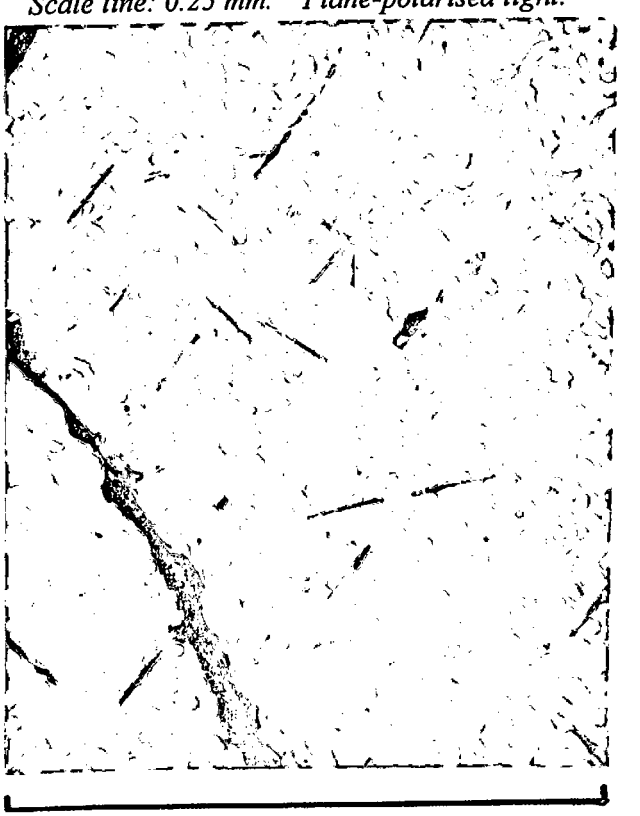

Figure 4.6 Textures of the pyroxenite suite (caption on previous page).

4 .4 DISCUSSION

Modal mineralogy

Harzburgite and lherzolite suite xenoliths dominate over the pyroxenite suite xenoliths at both the Arnie and Pigeon kimberlite localities. Misery, located just 20km SSW of Arnie, has a far larger proportion of eclogitic and pyroxenite suite xenoliths than the other two localities. This observation is based on both the relative proportion of the samples in this study (table 4.5), and on observed proportions of peridotitic to eclogitic xenoliths during initial sample selection.

The garnet-bearing xenoliths from the Pigeon kimberlite contain relatively more clinopyroxene than the garnet-bearing xenoliths from both the Arnie and Misery kimberlites. Primary chromite is more abundant in the xenoliths from the Arnie kimberlite than in those from the Misery or Pigeon kimberlites. Whereas this feature may be an artefact of the small sample size, the fact that garnet-orthopyroxene-olivine-bearing xenoliths were preferentially selected, and that the xenoliths are all of a similar size, means the secondary mineral association (clinopyroxene and/or chromite) of the garnet-bearing xenoliths ought to be independent of sample selection. The abundance is therefore believed to be a true representation of the mineral abundance at the respective localities rather than a relic of sampling bias. The different modal abundances of minerals in the xenoliths from the different kimberlites would suggest small scale heterogeneities within the mantle beneath the Slave province.

Table 4.5 Summary of the mineral associations of the prepared xenoliths in the study.

Mineral combinations	Number of Samples				Percentage (%) per Pipe		
	Arnie	Pigeon	Misery	Total	Arnie	Pigeon	Misery
Harzburgite Suite	22	12	10	*48*	67	38	50
Lherzolite Suite	9	17	5	*27*	27	53	25
Pyroxenite Suite	2	3	5	*10*	6	9	25
Total	**33**	**32**	**20**	***85***	**100**	**100**	**100**

Textural features

The samples from the three kimberlite localities can be divided into four main textural groupings:

- Coarse equant (Harte, 1977) - most grains in xenolith >2*2mm,
- Granuloblastic (Harte, 1977) - most grains in xenolith <2*2mm,
- Porphyroclastic (Harte, 1977) - where larger olivine occur within a matrix of recrystallized olivine,
- Poikilitic xenoliths - one mineral encloses finer, sub-rounded grains of other minerals.

Most textures are observed in xenoliths from all three kimberlite localities. Xenoliths from every locality exhibit evidence of recrystallization and exsolution processes, yet they appear to variable degrees.

The poikilitic texture is the most dominant texture noted within the xenoliths from the Arnie and Pigeon kimberlites (table 4.6). Coarse equant textured xenoliths are the second most dominant textural type noted from these kimberlites. The most dominant texture of the xenoliths from the Misery kimberlite is the coarse equant texture. No granuloblastic textured xenoliths are evident within the Pigeon kimberlite xenoliths, however, the only xenoliths with porphyroclastic textures originate from the Pigeon kimberlite locality.

Poikilitic textures may not be indicative of the overall texture of a larger rock package, but may represent localised textures within coarser grained rocks. Even within the small samples in this study (0.5 - 1.5 cm), there is evidence that it forms part of a coarser grained texture (figure 4.4). The high proportion of this texture may reflect the competence of the poikilitic grains. These coherent nodules may have remained intact whereas the surrounding rock disintegrated during the preliminary crushing phase of the exploration process.

Table 4.6 Summary of the textures of all the prepared xenoliths in the study.

Texture	Number of Samples			Percentage of Samples		
	Arnie	Pigeon	Misery	Arnie	Pigeon	Misery
Coarse equant	9	14	9	27	44	45
Granuloblastic	6	0	4	18		20
Porphyroclastic	0	3	0		9	
Poikilitic xenoliths (host mineral):	18	15	7	55	47	35
Poikilitic (gt)	*10*	*10*	*5*	*31*	*31*	*25*
Poikilitic (cpx)	*0*	*2*	*1*		*6*	*5*
Poikilitic (opx)	*0*	*3*	*1*		*10*	*5*
Poikilitic (ol)	*8*	*0*	*0*	*24*		
Total	**33**	**32**	**20**	**100**	**100**	**100**

Exsolution and Recrystallisation features

Exsolution is more common in the xenoliths from the Misery kimberlite than the other two localities. Especially common is spinel exsolution from both orthopyroxene and clinopyroxene mineral grains. Microscopic needles within garnet are also common (MIS438 and 454). Kopylova et al. (1999a) also noted needles within garnets from the Jericho kimberlite (NWT), and indicated that they were rutile needles. One clinopyroxenite xenolith from the Misery kimberlite (MIS428) exhibits both garnet and spinel exsolution from clinopyroxene, and a well developed necklace texture where smaller, recrystallized garnet and orthopyroxene surround the clinopyroxene grains. Neither the xenoliths from the Arnie kimberlite, nor those from the Pigeon kimberlite exhibit extensive exsolution features. Only one xenolith from Arnie featured spinel exsolution in orthopyroxene (ARN019), and one from the Pigeon kimberlite (MIS417). Hence the amount of exsolution noted within the xenoliths is greater in

the southerly kimberlite (Misery kimberlite) than the two northerly kimberlites (Pigeon and Arnie kimberlites).

Recrystallization of constituent minerals is evident in a number of xenoliths from each pipe. For example, pyroxenite xenoliths from both the Arnie and Misery kimberlites have finer grained, rounded garnets at the 120° triple junction of clinopyroxene grains (ARN028, ARN031 and MIS428). Olivine-rich xenoliths from the Pigeon kimberlite show evidence of recrystallization of olivine to form a porphyroclastic texture (e.g. PGN307 and PGN316).

Exsolution of garnet lamellae from eclogitic clinopyroxene is fairly common (Harte and Gurney, 1975; Jerde et al., 1993; Bilal and Touret, 2001), whereas exsolution of orthopyroxene and spinel from clinopyroxene is less common. The latter has been noted in localities such as: the Hawaiian chain (Sen, 1987) and the Syrian Rift on the extension of the Dead Sea fault (Bilal and Touret, 2001). Exsolution is a texture that records transitional stages in a re-equilibration process (Tuttle and Bowen, 1958; Field and Haggerty, 1994; Pearson et al., 1995). Various studies have shown that the development of garnet exsolution lamellae suggest slow cooling and re-equilibration of Al-rich pyroxenes from near solidus conditions (1400°C) towards normal mantle lithosphere temperatures (Harte and Gurney, 1975; Sautter and Harte, 1988; Pearson et al., 1995; Chen et al., 1996; Zhang and Liou, 1999). The abundant exsolution features within many of the pyroxenites from the Misery kimberlite suggests that they have experienced a change in pressure and temperature conditions. This re-equilibration process was arrested at the time of entrainment into the kimberlite magma.

5. MAJOR ELEMENT MINERAL CHEMISTRY

5.1 INTRODUCTION

Major element mineral compositions from the eighty-five samples described in the petrographic chapter were determined using a wavelength disperse electron microprobe in the Department of Geological Sciences, University of Cape Town, RSA. Operating conditions and lower limits of detection are included in Chapter 3.

Duplicate or triplicate analyses were obtained from each mineral in a xenolith. The freshest, least fractured grains were preferentially selected for analysis. The presence of compositional zoning was evaluated by analysing the core and rim of individual grains. The majority of the grains were found to be homogeneous and were averaged to provide a representative composition for each xenolith.

A few garnets showed subtle, but random variations in CaO (<0.89 wt% in 6.13 wt%) and Cr_2O_3 (<0.89 wt% in 8.92 wt%). The maximum variation in CaO and Cr_2O_3 content was noted in MIS413, smaller, but marked variation was noted in ARN026 and MIS412. A few orthopyroxene grains (ARN013, ARN018, MIS420) similarly showed subtle variation in Al_2O_3 (<0.19 wt% in 0.65 wt%) and Cr_2O_3 (0.20 wt% in 0.36 wt%). Maximum variation noted in ARN013 and MIS420 respectively. These analyses were also averaged. The variations in the garnets and orthopyroxenes are attributed to alteration of the grains near grain boundaries and fractures, or due to exsolution processes. Compositional variation between different chromite crystals in a single sample are large. For this reason, *none* of the chromite analyses were averaged.

Geochemical classification

Orthopyroxene and olivine, the major mineralogical components of peridotitic xenoliths have relatively simple crystallographic structures which allow for few elemental variations. In contrast, clinopyroxene and garnet are structurally more complex (Deer, Howie and Zussman, 1995). The garnet structure especially, allows for greater geochemical diversity than the other minerals commonly found within ultramafic nodules. This variety may be used to discriminate between different parageneses and as a tracer for petrogenetic processes taking place within the mantle. Garnet geochemistry has therefore been the focus of many mantle xenolith studies (Gurney and Switzer, 1973; Gurney, 1984; Kopylova et al., 2000). Dawson and Stephens (1975) were among the first to attempt to classify garnets according to their composition. They discriminated twelve coherent groups on the basis of five oxides, namely

Cr_2O_3, TiO_2, MgO, FeO and CaO. For example: peridotitic garnets are generally Cr-rich (>2 wt% Cr_2O_3), whereas pyroxenitic and eclogitic garnets are generally Cr-poor (<2 wt%) (Dawson and Stephens, 1975; Fipke et al., 1995).

Within the peridotitic field (>2wt% Cr_2O_3) the 85% line of Gurney (1994) is widely used today to distinguish between sub-calcic (harzburgitic) and high-Ca (lherzolitic) garnets. This has found application both in kimberlitic xenolith studies and in the diamond exploration industry (Fipke et al., 1995). This is an empirical line that apportioned 85% of the known garnet inclusions in diamond within the Ca-poor field (Gurney, 1984). For the purposes of this study, this line has been approximated to be: (Cr_2O_3 wt%) = 3.9(CaO wt%)-13.6 on a plot of Cr_2O_3 vs CaO in garnet (as deduced from Gurney, 1984).

Based on garnet composition and the 85% line of Gurney (1994) the harzburgitic suite may be divided into two groups, namely a low-Ca and a high-Ca harzburgite group. Whereas the high-Ca garnets are more alike the lherzolite suite in major element composition, their trace element chemistry is more alike that of the low-Ca harzburgitic suite.

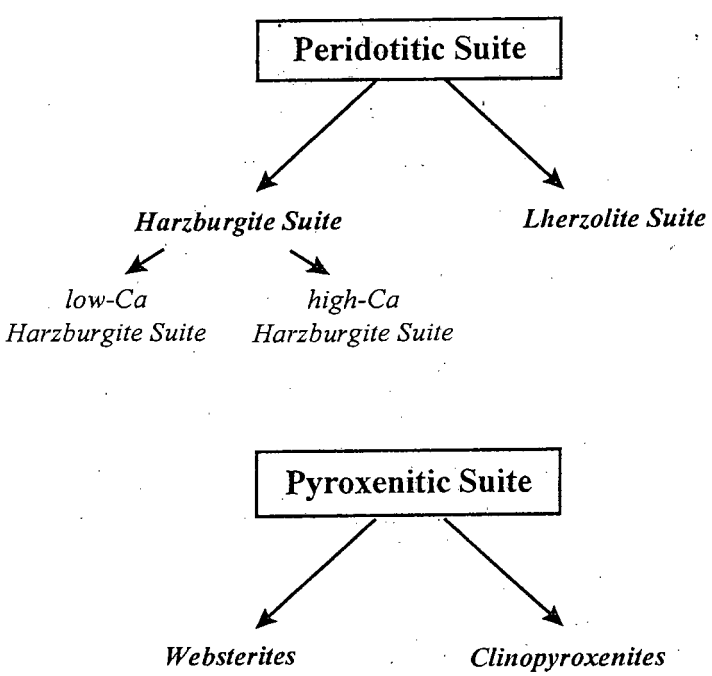

Figure 5.1 The subdivision of the samples based on petrography and major element compositions. The subdivision of the harzburgite suite is based primarily on the CaO and Cr_2O_3 content in garnet in conjunction with the 85% line of Gurney (1984).

5.2 CHEMICAL CHARACTERISATION

Harzburgite Suite

Low-Ca Harzburgite Suite

The garnets of the low-Ca harzburgite suite are all pyrope in composition (table 5.2 and figure 5.2). They have high Mg#'s (81.4-85.3, figure 5.3, Mg# = 100*Mg/(Mg+Fe)), and contain between 1.0 to 5.5 wt% CaO, and between 4.6 and 10.2 wt% Cr_2O_3 (figure 5.4). They all have TiO_2 contents below 0.1 wt% (figure 5.5).

The orthopyroxenes of the low-Ca harzburgite suite are enstatite, and are all Mg-rich (Mg# 93.0-94.0, table 5.5 and figure 5.6 and 5.7). All but one have CaO content below 0.3 wt% (MIS463 has an elevated CaO content of 0.63 wt%). There is a significant range in Cr_2O_3 (0.20-0.52 wt%) and Al_2O_3 (0.27-0.92 wt%) content in the orthopyroxenes (figure 5.8). This has implications for the derived pressure of equilibration for the harzburgitic xenoliths, as discussed in chapter 7.

The olivine of the low-Ca harzburgitic suite is Mg-rich (Mg#'s 91-93), and their NiO contents range from 0.32 to 0.50 wt% (table 5.3). One sample lies outside this range (PGN301)with Mg# 93.7, and NiO 0.15 wt% (figure 5.9), and a noticeably higher CaO, Cr_2O_3 and MnO content. The olivine is cloudy, and the anomalous chemistry is interpreted to be a reflection of the secondary alteration.

The low-Ca harzburgitic chromites have high Cr_2O_3 contents (60.2-63.2 wt%) and low Al_2O_3 contents (5.8-8.2 wt%). The chromite of ARN019 has exsolved out of the orthopyroxene and has a slightly lower average Cr_2O_3 content (58.6 wt%) and a higher Al_2O_3 content (10.0 wt%) (figure 5.10, table 5.4). The chromites have a MgO content between 11.4 and 13.5 wt% (Mg# 51.1-60.3).

High-Ca Harzburgite Suite

The garnets of the high-Ca harzburgites have higher CaO (5.2-7.7 wt%) and have a larger range in Mg#'s (77.9-84.7) than the low-Ca harzburgitic garnets (figure 5.3). 76.5 to 84.7, and the CaO content from 5.2 to 7.7 wt%. The garnet of MIS420 has a lower Mg# (76.5) and higher CaO (9.6 wt%) contents, but this sample is extremely altered. The Cr_2O_3 (5.5-11.5 wt%) and TiO_2 (<0.1 wt%) content of the high-Ca harzburgitic garnets is similar to that of the low-Ca harzburgitic garnets (figure 5.4, figure 5.5).

The majority of the high-Ca harzburgitic orthopyroxenes have high Mg#'s (93.0-93.6) and low CaO contents (less than 0.41 wt%). They have a large range in Cr_2O_3 (0.08-0.49 wt%) and Al_2O_3 (0.28-0.70 wt%) content (figure 5.8).

The olivine in the high-Ca harzburgite suite is similar to that of the low-Ca harzburgitic olivine, with a marginally larger range in Mg# (90.0-94.2), and a similar NiO content (0.35-0.51 wt%). The Mg-rich ($Fo_{94.2}$) olivine of sample ARN030 is a single olivine grain (<0.5mm) on the edge of a garnet fragment and the cloudy appearance suggests it has undergone secondary alteration.

There are two clusters of chromites, a small group similar to the majority of the low-Ca harzburgitic chromites, and a larger group akin to the exsolved chromite of ARN019 (figure 5.10). The first group has high Cr_2O_3 contents (60.8-61.8 wt%) and low Al_2O_3 contents (6.2-6.5 wt%), whereas the second group has slightly lower Cr_2O_3 contents (56.8-59.5 wt%) and higher Al_2O_3 contents (10.2-11.7 wt%). The chromites have a MgO content between 11.2-12.8 wt%, (Mg# 51.5-55.9).

The minerals within sample MIS413 are generally more Fe-rich than those of the other harzburgitic samples. The mineral chemistry has therefore not been included in the Mg# ranges reported above. The Mg#'s are as follows: garnet (70.4), orthopyroxene (89.6) and olivine (87.4). The olivine also has a lower NiO content (0.30 wt%). Although the best available grains were analysed, the minerals in MIS413 are highly altered. The Fe-rich nature of the minerals in MIS413 may reflect secondary Fe-enrichment.

Lherzolite Suite

The lherzolitic garnets are marginally more Fe- and more Ca-rich than the low-Ca harzburgitic garnets (figure 5.2, 5.3 and 5.4). The lherzolitic garnets have Mg#'s between 70.0 to 84.5, and CaO contents between 4.9 to 7.1 wt%. The Cr_2O_3 range is larger than that of the high-Ca harzburgites, ranging from 2.8 to 11.8 wt%. The TiO_2 content is also higher, ranging up to 0.9 wt% TiO_2 (figure 5.5). Lherzolitic garnets (clinopyroxene-bearing) generally have a higher Al/Cr cation ratio, than those of the harzburgite suite (clinopyroxene-free), table 5.2.

The clinopyroxenes of the lherzolite suite are all Mg-rich, with Mg#'s between 90.7 and 94.6 (figure 5.12), and Ca# 41.7-50.3 (Ca# = 100*Ca/(Ca+Mg)). Three clusters are noted within based on Al_2O_3 and Cr_2O_3 content (figure 5.13). The majority of the clinopyroxenes have a low Al_2O_3 contents (1.0-2.4 wt%), and fall into two clusters based on Cr_2O_3 content: a high Cr_2O_3 (2.2 to 3.7 wt%) and a low Cr_2O_3 content (0.8-1.3 wt%) group. Those clinopyroxenes with a high Cr_2O_3 content have generally equilibrated with high-Cr garnet, or are garnet-free. The third cluster (with a higher Al_2O_3 content:

3.4-3.9 wt%) consists of four samples, all of which have equilibrated with primary chromite. The lherzolitic clinopyroxenes all have low TiO_2 contents (<0.4 wt%), and a small range in CaO (18.3-21.3 wt%) and Na_2O (0.9-2.0 wt%) content (figure 5.14).

The orthopyroxenes of the lherzolite suite are more Ca-rich (0.14-0.97 wt% CaO) and Fe-rich (Mg# 91.2-93.7) than those of the harzburgite suite (92.4-94.0) (figure 5.7). The lherzolitic orthopyroxenes have a larger range in Cr_2O_3 (0.15 - 0.74 wt%) and Al_2O_3 (0.44 - 1.16 wt%) than the harzburgitic orthopyroxenes (figure 5.8). The Na_2O content is below 0.17 wt%. The TiO_2 content of the lherzolitic orthopyroxenes is low (0.13 wt%), but is greater than those of the harzburgitic orthopyroxenes.

The olivine of the lherzolite suite has a range in forsterite content from $Fo_{90.4}$ to $Fo_{92.7}$, and a larger range in NiO content (0.26-0.47 wt%) than the harzburgitic olivines.

Two distinct groups of chromites are observed: a low Al_2O_3 and a high Al_2O_3 group (figure 5.10). The low Al_2O_3 group (ARN032, ARN033 and PGN333) are similar in chemistry to the harzburgitic chromites. They have Al_2O_3 contents of 6.1-7.7 wt%, high Cr_2O_3 contents (57.6-60.2 wt%), and MgO contents between 10.1 and 12.9 wt%. Those chromites with high Al_2O_3 (15.6-24.5 wt%) have high MgO contents (11.3-15.1 wt%) and low Cr_2O_3 (42.0-50.5 wt%). There is a general trend in the lherzolitic chromites from chromite compositions to more pleonaste compositions, becoming more Al- and Fe^{3+}- rich.

Disequilibrium is noted between the chromite grains of MIS409: three chromite grains were analysed from MIS409, two in close spatial relation to orthopyroxene and clinopyroxene and the third completely surrounded by garnet. The chromites are not homogeneous: the chromite grain surrounded by the garnet has slightly higher MgO and Al_2O_3, and lower Cr_2O_3 contents than the chromite grains adjacent the pyroxenes (figure 5.11).

Two lherzolitic xenoliths contained phlogopite (ARN033 and PGN338). The phlogopite in ARN033 was removed during sample preparation.

The phlogopite in PGN338 has high SiO_2 contents (43.8%) and very low TiO_2 contents (0.07 wt%). In other respects it typical of other mantle derived phlogopites, having 13.5% Al_2O_3, 3.0% FeO, 24.6% MgO and 9.5% K_2O, as shown in table 5.1.

Table 5.1 Major element composition of phlogopite in PGN338.

Sample No.	PGN338
SiO_2	43.82
TiO_2	0.07
Al_2O_3	13.49
FeO	2.96
MnO	<0.05
MgO	24.63
CaO	<0.03
Na_2O	<0.03
K_2O	9.46
Total	94.50
Atomic Proportions based on 24(O, OH, F)	
Si	6.703
Ti	0.008
Al	2.433
Fe	0.379
Mn	0.005
Mg	5.618
Ca	0.001
Na	0.005
K	1.846
Total	16.998

Pyroxenite Suite

All the minerals of the pyroxenitic suite xenoliths are more Fe-rich, and have lower Cr_2O_3 contents than the minerals of the peridotitic suite xenoliths. The pyroxenite suite consists of two garnet-websterites and eight garnet-clinopyroxenites.

Websterites

The garnets of the granoblastic websterites are the most Fe-rich of all the garnets in this study (Mg# 45.3 and 54.7). They are Cr-poor (below 0.45 wt% Cr_2O_3), with CaO (5.4 and 5.7 wt%) and TiO_2 contents below 0.08 wt%. They have much higher Al/Cr ratios (75.8 and 122.2) than the peridotitic garnets (1-12) and the clinopyroxenite garnets (7.0-76.4, table 5.2).

The clinopyroxenes of the websterites distinguish these samples from the other pyroxenitic suite samples. The clinopyroxenes have lower Mg# (83.5 and 85.3), and higher Al_2O_3 contents (4.4 and 5.1 wt%) than the other clinopyroxenes. They have similar CaO (21.0 and 22.2 wt%) and Na_2O (1.2 and 1.8 wt%) contents to the peridotitic and other pyroxenitic clinopyroxenes. They have high TiO_2 contents (0.6 wt%), and similar Cr_2O_3 contents (0.2 and 0.3 wt%) to the recrystallized garnet-clinopyroxenes.

The websteritic orthopyroxenes are Fe-rich (Mg#'s 74.6 and 81.0). Cr_2O_3 contents are low (0.9 and 0.13 wt%), whereas the Al_2O_3 contents are high (1.7 and 2.0 wt%). The CaO content is also low (0.2 and 0.4 wt%). MIS438 has a high TiO_2 content (0.2 wt%).

Clinopyroxenites

The clinopyroxenites may be divided into two subgroups types based on texture, and the Al_2O_3 content in clinopyroxene.

The clinopyroxenitic garnets are all more Fe-rich than the peridotitic garnets (Mg#'s 59.5 to 81.0). The garnets within the sample MIS428 (contains exsolved orthopyroxene) are more Fe-rich than those samples only with exsolved garnet, whereas PGN320 and PGN322 are more Mg-rich. The garnets have low TiO_2 contents (<0.15 wt%). The clinopyroxenitic garnets have a small range in CaO content (4.2-6.1 wt%), apart from PGN320 and PGN322 (10.0 wt% CaO) figure 5.3. The garnets have low Cr_2O_3 contents (<2.3 wt%) apart from ARN028 (4.17 wt%). ARN028 has compositional (high Mg#), and petrographic affinities with the pyroxenitic suite, and has therefore been included in the pyroxenite suite.

The clinopyroxenes of samples ARN028, ARN031 and MIS428 (with recrystallized textured) have similar Mg#'s to the lherzolite suite clinopyroxenes, 89.7-92.4 (figure 5.12). They continue the trends of the lherzolite suite clinopyroxenes to lower Cr_2O_3 (0.1-0.4 wt%), Al_2O_3 (0.4-1.2 wt%) and Na_2O (0.4-0.5 wt%) contents, and higher CaO (22.0-23.8 wt%) contents. The clinopyroxenes of the coarse equant textured clinopyroxenites do not act as one coherent group. Two of the five samples (PGN319 and MIS451) have clinopyroxenes with low Cr_2O_3 contents (0.2-0.3 wt%), whereas the remaining three samples (MIS454, PGN320, PGN322) have a higher Cr_2O_3 content (1.2-1.4 wt%). The clinopyroxene in PGN319 has a much lower Mg# (83.3) and CaO content (19.3) than the other clinopyroxenes (Mg# 92.9 to 94.4; 20.9-22.3 wt% CaO). The clinopyroxenes have a similar Al_2O_3 (2.9-4.3 wt%) and Na_2O contents (1.6-2.4 wt%). The clinopyroxenes in the two samples that equilibrated with high-Ca garnets (~10wt%) have slightly higher Al_2O_3 and Cr_2O_3 contents than those of the other coarse equant garnet-clinopyroxenites.

Only one of the three recrystallized garnet-clinopyroxene samples contains orthopyroxene (MIS428). This orthopyroxene is Fe-rich (Mg# 85.8), with low Al_2O_3, Cr_2O_3 and CaO contents (0.56 wt%, 0.15 wt% and 0.2 wt% respectively).

* Figure 5.39 (page 5.37) is a schematic summary of the main chemical differences of the xenolith suites as described in the preceding sections.

Table 5.2 Selected major element mineral compositions - Harzburgitic garnets

	Low-Ca Harzburgitic garnets							High-Ca Harzburgitic garnets					
Sample No.	ARN007	ARN008	ARN019	ARN025	ARN026	MIS401	PGN340	ARN003	ARN005	ARN006	MIS413	MIS417	PGN311
SiO_2	41.36	42.18	42.33	41.59	42.28	41.27	41.83	40.93	40.64	41.20	39.74	41.02	41.77
TiO_2	<0.04*	<0.04	0.07	<0.04	0.04	<0.04	<0.04	<0.04	<0.04	<0.04	<0.04	<0.04	<0.04
Al_2O_3	18.20	20.11	19.63	18.97	20.96	18.11	18.44	17.94	18.13	19.70	16.67	19.52	20.43
Cr_2O_3	7.12	4.91	5.86	7.26	4.70	8.21	8.01	8.02	7.70	5.50	8.92	5.59	3.79
FeO	6.99	7.78	7.72	7.07	7.36	7.42	7.31	7.06	7.38	8.22	11.83	8.42	7.65
MnO	0.42	0.43	0.44	0.42	0.40	0.50	0.47	0.48	0.42	0.58	0.71	0.52	0.30
MgO	22.63	22.47	20.23	20.95	20.49	22.91	21.28	19.19	18.27	18.92	15.79	17.87	20.12
CaO	2.96	1.35	3.28	3.49	3.96	1.10	2.36	6.60	6.89	5.92	6.13	6.97	5.16
Na_2O	0.04	0.03	ND	0.04	0.02	0.04	ND	0.04	0.02	0.04	0.02	0.02	0.04
Total	**99.73**	**99.27**	**99.72**	**99.79**	**100.21**	**99.56**	**99.83**	**100.27**	**99.45**	**100.09**	**99.80**	**99.93**	**99.26**
Atomic Proportions based on 12 Oxygens													
Si	2.981	3.020	3.040	2.996	3.010	2.978	3.012	2.975	2.981	2.983	2.978	2.987	3.013
Ti	0.001	0.000	0.004	0.000	0.002	0.000	0.000	0.000	0.000	0.000	0.000	0.000	0.000
Al	1.546	1.697	1.662	1.610	1.759	1.540	1.565	1.536	1.567	1.681	1.472	1.675	1.736
Cr	0.406	0.278	0.333	0.413	0.265	0.468	0.456	0.461	0.446	0.315	0.528	0.322	0.216
Fe	0.421	0.466	0.463	0.426	0.438	0.448	0.440	0.429	0.453	0.498	0.741	0.513	0.462
Mn	0.026	0.026	0.027	0.026	0.024	0.031	0.029	0.030	0.026	0.035	0.045	0.032	0.018
Mg	2.432	2.399	2.167	2.250	2.175	2.464	2.284	2.079	1.997	2.043	1.764	1.940	2.164
Ca	0.228	0.103	0.252	0.269	0.302	0.085	0.182	0.514	0.541	0.460	0.492	0.544	0.399
Na	0.005	0.005	0.022	0.006	0.003	0.006	0.018	0.008	0.003	0.006	0.003	0.003	0.005
Total	**8.045**	**7.994**	**7.969**	**7.995**	**7.977**	**8.020**	**7.987**	**8.031**	**8.014**	**8.021**	**8.023**	**8.016**	**8.013**
Mg#	85.23	83.74	82.38	84.09	83.22	84.62	83.84	82.90	81.53	80.41	70.42	79.08	82.42
Al/Cr ratio	3.81	6.10	4.99	3.90	6.65	3.29	3.43	3.33	3.51	5.34	2.79	5.20	8.02
# Analyses	7	9	4	11	5	4	4	4	5	5	9	12	7

* <LLD

Table 5.2 continued: Selected major element mineral compositions - Lherzolitic and Pyroxenitic garnets

	Lherzolite						Clinopyroxenite						Websterite	
Sample No.	MIS409	PGN310	PGN329	PGN336	PGN337	PGN338	ARN028	ARN031	MIS428	MIS454	PGN319	PGN322	MIS438	MIS439
SiO_2	41.68	41.19	41.49	40.84	42.28	41.01	40.59	41.56	40.46	42.15	39.95	40.94	38.91	39.30
TiO_2	<0.04	0.11	0.86	0.17	0.62	0.04	0.11	0.05	0.05	0.13	<0.04	<0.04	0.08	0.06
Al_2O_3	21.24	18.26	19.52	16.75	20.77	15.17	19.67	22.21	21.02	22.35	22.34	22.96	22.26	22.44
Cr_2O_3	3.64	7.19	4.45	8.99	3.39	11.73	4.17	1.72	2.04	2.03	0.65	2.13	0.44	0.27
FeO	8.16	7.26	8.10	7.54	8.50	6.80	12.66	10.04	16.58	9.15	18.26	8.39	22.03	18.73
MnO	0.41	0.39	0.38	0.38	0.35	0.42	0.48	0.41	0.78	0.41	0.36	0.14	0.51	0.50
MgO	19.36	19.41	19.70	18.10	19.47	17.28	16.38	19.30	13.70	19.05	14.53	16.14	10.25	12.67
CaO	5.17	5.56	5.33	6.92	4.92	7.10	6.09	4.84	6.00	4.68	4.29	10.00	5.66	5.39
Na_2O	0.02	ND	0.05	ND	ND	ND	0.02	0.02	0.02	0.03	0.03	0.02	0.02	0.02
Total	**99.68**	**99.49**	**99.87**	**99.82**	**100.48**	**99.68**	**100.18**	**100.16**	**100.64**	**99.98**	**100.42**	**100.70**	**100.14**	**99.38**
Atomic Proportions based on 12 Oxygens														
Si	2.998	3.000	2.994	3.000	3.018	3.032	2.988	2.982	2.998	3.014	2.959	2.944	2.955	2.958
Ti	0.000	0.006	0.047	0.009	0.033	0.002	0.006	0.003	0.003	0.007	0.000	0.000	0.004	0.003
Al	1.801	1.567	1.660	1.450	1.747	1.321	1.706	1.878	1.835	1.883	1.950	1.945	1.992	1.990
Cr	0.207	0.414	0.254	0.522	0.191	0.685	0.243	0.098	0.120	0.115	0.038	0.121	0.026	0.016
Fe	0.491	0.442	0.489	0.463	0.507	0.421	0.779	0.603	1.027	0.547	1.131	0.504	1.399	1.179
Mn	0.025	0.024	0.023	0.023	0.021	0.026	0.030	0.025	0.049	0.025	0.023	0.008	0.033	0.032
Mg	2.077	2.108	2.119	1.982	2.072	1.904	1.798	2.065	1.513	2.030	1.604	1.730	1.161	1.421
Ca	0.399	0.434	0.412	0.544	0.377	0.562	0.481	0.372	0.476	0.358	0.340	0.770	0.460	0.435
Na	0.003	0.017	0.007	0.021	0.025	0.019	0.002	0.002	0.002	0.004	0.005	0.001	0.000	0.004
Total	**7.999**	**8.012**	**8.005**	**8.015**	**7.992**	**7.973**	**8.033**	**8.028**	**8.023**	**7.983**	**8.050**	**8.024**	**8.031**	**8.038**
Mg#	80.89	82.65	81.25	81.06	80.33	81.90	69.76	77.40	59.57	78.77	58.65	77.42	45.35	54.67
Al/Cr ratio	8.70	3.79	6.53	2.78	9.14	1.93	7.03	19.22	15.32	16.41	51.52	16.08	75.84	122.24
# Analyses	5	7	5	4	4	4	8	7	4	3	5	4	3	4

Table 5.3 Selected major element mineral compositions - Harzburgitic and Lherzolitic olivines

	Low-Ca Harzburgite						High-Ca Harzburgite						Lherzolite			
Sample No	ARN007	ARN008	ARN025	ARN026	MIS408	PGN340	ARN003	ARN005	ARN006	MIS413	MIS417	PGN315	ARN034	MIS426	PGN310	PGN336
SiO_2	40.51	41.18	40.29	40.98	40.56	41.46	40.55	41.40	41.28	40.17	40.98	40.10	40.24	41.35	39.48	40.81
TiO_2	<0.04	<0.04	<0.04	<0.04	<0.04	<0.04	<0.04	<0.04	<0.04	<0.04	<0.04	<0.04	<0.04	<0.04	<0.04	<0.04
Al_2O_3	0.03	0.04	<0.03	<0.03	<0.03	<0.03	<0.03	<0.03	0.03	0.03	<0.03	<0.03	<0.03	<0.03	<0.03	0.03
Cr_2O_3	0.05	0.06	0.03	<0.04	0.04	0.05	0.04	0.05	<0.04	<0.04	<0.04	<0.04	<0.04	<0.04	0.13	0.07
FeO	7.38	6.93	7.15	7.34	7.12	7.75	7.54	7.91	7.69	11.98	6.97	7.02	7.70	7.38	7.72	9.39
MnO	0.11	0.11	0.11	0.07	0.10	0.13	0.12	0.09	0.11	0.15	0.08	0.08	0.10	0.07	0.09	0.15
MgO	50.79	51.07	51.38	50.36	51.46	51.15	50.10	50.20	50.34	46.52	50.78	52.17	51.95	50.55	50.98	49.93
CaO	<0.03	<0.03	<0.03	<0.03	<0.03	<0.03	<0.03	<0.03	<0.03	0.04	0.06	<0.03	<0.03	<0.03	0.03	0.04
NiO	0.35	0.42	0.37	0.35	0.32	0.36	0.38	0.42	0.38	0.30	0.42	0.41	0.31	0.27	0.46	0.41
Total	**99.23**	**99.83**	**99.37**	**99.12**	**99.65**	**100.92**	**98.76**	**100.11**	**99.86**	**99.21**	**99.32**	**99.80**	**100.38**	**99.67**	**98.90**	**100.85**
Atomic Proportions based on 4 Oxygens																
Si	0.992	0.999	0.985	1.002	0.988	0.998	0.998	1.005	1.004	1.003	0.999	0.976	0.977	1.005	0.975	0.992
Ti	0.000	0.000	0.000	0.000	0.000	0.000	0.000	0.000	0.000	0.000	0.000	0.000	0.000	0.000	0.000	0.000
Al	0.001	0.001	0.000	0.000	0.001	0.001	0.001	0.000	0.001	0.001	0.000	0.000	0.000	0.000	0.000	0.001
Cr	0.001	0.001	0.001	0.000	0.001	0.001	0.001	0.001	0.000	0.000	0.000	0.000	0.001	0.001	0.003	0.001
Fe	0.151	0.141	0.146	0.150	0.145	0.156	0.155	0.161	0.156	0.250	0.142	0.143	0.156	0.150	0.159	0.191
Mn	0.002	0.002	0.002	0.001	0.002	0.003	0.002	0.002	0.002	0.003	0.002	0.002	0.002	0.001	0.002	0.003
Mg	1.853	1.847	1.873	1.836	1.868	1.836	1.837	1.817	1.825	1.732	1.846	1.894	1.880	1.832	1.876	1.809
Ca	0.001	0.000	0.001	0.000	0.001	0.000	0.000	0.000	0.000	0.001	0.002	0.000	0.000	0.000	0.001	0.001
Ni	0.007	0.008	0.007	0.007	0.006	0.007	0.008	0.008	0.007	0.006	0.008	0.008	0.006	0.005	0.009	0.008
Total	**3.007**	**3.000**	**3.015**	**2.998**	**3.011**	**3.001**	**3.002**	**2.994**	**2.996**	**2.996**	**3.000**	**3.023**	**3.023**	**2.994**	**3.024**	**3.007**
Mg#	92.47	92.93	92.76	92.44	92.80	92.17	92.22	91.88	92.11	87.38	92.85	92.99	92.32	92.43	92.17	90.46
Fo	92.47	92.93	92.76	92.44	92.80	92.17	92.22	91.88	92.11	87.38	92.85	92.99	92.32	92.43	92.17	90.46
Fa	7.53	7.07	7.24	7.56	7.20	7.83	7.78	8.12	7.89	12.62	7.15	7.01	7.68	7.57	7.83	9.54
# Analyses	3	3	5	3	2	2	3	2	2	2	5	3	2	2	3	2

Table 5.4 Selected major element mineral compositions - Peridotitic chromites and Cr-spinels

	Low-Ca Harzburgite					High-Ca Harzburgite				Lherzolite			
Sample No	ARN007	ARN017	ARN019	ARN019	ARN025	ARN006	ARN009	MIS413	MIS417	MIS409	MIS409	MIS426	PGN333
SiO_2	0.03	0.07	0.00	0.00	0.04	0.02	0.06	0.09	0.00	0.02	0.03	0.00	0.07
TiO_2	0.07	0.07	0.62	0.55	<0.05	<0.05	0.25	1.02	0.05	0.29	0.27	0.54	0.25
Al_2O_3	8.20	7.50	9.96	10.03	7.33	10.55	6.41	10.41	11.68	21.29	24.30	17.00	7.68
Cr_2O_3	61.87	61.77	58.95	57.88	61.23	58.93	61.10	52.50	57.10	45.17	42.05	49.75	60.17
FeO	12.73	13.67	15.22	14.77	13.52	14.97	13.68	15.97	14.95	14.09	12.75	17.00	15.00
Fe_2O_3	3.17	3.42	2.46	3.19	4.29	3.14	5.10	6.86	3.99	3.93	4.73	4.28	5.03
MnO	0.29	0.27	0.30	0.21	0.33	0.40	0.33	0.38	0.39	0.17	0.13	0.22	0.31
MgO	13.28	12.58	12.13	12.30	12.53	12.02	12.55	11.85	12.25	13.74	15.08	11.90	12.05
CaO	<0.02	<0.02	<0.02	<0.02	0.02	<0.02	<0.02	<0.02	<0.02	<0.02	<0.02	0.02	0.02
Total	**99.65**	**99.35**	**99.65**	**98.93**	**99.30**	**100.02**	**99.48**	**99.08**	**100.42**	**98.69**	**99.35**	**100.71**	**100.58**
Atomic Proportions based on 4 Oxygens													
Si	0.001	0.002	0.000	0.000	0.001	0.001	0.002	0.003	0.000	0.001	0.001	0.000	0.002
Ti	0.002	0.002	0.015	0.014	0.000	0.000	0.006	0.026	0.001	0.007	0.006	0.013	0.006
Al	0.319	0.295	0.387	0.392	0.290	0.409	0.255	0.413	0.449	0.790	0.881	0.640	0.302
Cr	1.615	1.631	1.536	1.519	1.625	1.531	1.630	1.396	1.474	1.124	1.022	1.256	1.585
Fe^{2+}	0.352	0.382	0.419	0.410	0.379	0.411	0.386	0.449	0.408	0.371	0.328	0.454	0.418
Fe^{3+}	0.079	0.086	0.061	0.080	0.108	0.078	0.129	0.174	0.098	0.093	0.109	0.103	0.126
Mn	0.008	0.008	0.008	0.006	0.010	0.011	0.009	0.011	0.011	0.004	0.003	0.006	0.009
Mg	0.654	0.626	0.596	0.609	0.627	0.589	0.632	0.595	0.596	0.645	0.691	0.567	0.599
Ca	0.000	0.000	0.000	0.000	0.001	0.000	0.000	0.000	0.000	0.000	0.000	0.001	0.001
Total	**3.030**	**3.033**	**3.023**	**3.030**	**3.041**	**3.029**	**3.049**	**3.067**	**3.037**	**3.035**	**3.042**	**3.039**	**3.048**
Mg#	60.31	57.24	55.36	55.42	56.24	54.64	55.06	48.84	54.08	58.14	61.25	50.43	52.37
Cr#	83.50	84.68	79.88	79.47	84.85	78.94	86.48	77.19	76.63	58.74	53.72	66.25	84.02
# Analyses	1	1	1	1	1	1	1	1	1	1	1	1	1
Type	Primary	Primary	Exsolved	Needle in Exsolved Opx		Exsolved	Primary	Secondary	Exsolved	Primary adjacent pyx	- Primary within gt	- Primary	Primary

Table 5.5 Selected major element mineral compositions - Harzburgitic and Lherzolitic orthopyroxene (Pyroxenitic orthopyroxenes continue on following page).

	Low-Ca Harzburgite					High-Ca Harzburgite				Lherzolite				
Sample No	ARN008	ARN019	ARN025	MIS401	PGN340	ARN005	MIS413	MIS417	PGN311	MIS409	MIS426	PGN310	PGN329	PGN338
SiO_2	57.78	58.37	57.52	58.67	57.91	57.58	56.85	57.52	56.75	57.47	58.61	57.95	57.37	58.73
TiO_2	<0.04	<0.04	<0.04	<0.04	<0.04	<0.04	<0.04	<0.04	<0.04	<0.04	0.05	0.05	0.13	<0.04
Al_2O_3	0.61	0.53	0.59	0.48	0.45	0.60	0.28	0.43	0.63	0.88	0.74	0.57	0.63	0.44
Cr_2O_3	0.28	0.26	0.40	0.34	0.24	0.34	0.16	0.10	0.18	0.30	0.30	0.32	0.21	0.41
FeO	4.18	4.14	4.34	4.36	4.24	4.47	7.23	4.57	5.55	4.43	4.47	4.71	5.77	4.46
MnO	0.10	0.10	0.12	0.13	0.11	0.12	0.19	0.12	0.12	0.09	0.07	0.10	0.12	0.11
MgO	36.83	36.52	36.94	36.22	36.98	35.48	34.88	36.55	35.08	36.36	35.52	35.77	35.09	35.86
CaO	0.12	0.17	0.24	0.07	0.15	0.33	0.05	<0.05	0.93	0.14	0.19	0.52	0.85	0.50
Na_2O	0.09	0.08	0.13	0.07	0.01	0.03	0.04	0.03	0.13	0.03	0.02	0.14	0.15	0.11
Total	**100.25**	**100.20**	**100.30**	**100.36**	**100.11**	**99.16**	**99.84**	**99.52**	**99.38**	**99.80**	**100.00**	**100.14**	**100.34**	**100.64**
Atomic Proportions based on 6 Oxygens														
Si	1.972	1.987	1.964	1.994	1.976	1.987	1.975	1.979	1.968	1.970	1.999	1.982	1.972	1.995
Ti	0.000	0.001	0.000	0.000	0.000	0.000	0.000	0.000	0.000	0.000	0.001	0.001	0.003	0.000
Al	0.025	0.021	0.024	0.019	0.018	0.024	0.011	0.017	0.026	0.036	0.030	0.023	0.025	0.018
Cr	0.007	0.007	0.011	0.009	0.007	0.009	0.004	0.003	0.005	0.008	0.008	0.009	0.006	0.011
Fe	0.119	0.118	0.124	0.124	0.121	0.129	0.210	0.132	0.161	0.127	0.128	0.135	0.166	0.127
Mn	0.003	0.003	0.003	0.004	0.003	0.003	0.005	0.003	0.003	0.003	0.002	0.003	0.004	0.003
Mg	1.874	1.853	1.880	1.835	1.881	1.825	1.807	1.875	1.814	1.858	1.806	1.824	1.798	1.816
Ca	0.004	0.006	0.009	0.003	0.005	0.012	0.002	0.000	0.034	0.005	0.007	0.019	0.031	0.018
Na	0.006	0.005	0.008	0.005	0.000	0.002	0.003	0.002	0.009	0.002	0.001	0.009	0.010	0.007
Total	**4.021**	**4.001**	**4.023**	**3.993**	**4.012**	**4.001**	**4.018**	**4.012**	**4.021**	**4.009**	**3.982**	**4.005**	**4.015**	**3.995**
Mg#	94.01	94.02	93.81	93.68	93.95	93.40	89.58	93.44	91.86	93.61	93.40	93.12	91.56	93.48
Ca#	0.23	0.33	0.46	0.15	0.29	0.67	0.10	0.00	1.86	0.27	0.38	1.03	1.71	0.99
# Analyses	4	2	4	4	4	5	4	4	4	7	2	3	2	2
En	0.94	0.93	0.94	0.92	0.94	0.91	0.90	0.94	0.91	0.93	0.90	0.91	0.90	0.91
Fs	0.06	0.06	0.06	0.06	0.06	0.06	0.11	0.07	0.08	0.06	0.06	0.07	0.08	0.06

Table 5.5 cont. Pyroxenitic Orthopyroxene.

	Clino-pyroxenite	Websterite	
Sample #	MIS428	MIS438	MIS439
SiO_2	57.27	54.46	55.54
TiO_2	0.06	0.21	0.05
Al_2O_3	0.56	1.71	2.02
Cr_2O_3	0.15	0.13	0.09
FeO	9.64	16.48	12.62
MnO	0.13	0.15	0.13
MgO	32.65	27.10	30.22
CaO	0.25	0.35	0.20
Na_2O	0.01	0.02	0.03
Total	**100.74**	**100.62**	**100.89**
Atomic Proportions based on 6 Oxygens			
Si	1.987	1.955	1.951
Ti	0.002	0.006	0.001
Al	0.023	0.072	0.084
Cr	0.004	0.004	0.002
Fe	0.280	0.495	0.371
Mn	0.004	0.004	0.004
Mg	1.689	1.451	1.583
Ca	0.009	0.014	0.008
Na	0.000	0.002	0.002
Total	**3.998**	**4.002**	**4.006**
Mg#	85.79	74.56	81.02
Ca#	0.54	0.93	0.48
# Anal*	3	3	2
En	0.84	0.73	0.79
Fs	0.14	0.25	0.19

Key:
*) # Anal. = Number of analyses
**) CaTs = Ca-Tschermacks

Table 5.6 Selected major element mineral compositions - Lherzolitic and Pyroxenitic clinopyroxene.

	Lherzolite (no garnet)	Lherzolite				Clinopyroxenite				Websterite
Sample #	ARN033	MIS409	MIS426	PGN310	PGN329	ARN028	MIS428	MIS454	PGN322	MIS438
SiO_2	54.45	54.14	54.17	54.50	54.67	53.81	53.92	54.36	52.99	52.16
TiO_2	0.17	<0.04	0.15	0.10	0.25	<0.04	0.07	0.28	0.12	0.60
Al_2O_3	1.35	3.42	3.80	1.89	1.70	0.44	1.21	3.35	4.32	4.41
Cr_2O_3	2.19	2.26	2.32	2.23	1.00	0.24	0.38	1.42	1.26	0.30
FeO	2.30	1.57	1.67	2.36	3.26	3.74	2.63	2.04	1.75	5.10
MnO	0.10	0.06	0.06	0.08	0.09	0.11	0.05	<0.06	<0.06	0.07
MgO	16.48	15.40	14.65	16.87	18.12	18.26	16.60	15.00	15.84	14.48
CaO	21.27	20.83	20.17	19.31	19.00	22.01	23.75	20.91	22.27	22.19
Na_2O	1.72	2.35	2.69	2.11	1.44	0.49	0.49	2.40	2.38	1.21
Total	**100.09**	**100.03**	**99.70**	**99.56**	**99.58**	**99.17**	**99.10**	**99.82**	**100.90**	**100.50**
Atomic Proportions based on 6 Oxygens										
Si	1.978	1.958	1.963	1.981	1.982	1.978	1.979	1.970	1.909	1.905
Ti	0.005	0.000	0.004	0.003	0.007	0.001	0.002	0.008	0.003	0.016
Al	0.058	0.146	0.162	0.081	0.073	0.019	0.053	0.143	0.184	0.190
Cr	0.063	0.064	0.066	0.064	0.029	0.007	0.011	0.041	0.036	0.009
Fe	0.070	0.047	0.051	0.072	0.099	0.115	0.081	0.062	0.053	0.156
Mn	0.003	0.002	0.002	0.002	0.003	0.003	0.002	0.002	0.000	0.002
Mg	0.892	0.830	0.792	0.914	0.980	1.001	0.908	0.810	0.851	0.788
Ca	0.828	0.807	0.783	0.752	0.738	0.867	0.934	0.812	0.860	0.869
Na	0.121	0.164	0.189	0.149	0.101	0.035	0.035	0.169	0.166	0.086
Total	**4.018**	**4.019**	**4.013**	**4.018**	**4.011**	**4.026**	**4.004**	**4.015**	**4.061**	**4.022**
Mg#	92.74	94.61	93.99	92.72	90.83	89.70	91.85	92.92	94.17	83.49
Ca#	48.12	49.29	49.73	45.13	42.97	46.41	50.70	50.05	50.26	52.42
# Anal.*	2	6	2	5	2	5	3	2	2	3
Wollastonite	0.405	0.382	0.375	0.368	0.364	0.423	0.458	0.395	0.386	0.395
Enstatite	0.446	0.415	0.396	0.457	0.490	0.500	0.454	0.405	0.425	0.394
Ferrosilite	0.035	0.024	0.025	0.036	0.049	0.057	0.040	0.031	0.026	0.078
Acmite	0.035	0.038	0.026	0.036	0.022	0.051	0.009	0.030	0.122	0.043
CaTs**	0.017	0.042	0.033	0.016	0.011	0.021	0.019	0.023	0.088	0.078
Jadeite	0.086	0.126	0.164	0.113	0.079	0.000	0.026	0.138	0.044	0.042

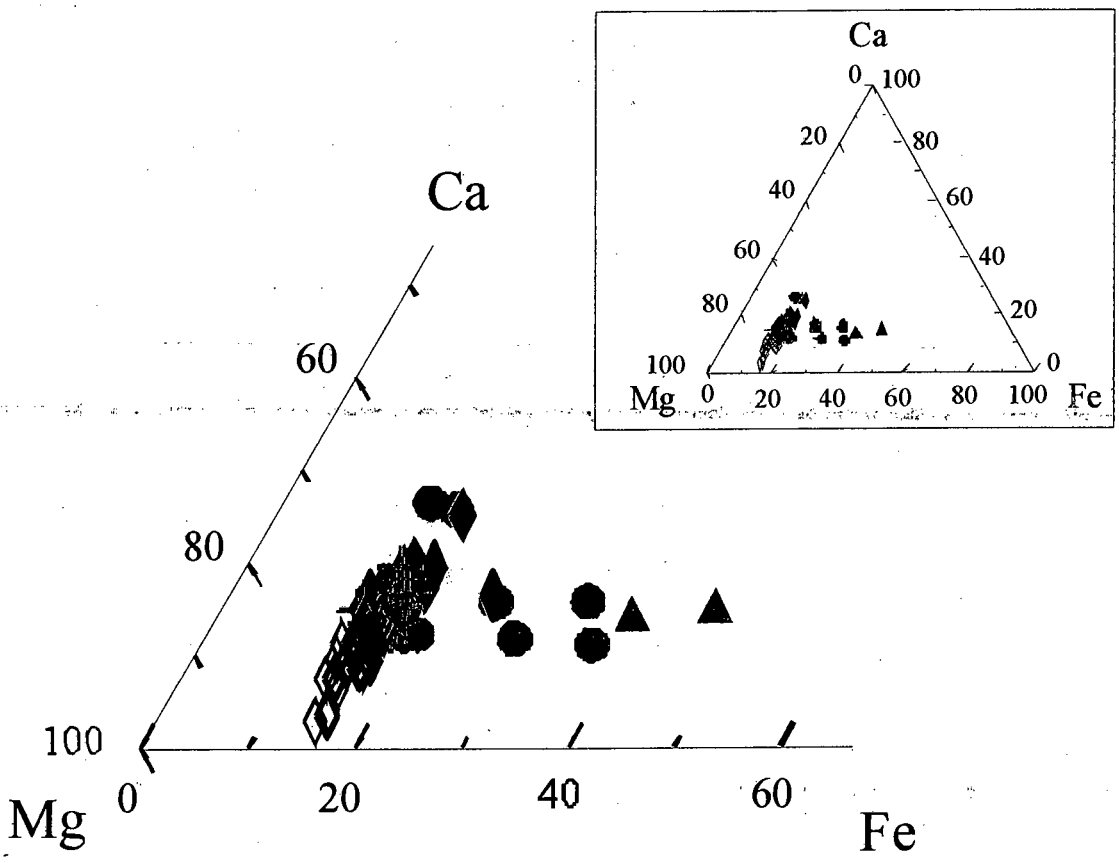

Figure 5.2 Ca, Mg and Fe compositions of xenolith garnets. The low-Ca harzburgites are more Mg-rich than the high-Ca harzburgitic and lherzolitic garnets. The clinopyroxenites and websterites are more Fe-rich than the peridotitic garnets.(Symbols as for figure 5.3)

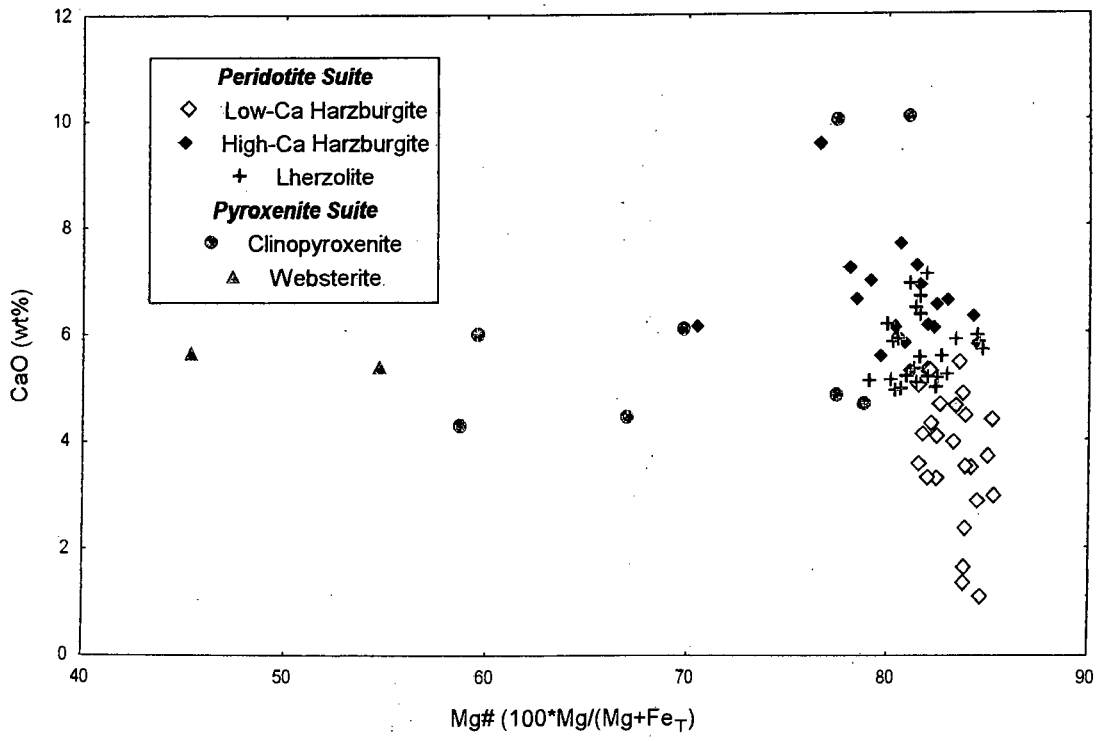

Figure 5.3 Mg# versus CaO in garnet. The peridotitic garnets have a small range in Mg# (76.5-85.3) in comparison to the pyroxenitic garnets (45.3-78.8), and mark a subtle negative relationship between the CaO content and Mg#. The garnet in MIS413 is more Fe-rich (Mg# 70.4) than the other peridotitic garnets. The clinopyroxenitic garnets have a narrow range in CaO content (4.2 - 6.1 wt%), apart from PGN320 and PGN322 (with 10 wt% CaO).

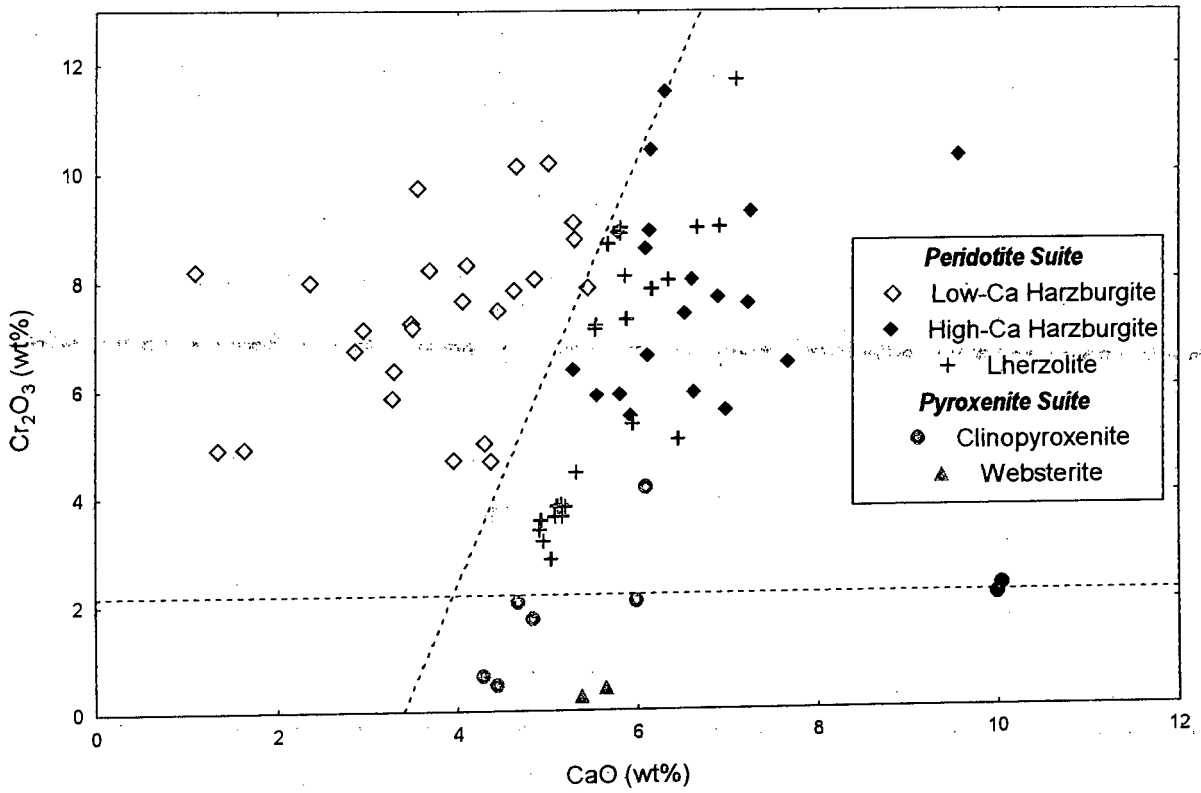

Figure 5.4 Cr_2O_3 vs CaO in garnet. The peridotitic garnets have >2 wt% Cr_2O_3, and the majority of the pyroxenitic garnets <2 wt% (ARN028 has 4.2 wt%). The 85% line of Gurney (1984) divides the harzburgitic suite into a low-Ca group and a high-Ca group. The lherzolitic garnets all plot in the high-Ca quadrant.

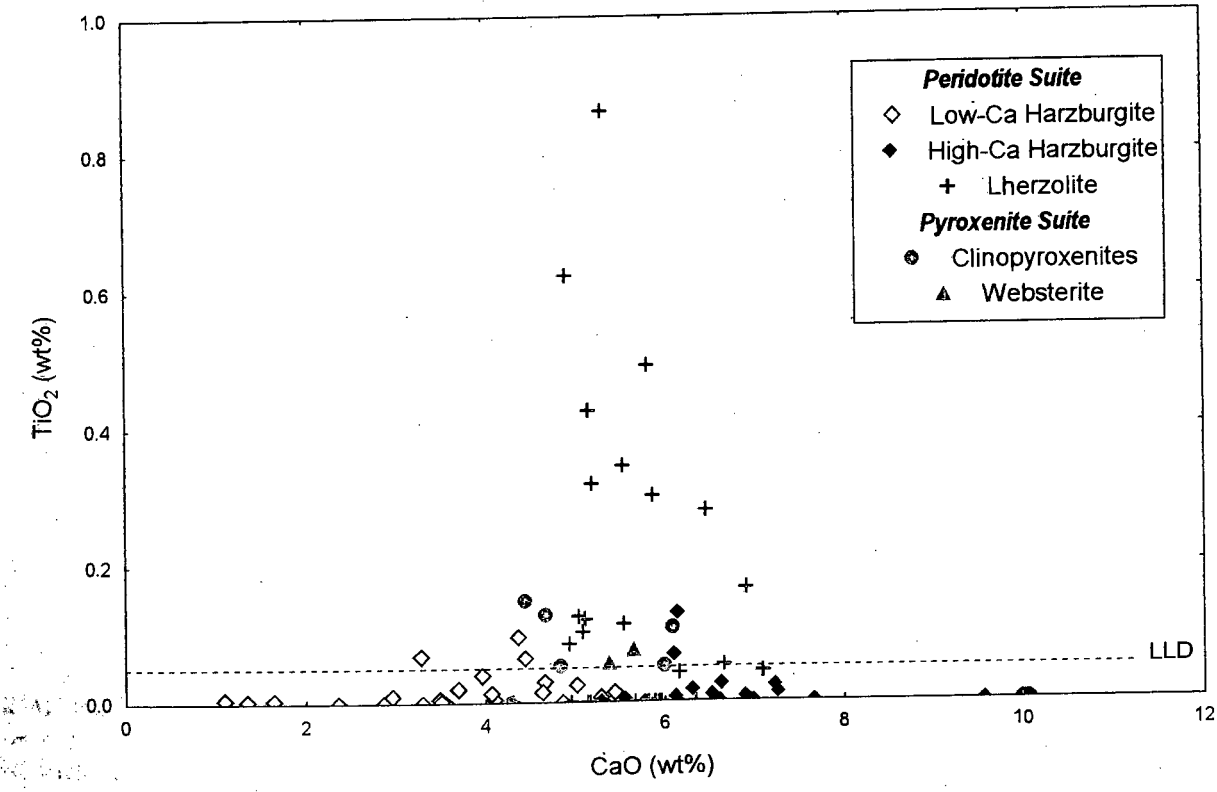

Figure 5.5 The low-Ca and high-Ca harzburgitic garnets all have low TiO_2 contents (<0.15 wt%). The lherzolitic garnets (4.9-7.0 wt% CaO) have high TiO_2 contents (0-0.9 wt%).

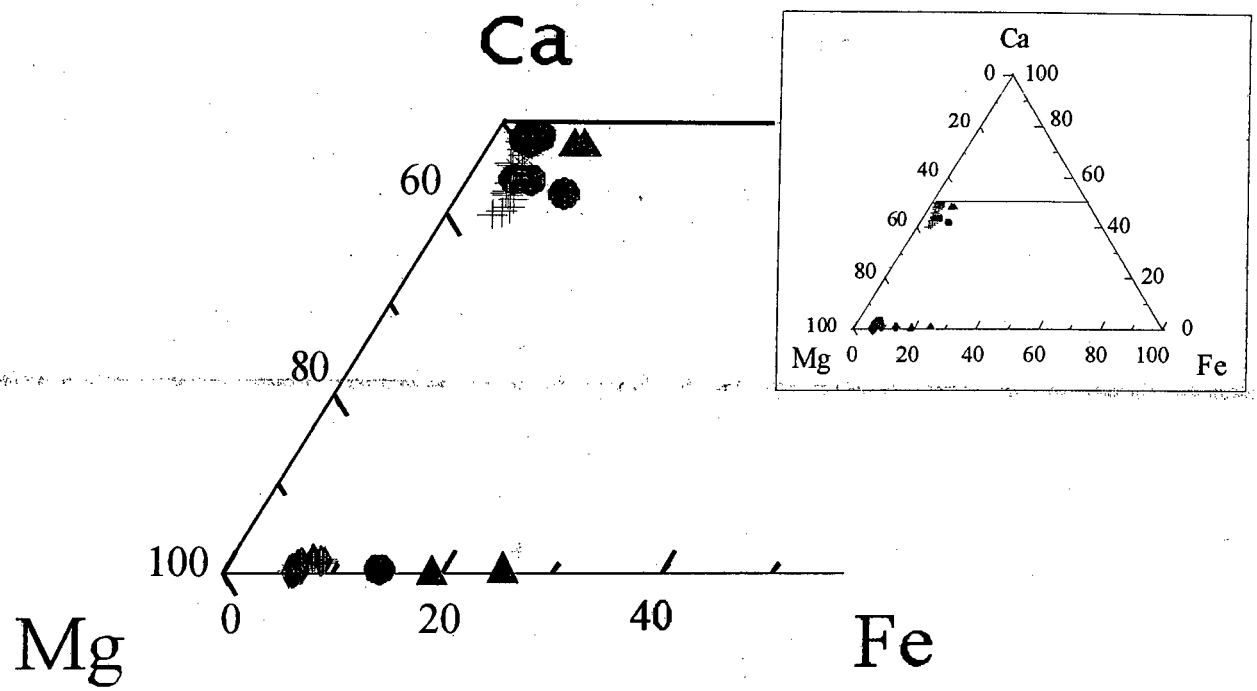

Figure 5.6 Ca, Mg, Fe compositions of orthopyroxene and clinopyroxene. (Symbols as for fig 5.3)

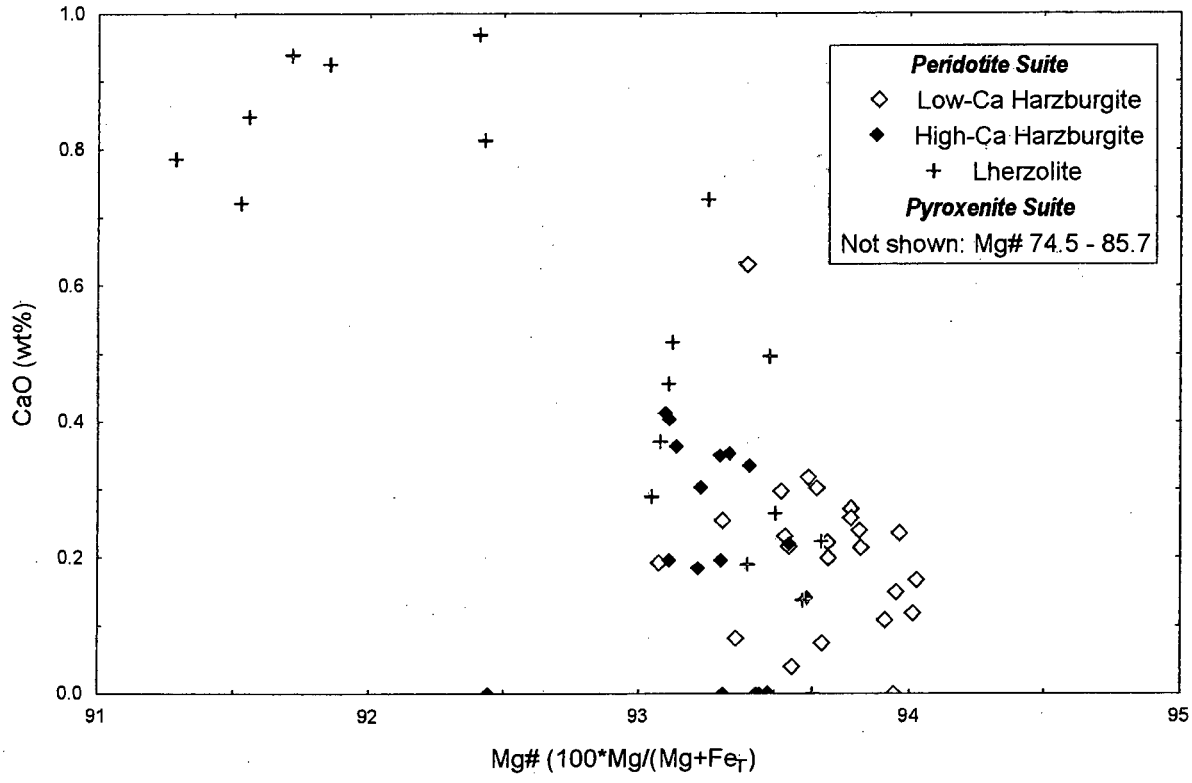

Figure 5.7 CaO vs Mg# in orthopyroxene. The harzburgitic orthopyroxenes have lower CaO contents than the lherzolitic orthopyroxenes (LLD-0.4 wt%, and LLD-1.0 wt% respectively). One harzburgitic orthopyroxene (MIS463) has a higher CaO content of 0.6 wt%. The lherzolitic orthopyroxenes (Mg# 91.2-93.7) are more Fe-rich than those of the harzburgitic suite (Mg# 93.0-94.0). The pyroxenitic orthopyroxenes (not shown) are more Fe-rich than the peridotitic orthopyroxenes (Mg# 74.5-85.7).

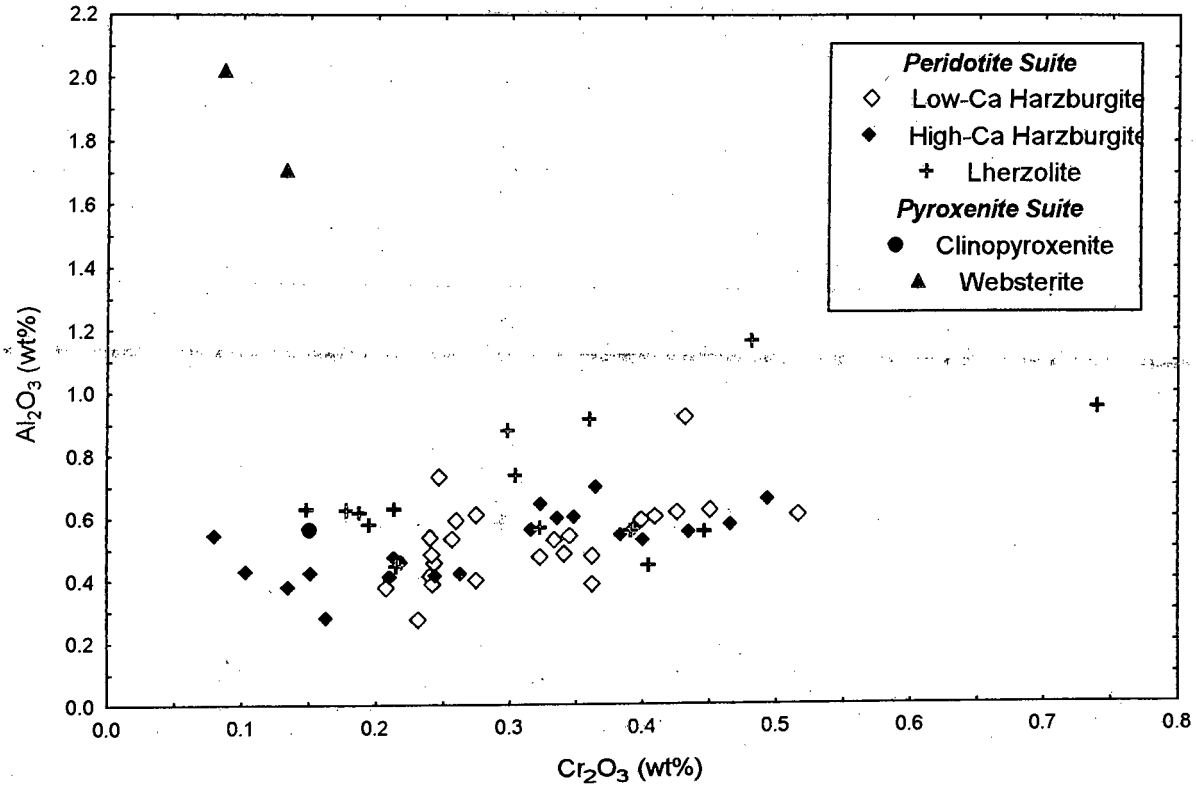

Figure 5.8 Al_2O_3 vs Cr_2O_3 in orthopyroxene. The websteritic orthopyroxenes have higher Al_2O_3 contents (1.7-2.0 wt%) than the peridotitic and clinopyroxenitic orthopyroxenes (0.2-1.2 wt%). The peridotitic orthopyroxenes define a rough positive relationship between Al_2O_3 and Cr_2O_3.

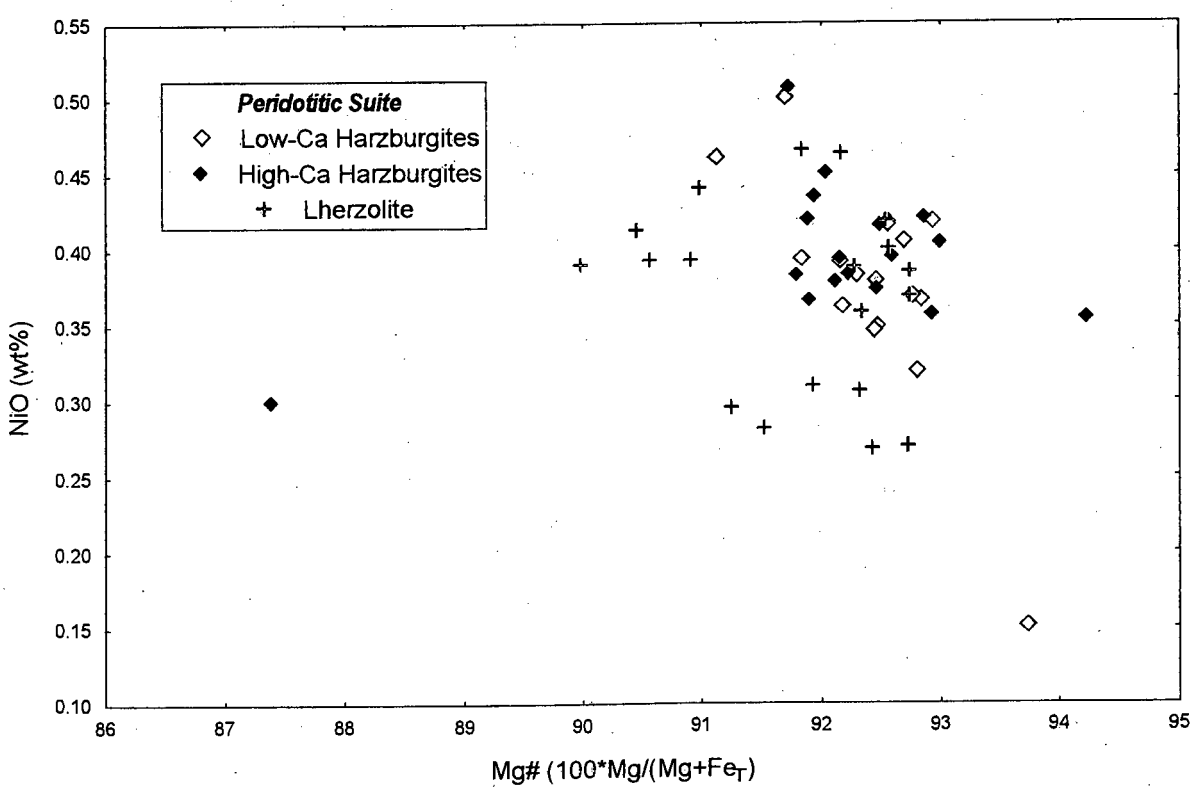

Figure 5.9 NiO vs Mg# in olivine. The majority of the olivines have Mg#'s 89.9 - 93.0. The three outliers are: MIS413 (Mg# 87.38), ARN030 (Mg# 94.22) and PGN301 (NiO 0.15, Mg# 93.7).

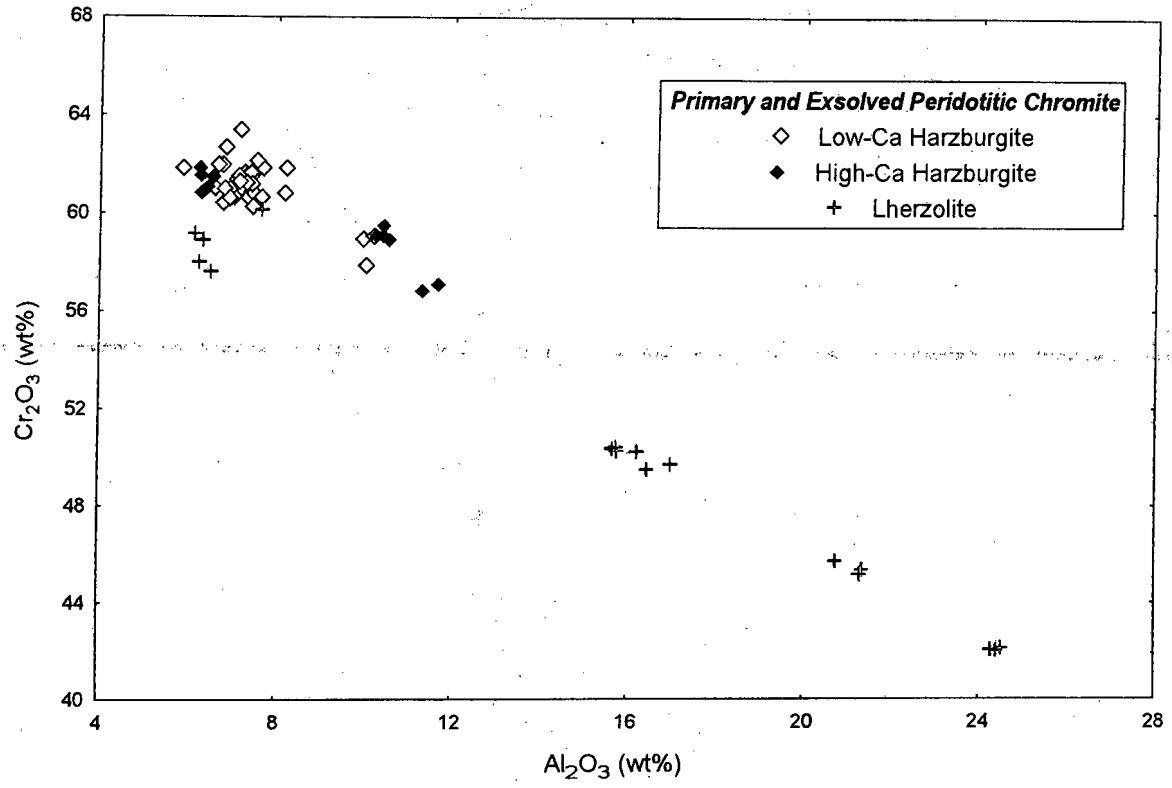

Figure 5.10 Cr_2O_3 vs Al_2O_3 in chromite. The harzburgitic chromites all have high Cr_2O_3 contents (58.6-63.4 wt%) and low Al_2O_3 contents (5.8-11.7 wt%). The lherzolitic chromites have a large range in Cr_2O_3 (42.0-59.2 wt%) and Al_2O_3 content (6.1-24.6 wt%).

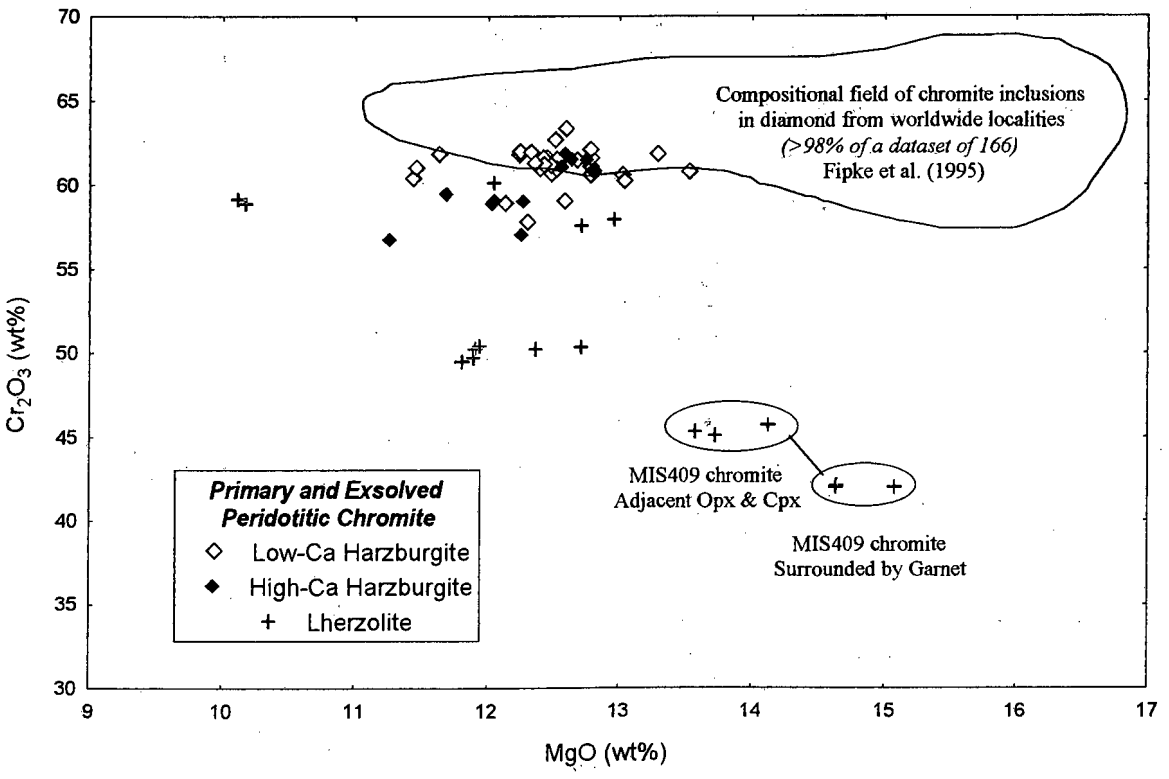

Figure 5.11 Cr_2O_3 vs MgO in chromite. The majority of the harzburgitic chromites plot within, or close to the compositional field for chromite inclusions in diamond. All the lherzolitic chromites plot outside this field, having lower Cr_2O_3 contents. The chromite grains in sample MIS409 situated adjacent pyroxene have a different chemistry to those grains totally enclosed by garnet.

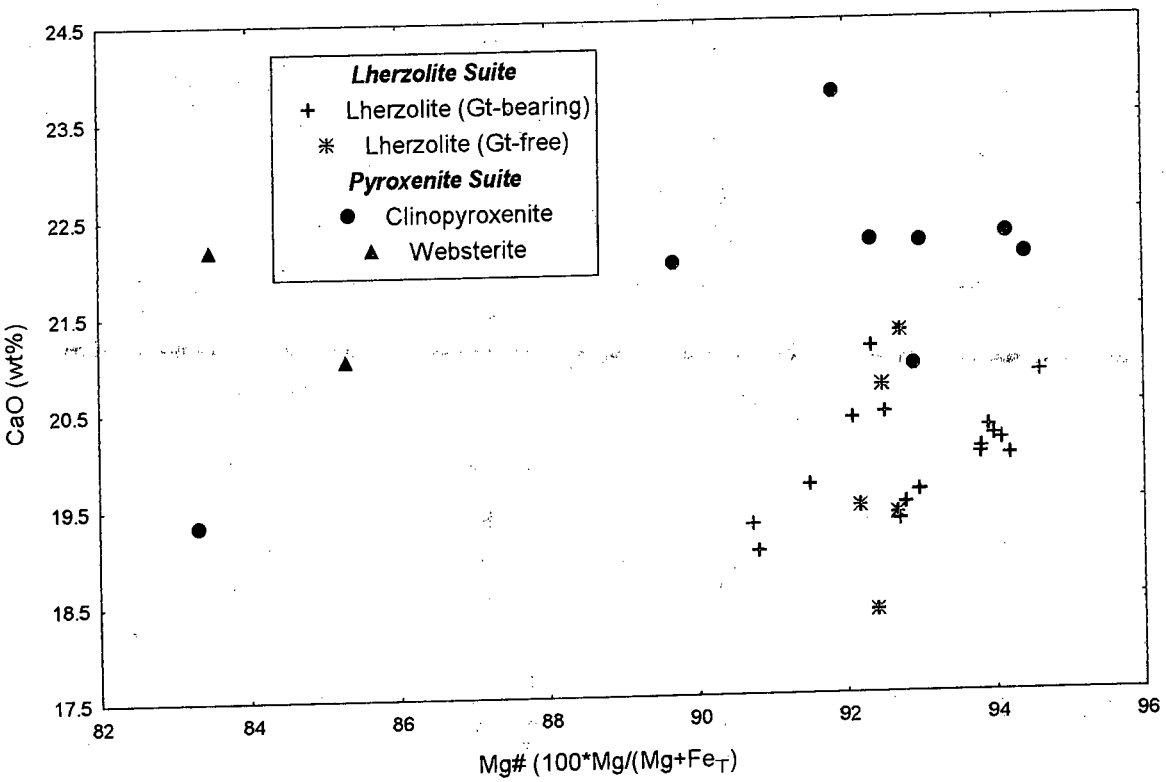

Figure 5.12 CaO vs Mg# in clinopyroxene. The lherzolitic clinopyroxenes have a small range in Mg# (90.7 - 94.6) compared to the pyroxenitic clinopyroxenes (Mg# 83.3-94.4). The clinopyroxene in PGN319 and the websterites (MIS438, MIS439) are more Fe-rich than the other samples.

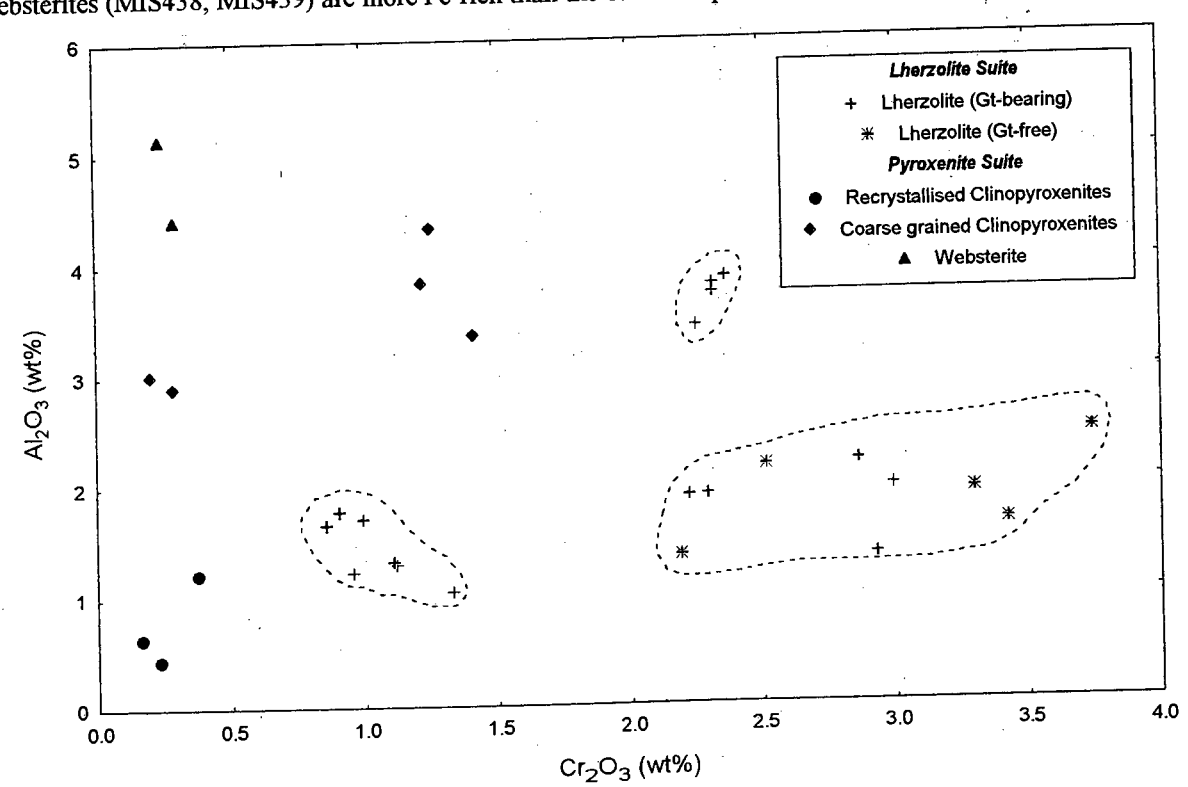

Figure 5.13 Al_2O_3 vs Cr_2O_3 in clinopyroxene. Three clusters are noted within the lherzolitic clinopyroxenes: a low Al_2O_3 and Cr_2O_3 cluster; a low Al_2O_3 and high Cr_2O_3 cluster (some of these samples contain no garnet); and a high Al_2O_3 and Cr_2O_3 cluster (all in equilibrium with primary chromite). The pyroxenitic clinopyroxenes generally have higher Al_2O_3, and lower Cr_2O_3 contents than those of the lherzolite suite.

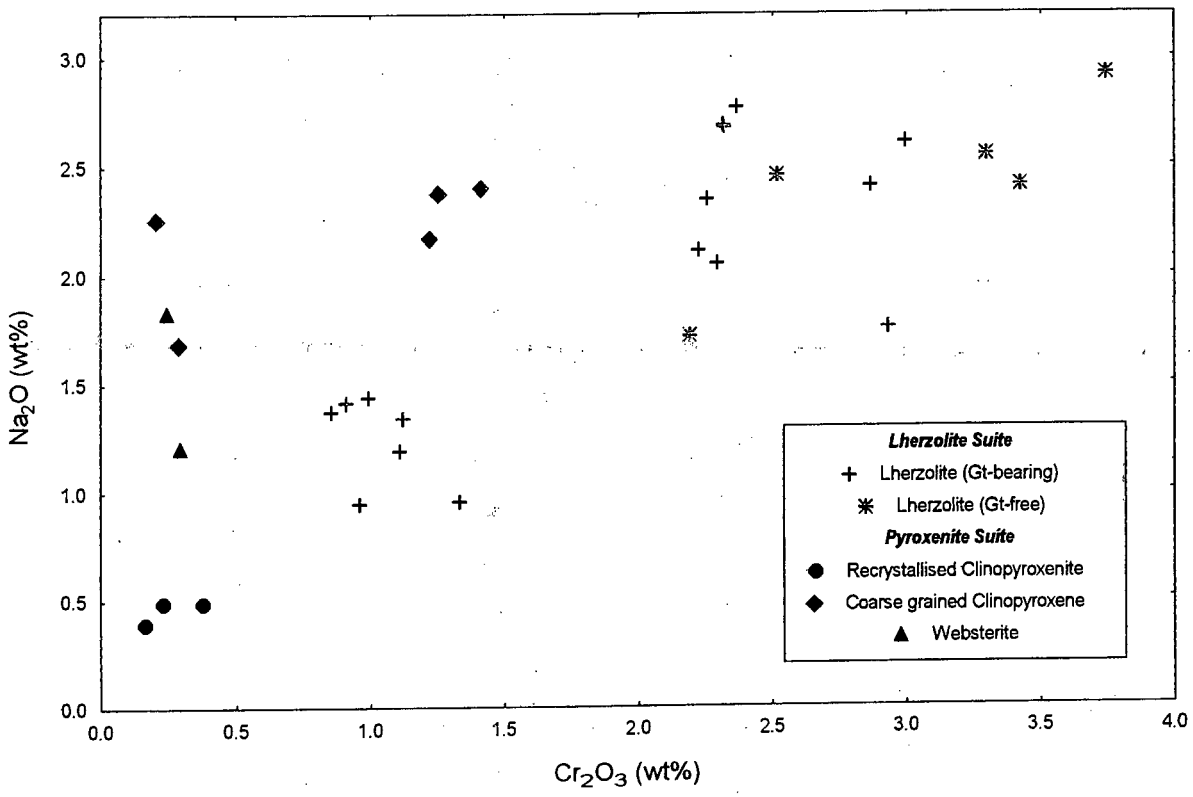

Figure 5.14 Cr_2O_3 vs Na_2O in clinopyroxene. The lherzolitic clinopyroxenes define a positive relationship between Cr_2O_3 and Na_2O.

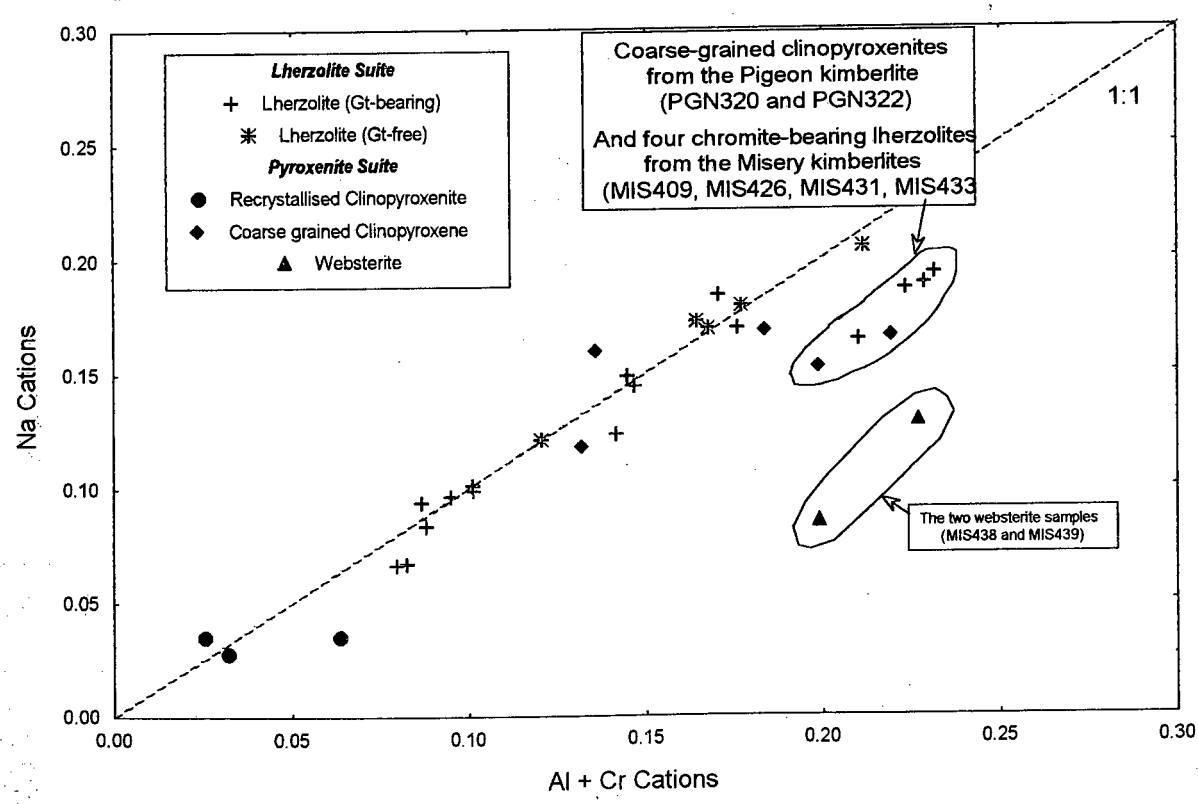

Figure 5.15 A coupled substitution of Na^{1+} with Al^{3+} or Cr^{3+} would be indicated by points lying on the 1:1 line. The clinopyroxenes in eight samples indicated by the fields above are enriched in Cr and Al relative to Na.

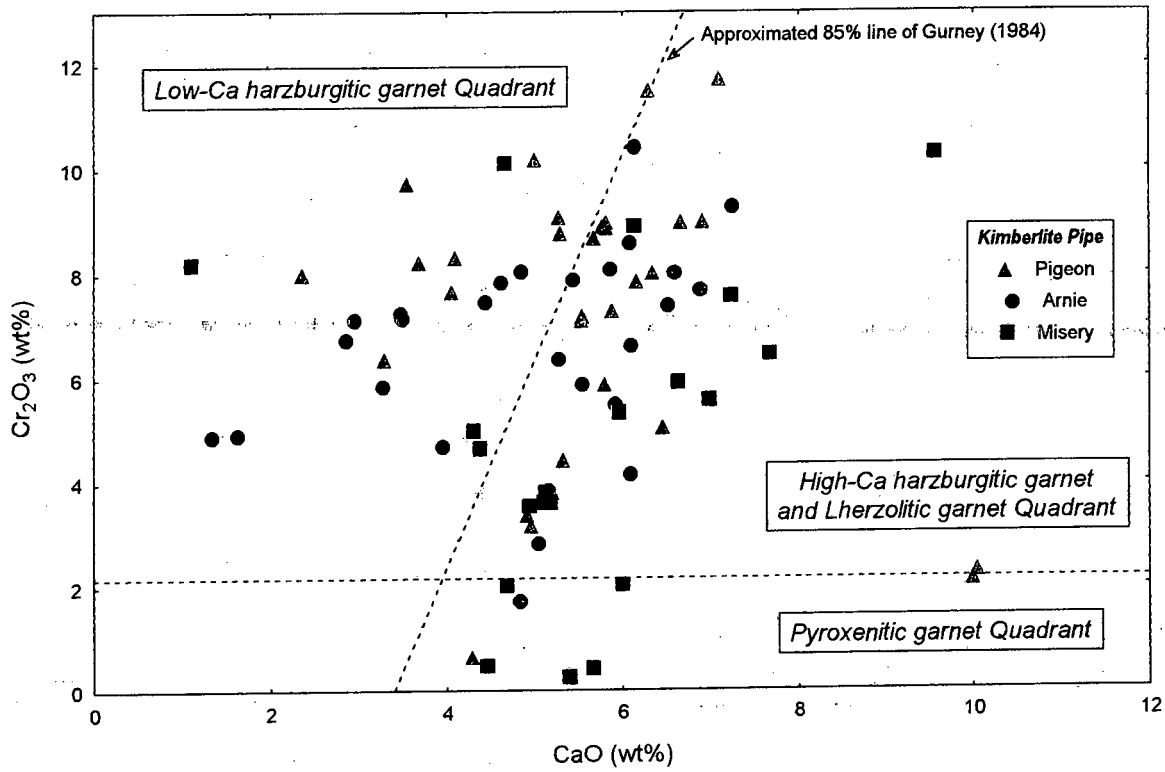

Figure 5.16 Cr_2O_3 vs CaO in garnet. The low-Ca harzburgitic garnets from the Pigeon kimberlite are more Cr-rich than those from the Arnie kimberlite. The Misery kimberlite has a lower proportion of low-Ca harzburgitic, and higher proportion of pyroxenitic garnets (<2 wt% Cr_2O_3) than the Arnie and Pigeon kimberlites. Rock types indicated in figure 5.4.

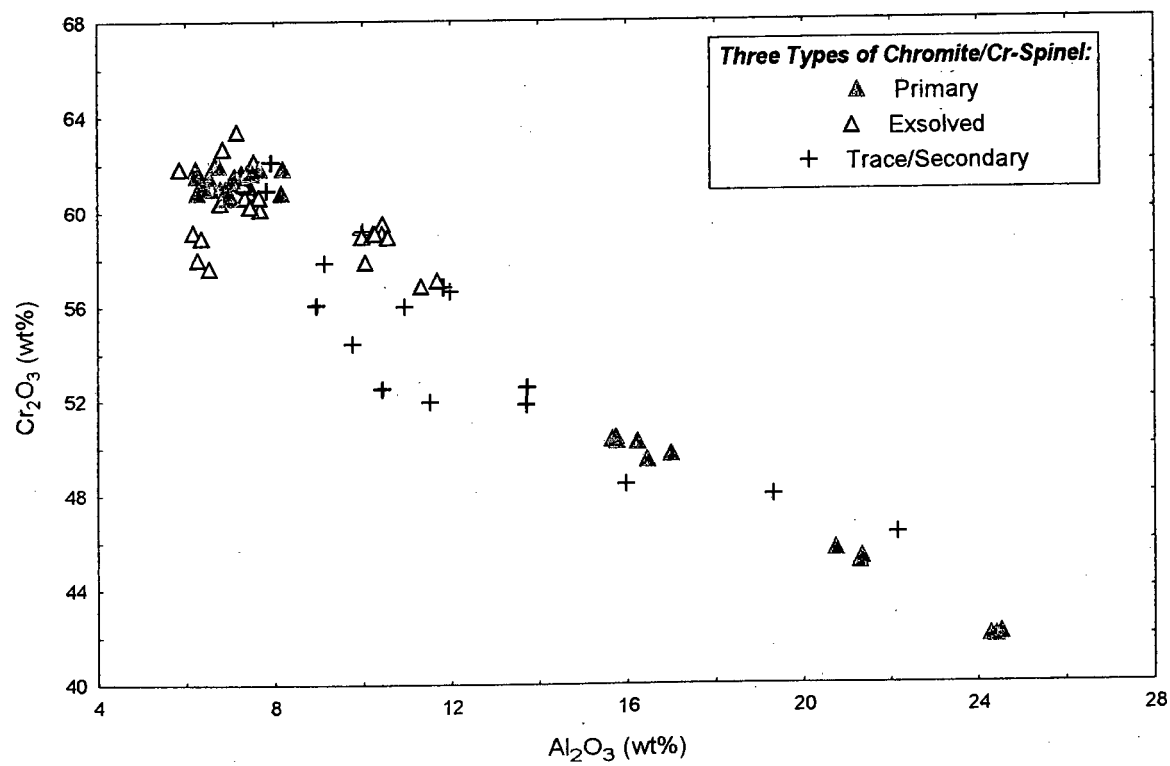

Figure 5.17 The exsolved chromites have a larger compositional range than the primary chromites. The primary Cr-spinels (<51% Cr_2O_3) are lherzolitic in nature (figure 5.10). The secondary Cr-spinels, located in zones of alteration, tend toward more pleonaste compositions (more Fe- and Al-rich).

General Chemical Trends

Garnet trends

Mg# and Cr_2O_3 content are the best discriminating factors between the peridotite suite and the pyroxenitic suite. The peridotitic garnets have a higher Cr_2O_3 and MgO content than the pyroxenitic suite garnets. The peridotitic garnets define a negative trend of decreasing CaO with increasing Mg# (figure 5.3). The range in Mg# is more restricted (77.9 to 85.3) than those of the pyroxenitic suite (45.3-81.0).

A distinct positive trend is defined by the lherzolite suite samples in a plot of CaO vs Cr_2O_3 (figure 5.4). This is a narrow band with an approximate Ca:Cr ratio of 2.2:1 cations. Since the 1970's studies such as Gurney and Switzer (1973), Sobolev et al. (1973) and Sobolev (1977) have all noted this trend for lherzolitic garnets in equilibrium with clinopyroxene.

All the low-Ca harzburgitic samples have TiO_2 contents below 0.1 wt%. The lherzolitic and high-Ca harzburgitic garnets have measurable TiO_2 contents, with a sharp rise in TiO_2 contents for garnets with CaO contents greater than 4.9 wt% (figure 5.5).

A negative correlation between Mg# and Al_2O_3, CaO and MnO was noted for all the peridotitic garnets. The garnets displays a negative correlation between Cr_2O_3 and Al_2O_3, as expected from the substitution of Cr^{3+} for Al^{3+} in the garnet structure. The negative correlation of Mg# with Al_2O_3; and between Cr_2O_3 with Al_2O_3 translates into a positive correlation between Cr_2O_3 and Mg# in garnet.

Clinopyroxene trends

None of the clinopyroxenes in the pyroxenitic suite have an omphacitic composition (figure 5.6 inset). This fact was verified using the classification by Morimoto (1988). The Ca-Mg-Fe nature of the clinopyroxenes of the pyroxenite suite (figure 5.6) imply that the samples do not have a classical eclogitic nature, in which the clinopyroxenes have an omphacitic composition.

Most of the peridotitic clinopyroxenes define a positive trend between Al_2O_3 and Cr_2O_3, with a ratio of Al_2O_3: Cr_2O_3 of 0.2:1 (figure 5.13). Four clinopyroxenes from the Misery kimberlite lie off this trend. All four of these samples (MIS409, MIS426, MIS431, MIS433) contain primary spinel. The Cr_2O_3 content in these clinopyroxenes may have been preferentially partitioned into the chromite, leaving the clinopyroxene Cr-poor in relation to the other clinopyroxenes. PGN333, the only other lherzolitic sample that contains spinel, lies in the positive lherzolitic trend. The modal proportion of

spinel in PGN333 is much smaller than the other four spinel-bearing samples, due to this fact the Cr_2O_3 content of the clinopyroxene in PGN333 may not have been affected by the spinel formation.

A similar positive correlation is noted between Na_2O and Cr_2O_3, with a ratio of Na_2O: Cr_2O_3 of 0.7:1 (figure 5.14). The pyroxenitic suite samples have a highly variable Al_2O_3 and Na_2O content and low Cr_2O_3 content below 0.5 wt% (apart from PGN320, PGN322, MIS454, which have Cr_2O_3 contents around 1.3 wt%). A coupled substitution of Na^{1+} with Al^{3+} or Cr^{3+} would be indicated by points lying on the 1:1 line (figure 5.15). The clinopyroxenes in eight samples are enriched in Cr and Al relative to Na, namely the websteritic clinopyroxenes (MIS438, MIS439), the coarse equant clinopyroxenites PGN320, PGN322, and the four clinopyroxenes in equilibrium with primary chromite (MIS409, MIS426, MIS431, MIS433).

Orthopyroxene

The peridotitic orthopyroxenes define a positive correlation between Al_2O_3 and Cr_2O_3 (figure 5.8), and a slight negative correlation between MnO and Mg#, and CaO and Mg#. Based on Mg# and CaO two subtle groups can be defined within the lherzolitic orthopyroxenes: a more Fe-rich group with higher CaO values, and a Mg-rich group with lower CaO contents (figure 5.7).

Olivine

The olivine in the harzburgites and lherzolites are very similar, and no compositional trends were noted. It should however be noted that three samples have anomalous olivine compositions. The olivine in MIS413 is more Fe-rich than the other olivines, and the olivine in ARN030 more Mg-rich. PGN301 has a very low NiO content. The cloudy appearance of the olivines suggests that they may have undergone secondary alteration.

Chromite

Three different forms of chromite were noted in the petrographic study, namely: primary, exsolved and trace chromites. The primary and exsolved spinels of the harzburgite suite are similar in nature, and have a chromite composition (>56.8 wt% Cr_2O_3). The exsolved chromite (56.8-63.4 wt% Cr_2O_3) has a slightly larger compositional range than the primary chromites (60.6-62.0 wt% Cr_2O_3, figure 5.17). The chromite within the lherzolite suite samples contain progressively more Al_2O_3 and less Cr_2O_3 than the harzburgite suite chromites (60.1-42.0 wt% Cr_2O_3, and 6.1-24.5 wt% Al_2O_3), thus tending toward pleonaste compositions. None of the pyroxenitic suite samples contained primary chromite.

The secondary trace chromites are located in the alteration rims of minerals, especially the kelyphitic rims of garnet. They trend toward higher MgO and Al_2O_3 contents with decreasing Cr_2O_3. They also

tend to have higher TiO_2, MnO and Fe_2O_3 contents than the exsolved and primary chromites. There is a direct correlation between the size of the chromite and it's chemistry. As the chromites become smaller they tend toward more pleonaste compositions, becoming more Al- and Fe^{3+}- rich.

5.3 DISCUSSION

Comparison between Lac de Gras and Kaapvaal peridotites

Major element compositions from coarse granular, low temperature peridotites from the Bultfontein, Bultfontein Floors, De Beers, Dutoitspan, Finsch, Frank Smith, Jagersfontein, Koffiefontein, Monastery, Mothae, Orapa-01, River Ranch, Roberts Victor and Wesselton kimberlites were obtained from the Kimberlite Research Group's Database at the University of Cape Town. The major element data from these localities on the Kaapvaal craton were combined into one data set and compared with the major element compositions of the peridotitic minerals from the three kimberlite localities in this study.

Figures 5.18 to 5.38 show that the major element composition of the peidotitic minerals from the Lac de Gras region are similar to those from various localities on the Kaapvaal craton. The garnets from the peridotites in this study extend to slightly lower Mg#'s (fig 5.18), but are more Cr_2O_3-rich (fig 5.21) than the majority of the garnets from the Kaapvaal craton. The chromites are also more Cr_2O_3-rich (fig 5.36), and MgO-poor (fig 5.37) than those from the Kaapvaal craton. The harzburgitic orthopyroxenes from the Lac de Gras region are depleted in Al_2O_3 relative to those from the Kaapvaal craton (fig 5.25).

Garnet and chromite mineral chemistry in relation to diamond bearing capacity

A large number of the garnets from both the Pigeon and Arnie kimberlites are low-Ca harzburgitic garnets, whereas only four low-Ca harzburgitic garnets from the Misery kimberlite were analysed (figure 5.16). In addition a large number of the chromites from the Arnie kimberlite plot close to the diamond stability field (figure 5.11, table 5.4), whereas those of the Misery kimberlite do not. The Misery kimberlite is however presently being mined by BHP. The diamonds from the Misery kimberlite are predominantly eclogitic (J.J. Gurney, pers comm. 2001), a fact that would be corroborated by the high proportion of eclogitic and websteritic xenoliths from the Misery kimberlite. This highlights the importance of investigating the eclogitic population in any diamond exploration and feasibility study.

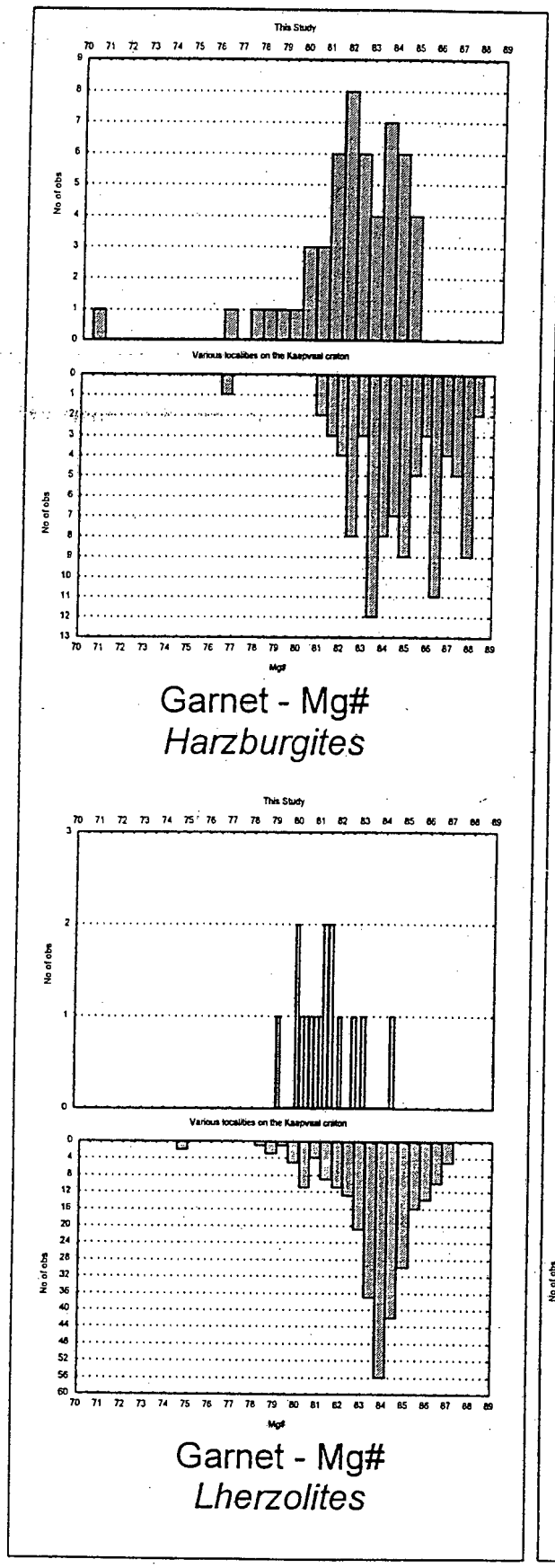

Figure 5.18 A comparison between the Mg# in garnet for the peridotites in this study (upper histogram) and those from various localities on the Kaapvaal craton (lower histogram).

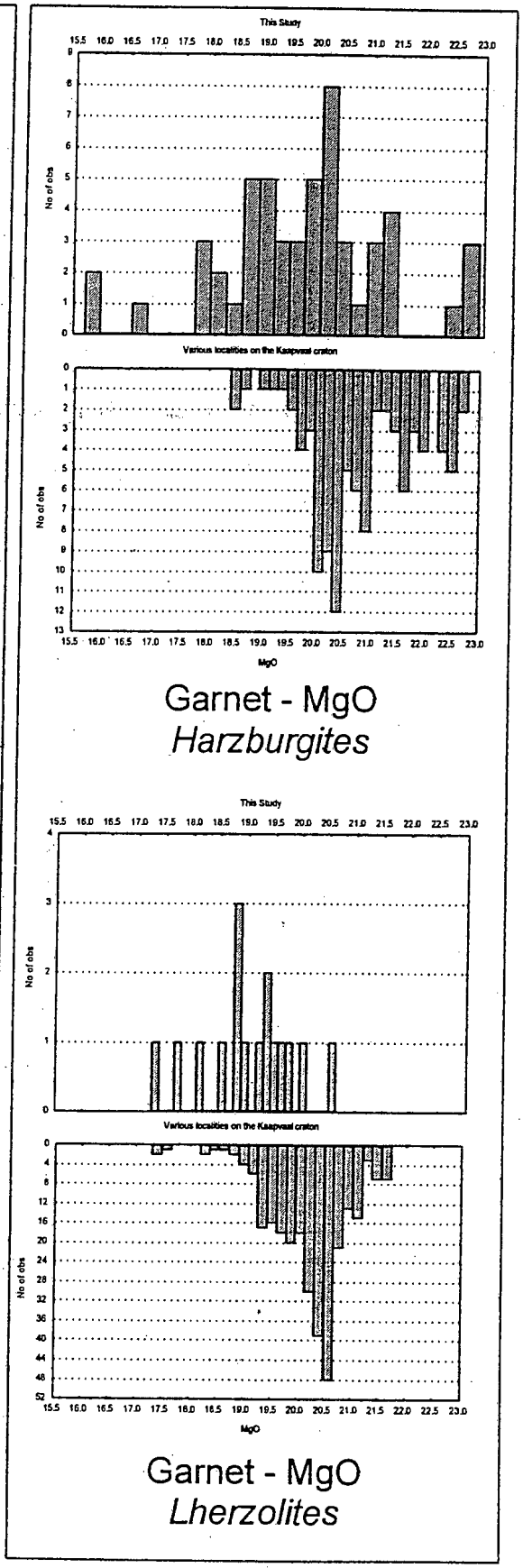

Figure 5.19 A comparison between the MgO in garnet for the peridotites in this study (upper histogram) and those from various localities on the Kaapvaal craton (lower histogram).

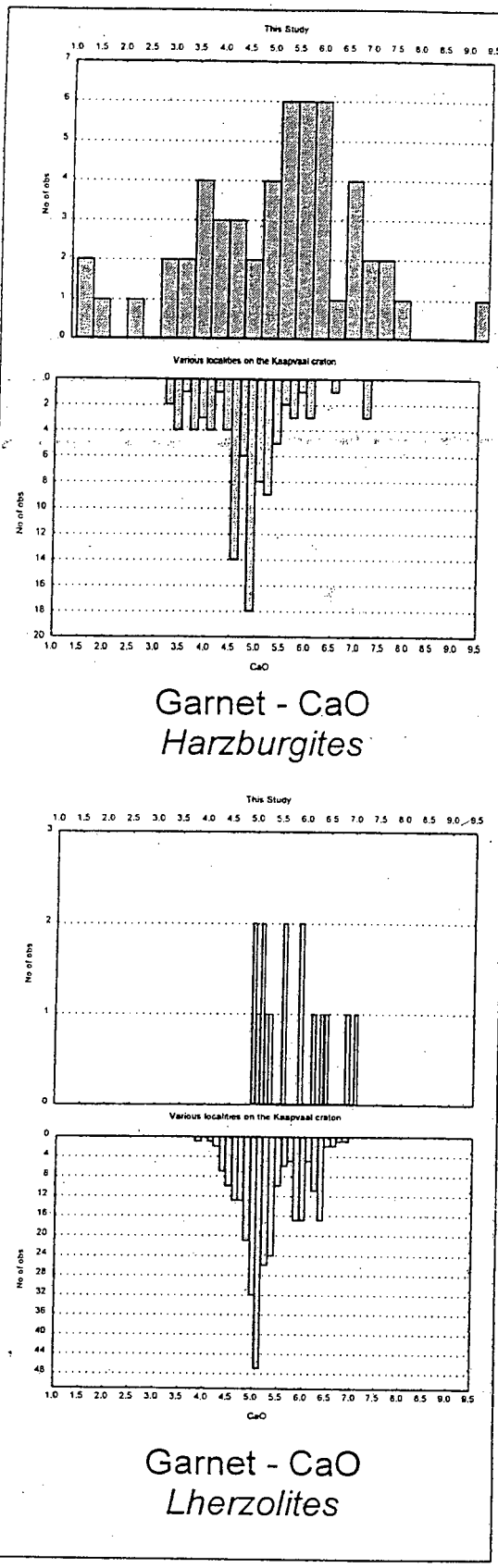

Figure 5.20 A comparison between the CaO in garnet for the peridotites in this study (top histogram) and those from various localities on the Kaapvaal craton (bottom histogram).

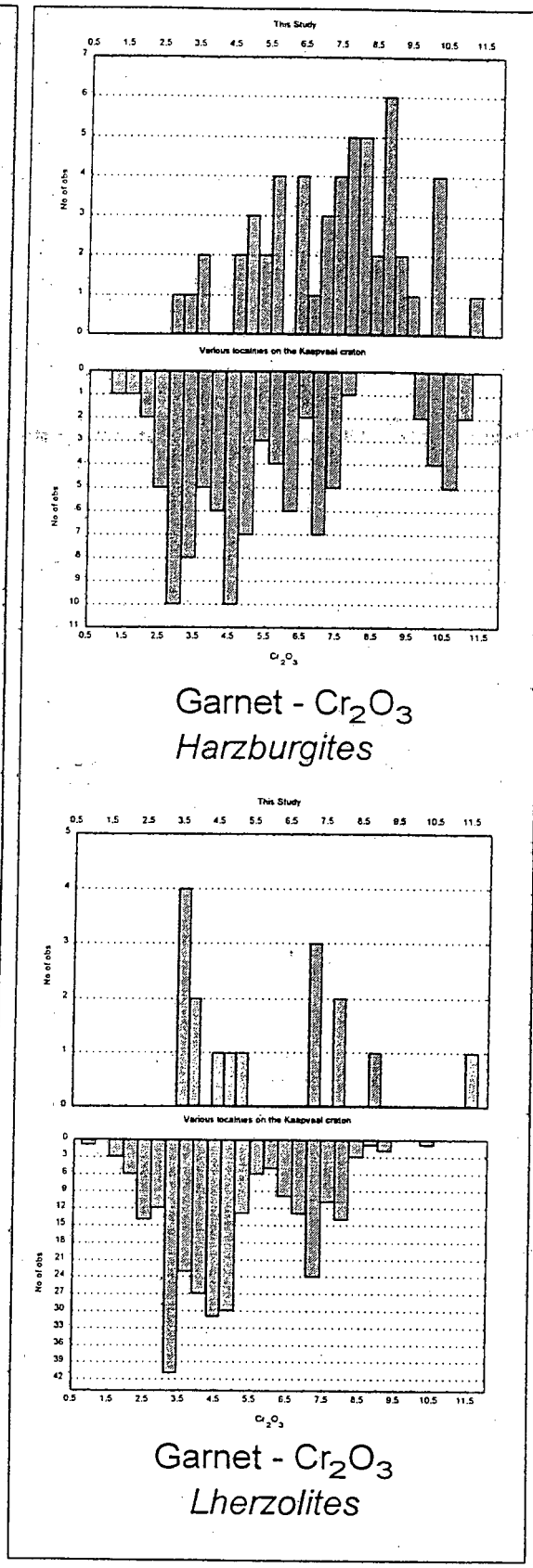

Figure 5.21 A comparison between the Cr_2O_3 in garnet for the peridotites in this study (top histogram) and those from various localities on the Kaapvaal craton (bottom histogram).

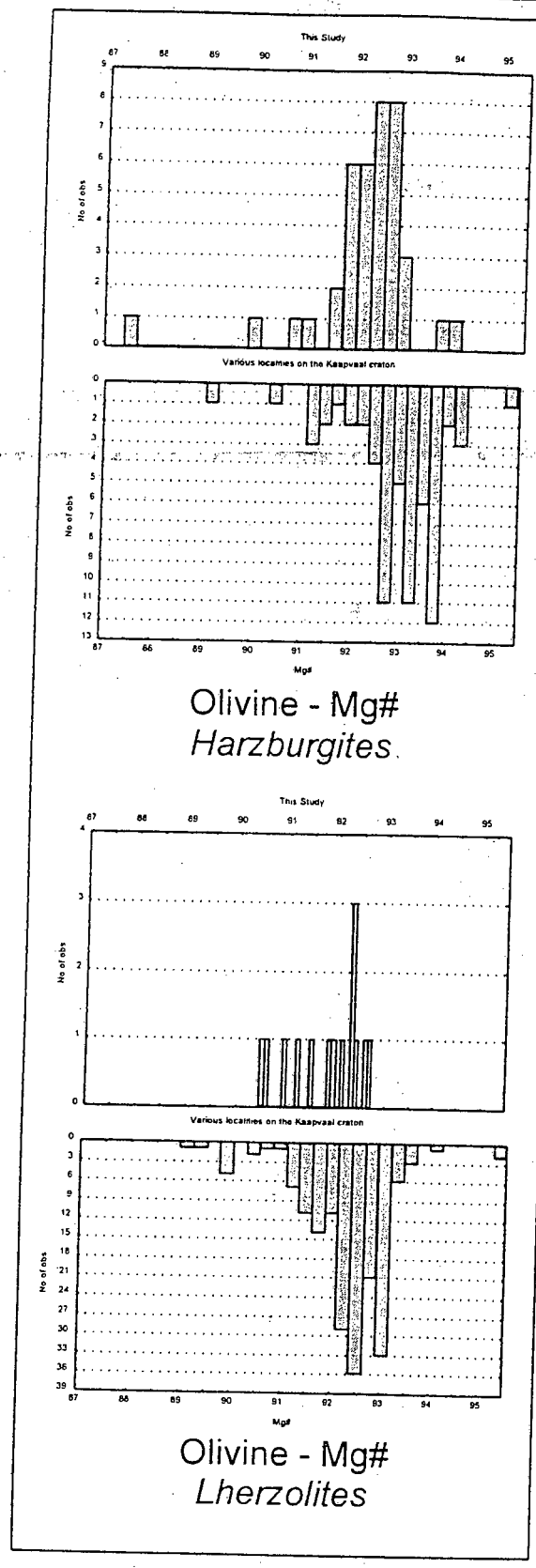

Olivine - Mg#
Harzburgites

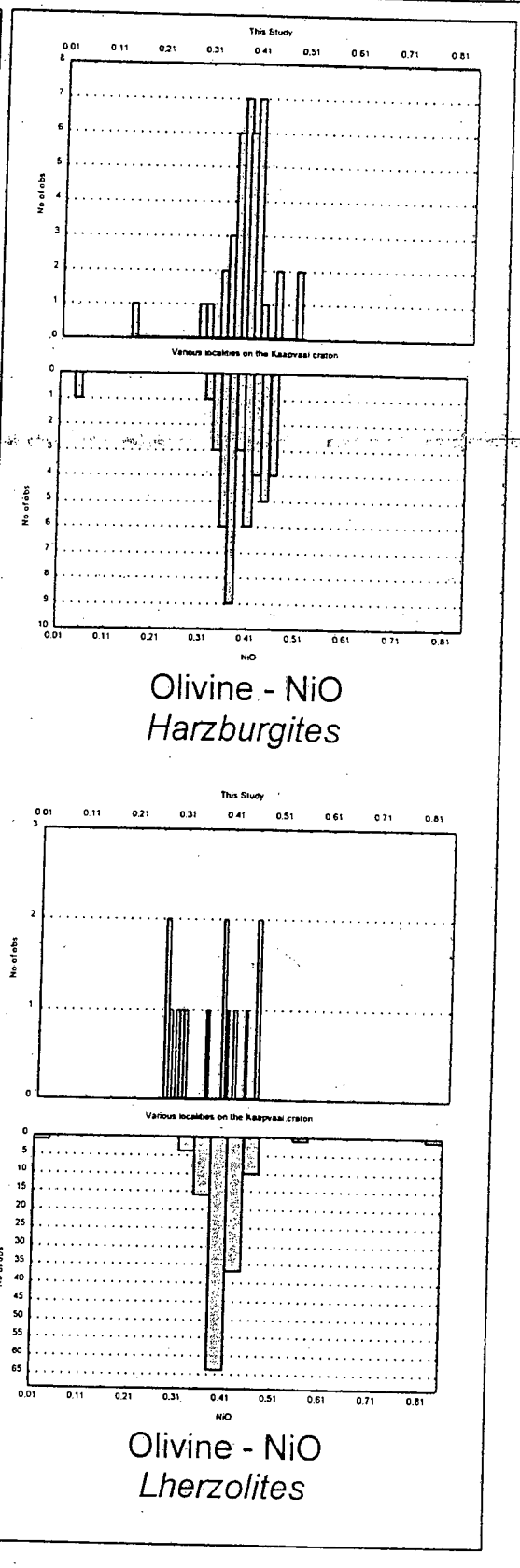

Olivine - NiO
Harzburgites

Olivine - Mg#
Lherzolites

Olivine - NiO
Lherzolites

Figure 5.22 A comparison between the Mg# in olivine for the peridotites in this study (upper histogram) and those from various localities on the Kaapvaal craton (lower histogram).

Figure 5.23 A comparison between the NiO in olivine for the peridotites in this study (upper histogram) and those from various localities on the Kaapvaal craton (lower histogram).

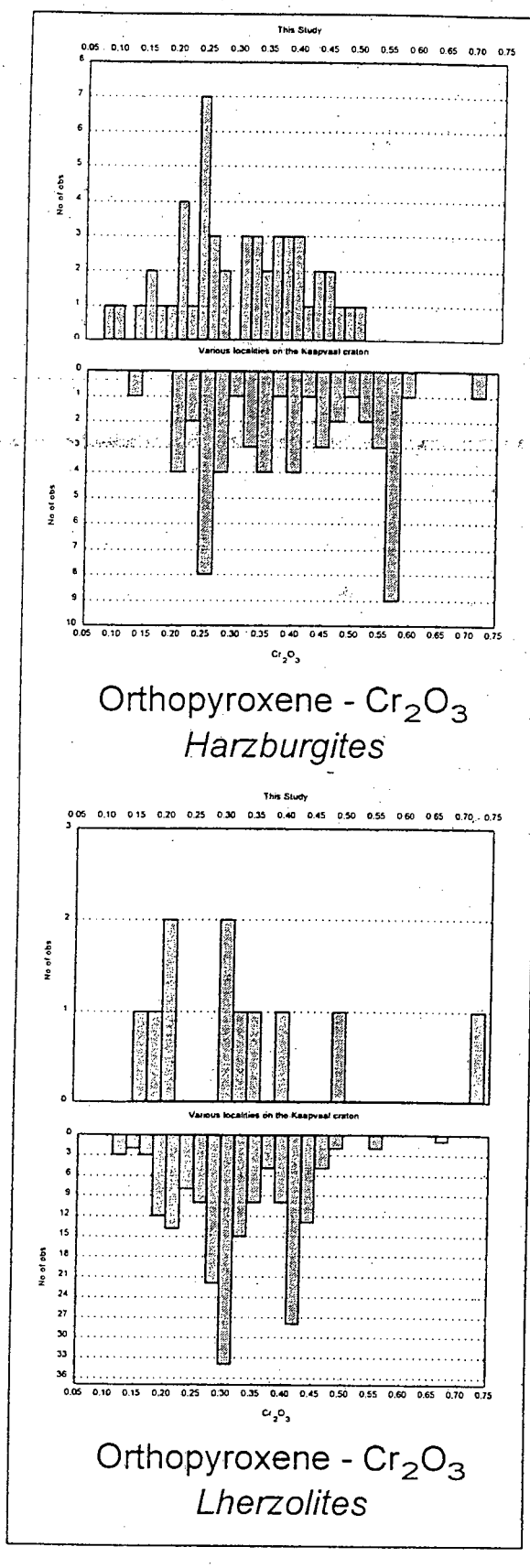

Figure 5.24 A comparison between the Cr_2O_3 in orthopyroxene for the peridotites in this study (upper histogram) and those from various localities on the Kaapvaal craton (lower histogram).

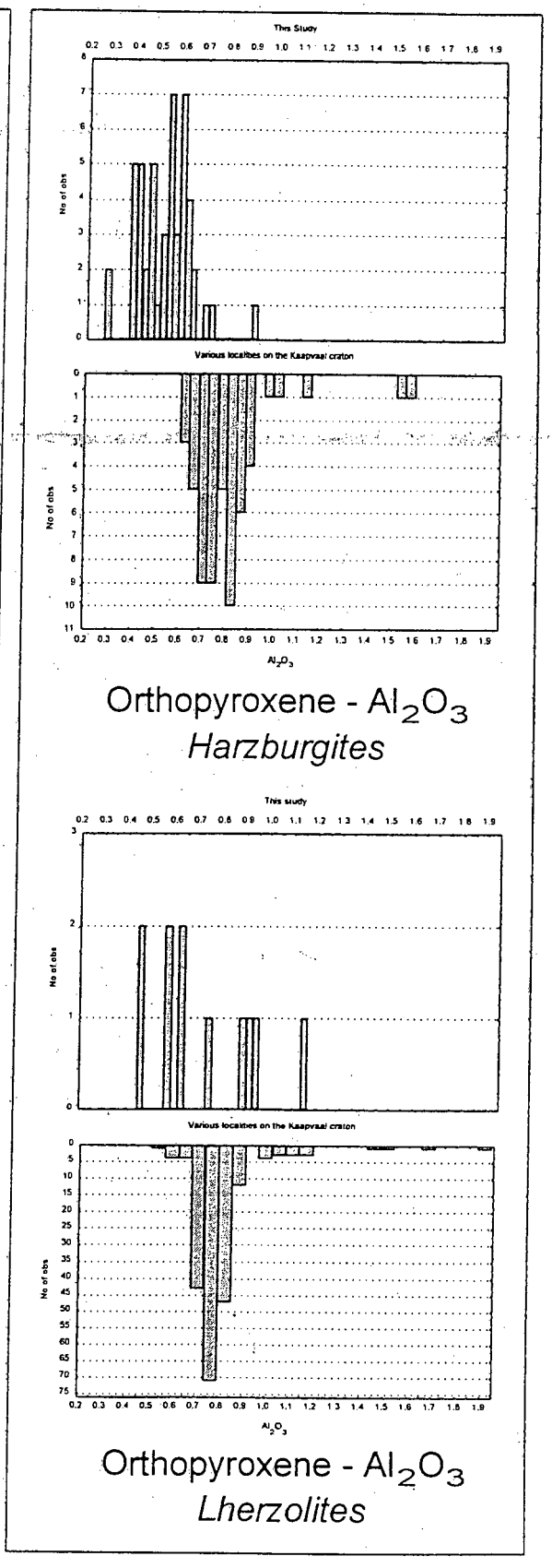

Figure 5.25 A comparison between the Al_2O_3 in orthopyroxene for the peridotites in this study (upper histogram) and those from various localities on the Kaapvaal craton (lower histogram).

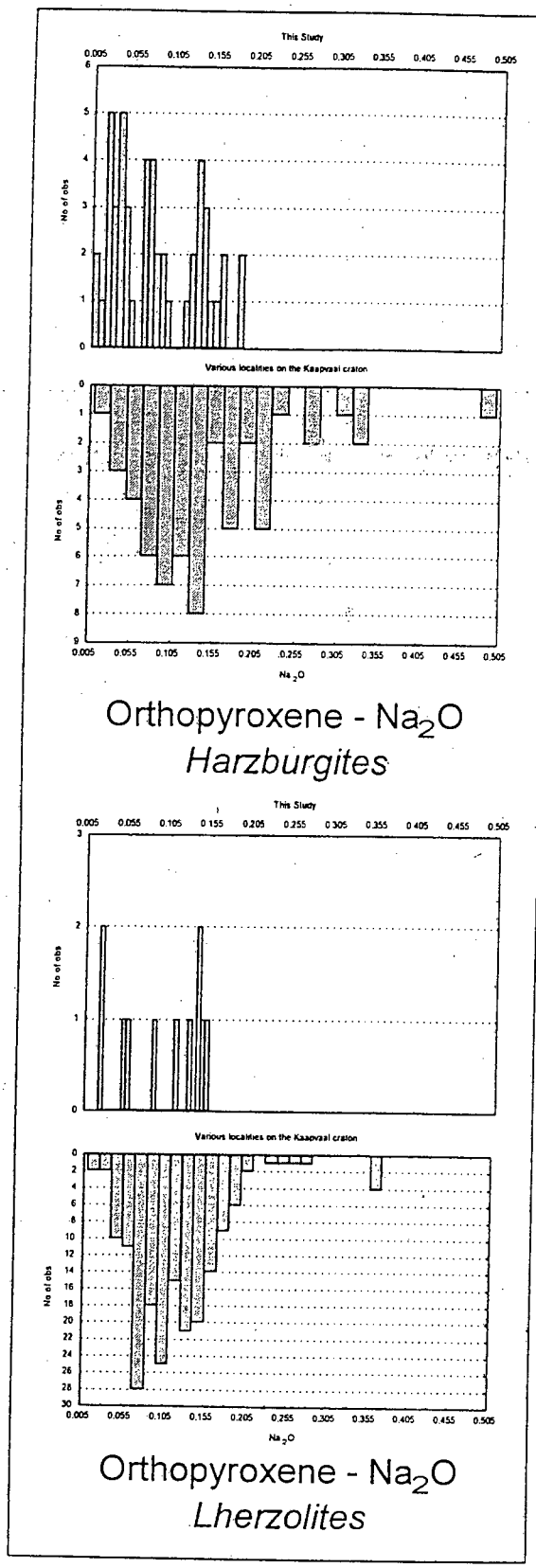

Figure 5.26 A comparison between the Na_2O in orthopyroxene for the peridotites in this study (upper histogram) and those from various localities on the Kaapvaal craton (lower histogram).

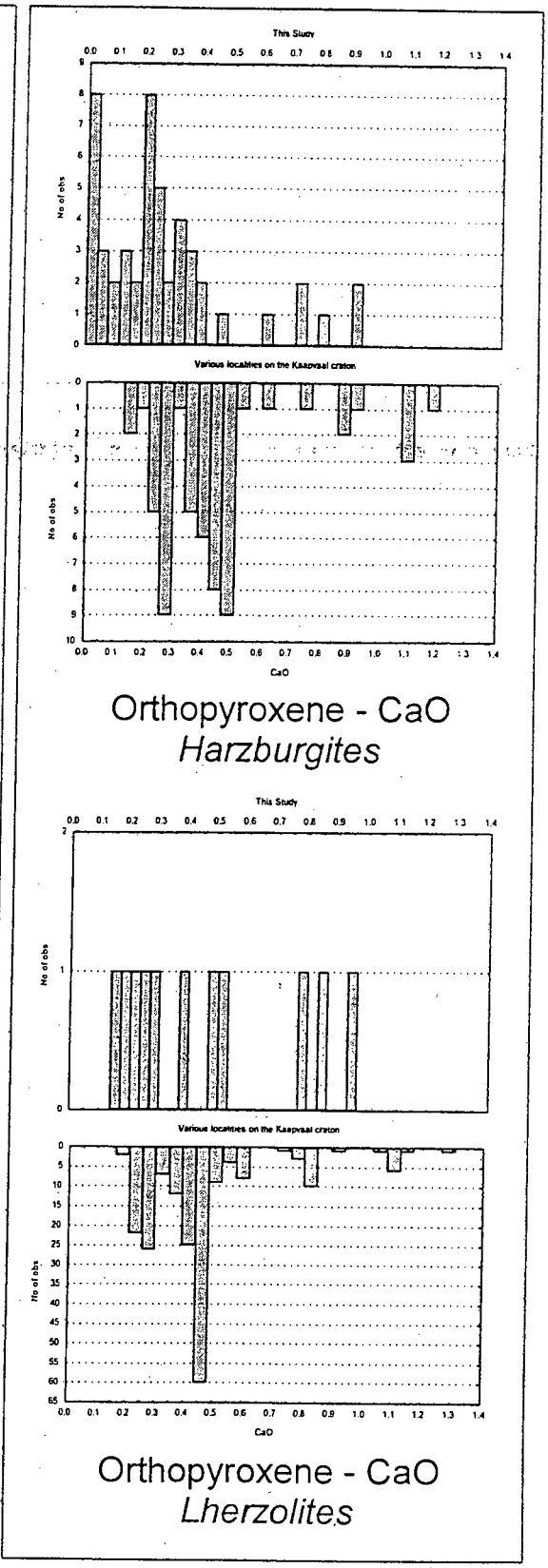

Figure 5.27 A comparison between the CaO in orthopyroxene for the peridotites in this study (upper histogram) and those from various localities on the Kaapvaal craton (lower histogram).

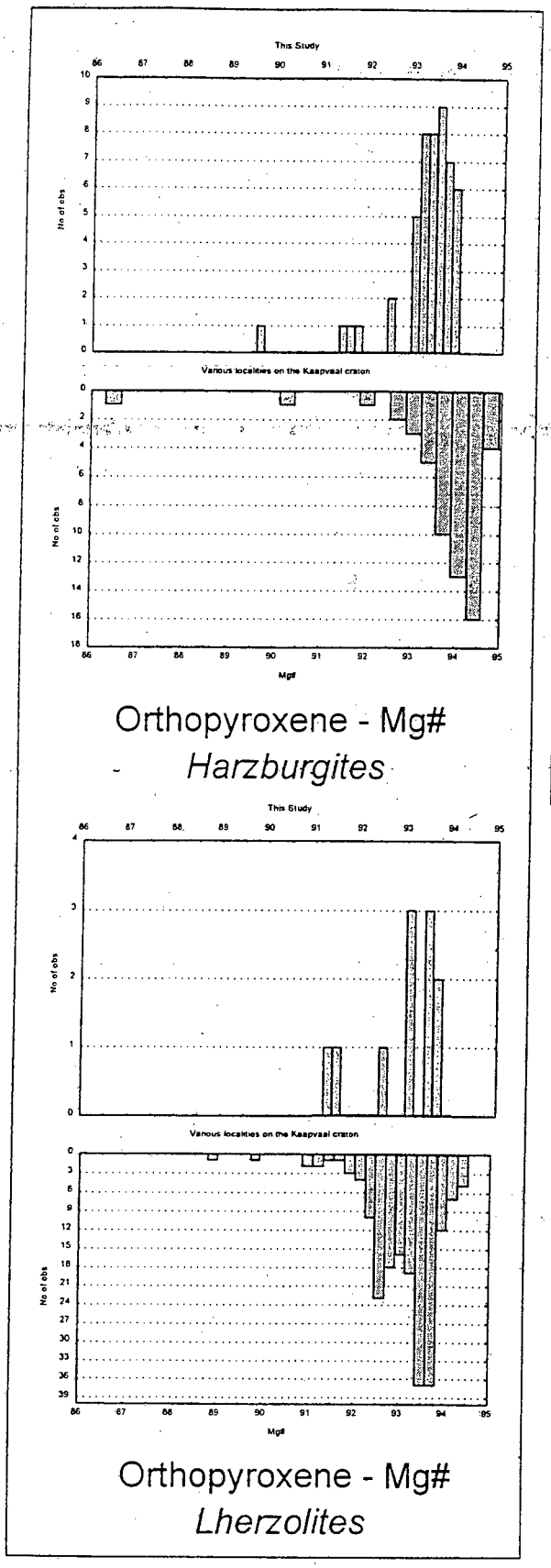

Figure 5.28 A comparison between the Mg# in orthopyroxene for the peridotites in this study (upper histogram) and those from various localities on the Kaapvaal craton (lower histogram).

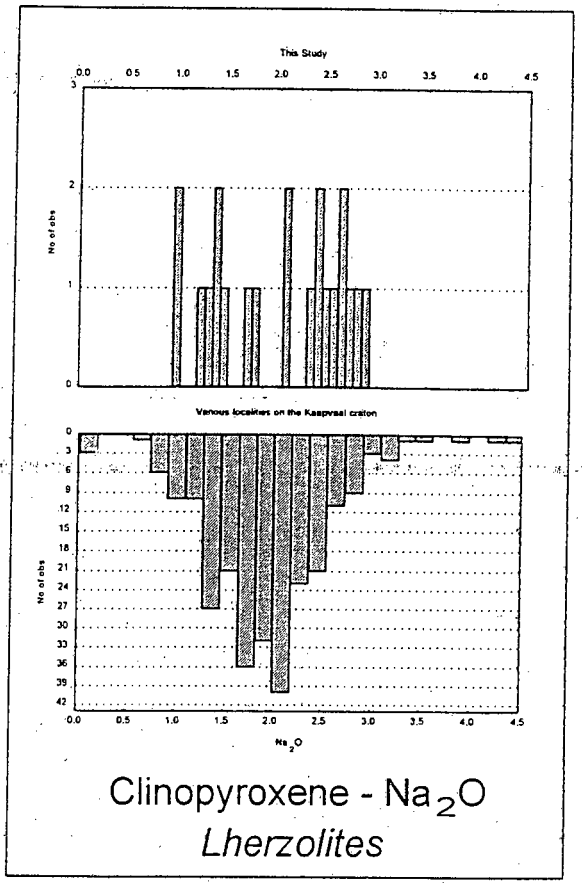

Figure 5.29 A comparison between the Na_2O in clinopyroxene for the peridotites in this study (upper histogram) and those from various localities on the Kaapvaal craton (lower histogram).

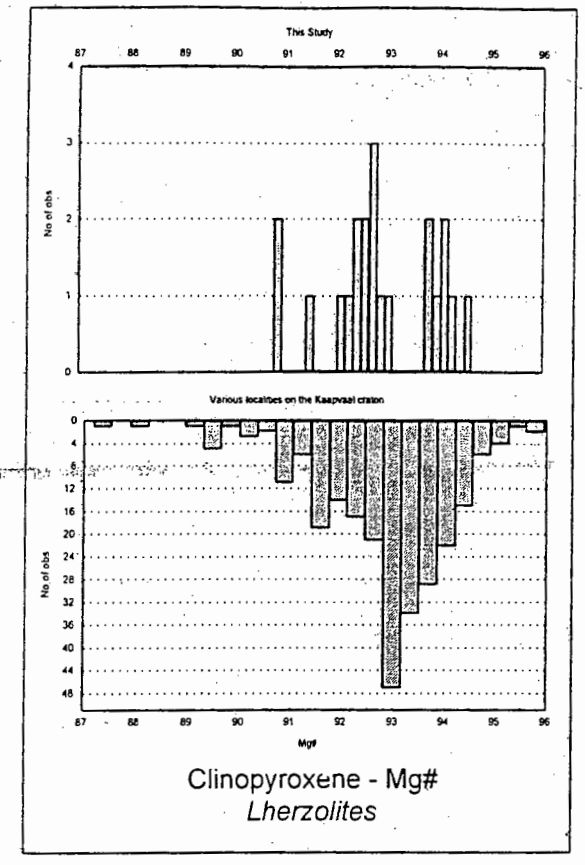

Figure 5.30 A comparison between the Mg# in clinopyroxene for the peridotites in this study and those from various localities on the Kaapvaal craton.

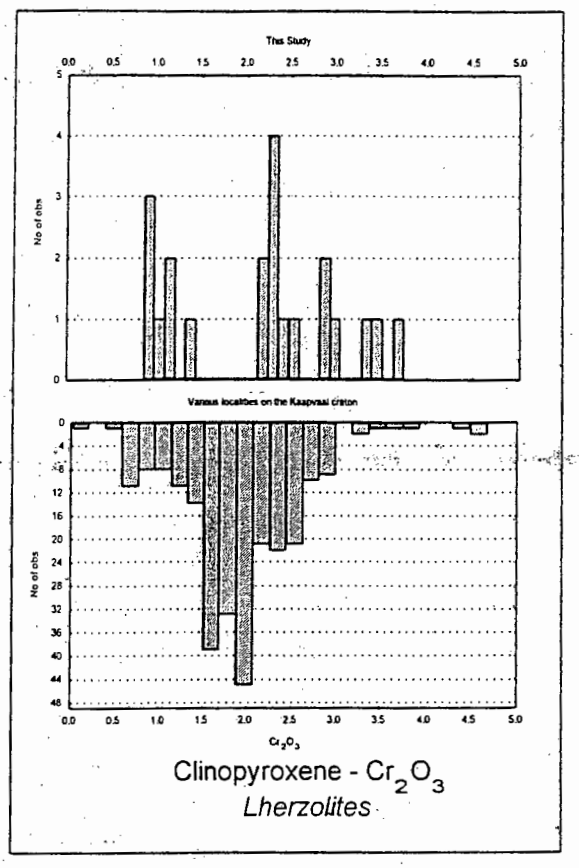

Figure 5.31 A comparison between the Cr_2O_3 in clinopyroxene for the peridotites in this study and those from various localities on the Kaapvaal craton.

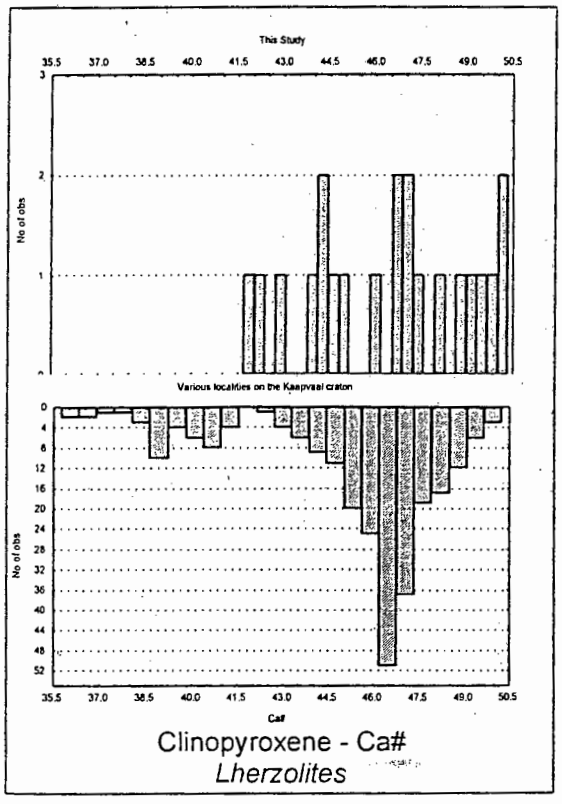

Figure 5.32 A comparison between the Ca# in clinopyroxene for the peridotites in this study and those from various localities on the Kaapvaal craton.

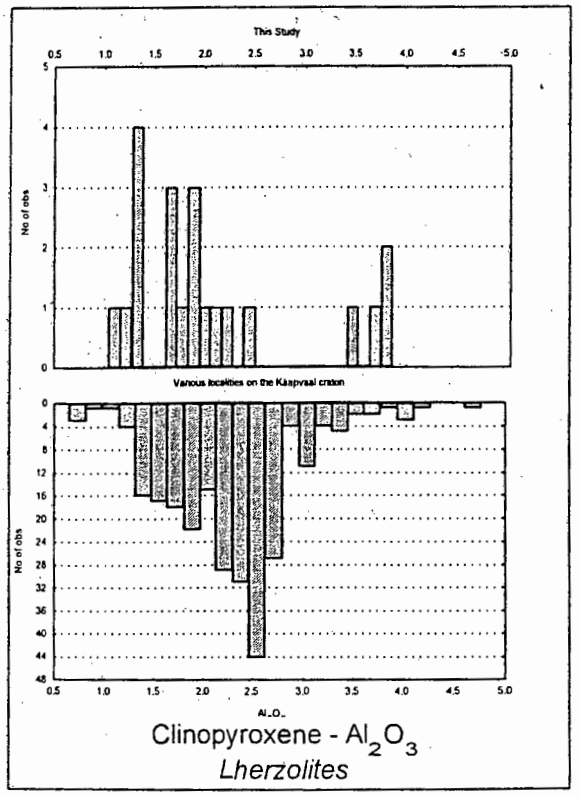

Figure 5.33 A comparison between the Al_2O_3 in clinopyroxene for the peridotites in this study and those from various localities on the Kaapvaal craton.

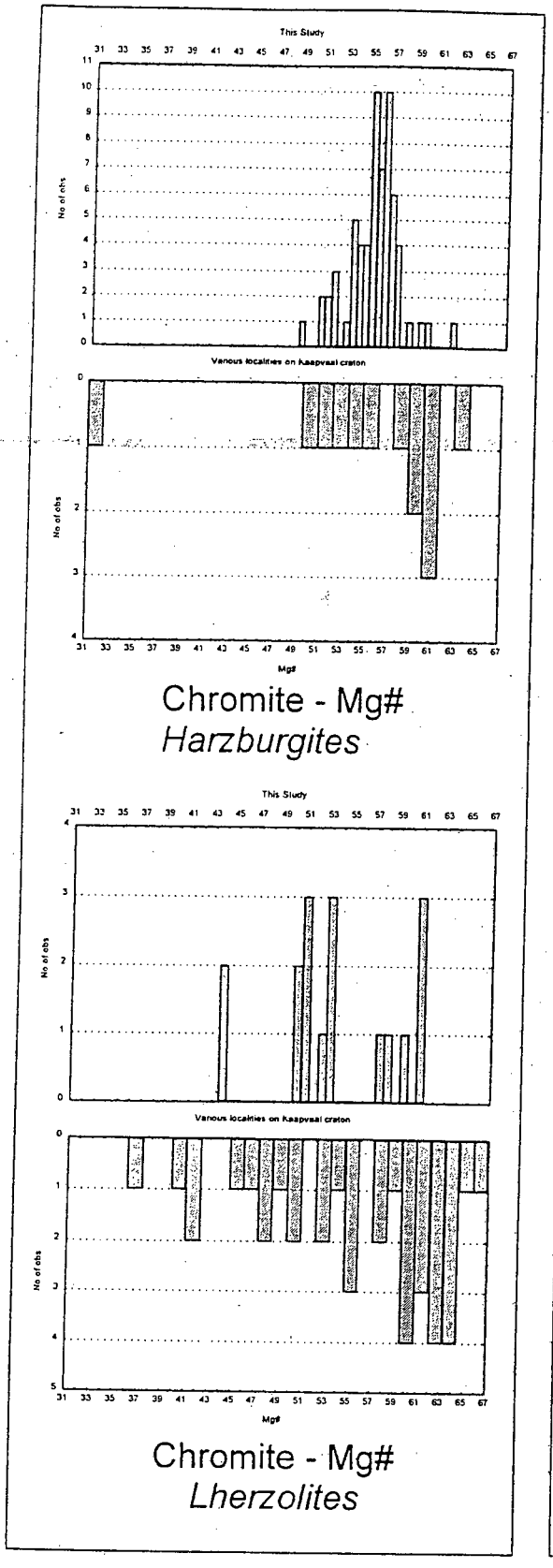

Figure 5.34 A comparison between the Mg# in chromite for the peridotites in this study (upper histogram) and those from various localities on the Kaapvaal craton (lower histogram).

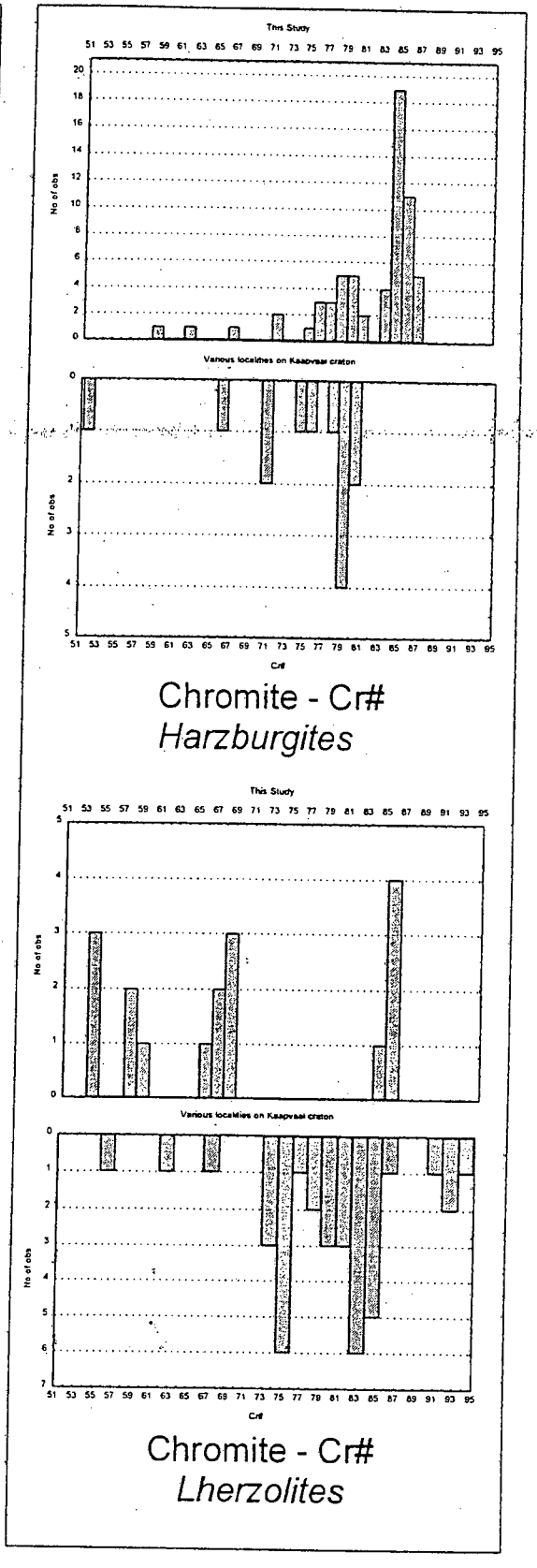

Figure 5.35 A comparison between the Cr# in chromite for the peridotites in this study (upper histogram) and those from various localities on the Kaapvaal craton (lower histogram).

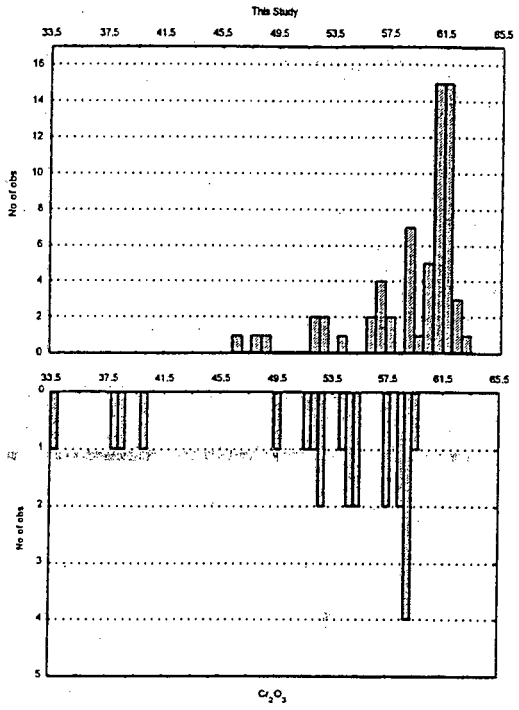

Chromite - Cr_2O_3
Harzburgites

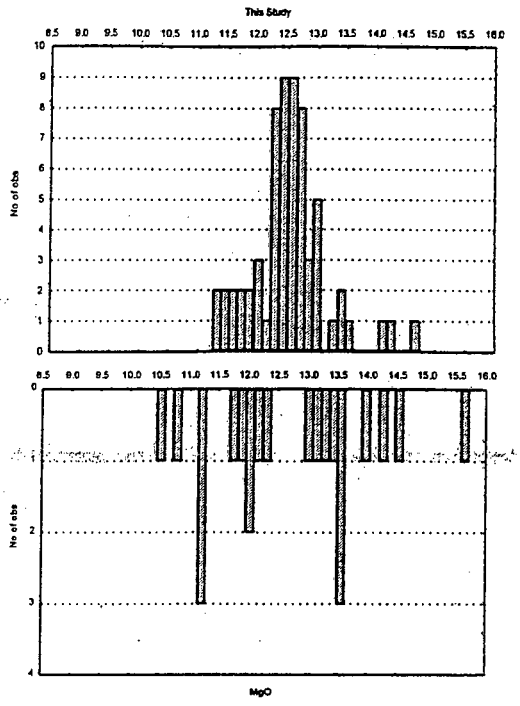

Chromite - MgO
Harzburgites

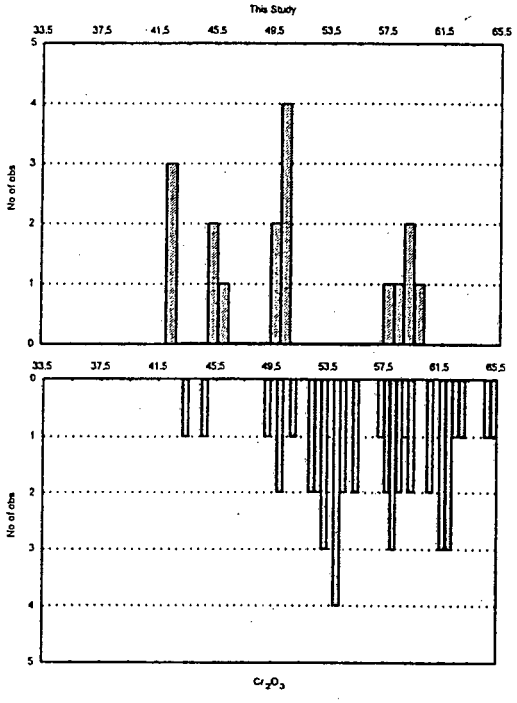

Chromite - Cr_2O_3
Lherzolites

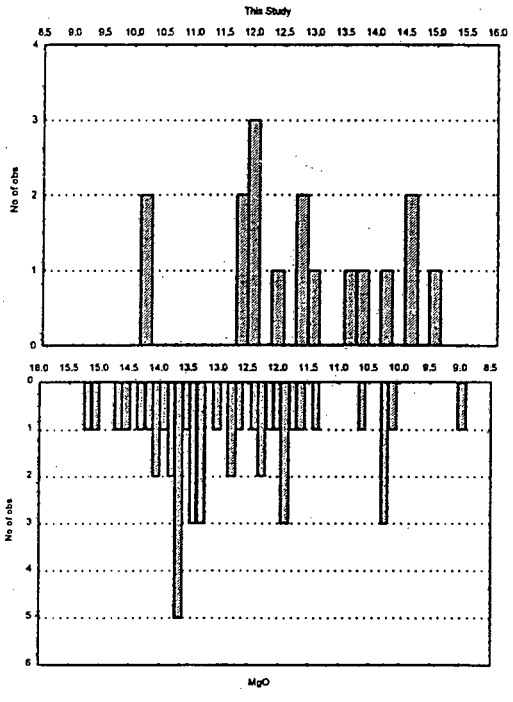

Chromite - MgO
Lherzolites

Figure 5.36 A comparison between the Cr_2O_3 in chromite for the peridotites in this study (upper histogram) and those from various locations on the Kaapvaal craton (lower histogram).

Figure 5.37 A comparison between the MgO in chromite for the peridotites in this study (upper histogram) and those from various locations on the Kaapvaal craton (lower histogram).

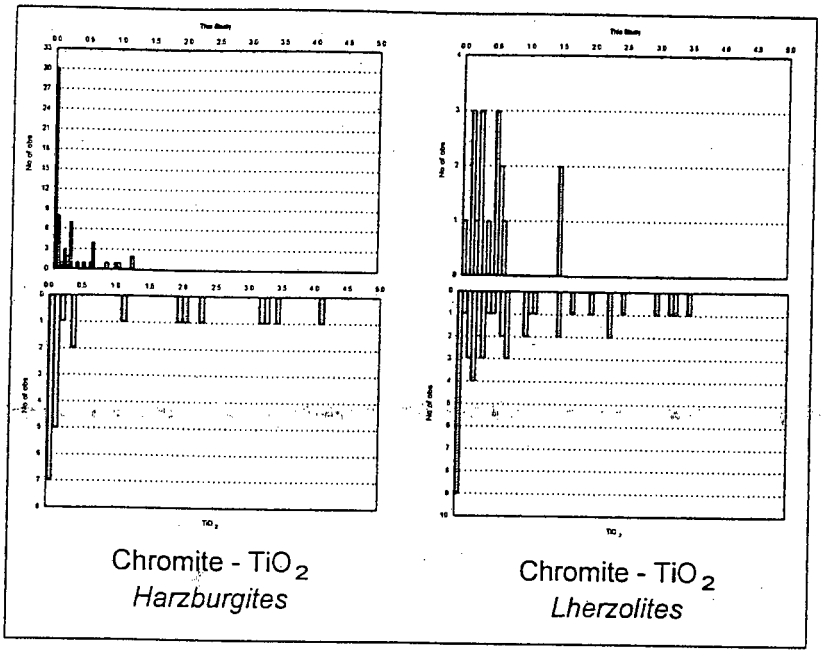

Figure 5.38 A comparison between the TiO_2 in chromite for the peridotites in this study (upper histogram) and those from various localities on the Kaapvaal craton (lower histogram).

Mg# ratios between coexisting pyroxenes

A ratio of the orthopyroxene Mg# to the clinopyroxene Mg# was computed for all samples which contained both orthopyroxene and clinopyroxene grains within the small xenolith fragment. Averages were computed for eleven lherzolitic and three pyroxenitic xenoliths. An average of the Mg# of orthopyroxene to clinopyroxene for the lherzolitic xenoliths is 1.00 +/- 0.0068. The average ratio of Mg# of orthopyroxene to clinopyroxene is however lower for the pyroxenitic samples (0.93 +/- 0.0293). This difference may be due to a compositional effect, or be an indication of disequilibrium between the orthopyroxene and clinopyroxene in the pyroxenitic xenoliths.

Possible relations between different suites

The garnets and clinopyroxenes of the recrystallized garnet-clinopyroxenite samples continue the trend of the lherzolite samples to lower Cr_2O_3 and Al_2O_3 contents. They are slightly more Fe-rich than the minerals of the peridotite suite, and yet less Fe-rich than the granoblastic websterites. They may therefore be a gradational link between the peridotite samples and the websteritic samples. This can also be attested by the intermediate composition of the recrystallized orthopyroxene in sample MIS428.

Possible causes for the compositional trends within garnet

The low-Ca harzburgitic garnets from individual kimberlites Pigeon and Arnie form rough fields of increasing CaO with increasing Cr_2O_3. This rough correlation is a less Cr-enriched trend than the "lherzolite trend" (figure 5.16).

The "lherzolite trend", a steep correlation between CaO and Cr_2O_3 in lherzolitic garnets was first noted in the 1970's (Gurney and Switzer, 1973; Sobolev et al., 1973; Sobolev, 1977). It has since been well documented in numerous on- and off-craton kimberlite localities (Burgess and Harte, 1999; Grütter et al., 1999; Steifenhofer et al., 1999). Hatton (1978) proposed that the lherzolite trend could be explained by a buffering of Ca^{2+} in the garnet by a reaction also involving orthopyroxene and clinopyroxene. Harzburgitic garnets, not being in equilibrium with clinopyroxene, do not lie on the lherzolite trend. Gurney (1984) found that the garnets on the Ca-poor side of the lherzolite trend (the harzburgitic garnets) were under-saturated with respect to Ca, and have a similar composition to garnets found in diamond inclusions. Yet no distinct trends are known within the Ca-poor field, which makes the roughly positive Ca-Cr correlation of the low-Ca harzburgites from individual kimberlites in this study unusual.

Within the garnets from the spinel-garnet peridotite from the Jericho kimberlite (about 150 km north of Lac de Gras) Kopylova et al. (2000) have noted a trend of lower Cr-enrichment with increasing CaO than the normal lherzolite trend. They attributed this trend to the buffering effect of spinel and

clinopyroxene in equilibrium with garnet. The less-Cr-enriched nature of this trend is similar to the rough correlation noted in the low-Ca harzburgite suite. Many of the low-Ca harzburgitic garnets have equilibrated with chromites, but are under-saturated with respect to calcium, implying that they have not equilibrated with clinopyroxene (Harte et al., 1980; Boyd and Gurney, 1982). Hence the formation of the correlation in Cr_2O_3-CaO could not be due to the same garnet-spinel-clinopyroxene equilibration and buffering as suggested by Kopylova et al. (2000) for the exotic trend from the Jericho kimberlite.

An alternative means of creating the Cr_2O_3-CaO trend is by metasomatism or melt interaction, modifying a homogeneous precursor to different degrees by Ca-enrichment or by Ca-depletion. Cr_2O_3-CaO zoning within individual garnet grains has lead numerous authors to suggest that the low-Ca harzburgites can be modified to more enriched lherzolitic compositions by interaction with a melt, be it a megacrystic melt, a proto-kimberlitic fluid or an Asthenospheric melt (Burgess and Harte, 1999; Griffin et al., 1999b; Pokhilenko et al., 1999; Stachel et al., 1999). Luth (1999) however suggests that interaction of harzburgites with a liquid carbonate would deplete harzburgitic garnets of Ca.

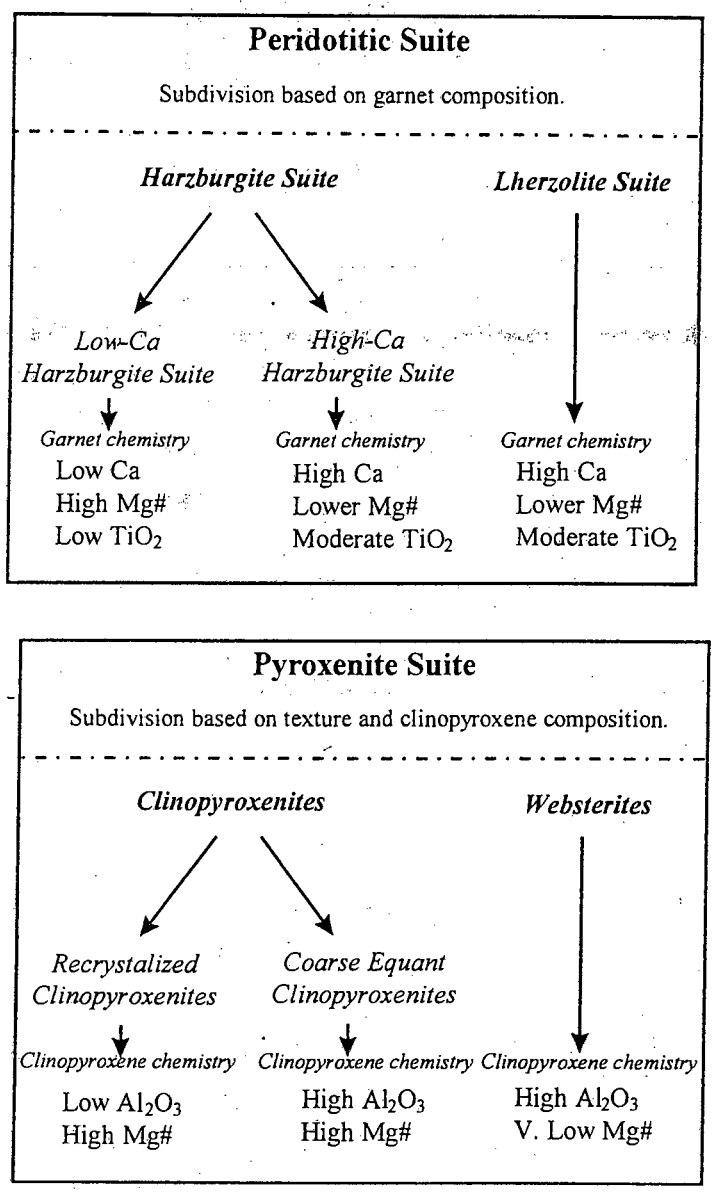

Figure 5.39 Summary of the different chemical characteristics of the subgroups within the peridotite and pyroxenite suite samples respectively. The subdivision of the peridotite suite sample suite is based on the garnet composition, whereas that of the pyroxenite suite is based on texture and the clinopyroxene composition.

6. TRACE ELEMENT MINERAL CHEMISTRY

6.1 INTRODUCTION

Trace elements may be considered as those elements that constitute <0.1% of a melt and that obey Henry's Law for dilute solutions. They may be considered as "those elements that are not stoichiometric constituents of phases in the system of interest" (White, 1997). The application of this definition depends on the system of interest, for example K may be considered a trace element in a basaltic system, but not in a granitic system.

Trace elements, and particularly rare earth element (REE) studies of minerals can be used to infer partial melting, crystal fractionation and metasomatic processes, such as cryptic metasomatism (Harte, 1987). Small scale mantle heterogeneity suggests that processes affecting one portion of the mantle may not have affected others. Hence not all mantle rocks may have experienced metasomatic processes, but all would experience mineral-mineral trace element interactions. These interactions may have important application in understanding the state of equilibrium between minerals (van Agterburgh et al., 1998), and have geothermobarometric applications (Griffin et al., 1989; Ryan et al., 1996; Canil, 1999).

Garnet and clinopyroxene are the two main REE repositories within the diamond stability region (Wang and Gasparik, 2001) as the incompatible trace elements are hosted more readily in the complex crystallographic structures of these minerals than in the other ultramafic minerals (olivine and orthopyroxene). The heavy REE's partition well into the garnet structure, substituting for Mg. (Shimizu and Kushiro, 1975), whereas the light REE's partition well into the clinopyroxene structure (Wang and Gasparik, 2001).

General Trace Element Characteristics

The behaviour of trace elements is largely determined by their radius and ionic charge. These characteristics determine the nature of the bonds they form, and the relative ease with which they substitute into the structure of minerals. The trace elements studied within this chapter may broadly be grouped into four categories, namely the large ion lithophile elements (LILE), the high field strength elements (HFSE), the first series transition metals and the rare earth elements (REE).

K, Rb, Sr, Cs and Ba are collectively known as the large ion lithophile elements (LILE). These elements have a large ionic radius (1.21Å for Sr and 1.78Å for Cs, after Whittaker and Muntus, 1970) and low ionic charge (+2 or +1). The ionic radii of the LILE's are larger than those elements that normally compose the major minerals in mafic and ultramafic rocks. Substitution of the LILE's into the mineral structure of these rocks therefore causes distortion of the tetrahedral and octahedral sites, which is energetically unfavourable (White, 1997). LILE's are therefore generally considered incompatible elements in mafic and ultramafic rock-mineral systems.

High field strength elements (HFSE) have smaller ionic radii and higher ionic charge than the large ion lithophile elements (LILE). Zr and Hf both have a +4 valence state and ionic radius of ~0.80Å, whereas Nb and Ta both have a +5 valence state, and an ionic radius of 0.72Å (after Whittaker and Muntus, 1970). Th (+4) and U (+4 or +6) are sometimes included in this group due to their high valence states. In the mineral-melt system, the HFSEs are incompatible elements in silicate minerals. Their high ionic charge makes substitution for the common mafic and ultramafic elements (Mg^{2+}, Fe^{2+}, Ca^{2+}) unfavourable, and coupled substitutions would be required to maintain charge balance. The first series transition metals (Sc, Ti, V, Cr, Co, Ni, Cu and Zn) are all siderophile and/or chalcophile in nature, apart from Mn which is a lithophile.

The REE's are part of the lanthanide series of elements, and usually act as a coherent group. They are used extensively in trace element studies to define processes affecting the mantle. The REE's all have a 3+ valence state, apart from two elements which may have a second valence state, namely Ce (+3 and +4) and Eu (+2 and +3). These valence characteristics are useful for defining oxygen fugacities and partial melt processes. REE concentrations are typically normalised to chondritic values to remove the saw-tooth effect caused by the absolute abundance of elements, and allows for the comparison of REE patterns between different phases.

A quantitative analysis of the following elements was undertaken using the LA-ICP-MS at UCT:
LILE: Rb, Sr, Ba
HFSE: Zr, Nb, Hf, Ta, Y, Th, U
REE: La, Ce, Nd, Sm, Eu, Gd, Dy, Er, Yb
First Series Transition Metals and Compatible Elements: Sc, Ti, V, Co, Ni

The trace element concentration of garnet and clinopyroxene are discussed in detail as these two minerals are the main two repositories for trace elements in ultramafic xenoliths. The compatible elements within orthopyroxene and olivine will be discussed briefly.

Method

Trace element compositions for individual minerals were obtained using the Perkin Elmer Elan 6000 Inductively Coupled Plasma-Mass Spectrometer (ICP-MS) coupled to a CETAC LSX-200 UV Laser in the Department of Geological Sciences, UCT. A minimum of three analyses were obtained per mineral. A single analysis consisted of three replicates of a hundred readings each. Methods and standardisation procedures are detailed in chapter 3.

The REE's were normalised according to the chondritic values defined by Anders and Grevesse (1989), and the trace elements are normalised to the primitive mantle values given by McDonough and Sun (1995). In these plots the trace elements are presented in decreasing order of incompatibility from left to right (figures 6.8-6.14). Rb and Ba as most incompatible on the left, and Co and Ni as the most compatible on the right.

As minerals/mineral partition coefficients are of interest to unravelling mantle processes, where mineral/mineral partition coefficients were not available they were inferred by dividing published mineral/melt by mineral/melt partition coefficients for similar melts.

6.2 CHEMICAL CHARACTERIZATION

Harzburgite Suite

Due to the similar trace element characteristics of the low-Ca and high-Ca harzburgitic suite minerals, they have been described together as a single suite below.

Large Ion Lithophile Elements (LILE) and High Field Strength Elements (HFSE)

The harzburgitic garnets have higher Sr contents (LLD - 6.7 ppm) than in the lherzolites or pyroxenites (<1 ppm). The harzburgitic garnets have a wide range in Zr content (0.4-64 ppm), and lower Y contents (<2.8 ppm) than the lherzolitic and pyroxenitic garnets (2.3-47.0 ppm). The garnets in ARN003 are exceptional and have elevated Y (35 ppm) and Zr (107 ppm) contents (figure 6.1).

First Series Transition Metals

The harzburgitic garnets have low Ti contents (<371 ppm), and a large range in Sc content (117-448 ppm), figure 6.2. The abundance of Sc appears to be related to the Mg# in the garnet, as Mg# increases, so does the abundance of Sc (figure 6.3). The harzburgitic garnets have lower Ni (11-56 ppm) contents and similar Co (32-50 ppm) contents to the lherzolitic garnets (figure 6.4), the garnet in ARN025 however contains more Co (70 ppm).

Neither the orthopyroxene, nor the olivine of the low-Ca harzburgitic suite contain many detectable incompatible trace elements. They do however contain appreciable amounts of compatible elements: the orthopyroxene contains 434-797 ppm Ni, and 34-48 ppm Co (figure 6.5), and the olivine contains 2264-2881 ppm Ni and 108-127 ppm Co (figure 6.6).

Rare Earth Elements (REE)

Three distinct REE patterns are found within the garnets of the low-Ca harzburgites: a MREE-enriched pattern, a sinusoidal pattern and a LREE-depleted pattern (figure 6.7). The MREE-enriched pattern is characterised by enriched MREE (~20 times chondrite) relative to the LREE's and HREE's (~5 times chondrite). The maximum is around Sm. The sinusoidal pattern is LREE enriched (~10 times chondrite) compared to the MREE (~2 times chondrite) and HREE's (~ chondritic). In contrast to the MREE-enriched pattern, the sinusoidal pattern has a smaller maximum around Nd, and a minimum around Dy-Er. The third pattern is a simple pattern of LREE depletion, where the LREE's have chondritic values, and the HREE's are about five times the chondritic value. It is interesting to note that all the garnets that have MREE-enriched patterns coexist with primary chromites (ARN007, ARN017, ARN025, ARN027).

The high-Ca harzburgitic garnets have similar chondrite normalised REE patterns to those of the low-Ca harzburgite garnets. The sinusoidal and LREE depleted enriched patterns are identical, whereas the MREE-enriched pattern varies slightly (figure 6.7). The MREE-enriched pattern of the garnet in ARN013 has considerably lower abundance's of the MREE (~chondrite) than the other MREE-enriched garnets (~20 times chondrite). ARN003 on the other hand has an enriched REE abundance (~50 times chondrite, Gd maximum), in contrast to the other MREE-enriched garnets (with a maximum around Sm).

Trace element abundance's relative to Primitive Mantle

Although the REE patterns of the harzburgitic garnets differ, the majority of the garnets have similar trace element characteristics. The garnets that displayed sinusoidal REE patterns (MIS401, MIS408 and PGN340) have lower Sm, Zr, Hf, Eu and Gd concentrations, and higher Sr contents than the other harzburgitic garnets (figure 6.8 and 9). All the garnets are depleted in Dy, Y, Er and Yb apart from that of sample ARN003. The garnets of ARN003 are enriched in trace elements relative to the other harzburgitic garnets, particularly the compatible elements Sm, Zr, Hf, Eu, Gd, Dy, Y, Er, Yb and Sc. ARN026 is enriched in Zr and Hf relative to the other garnets. Generally the low-Ca harzburgitic garnets are slightly more depleted in Nb, Sr and Ti, and enriched in Sc than the high-Ca harzburgitic garnets.

lherzolite Suite

Large Ion Lithophile Elements (LILE) and High Field Strength Elements (HFSE)

The lherzolitic garnets have similar Zr contents to those of the harzburgite suite (4-54 ppm), and higher Y contents (1.4-17 ppm; figure 6.1). They all have low (<1 ppm) Sr contents.

Apart from Sr, the lherzolitic clinopyroxenes have low LILE abundance's (<13 ppm Ba, and <5 ppm Rb). The majority of the lherzolitic clinopyroxenes contain between 109 and 332 ppm Sr, and have low HFSE contents (<10 ppm Zr; <5 ppm Hf, Nb, Ta). The clinopyroxene in ARN032 is an exception and has much higher Sr (1803 ppm) and Zr content (58 ppm) than the other clinopyroxenes.

First Series Transition Metals

The lherzolitic garnets have higher Ti contents (500-3878 ppm) than those in other suites (figure 6.2), and have a small range in Sc content (99-148 ppm). Apart from the garnet in MIS409, the Ni content of the lherzolitic garnets (53-101 ppm) is higher than those of the harzburgitic suite, but have similar Co contents (37-54 ppm). Garnets in MIS409 have a lower Ni and subtly lower Co content (13 and 31 ppm respectively; figure 6.4).

The lherzolitic clinopyroxenes have lower abundances of the compatible elements Co (10-26 ppm) and Ni (188-143 ppm) than the pyroxenites (figure 6.10), but V (128-328 ppm) and Sc (9-31 ppm) are more abundant than in the clinopyroxenes from the clinopyroxenites (figure 6.11). The lherzolitic clinopyroxenes contain between 94 and 1180 ppm Ti. The trace element content of ARN032 is higher than the lherzolitic clinopyroxenes (102 ppm Sc).

The compatible element content of the lherzolitic orthopyroxenes is higher than that of the harzburgitic orthopyroxenes (46-52 ppm Co; 620-800 ppm Ni; figure 6.5). The orthopyroxene in MIS409 is however much lower than any of the other peridotitic orthopyroxenes, with 444 ppm Ni and 29 ppm Co. The lherzolitic orthopyroxenes contain more Ti than the harzburgitic orthopyroxenes (177-653 ppm Ti), but have a similar V content (33-44 ppm).

The lherzolitic olivines have lower Ni (2061-2552 ppm) and Co (107-119 ppm) abundance's than the harzburgitic olivines (figure 6.6).

The trace element composition of the minerals in sample MIS409 are different to the other lherzolitic minerals. The garnet, clinopyroxene and orthopyroxene are all depleted in the compatible elements Ni

(13 ppm) and Co (31 ppm) compared to the other lherzolitic minerals (figure 6.4), and appears to be more like the harzburgitic minerals in this regard. Interestingly, MIS409 has a lower temperature of equilibration than the other lherzolitic samples (figure 6.20), and is the only lherzolitic sample that was analysed for trace elements that coexists with chromite.

Rare Earth Elements (REE)

In contrast to the three varieties of REE patterns noted in the harzburgitic garnets, only one pattern is noted in the lherzolitic garnets. The lherzolite garnets are all LREE depleted (<1 times chondrite) relative to HREE's (~10 times chondrite), figure 6.12.

Two REE patterns are noted in the lherzolitic clinopyroxenes (figure 6.13). The majority are slightly LREE enriched (>10 times chondrite) relative to the HREE (~3 times chondrite), forming a sinusoidal REE pattern. In contrast, MIS409 has a relatively flat (~3 times chondrite), slightly concave upward pattern (La ~ 5 times chondrite). One sample (ARN032) is extremely LREE enriched (>250 times chondrite) relative to HREE (~4 times chondrite).

Trace element abundance's relative to Primitive Mantle

The lherzolitic garnets have a distinctly different trace element profile to the harzburgites. Whereas they have a similar Sr depletion, they contain greater amounts of Ti and Nb than the harzburgitic garnets. The lherzolitic garnets are also enriched in the compatible elements Gd, Dy, Y, Er and Yb relative to the harzburgites, but are not as enriched in Sc (figure 6.8, 6.9 and 6.16).

Pyroxenite Suite

Large Ion Lithophile Elements (LILE) and High Field Strength Elements (HFSE)

The majority of the pyroxenitic garnets have low Sr (<1 ppm), Zr contents (<3 ppm), and Y contents (<20 ppm). The garnet in sample MIS438 has higher Y (47 ppm) and Zr contents (26 ppm). Their low Zr content may be used to discriminate them from the peridotitic garnets (figure 6.1).

The pyroxenitic clinopyroxenes have low LILE abundance's (<10 ppm Ba, and <2 ppm Rb), but higher Sr contents (8-368 ppm). Apart from the clinopyroxene in the websteritic sample MIS438 (Zr 54 ppm), the pyroxenitic clinopyroxenes all have low HFSE contents (<10 ppm Zr; <5 ppm Hf, Nb, Ta).

First Series Transition Metals

The pyroxenitic garnets have lower Sc contents than the peridotitic garnets (21-222 ppm), and moderate Ti contents (263-921 ppm). The Ni content (10-48 ppm) of the pyroxenitic garnets is similar

to that of the harzburgitic garnets, whereas the Co content is higher (websteritic garnets: 60 and 70 ppm Co; clinopyroxenitic garnets: 50-53 ppm Co; figure 6.4). The garnet in PGN319 has much higher Co content (101 ppm).

The pyroxenitic clinopyroxenes have high compatible element contents compared to the lherzolitic clinopyroxenes (318-573 ppm Ni; 16-50 ppm Co). The Sc (4-27 ppm) and V (92-212 ppm) content of the clinopyroxenite clinopyroxenes is lower than that of the websteritic clinopyroxenes (36-38 ppm Sc; 438-578 ppm V). The websterites have high Ti contents (2659-5219 ppm) in comparison to the other pyroxenites (74-727 ppm).

The orthopyroxene in the two websteritic samples (MIS438 and MIS439) have higher Co abundance's (99-108 ppm) than the peridotitic orthopyroxenes (figure 6.5). The Ni content of the orthopyroxene in MIS438 (517 ppm) is similar to that of the peridotitic orthopyroxenes, whereas the orthopyroxene in sample MIS439 is much higher (1080 ppm). The V content of the orthopyroxene in both the websteritic samples is much higher than those of the peridotitic suite (97 and 102 ppm), as is the Ti content (377 and 1174 ppm).

Rare Earth Elements (REE)

The garnets of the pyroxenite suite are similar to those of the lherzolite suite garnets in terms of both REE pattern and abundance (figure 6.14). They are LREE depleted (<1 times chondrite) and HREE enriched (~10 times chondrite) relative to chondrite. The websteritic garnets (MIS438, MIS439) are more HREE enriched (15-35 times chondrite) than the clinopyroxenitic garnets.

Two REE patterns are noted within the clinopyroxenes of the pyroxenite suite. The samples MIS438 and PGN319 form convex-upward REE patterns, with MREE's between 30-45 times chondrite, in comparison to the HREE's (<10 times chondrite). The second websteritic sample (MIS439) also has a convex-upward pattern, but with lower absolute REE concentrations than MIS438 and PGN319 (<7 times chondrite). These three clinopyroxenes are more Fe-rich than the other pyroxenitic clinopyroxenes (figure 5.12). The remaining clinopyroxenitic clinopyroxenes have flat to concave-upward patterns, being more enriched in LREE (10-15 times chondrite) than MREE (<10 times chondrite), figure 6.15.

Trace element abundance's relative to Primitive Mantle (PM)

The trace element content of the pyroxenitic and lherzolitic garnets are similar (figure 6.16 and 6.17), being enriched in the compatible elements Gd, Dy, Y, Er and Yb relative to the harzburgitic garnets. The negative Ti anomaly is not as marked as for the low-Ca harzburgites. The websteritic garnets

(MIS438, MIS439) are more enriched in the compatible elements Gd, Dy, Y, Er and Yb than the garnet-clinopyroxenite garnets. Whereas the lherzolitic garnets have lower Sc contents (5-7 times PM) than the harzburgitic garnets (10-30 times PM), the pyroxenitic garnets (apart from ARN028 and ARN031) have even lower Sc contents (1-5 times PM). The garnets in ARN028 and ARN031 have similar Sc contents to the harzburgites (14 times PM).

Table 6.1 Selected trace element abundances in garnet. Elemental abundance in ppm.

Suite	Low-Ca Harzburgite					High-Ca Harzburgite				Lherzolite				Clinopyroxenite		Websterite
Sample No	ARN007	ARN025	MIS401	PGN303	PGN314	ARN003	ARN004	ARN013	MIS417	MIS409	PGN307	PGN310	PGN337	ARN028	PGN320	MIS438
Sc	270	495	424	222	117	448	286	202	231	129	103	148	100	227	21	64
Ti	56	<25.62*	19	182	371	125	38	13	133	567	2241	1270	2850	537	385	921
V	176	319	153	297	269	288	297	167	233	106	355	344	290	538	67	132
Co	44	70	37	45	39	43	39	36	33	31	37	48	39	50	53	60
Ni	36	56	26	30	56	31	22	11	22	12	67	53	53	44	23	10.2
Rb	0.14	<0.74	0.13	1.5	<0.74	<0.055	<0.055	0.06	0.079	0.24	<0.74	<0.74	<0.74	<0.74	1.1	<0.74
Sr	1.2	1.8	2.3	0.75	0.57	1.8	1.8	0.18	0.71	0.22	0.87	0.82	0.54	<0.37	0.42	<0.367
Y	0.65	<0.71	1.3	2.4	2.1	35	1.2	0.09	1.4	8.6	4.1	14	12	9.6	2.3	47
Zr	32	53	5.7	27	29	107	3.3	0.70	4.2	4.7	15	54	27	1.9	1.2	26
Nb	0.33	0.50	0.19	0.84	<0.22	1.3	0.090	0.057	0.10	0.34	0.50	0.39	0.44	0.77	0.31	<0.224
Ba	0.50	2.78	0.23	2.86	<1.61	0.44	1.1	0.30	0.42	0.19	<1.61	1.6	<1.61	<1.61	<1.61	<1.611
La	0.13	0.92	0.73	0.52	0.44	0.25	0.67	0.15	0.33	0.05	<0.43	<0.43	<0.43	<0.43	<0.43	<0.433
Ce	1.3	2.3	5.5	2.85	0.44	2.0	5.4	0.32	2.6	0.15	0.78	0.66	0.16	0.27	0.21	0.69
Nd	5.2	9.4	5.4	3.32	1.4	7.7	6.2	0.47	6.0	0.27	2.19	2.44	0.75	0.54	0.87	1.1
Sm	3.4	5.1	0.63	0.98	0.50	5.5	0.92	0.17	1.3	0.36	0.77	2.1	0.54	<0.26	<0.26	1.3
Eu	0.94	1.3	0.15	<0.54	0.58	2.4	0.25	<0.051	0.30	0.24	<0.54	1.1	<0.54	<0.54	<0.54	0.9
Gd	2.2	3.6	0.42	0.67	0.85	10.2	0.49	0.17	0.62	1.2	0.96	3.2	1.3	<0.41	0.57	4.8
Dy	0.39	0.68	0.39	1.2	0.79	8.8	0.16	0.11	0.32	1.8	0.93	3.0	2.1	1.7	0.80	8.0
Er	<0.054	0.66	0.13	<0.47	0.57	3.2	0.15	<0.054	0.20	1.2	0.65	1.3	1.4	1.3	0.53	5.2
Yb	0.16	0.30	0.46	0.88	0.56	2.2	0.26	0.05	0.71	1.3	<0.26	1.3	1.6	1.3	0.48	5.7
Hf	0.63	1.0	0.084	0.78	0.66	1.7	0.082	<0.052	0.11	0.24	0.75	0.78	0.86	<0.474	<0.47	0.64
Ta	0.026	0.11	0.037	<0.045	<0.045	0.13	0.025	<0.005	0.057	0.11	0.094	0.076	<0.045	0.13	0.11	<0.045
Th	<0.029	0.45	0.13	<0.29	<0.29	0.037	0.11	<0.029	0.12	<0.029	<0.29	<0.29	<0.29	<0.29	<0.29	<0.288
U	0.046	0.21	0.21	0.35	<0.17	0.11	0.067	0.03	0.05	0.076	<0.17	<0.17	<0.17	<0.17	<0.17	<0.169
Y/Nd	0.13	Y <LLD	0.24	0.74	1.5	4.6	0.20	0.19	0.23	32	1.9	5.9	16	18	2.7	42
Ti/Nd	11	Ti <LLD	3.5.	55	272	16	6.2	27	22	2100	1022	520	3798	991	444	818
Spot size **	5	4	5	4	4	5	5	5	5	5	4	4	4	4	4	4
Garnet REE pattern	MREE-enriched	MREE-enriched	Sinusoidal	MREE-enriched	LREE-depleted	MREE-enriched	Sinusoidal	MREE-enriched	Sinusoidal	LREE-depleted	LREE-depleted	LREE-depleted	LREE-depleted	LREE-depleted	LREE-depleted	LREE-depleted

* < Lower Limit of Detection ** Laser beam spot size during analysis

Table 6.2 Selected trace element abundances in clinopyroxene. Elemental abundance in ppm.

Suite	Lherzolite				Clinopyroxenite			Websterite
Sample No	ARN032	MIS409	PGN310	PGN337	ARN028	PGN319	PGN320	MIS438
Sc	102	31	18	12	4.9	27	4.6	36
Ti	97	941	402	1075	74	550	647	5219
V	223	271	328	254	93	212	145	438
Co	12	10.4	19	25	32	50	16	40
Ni	188	197	315	350	430	558	442	318
Rb	3.5	1.0	<0.74*	<0.74	<0.74	<0.74	<0.74	<0.74
Sr	1803	109	332	132	8.2	368	195	29
Y	8.6	<0.71	1.7	1.6	<0.714	1.4	<0.714	4.1
Zr	58	4.0	9.7	3.3	0.90	5.8	1.1	54
Nb	1.4	0.56	1.00	0.42	0.49	<0.22	0.72	<0.22
Ba	2.8	2.6	4.6	6.0	9.4	<1.61	2.9	<1.61
La	59	1.2	4.0	2.4	2.4	8.3	2.0	4.7
Ce	170	2.3	15	8.4	3.7	24	4.7	18
Nd	90	1.5	13	5.7	1.0	19	1.9	19
Sm	11	0.41	2.4	1.1	0.36	2.4	<0.261	5.3
Eu	2.7	<0.54	0.63	<0.54	<0.54	0.75	<0.54	1.3
Gd	5.9	0.59	1.4	0.71	<0.414	1.5	<0.414	3.9
Dy	2.8	<0.50	<0.50	0.55	<0.50	0.57	<0.50	1.8
Er	0.82	<0.47	<0.47	<0.47	<0.47	<0.47	<0.47	<0.47
Yb	0.66	<0.26	<0.26	0.53	<0.26	0.32	<0.26	0.36
Hf	2.0	<0.47	0.63	<0.47	<0.47	0.51	<0.47	2.5
Ta	0.15	<0.045	0.054	<0.045	0.082	<0.045	0.19	<0.045
Th	0.79	<0.29	<0.29	<0.29	<0.29	<0.29	<0.29	<0.29
U	0.35	<0.17	0.24	<0.17	<0.17	0.42	<0.17	<0.17
Spot size**	4	4	4	4	4	4	4	4

* < Lower Limit of Detection ** Laser beam spot size during analysis

Table 6.4 Selected trace element abundances in olivine. Elemental abundance in ppm.

Suite	Low-Ca Harzburgite				High-Ca Harzburgite				Lherzolite			
Sample No	ARN025	ARN026	PGN314	PGN317	ARN003	ARN005	ARN013	MIS417	ARN032	PGN306	PGN310	PGN316
Sc	<3.77*	<3.77	<3.77	<3.77	<3.77	<3.77	<3.77	<3.77	2.3	<3.77	<3.77	<3.77
Ti	<25.62	<25.62	<25.62	<25.62	<25.62	<25.62	<25.62	<25.62	16	<25.62	49	38
V	<32.07	<32.07	<32.07	<32.07	<32.07	<32.07	<32.07	<32.07	5.0	<32.07	<32.07	<32.07
Co	108	111	110	115	114	127	120	109	117	120	107	116
Ni	2298	2264	2510	2496	2521	2881	2868	2547	2061	2340	2414	2552
Rb	0.90	<0.74	2.2	<0.74	2.4	0.80	0.76	<0.74	0.11	1.0	<0.74	1.2
Sr	0.41	1.3	2.0	<0.37	<0.37	<0.37	<0.37	<0.37	1.2	0.59	<0.37	0.44
Y	0.077	<0.71	<0.71	<0.71	<0.71	<0.71	<0.71	<0.71	<0.064	<0.71	<0.71	<0.71
Zr	<0.21	0.65	<0.21	0.44	0.34	0.51	0.58	0.33	0.44	0.59	<0.21	0.63
Nb	1.5	<0.22	0.77	0.50	3.5	<0.22	0.69	0.39	5.9	1.1	0.31	<0.22
Ba	<1.61	2.6	11	<1.61	<1.61	2.1	<1.61	<1.61	1.6	<1.61	<1.61	<1.61
La	0.80	1.2	<0.43	<0.43	<0.43	<0.43	0.74	<0.43	0.50	<0.43	<0.43	0.75
Ce	0.20	0.22	0.84	0.15	0.23	0.16	0.24	<0.13	0.38	0.23	0.28	<0.13
Nd	<0.21	0.31	0.61	<0.21	0.43	0.34	0.61	0.24	0.27	<0.21	0.30	0.32
Sm	0.77	0.99	<0.26	0.65	0.60	1.01	1.0	<0.26	0.081	<0.26	<0.26	<0.26
Eu	<0.54	0.89	<0.54	<0.54	<0.54	<0.54	<0.54	<0.54	<0.051	<0.54	<0.54	0.54
Gd	0.70	<0.41	<0.414	<0.41	0.44	0.58	0.79	<0.41	0.078	<0.41	<0.41	<0.41
Dy	<0.50	0.70	<0.50	<0.50	0.79	0.76	1.3	<0.50	<0.056	<0.50	<0.50	<0.50
Er	0.48	0.59	<0.47	<0.47	<0.47	1.1	<0.47	<0.47	<0.054	<0.47	<0.47	0.71
Yb	0.31	0.41	<0.26	0.66	1.3	0.70	0.89	<0.26	0.34	<0.26	<0.26	0.63
Hf	<0.47	<0.47	<0.47	<0.47	<0.47	<0.47	<0.47	<0.47	<0.052	<0.47	<0.47	<0.47
Ta	0.13	0.068	0.088	0.065	0.32	0.17	0.25	0.10	0.31	0.10	0.066	0.16
Th	<0.29	<0.29	<0.29	<0.29	<0.29	<0.29	<0.29	<0.29	<0.029	<0.29	<0.29	<0.29
U	<0.17	<0.79	0.17	<0.17	<0.17	<0.17	<0.17	<0.17	<0.013	<0.17	0.20	<0.17
Spot size **	4	4	4	4	4	4	4	4	5	4	4	4

* < Lower Limit of Detection ** Laser beam spot size during analysis

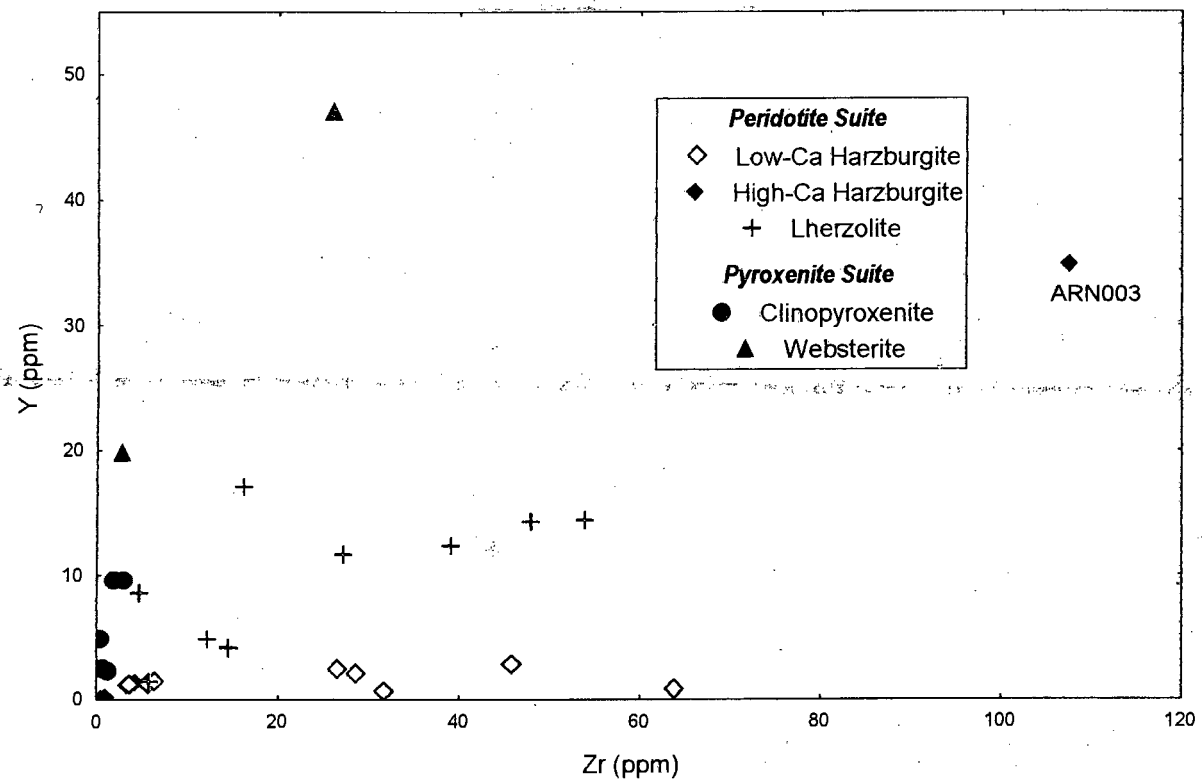

Figure 6.1 Y vs Zr in garnet. The pyroxenitic garnets have low Zr contents (0-26 ppm), whereas the peridotitic garnets have a wide range in Zr content (0-64 ppm). ARN003 has an exceptionally high Zr content (107 ppm). The harzburgitic garnets generally have lower Y contents than the lherzolitic and pyroxenitic garnets.

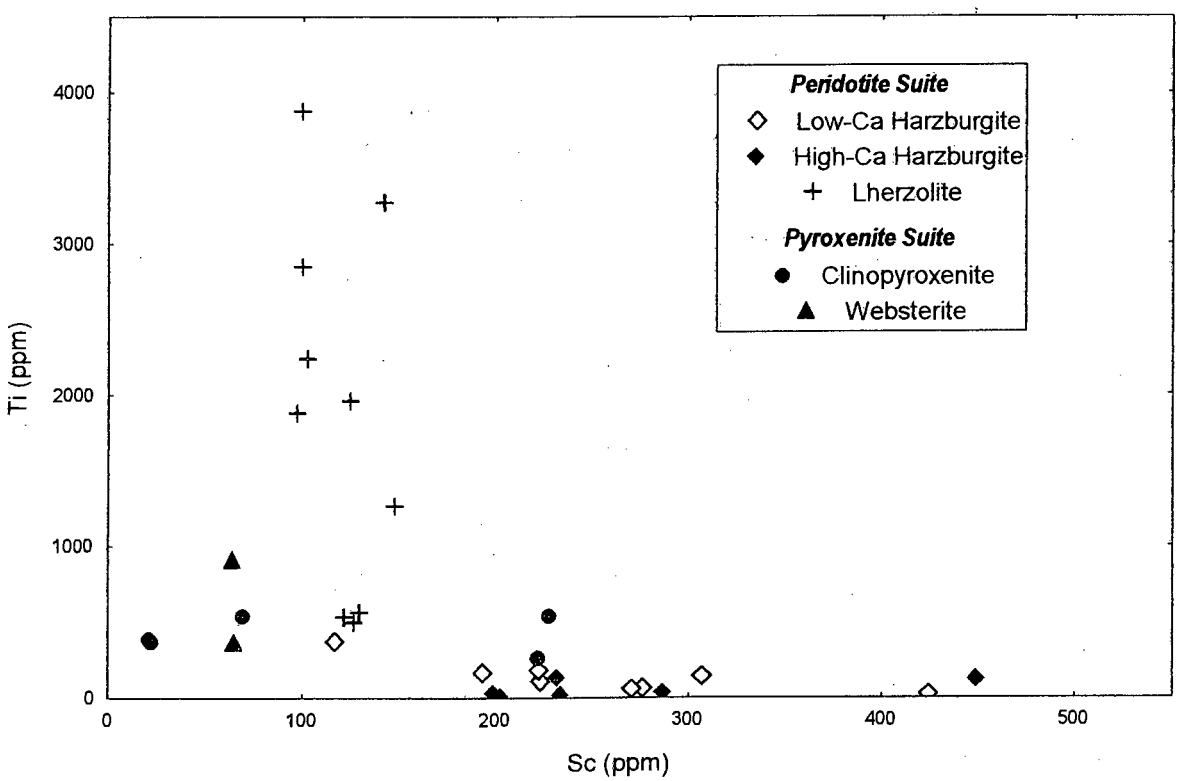

Figure 6.2 Ti vs Sc in garnet. The harzburgitic garnets have low Ti contents (<371 ppm), and a large range in Sc content (117-448 ppm).

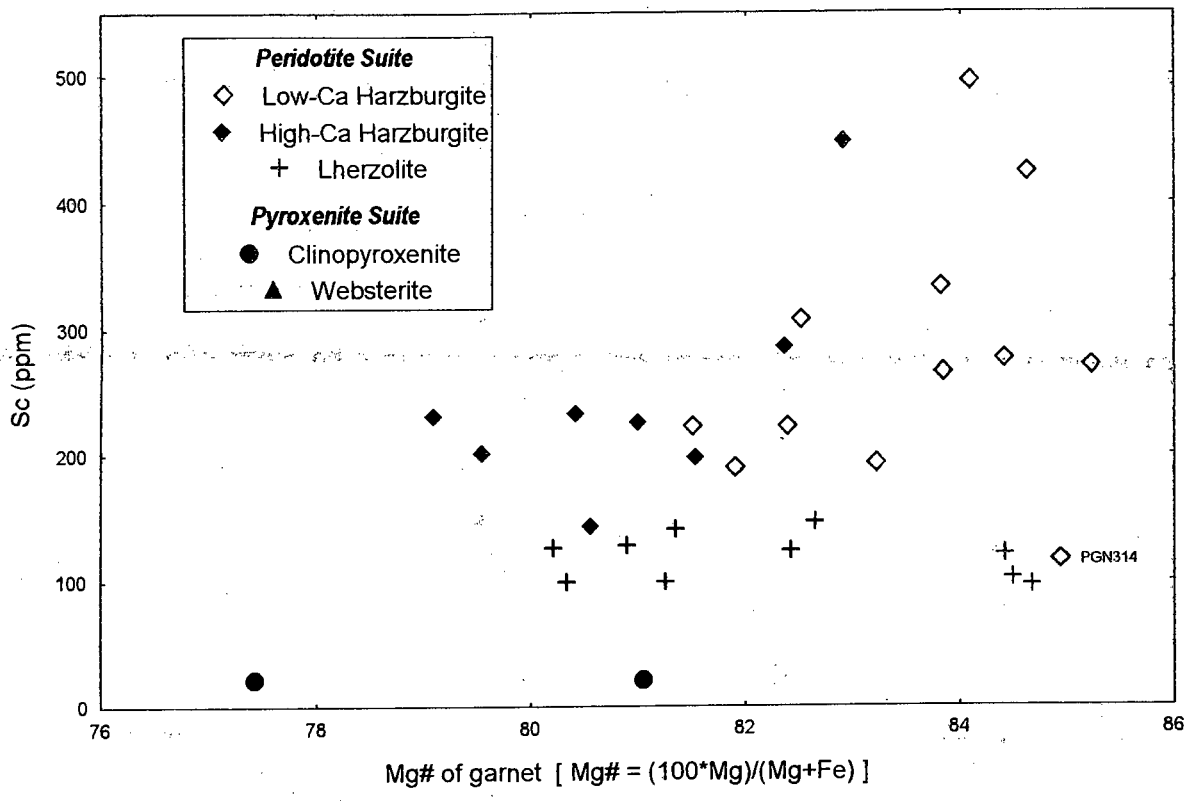

Figure 6.3 Sc vs Mg# in garnet. The harzburgitic garnets define a rough positive relationship between Mg# and Sc. Sc increases as Mg# increases. PGN314 has lower Sc contents than the other harzburgitic garnets (117 ppm), and lies off the positive trend.

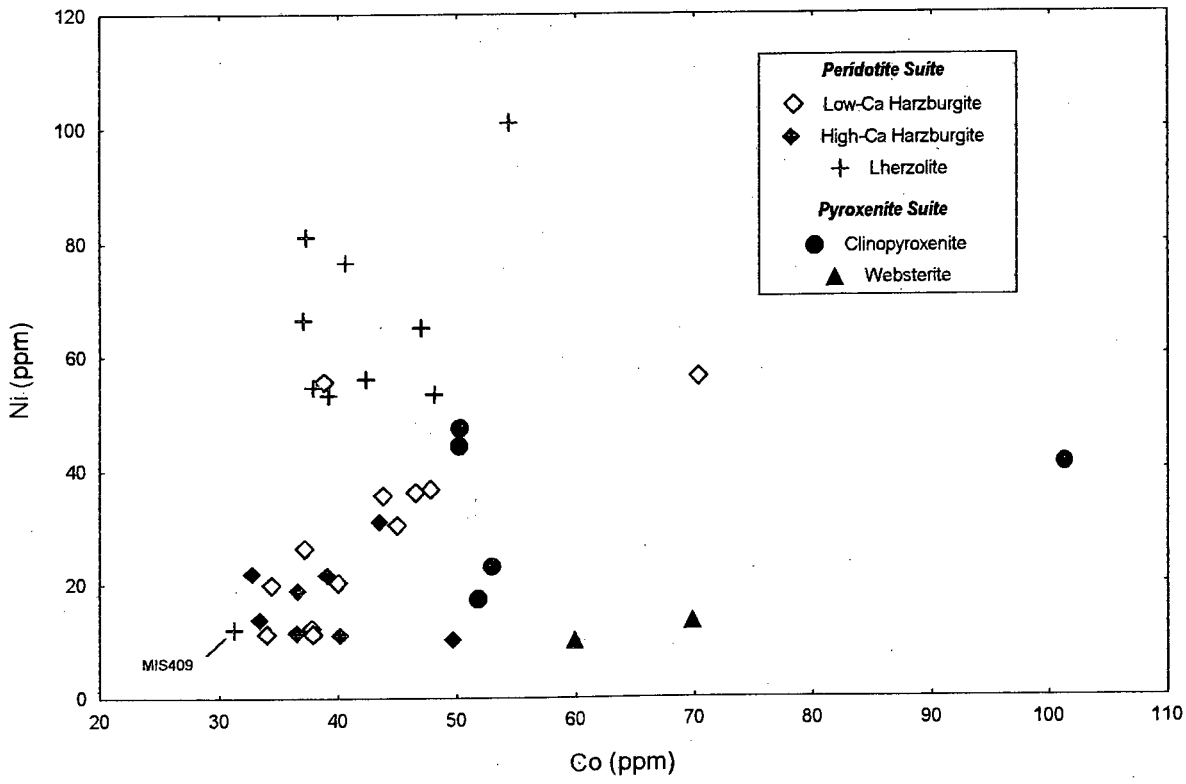

Figure 6.4 Ni vs Co in garnet. The lherzolitic garnets (apart from MIS409) have higher Ni contents (53-101 ppm) than the harzburgitic and pyroxenitic garnets (11-56 ppm). Whereas the pyroxenitic garnets contain similar Ni contents to the harzburgitic garnets, they have higher Co contents (50-101 ppm).

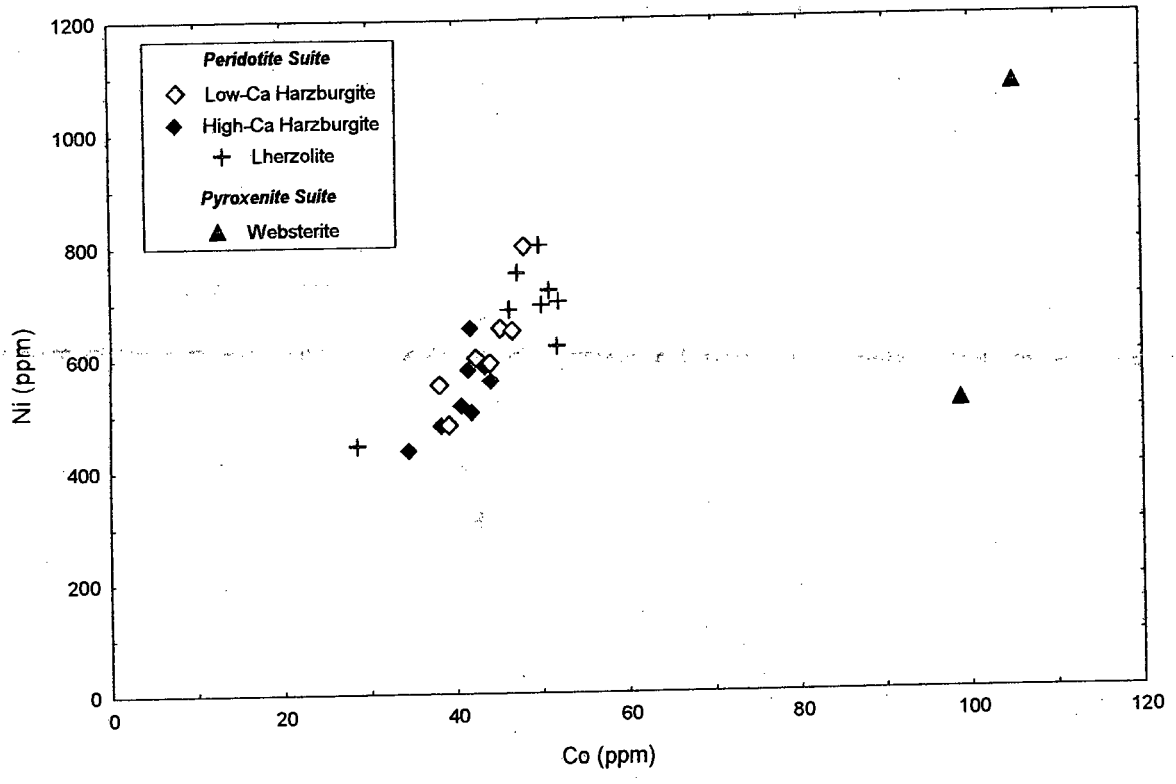

Figure 6.5 Ni vs Co in orthopyroxene. The websteritic orthopyroxenes have a higher Co content (99-105 ppm) than the peridotitic orthopyroxenes (28-52 ppm). The lherzolitic orthopyroxenes (apart from MIS409) have slightly higher Ni (620-800 ppm) and Co (56-62 ppm) contents than the harzburgitic orthopyroxenes (434-797 ppm Ni, and 34-48 ppm Co).

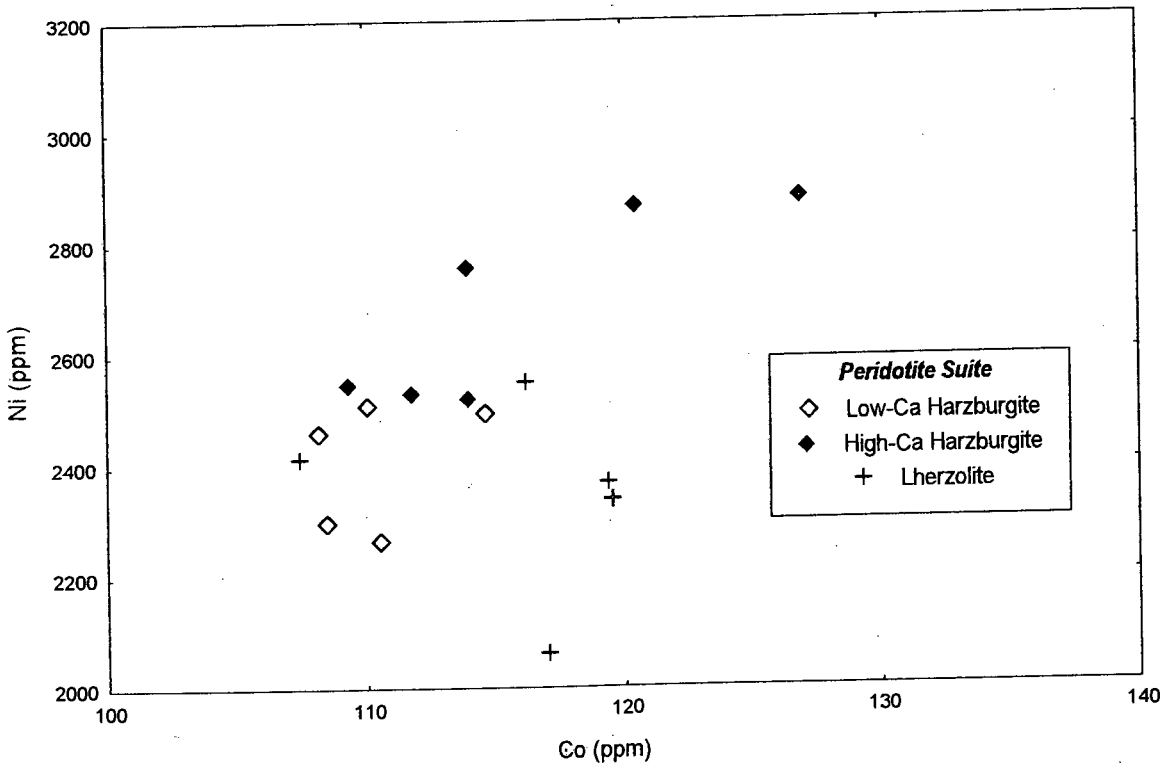

Figure 6.6 Ni vs Co in olivine. The trace element content in harzburgitic and lherzolitic olivine is very similar. The high-Ca harzburgites have a slightly higher Ni content (2521-2881 ppm) than the lherzolites and low-Ca harzburgites (2061-2552 ppm).

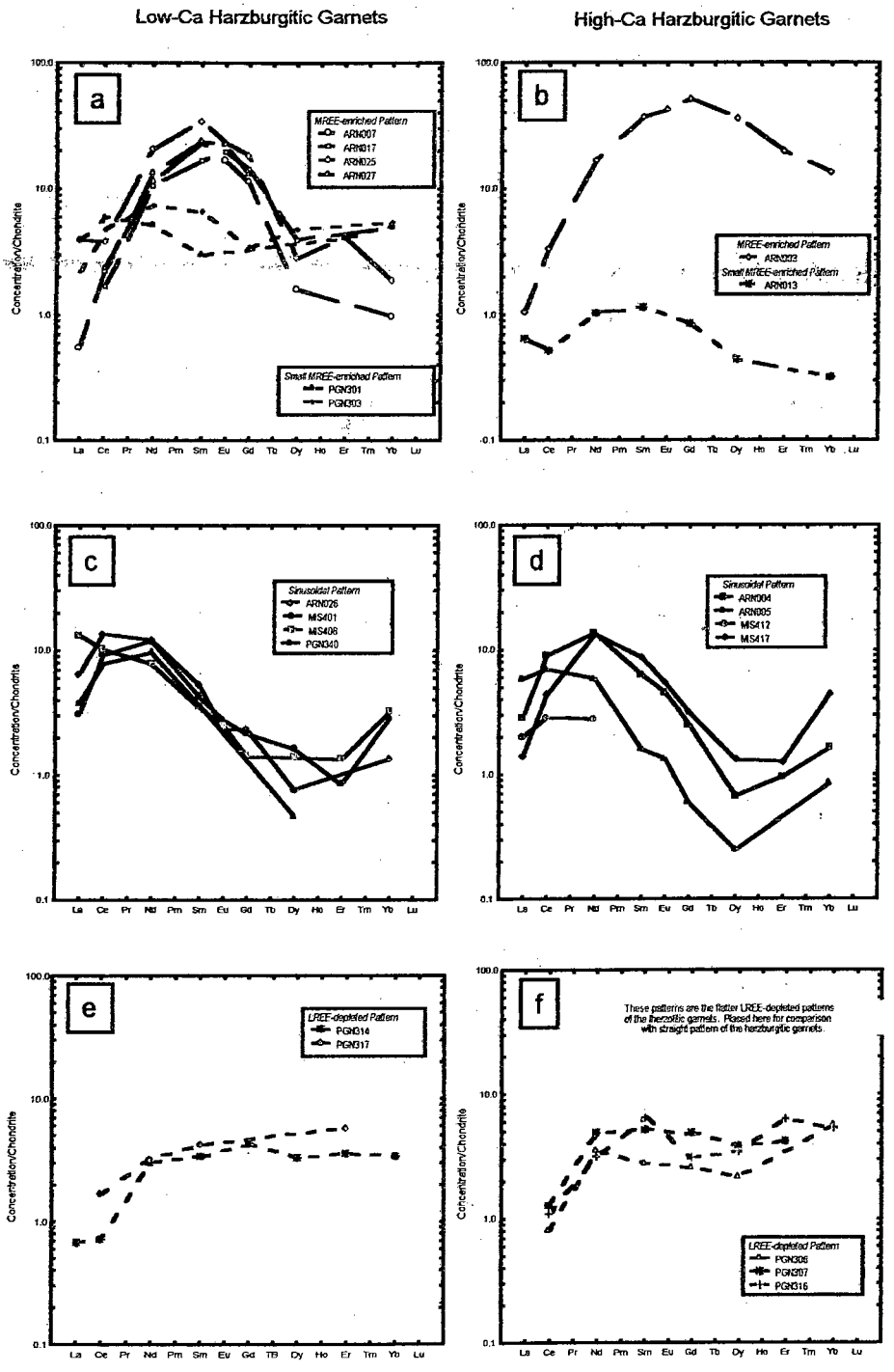

Figure 6.7 Chondrite normalised REE diagrams of harzburgitic garnets (a-e). The MREE-enriched (a and b) and sinusoidal REE patterns (c and d) are characteristic of the harzburgitic garnets. The straight pattern (e) is more alike the LREE-depleted pattern of the lherzolitic garnets (f).

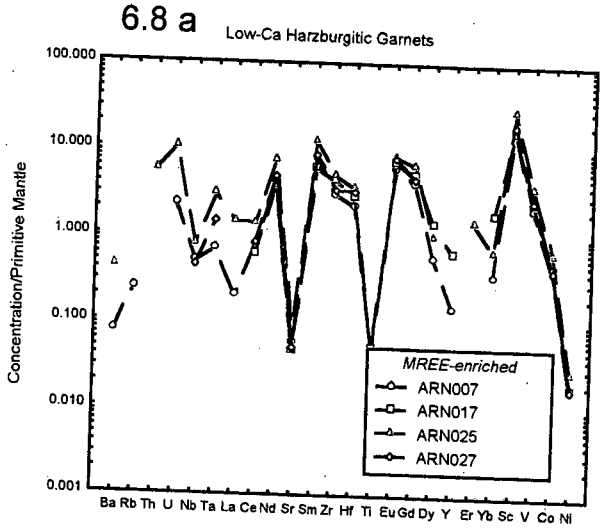

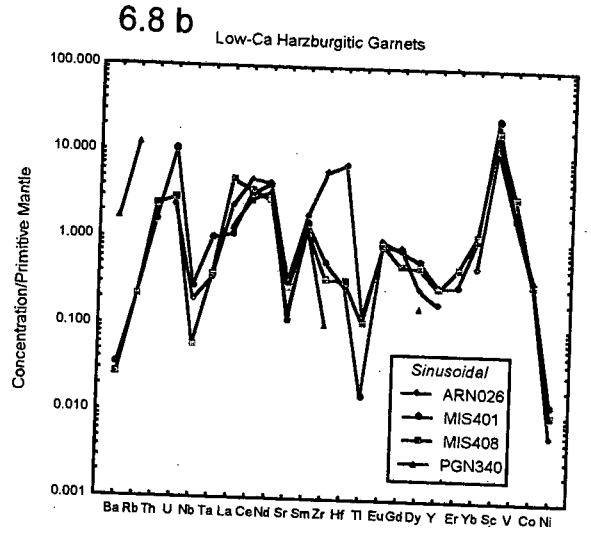

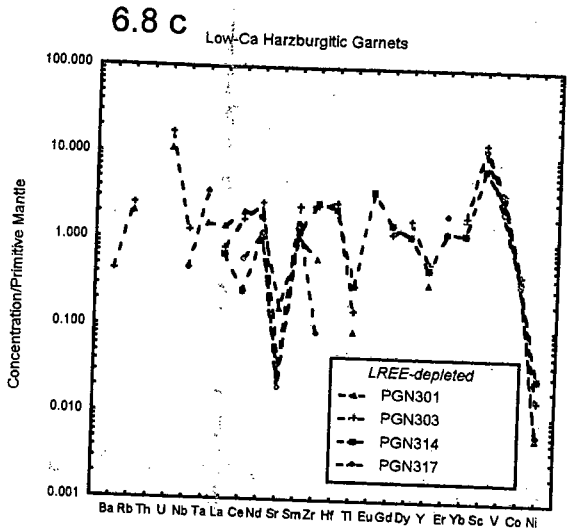

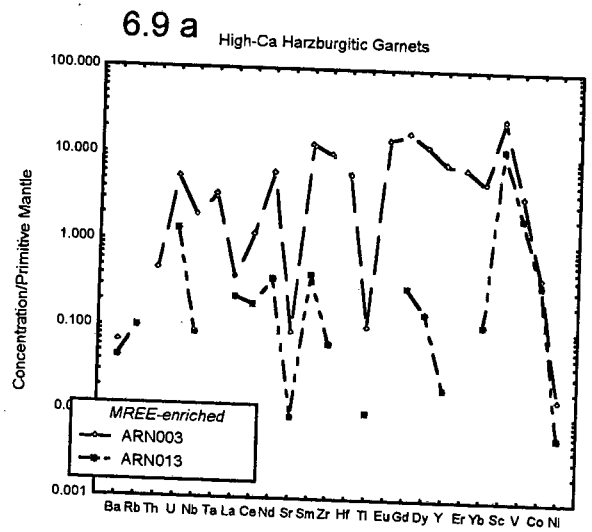

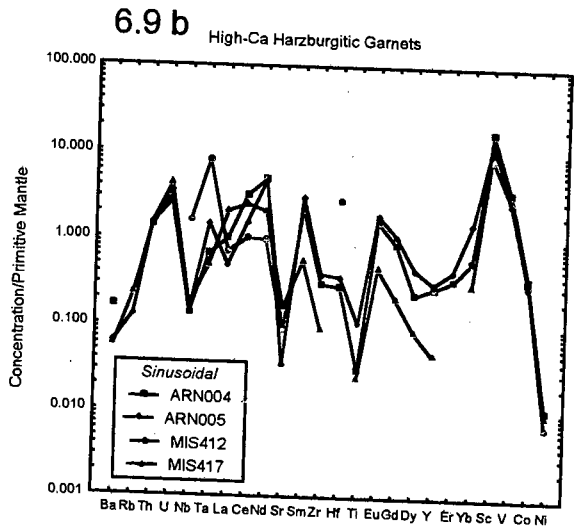

Figure 6.8 Primitive mantle normalised trace element diagrams for the low-Ca harzburgitic garnets. They have low Sr and Ti contents, and high Sc contents. The garnet in ARN026 is enriched in Zr and Hf relative to the other garnets.

Figure 6.9 Primitive mantle normalised trace element diagrams for the high-Ca harzburgitic garnets. The garnet in ARN003 is more enriched in trace elements than the other harzburgitic garnets.

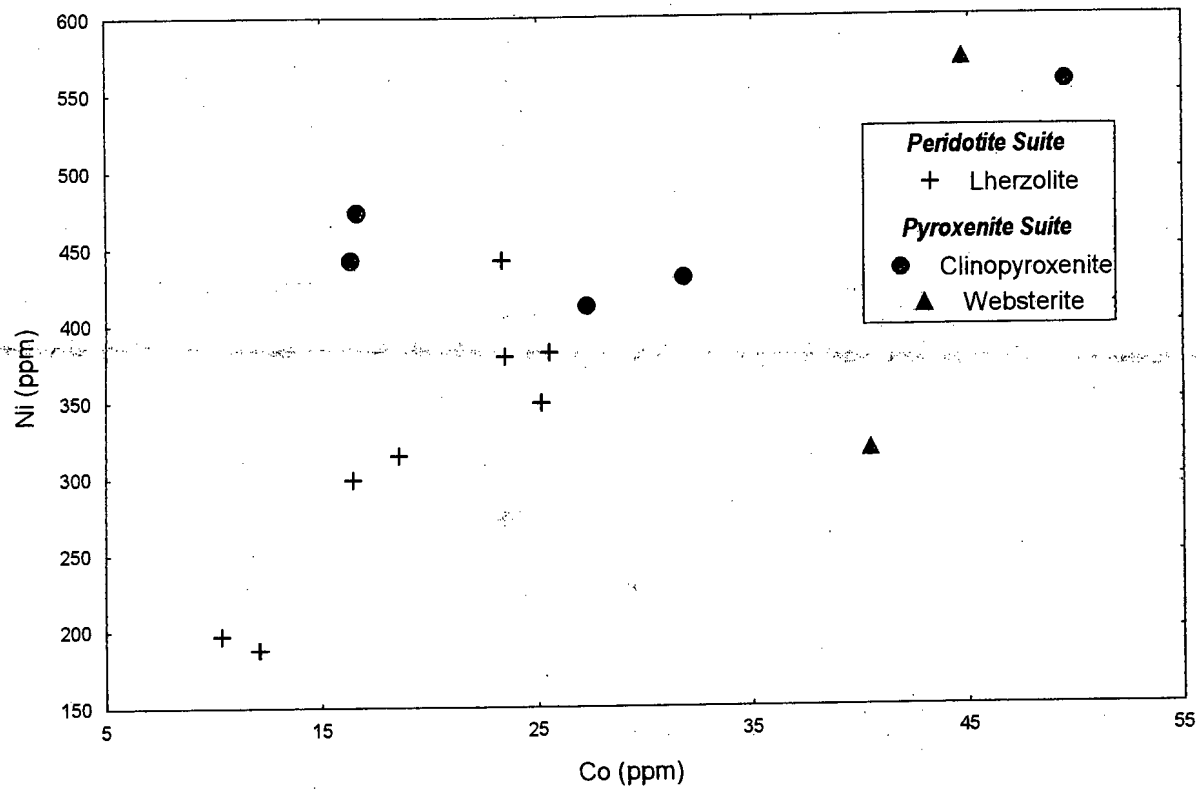

Figure 6.10 Ni vs Co in clinopyroxene. The lherzolitic clinopyroxenes have lower abundances of the compatible elements Co and Ni than the pyroxenitic clinopyroxenes.

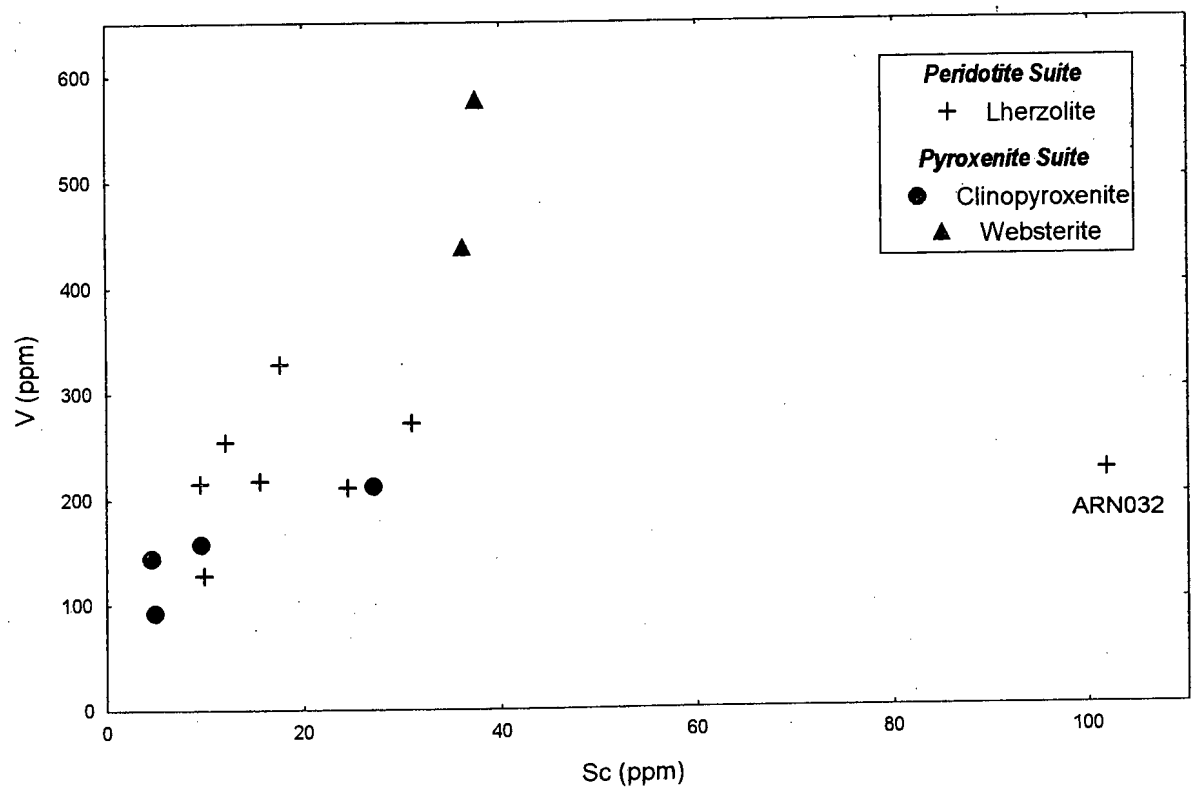

Figure 6.11 V vs Sc in clinopyroxene. The websterites are more enriched in V and Sc than the lherzolitic clinopyroxenes; and the lherzolitic clinopyroxenes are more enriched in these elements than the clinopyroxenes of the clinopyroxenite xenoliths. ARN032 is highly enriched in Sc (102 ppm).

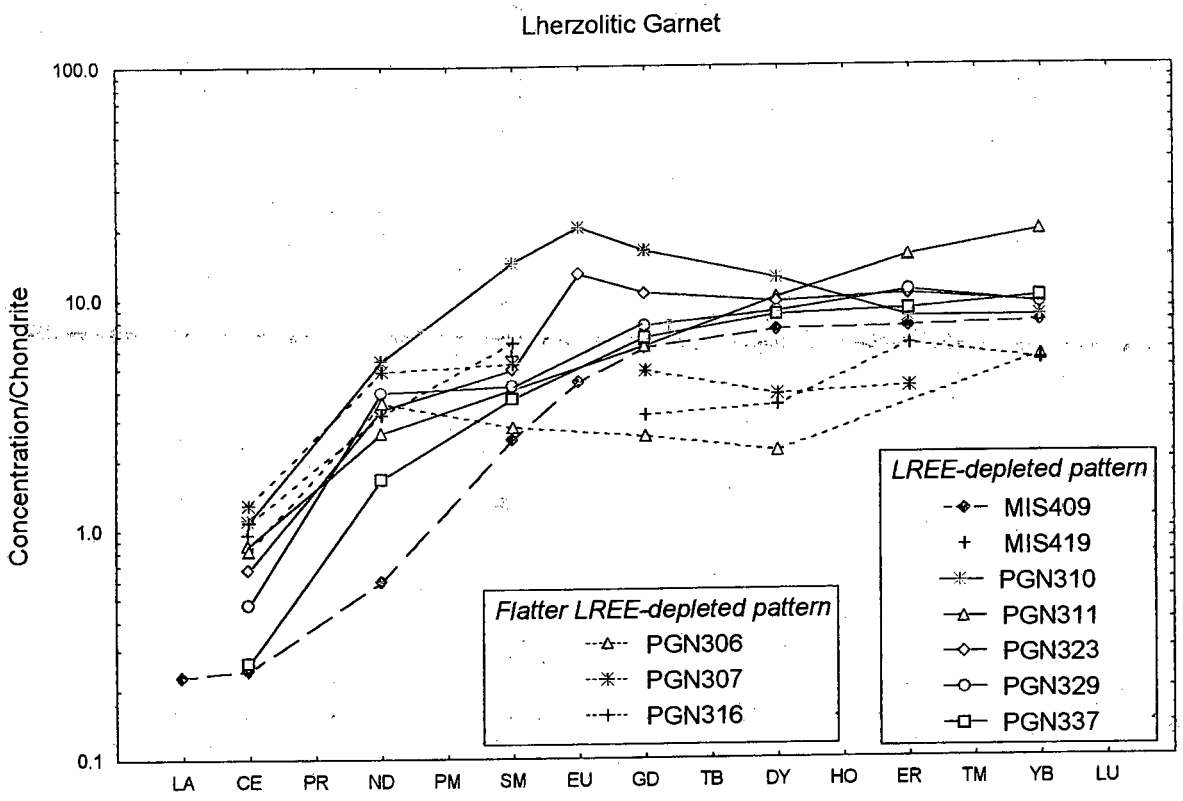

Figure 6.12 Chondrite normalised REE pattern for lherzolitic garnets. Lherzolitic garnets all have LREE-depleted patterns. The garnets in PGN306, PGN307 and 316 are slightly depleted in HREE's relative to the other lherzolitic garnets.

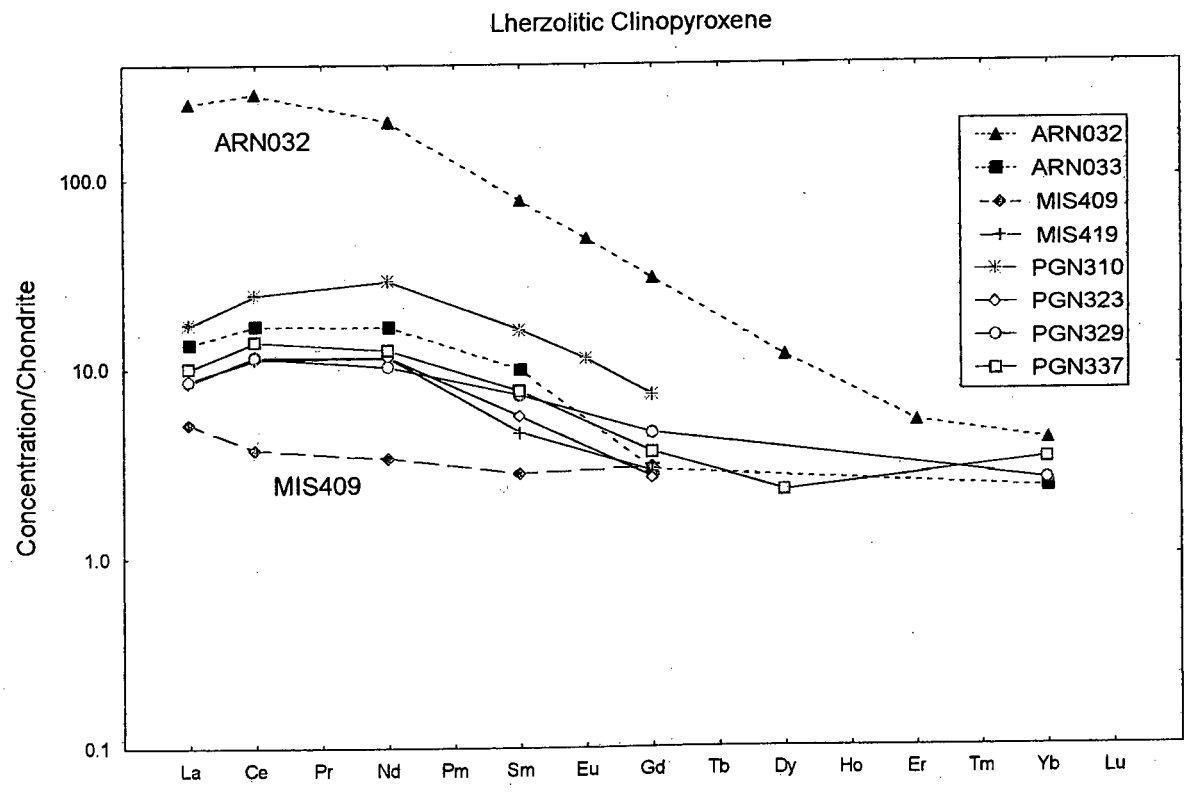

Figure 6.13 Chondrite normalised REE pattern for lherzolitic clinopyroxenes. The majority of the clinopyroxenes have a moderately LREE-enriched pattern. There are two exceptions: the clinopyroxene in ARN032 is highly enriched in LREE's, whereas that in MIS409 shows no enrichment in LREE's.

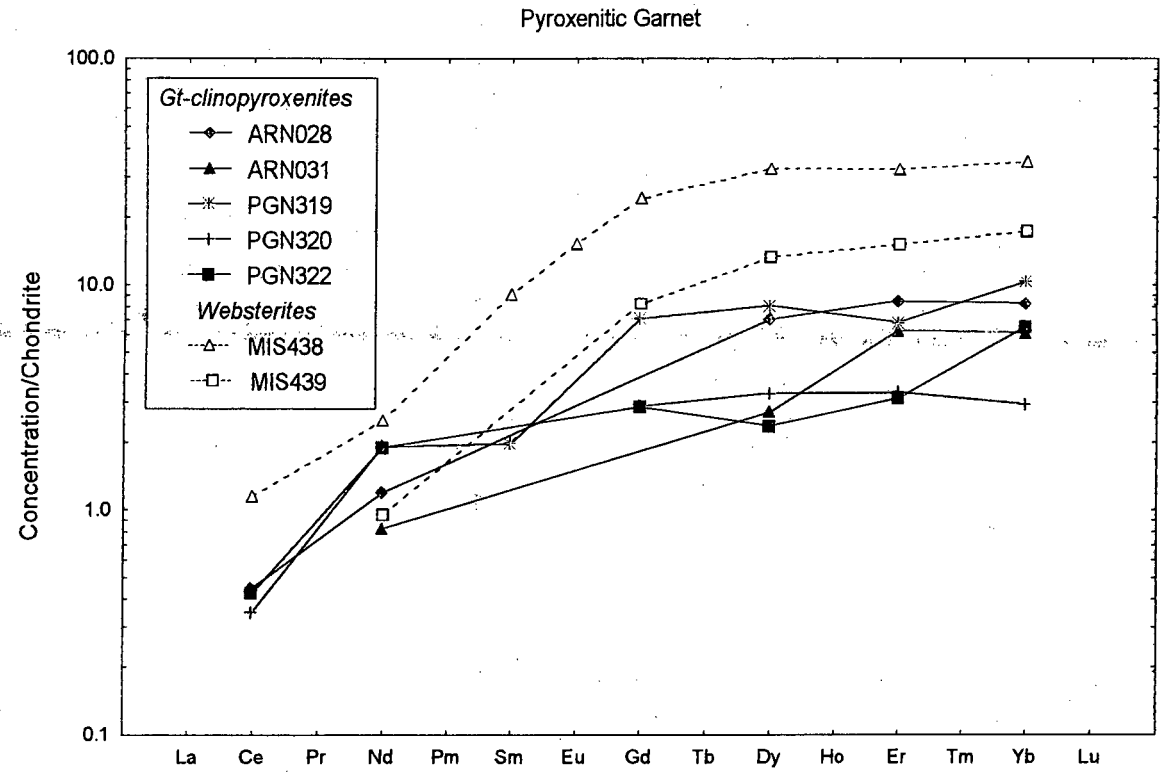

Figure 6.14 Chondrite normalised REE pattern for pyroxenitic garnets. The pyroxenitic garnets have LREE-depleted patterns like the lherzolitic garnets. The websterites are more enriched in HREE's than the other pyroxenitic garnets.

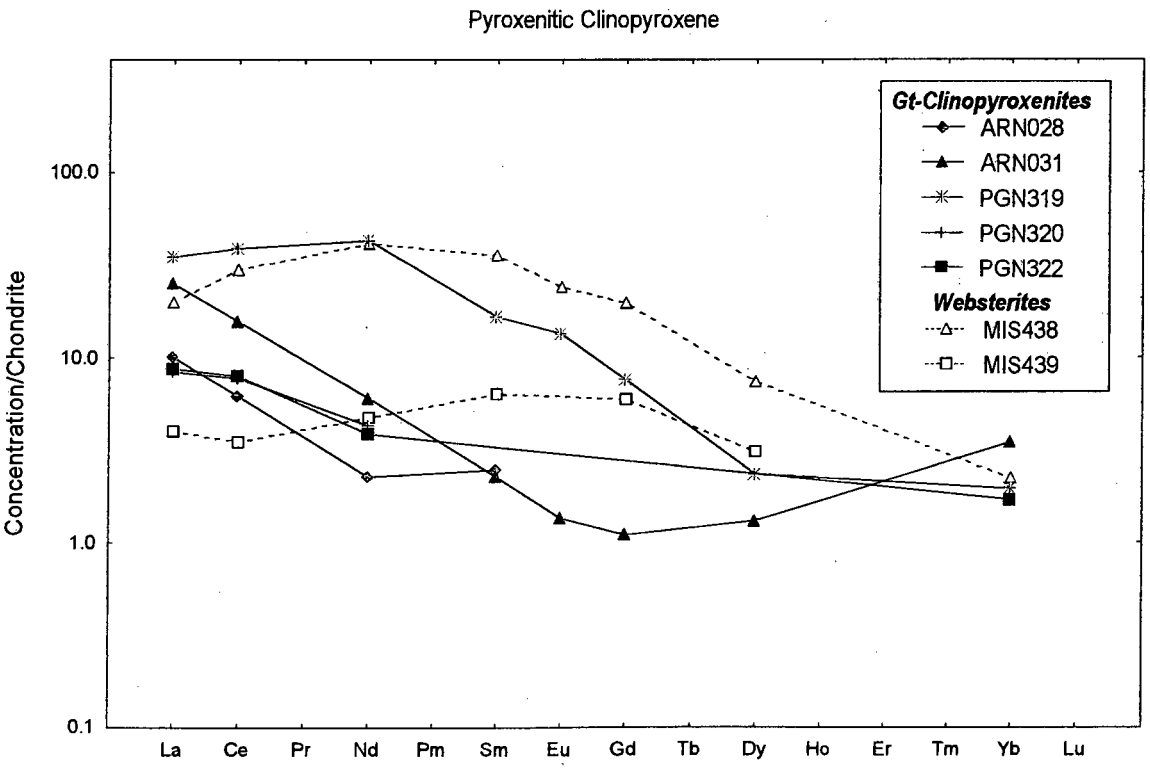

Figure 6.15 Chondrite normalised REE pattern for pyroxenitic clinopyroxenes. The three Fe-rich clinopyroxenes MIS438, PGN319, and MIS439 (figure 5.12) have convex-upward patterns, with high MREE content relative to LREE content. The remaining clinopyroxenitic clinopyroxenes have flat or concave-upward REE patterns.

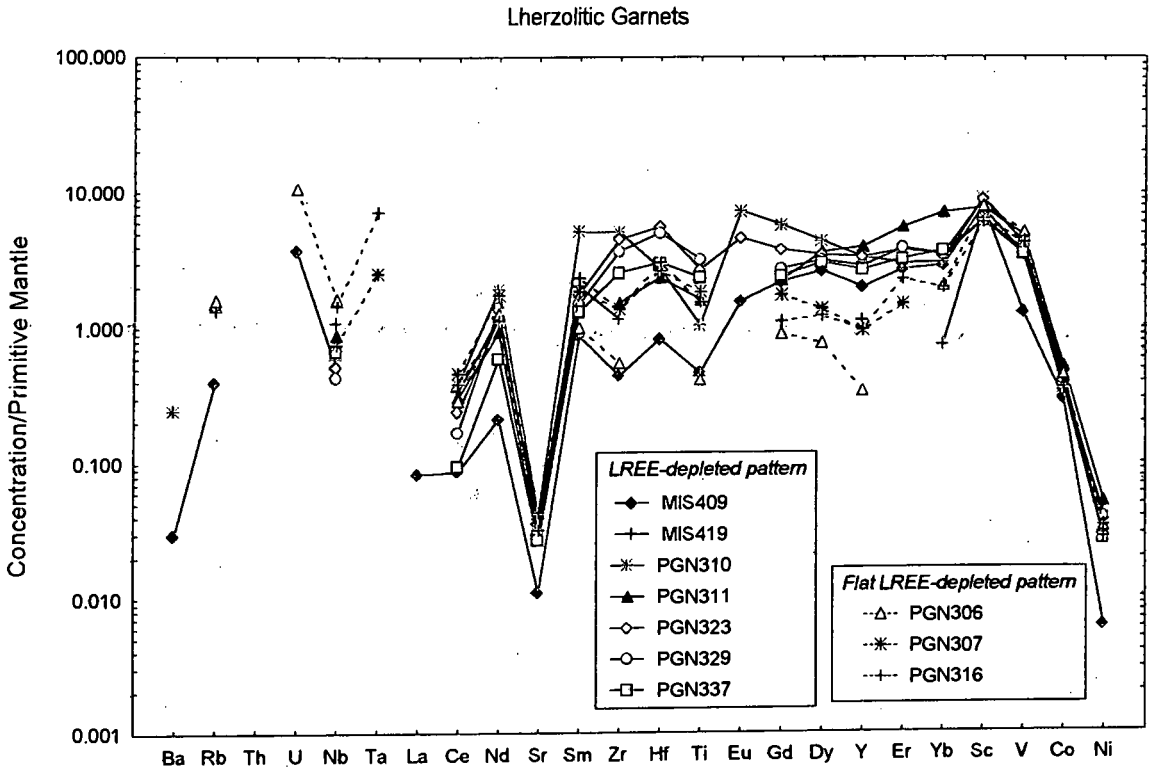

Figure 6.16 Primitive mantle normalised lherzolitic garnets. The lherzolitic garnets are more enriched in the compatible elements Gd, Dy, Y, Er and Yb relative to the harzburgites, but are depleted in Sc.

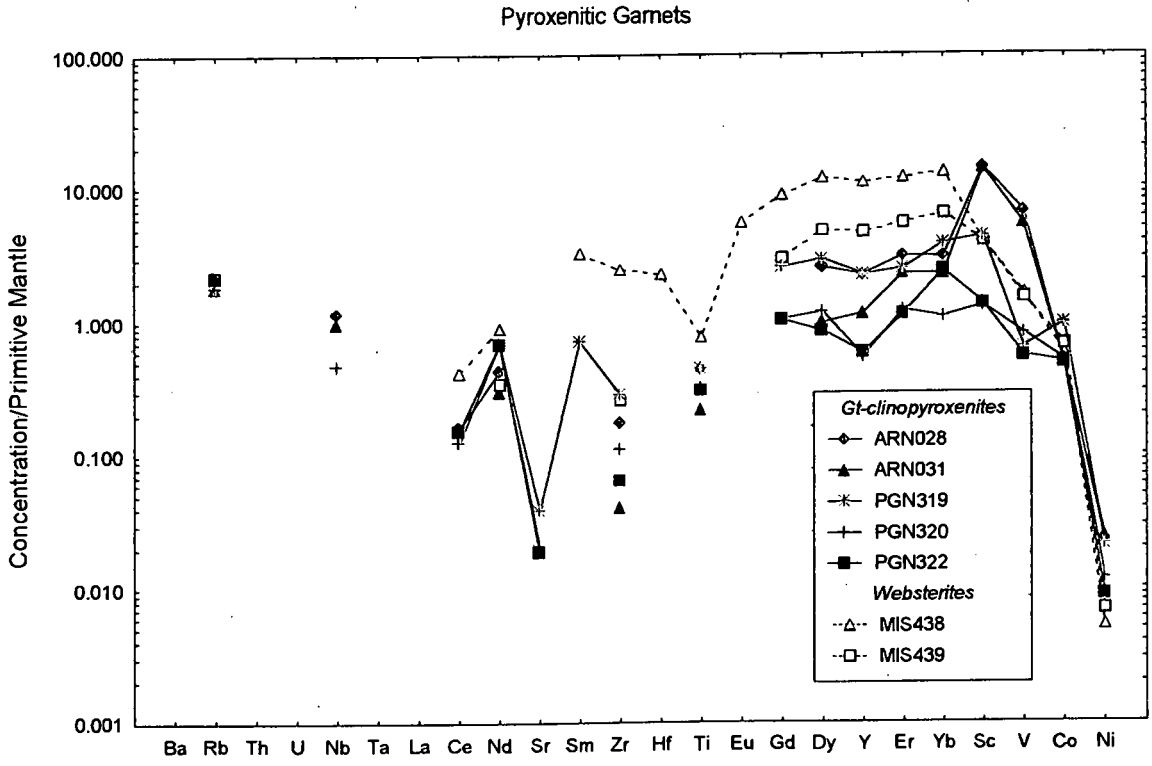

Figure 6.17 Primitive mantle (PM) normalised pyroxenitic garnets. The pyroxenitic and lherzolitic garnets have similar trace element compositions (figure 6.16). Apart from ARN028 and ARN031, the pyroxenitic garnets have lower Sc contents (1-5 times PM) than the lherzolitic garnets (5-9 times PM). The garnets in ARN028 and ARN031 have similar Sc contents (14 times PM) to the harzburgitic garnets (10-30 times PM).

Texture and Rare Earth Element (REE) patterns

Many of the pyroxenite samples in this study displayed disequilibrium textures such as garnet exsolution and recrystallization from clinopyroxene (ARN028 and ARN031). The clinopyroxene in ARN031 has a concave upward REE pattern of moderate light REE enrichment of La and Ce relative to the middle REE's (figure 6.15). Eclogitic clinopyroxenes from Bellsbank (South Africa) and Obanazhënnaya (Yakutia, Russia) analysed by Jerde et al. (1993) have a similar REE pattern to the pyroxenitic clinopyroxene in ARN031, the garnets were however more HREE enriched (>10 times chondrite). Jerde et al. (1993) suggested that the REE patterns in the Bellsbank and Obanazhënnaya clinopyroxenes reflect metastable partitioning of REE during exsolution processes. The clinopyroxene REE patterns of the recrystallized sample ARN031 may therefore be attributed to metastable conditions.

Partition coefficients - $D_{Zr}^{cpx/gt}$

van Achterbergh et al. (2001) suggested that $D_{Zr}^{cpx/gt}$ partition coefficients may be used to indicate the state of equilibrium between the two minerals. They noted that equilibrium garnet-clinopyroxene pairs generally had $D_{Zr}^{cpx/gt} < 1.9$ and "most commonly" $D_{Zr}^{cpx/gt} < 0.2$. Gallahan and Nielsen (1992) have however shown that partition coefficients, particularly those of clinopyroxene are pressure, temperature and compositionally dependant. This study agrees, suggesting that the partitioning of Zr between garnet and clinopyroxene is more likely related to compositional or temperature effects than the state of equilibrium between the minerals, as shown below:

Table 6.5 shows that all but one of the lherzolitic samples have $D_{Zr}^{cpx/gt} < 0.2$ (MIS409 has a $D_{Zr}^{cpx/gt}$ of 0.85), the clinopyroxenites have $0.4 < D_{Zr}^{cpx/gt} < 2$ and websterites have $D_{Zr}^{cpx/gt} > 2$. The major element chemistry of the three different suites of xenoliths are markedly different, suggesting that the $D_{Zr}^{cpx/gt}$ is compositionally dependant. In particular, it appears to be related to the Cr_2O_3 content in garnet as $D_{Zr}^{cpx/gt}$ decreases with an increase in Cr_2O_3 (figure 6.19). In addition, according to van Achterbergh et al. (2001), the high $D_{Zr}^{cpx/gt}$ (>2) of the websteritic samples (MIS438 and MIS439) would suggest they are out of equilibrium, having a $D_{Zr}^{cpx/gt} > 1.9$. This would contradict the textural evidence. Both websterites have well equilibrated granoblastic textures with straight grain boundaries and 120° grain intersections, whereas many of the xenoliths with $D_{Zr}^{cpx/gt} < 1.9$ have poikilitic textures (MIS409, PGN323) or show evidence of recrystallization (ARN028).

The T_{Ni} temperatures obtained for the xenoliths also indicates that the $D_{Zr}^{cpx/gt}$ may be temperature dependant. Those xenoliths with high temperatures (1052-1185°C) have $D_{Zr}^{cpx/gt} < 0.18$, whereas

those xenoliths with lower temperatures of equilibration have higher $D_{Zr}^{cpx/gt}$ (0.48-2.49 at 664-1015°C). The findings of Grégoire et al. (in press, 2001) support this correlation with temperature. Within their sample suite which included both sheared and granular peridotites, they found that the lower temperature lherzolite xenoliths (841-999°C) had higher $D_{Zr}^{cpx/gt}$ values (1.25-1.82) than the xenoliths equilibrated at higher temperatures, two of which are deformed peridotites (1076-1306°C; $D_{Zr}^{cpx/gt}$ 0.39-0.49).

Table 6.5 Calculated Zr partition coefficients between garnet and clinopyroxene

Sample Number	Zr - Gt	Zr - Cpx	$D_{Zr}^{cpx/gt}$	Cr_2O_3 in garnet (wt%)	Temperature (°C) *	Rock Suite
MIS409	4.7	4.0	0.853	3.64	692	Lherzolite
MIS419	12.3	0.56	0.046	5.35	1208	Lherzolite
PGN310	54	9.7	0.180	7.19	1053	Lherzolite
PGN323	48	2.6	0.054	5.06	1070	Lherzolite
PGN329	39	3.5	0.090	4.45	1185	Lherzolite
PGN337	27	3.3	0.120	3.39	1052	Lherzolite
ARN028	1.9	0.90	0.484	4.17	994	Gt-Clinopyroxenite
ARN031	0.43	0.49	1.153	1.72	1015	Gt-Clinopyroxenite
PGN319	3.0	5.8	1.932	0.65	971	Gt-Clinopyroxenite
PGN320	1.2	1.1	0.951	2.29	824	Gt-Clinopyroxenite
PGN322	0.69	0.93	1.362	2.13	763	Gt-Clinopyroxenite
MIS438	26	54	2.067	0.44	664	Websterite
MIS439	2.8	6.8	2.488	0.27	712	Websterite

* Temperature obtained using T_{Ni} (Chapter 7).

Conclusion

The textural evidence of the clinopyroxenites supports the theory by Jerde et al. (1993) that the unusual REE pattern in clinopyroxene may be due to partial re-equilibration, whereas the textural evidence of the websterites contradicts the suggestion by van Achterberg (2001) that mineral pairs with $D_{Zr}^{cpx/gt}$ >2 are not in equilibrium. The $D_{Zr}^{cpx/gt}$ appears to be dependant on either temperature or composition (or both), rather than a test of elemental equilibration between minerals.

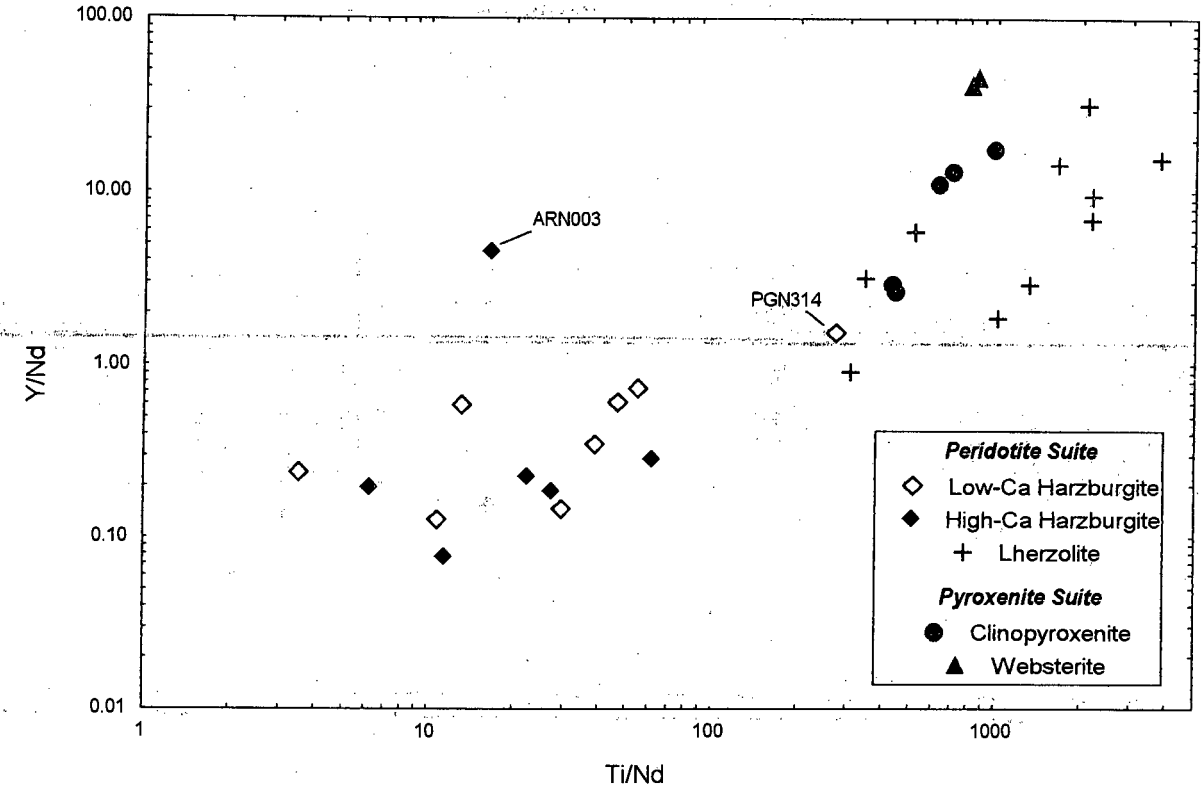

Figure 6.18 Ti/Nd vs Y/Nd in garnet. Harzburgitic garnets have lower Ti/Nd and Y/Nd ratios than the lherzolitic and pyroxenitic garnets.

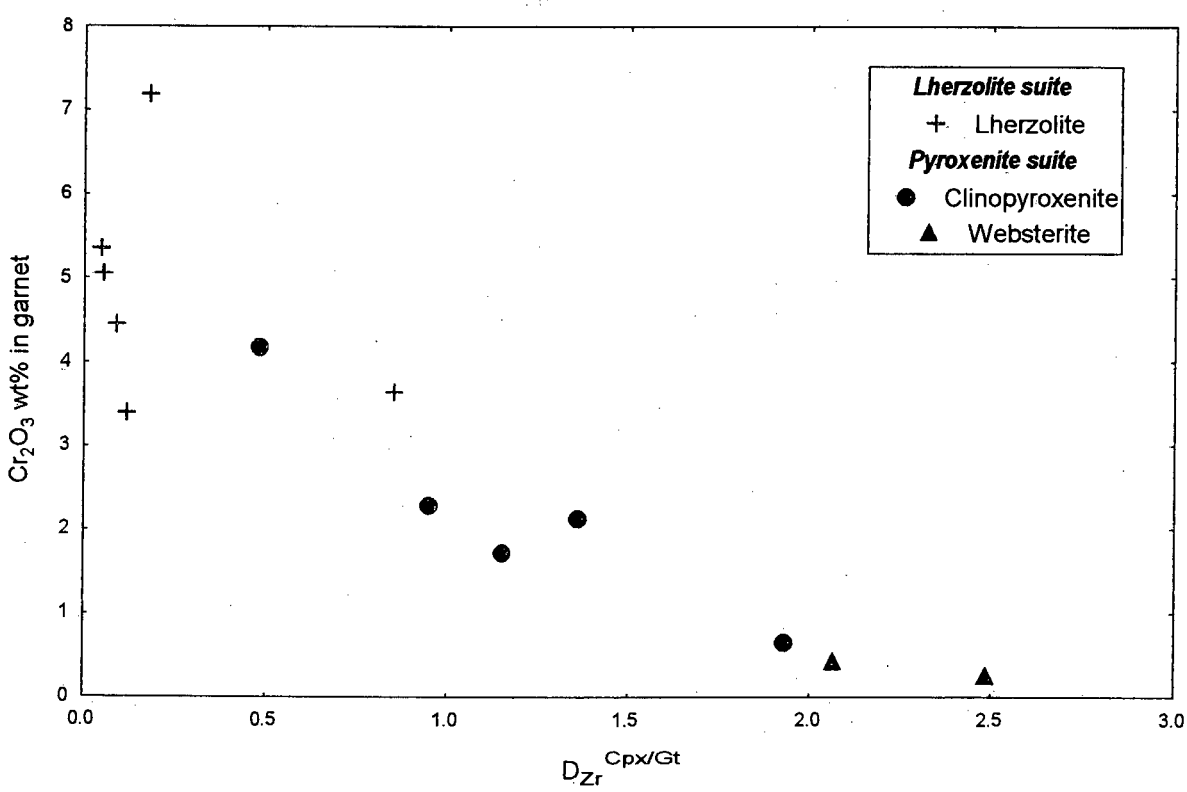

Figure 6.19 Cr_2O_3 (wt%) vs $D_{Zr}^{cpx/gt}$. The $D_{Zr}^{cpx/gt}$ ratio is compositionally dependant on Cr_2O_3 content within garnet: $D_{Zr}^{cpx/gt}$ decreases with an increase in Cr_2O_3 in garnet.

Garnet REE patterns

MREE-enriched REE pattern in harzburgitic garnets

The LREE depleted REE pattern of the lherzolite and pyroxenite garnets are the most common REE pattern noted in garnets, and are believed to reflect equilibrium conditions (Hoal et al., 1994). The MREE-enriched and sinusoidal REE patterns noted in the harzburgitic garnets have been well documented in numerous mantle derived sub-calcic garnets and garnets included in diamonds (Shimizu, 1975; Nixon et al., 1987; Hoal et al., 1994; Shimizu and Sobolev, 1995; Stachel et al., 1999; Stiefenhofer et al., 1999). The "sinusoidal" REE pattern in garnet discussed by Hoal et al. (1994) has a peak around Sm, more alike the MREE-enriched than the sinusoidal REE pattern described in this study. REE patterns from garnet inclusions in diamond have sinusoidal REE patterns that peak around Nd, similar to the sinusoidal pattern described in this study (Shimizu and Richardson, 1987).

Various suggestions have been proposed for the formation of the MREE-enriched REE pattern in the harzburgitic garnets. Most authors agree that the MREE-enriched pattern reflects a state of disequilibrium, and are related to partial re-equilibration with melt. Shimizu and Sobelev (1977) suggest that the disequilibrium may be due to rapid crystal growth relative to the rate of diffusive mass transport in the melt present, causing elevated incompatible trace element concentrations in the crystal relative to the equilibrium value. Hoal et al. (1994) suggest that the MREE-enriched REE pattern may be attributed to partial re-equilibration of the REE with LREE enriched metasomatic agents (figure 6.20). They suggest that the different partition coefficients for the LREE, MREE and HREE (K_D<0.1, 0.1<K_D<1.0 and K_D >1 respectively; Shimizu and Kushiro, 1975) may affect the rate of diffusion of the REE. They therefore propose that the LREE, MREE and HREE reach equilibrium at different times: the HREE's taking longer to re-equilibrate than the LREE's, thereby causing the MREE-enriched pattern (figure 6.7). Griffin et al. (1999b) however question how the LREE's, with a larger radius could have a faster rate of diffusion than the relatively smaller HREE's. Griffin et al. (1999b) suggest that the MREE-enriched pattern reflects a partial re-equilibration state of the harzburgitic garnets with a carbonatitic melt. The low HREE and enrichment in MREE's reflect the steep chondrite-normalised pattern of carbonatitic melts. The LREE's have a larger ionic radii (La^{3+}: 1.26Å) than the HREE's (Lu^{3+}: 1.05Å). The LREE's therefore typically replace Ca^{2+} (1.2Å) in the garnet structure. Due to the Ca-poor nature of the harzburgitic garnets, fewer sites are available for LREE substitution. Re-equilibration of the LREE's therefore lag behind that of the MREE and HREE's, causing the MREE-enriched pattern.

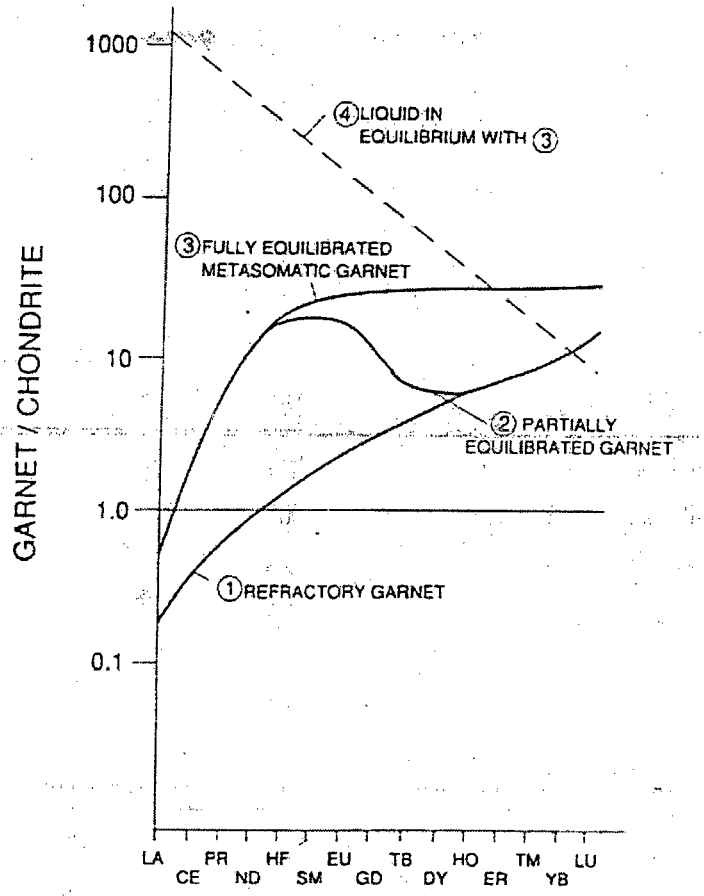

Figure 6.20 Schematic model by Hoal et al. (1994) to account for the MREE-enriched patterns noted in numerous sub-calcic garnets and garnet inclusions in diamond. Interaction of melt (4) with refractory garnet (1) produces a partially equilibrated garnet (2). If process had continued to completion, garnets with REE patterns of (3) would result.

Whereas both Hoal et al. (1994) and Griffin et al. (1999b) propose partial re-equilibration with a melt for the formation of the MREE-enriched pattern, the mechanism proposed by Griffin et al. (1999b) is favoured as the relation between diffusion rate and partition coefficient (Hoal et al., 1994) is not well understood. The intuitive observation by Griffin et al. (1999b) that the larger LREE's would have a slower rate of diffusion than the HREE's would nullify the argument by Hoal et al. (1994).

Interaction of the mantle beneath the Lac de Gras region with a LREE enriched fluid during the Archean is likely. Two regions of carbonatite magmatism of Archean age have been mapped within the Slave craton alone (Villeneuve and Relf, 1998). The extreme LREE enrichment in the clinopyroxene of ARN032 (figure 6.13) is likely to be evidence of interaction with a LREE enriched fluid, whether it be carbonatitic, or from metasomatic agents or from proto-kimberlite interaction.

Sinusoidal and LREE depleted REE patterns in harzburgitic garnets

Whereas numerous suggestions have been proposed for the MREE-enriched pattern, none have been proposed for the formation of the sinusoidal REE pattern. An overlay of the LREE-depleted patterns in the harzburgitic and lherzolitic garnets with the sinusoidal REE pattern of the harzburgitic garnets produced a spiralling pattern pivoting around the MREE's (figure 6.21). It would appear that as the LREE content decreases, the HREE content increases.

One possible mechanism for this change in REE abundance could be melt interaction. But by the mechanisms described by Hoal et al. (1994) and Griffin et al. (1999), melt interaction with low-Ca harzburgitic garnets would produce MREE-enriched patterns if arrested before equilibrium is reached. Yet the sinusoidal pattern is LREE enriched relative to both the MREE and HREE, hence an alternative mechanism needed to be sought to create, or preserve, the sinusoidal REE pattern in the harzburgitic garnets.

Exsolution of pyrope and pyroxene from majorite is a mechanism that may account for the original sinusoidal pattern, and provide a means of preserving the sinusoidal pattern in harzburgitic garnets, as described below:

The LREE enrichment relative to MREE and HREE content in the harzburgitic garnets with a sinusoidal pattern is very similar to the clinopyroxene REE pattern (figure 6.22). This raises the possibility of a relation between the two patterns via majorite, as majorite is a solid solution between garnet and pyroxene. Whereas majorite retains a garnet structure, it contains a large proportion of pyroxene in solid solution as pyroxene becomes more soluble in the garnet structure with increasing depth.

The mineral/melt partition coefficients of majorite are more alike those of clinopyroxene, than those of pyrope (Xie et al., 1995; table 6.6). This characteristic has an interesting implication for the original REE distribution within majorite, and for the distribution of REE's in the exsolution product:

1) The majoritic garnet REE pattern may look like that of clinopyroxene, i.e. it could initially be sinusoidal. The sinusoidal REE pattern in the low-Ca harzburgitic garnets may therefore reflect the original REE distribution within majorite.
2) The partition coefficients of the LREE in pyrope are lower than those of majorite, whereas those of the HREE's are higher for pyrope than majorite. Exsolved pyrope should therefore contain progressively more HREE's and less LREE's than majorite, pivoting around the MREE's, as shown in figure 6.21.

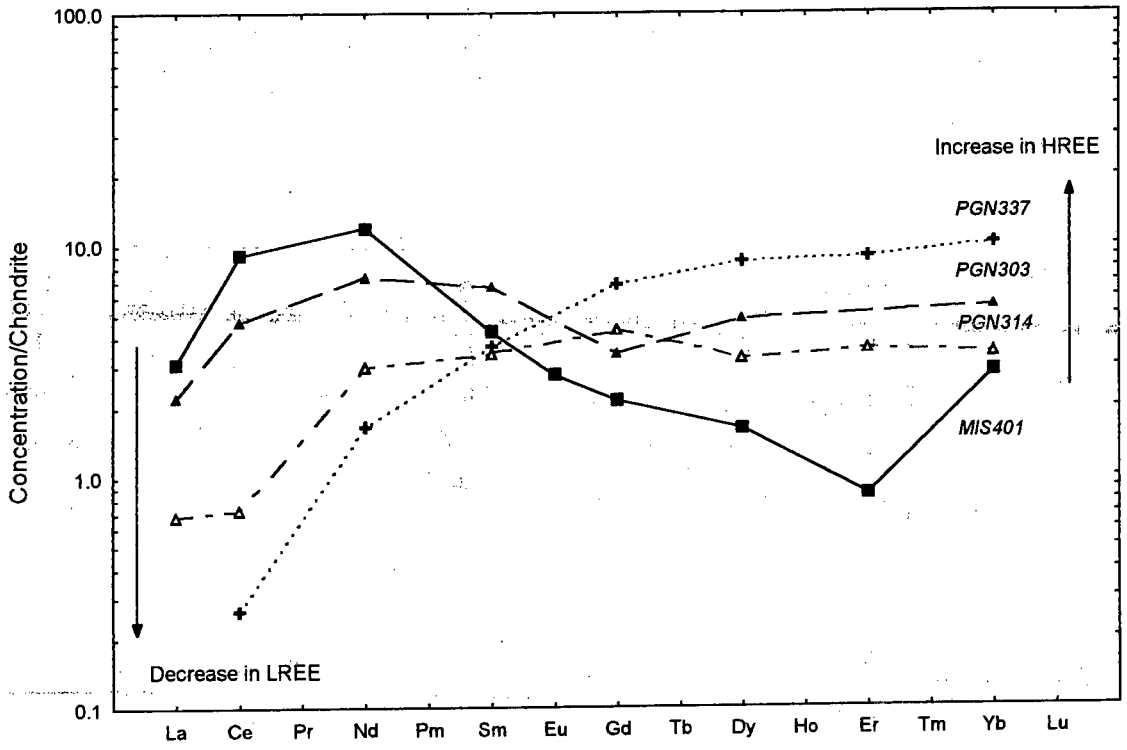

Figure 6.21 An overlay of the LREE-depleted patterns in the lherzolitic (PGN337) and harzburgitic (PGN314) garnets with the sinusoidal REE pattern of the harzburgitic garnets (PGN303, MIS401) produces a spiralling pattern pivoting around the MREE's. It would appear that as the LREE content decreases, the HREE content increases.

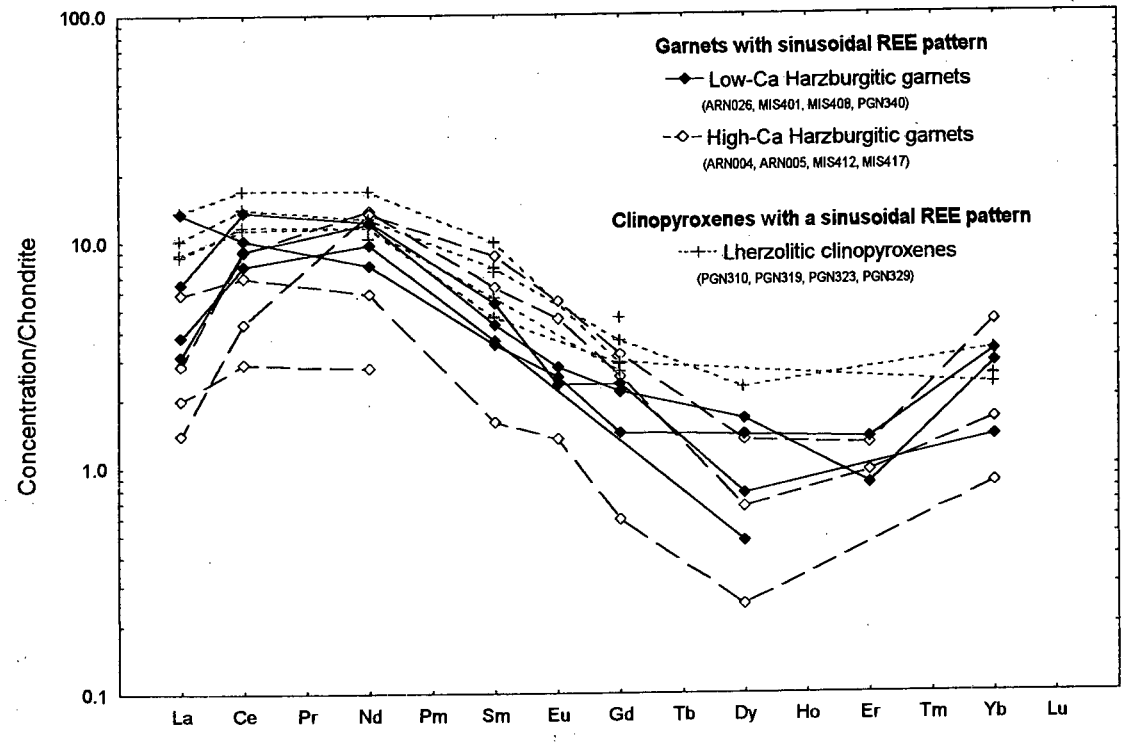

Figure 6.22 Chondrite normalised REE pattern for selected harzburgitic garnets and lherzolitic clinopyroxenes. There is a similarity between the clinopyroxene REE pattern and the sinusoidal REE pattern of the harzburgitic garnets.

Table 6.6 Mineral/Silicate Melt Partition coefficients for the minerals in ultramafic xenoliths (after Xie et al., 1995)

Element	Pyrope	Majorite	Clinopyroxene	Orthopyroxene	Olivine
La	0.01	0.09	0.054	0.002	0.005
Ce	0.02	0.095	0.098	0.003	0.005
Nd	0.005	0.1	0.05	0.01	0.01
Sm	0.22	0.2	0.26	0.01	0.005
Eu	0.32	0.2	0.31	0.013	0.007
Gd	0.5	0.26	0.3	0.016	0.006
Yb	4	1.4	0.28	0.049	0.002

But what supporting evidence is there for a majoritic component beneath the Slave province?

Haggerty (1995) noted that majoritic inclusions in diamond are recognisable as they retain their crystallographic structure, whereas majoritic rocks re-equilibrate by exsolution and may form "jigsaw"-like textures. Although the sample size in this study is small (<1.5 cm), those samples that have sinusoidal REE patterns in garnet do exhibit "jigsaw"-type textures (figure 4.5a).

Numerous super-deep mineral inclusions in diamond have been found in diamonds from the Lac de Gras region and the southern slave craton: five of thirty-seven mineral inclusions in diamond from the Tli Kwi Cho kimberlite complex (DO-27) were ferropericlase, and one had a majoritic component (Davies et al., 1999); and four of twelve garnet inclusions in diamond from the Snap Lake kimberlite contained a significant majoritic component (two eclogitic, and two peridotitic; Pokhilenko et al., 2001). The concentration of low-Ca harzburgitic garnets is also higher in the central region (Grütter et al., 1999). The presence of super-deep mineral inclusions in diamond (Davis et al, 1999) suggests that they had a super-deep origin. They may therefore either be plume related (Griffin et al., 1999a), or the continental keel may have been deeper then normal, possibly extending into the majorite stability zone (Helmstaedt and Gurney, 1992; Pokhilenko et al., 2001).

Quantitative modelling

A model was formulated to quantitatively predict the REE distribution between exsolution products from majorite based on the following equation:

Reaction: Majorite + Olivine → Pyrope + Orthopyroxene + Olivine

Intermediate phases: ↘ Majorite + Pyrope + Orthopyroxene + Olivine ↗

The calculations needed to include different modal proportions of the minerals present during the intermediate phases in order to mimic the exsolution process. It also needed to maintain a mass balance of the minerals present in the system in order to model closed system behaviour.

Various basic assumptions were made:

1) Modal proportion of starting material: 40% majorite, 60 % olivine.
2) Modal proportion of end product: 10% pyrope, 30% pyroxene, 60% olivine.
3) Olivine is excluded from the calculation based on two assumptions: 1) Olivine hosts negligible amounts of REE's and would therefore not influence trace element partitioning; and 2) as the relative start and end product contain the same amount of olivine, olivine is not involved in the exsolution process.
4) The initial concentration of REE's to be partitioned between the minerals during the exsolution process is equal to those present within the majorite i.e. 40% of the rock.
5) Closed system behaviour is assumed.

The exsolution process was modelled in five independent stages, as shown in table 6.7. The modal percentages of the minerals present varied in each stage from 100% majorite in Stage 1 to 0% majorite in Stage 5 (table 6.7).

Table 6.7 Hypothetical percentages of the minerals involved in the exsolution process in different stages. The ratio of pyrope:pyroxene is constant at 1:3.

Stage		% Majorite (%Maj)	% Pyrope (%Py)	% Pyroxene (%Pyx)
1	Initial	100	0	0
2	Intermediate	80	5	15
3	Intermediate	50	13	37
4	Intermediate	20	20	60
5	Final	0	25	75

An example of the calculation of the distribution of La between the various phases is as follows:

$[La]_{Maj} = [La]_{Innitial} / ((\%Maj) + (\%Py * D^{La}_{Py}/ D^{La}_{Maj}) + (\%Pyx * D^{La}_{Pyx}/ D^{La}_{Maj}))$

$[La]_{Py} = [La]_{Maj} * D^{La}_{Py}/ D^{La}_{Maj}$

$[La]_{Pyx} = [La]_{Maj} * D^{La}_{Pyx}/ D^{La}_{Maj}$

A mass balance cross-check was employed to verify that the distribution of the REE's between the minerals was correct. This was achieved by checking that the sum of the calculated concentrations multiplied by the modal percentage of the mineral equalled the initial REE concentration.

Calculation correct if: $[La]_{Initial} - (\%Maj*[La]_{Maj}) - (\%Py*[La]_{Py}) - (\%Pyx*[La]_{Pyx}) = 0$

Results

Initially two models were attempted. Both used the REE content of ARN026 as a starting material. Model (A) involved exsolution into pyrope and orthopyroxene (table 6.8), whereas Model (B) modelled exsolution into pyrope and clinopyroxene (table 6.9). Results of both models are detailed below. Model C is an extension of the basic calculation to include the exsolution of a small portion of clinopyroxene alongside pyrope and orthopyroxene (table 6.10).

Table 6.8 Results of Model (A). Elemental abundance in ppm.

Exsolution process: Majorite (1.0) → Pyrope (0.25) + Orthopyroxene (0.75). (x)= wt fraction.

Mineral	Majorite				Pyrope				Orthopyroxene			
Wt fraction	1.0	0.80	0.50	0.20	0.05	0.13	0.20	0.25	0.15	0.37	0.60	0.75
Stage	*1*	*2*	*3*	*4*	*2*	*3*	*4*	*5*	*2*	*3*	*4*	*5*
La	1.05	1.29	2.00	4.44	0.14	0.22	0.49	2.61	0.029	0.044	0.099	0.523
Ce	6.14	7.53	11.4	23.5	1.58	2.4	4.95	16.9	0.238	0.359	0.742	2.54
Nd	4.7	5.65	8.08	14.4	2.82	4.04	7.2	14.9	0.247	0.354	0.630	1.30
Sm	0.61	0.71	0.93	1.36	0.78	1.02	1.5	2.16	0.036	0.046	0.068	0.098
Eu	0.14	0.16	0.19	0.25	0.25	0.31	0.41	0.50	0.010	0.013	0.016	0.021
Gd	0.39	0.43	0.50	0.62	0.82	0.96	1.19	1.41	0.026	0.031	0.038	0.045
Dy	0.30	0.34	0.39	0.48	0.68	0.79	0.98	1.14	0.016	0.019	0.023	0.027
Er	0.17	0.18	0.18	0.20	0.58	0.60	0.64	0.66	0.009	0.009	0.010	0.010
Yb	0.40	0.42	0.45	0.51	1.21	1.3	1.45	1.55	0.015	0.016	0.018	0.019

Table 6.9 Results of Model (B). Elemental abundance in ppm.

Exsolution process: Majorite (1.0) → Pyrope (0.25) + Clinopyroxene (0.75). (x)= wt fraction.

Element	Majorite				Pyrope				Clinopyroxene			
Wt fraction	1.0	0.80	0.50	0.20	0.05	0.13	0.20	0.25	0.15	0.37	0.60	0.75
Stage	*1*	*2*	*3*	*4*	*2*	*3*	*4*	*5*	*2*	*3*	*4*	*5*
La	1.05	1.17	1.42	1.80	0.13	0.16	0.20	0.24	0.700	0.852	1.077	1.313
Ce	6.14	6.36	6.75	7.13	1.34	1.42	1.50	1.56	6.56	6.96	7.35	7.66
Nd	4.70	4.60	4.47	4.32	2.30	2.24	2.16	2.12	6.03	5.87	5.67	5.56
Sm	0.61	0.58	0.55	0.51	0.64	0.60	0.56	0.54	0.759	0.709	0.664	0.637
Eu	0.14	0.13	0.11	0.10	0.20	0.18	0.16	0.15	0.197	0.171	0.151	0.140
Gd	0.39	0.36	0.33	0.30	0.69	0.63	0.58	0.55	0.416	0.378	0.348	0.331
Dy	0.30	0.31	0.31	0.31	0.63	0.63	0.64	0.64	0.188	0.188	0.191	0.193
Er	0.17	0.17	0.16	0.16	0.55	0.52	0.51	0.49	0.073	0.069	0.067	0.066
Yb	0.40	0.41	0.42	0.45	1.18	1.21	1.29	1.33	0.082	0.085	0.090	0.093

Table 6.10 Results of Model (C). Elemental abundance in ppm. (x)= wt fraction.

Exsolution process: Majorite (1.0) → Pyrope (0.25) + Orthopyroxene (0.70) + Clinopyroxene (0.05)

	Majorite				Pyrope				Orthopyroxene				Clinopyroxene			
Wt frac.	1.0	0.80	0.50	0.20	0.05	0.13	0.20	0.25	0.14	0.35	0.57	0.70	0.01	0.02	0.03	0.05
Stage	1	2	3	4	2	3	4	5	2	3	4	5	2	3	4	5
La	1.05	1.28	1.96	4.13	0.14	0.22	0.46	1.58	0.029	0.043	0.092	0.317	0.770	1.17	2.48	8.55
Ce	6.14	7.44	10.98	21.08	1.57	2.31	4.44	10.23	0.235	0.347	0.666	1.534	7.67	11.32	21.75	50.11
Nd	4.70	5.56	7.75	12.90	2.78	3.87	6.45	10.62	0.243	0.339	0.564	0.929	7.30	10.17	16.93	27.87
Sm	0.61	0.70	0.89	1.26	0.77	0.98	1.38	1.80	0.035	0.045	0.063	0.082	0.910	1.16	1.63	2.12
Eu	0.14	0.16	0.19	0.23	0.25	0.30	0.38	0.43	0.010	0.012	0.015	0.018	0.243	0.288	0.364	0.420
Gd	0.39	0.42	0.49	0.59	0.81	0.93	1.13	1.28	0.026	0.030	0.036	0.041	0.486	0.560	0.680	0.765
Dy	0.30	0.33	0.38	0.47	0.68	0.78	0.95	1.08	0.016	0.018	0.022	0.025	0.204	0.235	0.286	0.325
Er	0.17	0.18	0.18	0.19	0.57	0.59	0.63	0.65	0.0089	0.0092	0.0098	0.0100	0.077	0.079	0.084	0.086
Yb	0.40	0.42	0.45	0.50	1.21	1.29	1.44	1.53	0.015	0.016	0.018	0.019	0.084	0.090	0.101	0.107

Figure 6.23 shows the different REE patterns produced at different stages during the exsolution process for models A and B. As predicted from the partition coefficients, the pyrope becomes more enriched in HREE's, and is relatively depleted in LREE's in comparison to majorite. Figure 6.23 also shows that when majorite exsolves into pyrope and orthopyroxene it retains the sinusoidal REE pattern, whereas when it exsolves into pyrope and clinopyroxene the REE pattern tends more towards the LREE depleted pattern of the lherzolitic garnets. Where both clinopyroxene and orthopyroxene exsolve, the REE pattern formed is intermediate between the two extremes of figure 6.23.

Conclusion

Whereas the absolute abundance's of the resultant phases from exsolution processes are dependant on the initial concentration, the model shows that:

1) Partition coefficients predict that the pyrope exsolving from a majoritic source would be become increasingly depleted in LREE, and enriched in HREE relative to the initial REE composition of majorite.
2) Due to the similar partition coefficients of clinopyroxene and majorite, the REE pattern of majorite may be sinusoidal in shape.
3) Majorite that exsolved into pyrope and orthopyroxene may retain the sinusoidal REE pattern of the majoritic source, whereas Ca-rich majorite exsolving into pyrope and clinopyroxene would produce the LREE depleted REE pattern noted in the lherzolitic garnets.

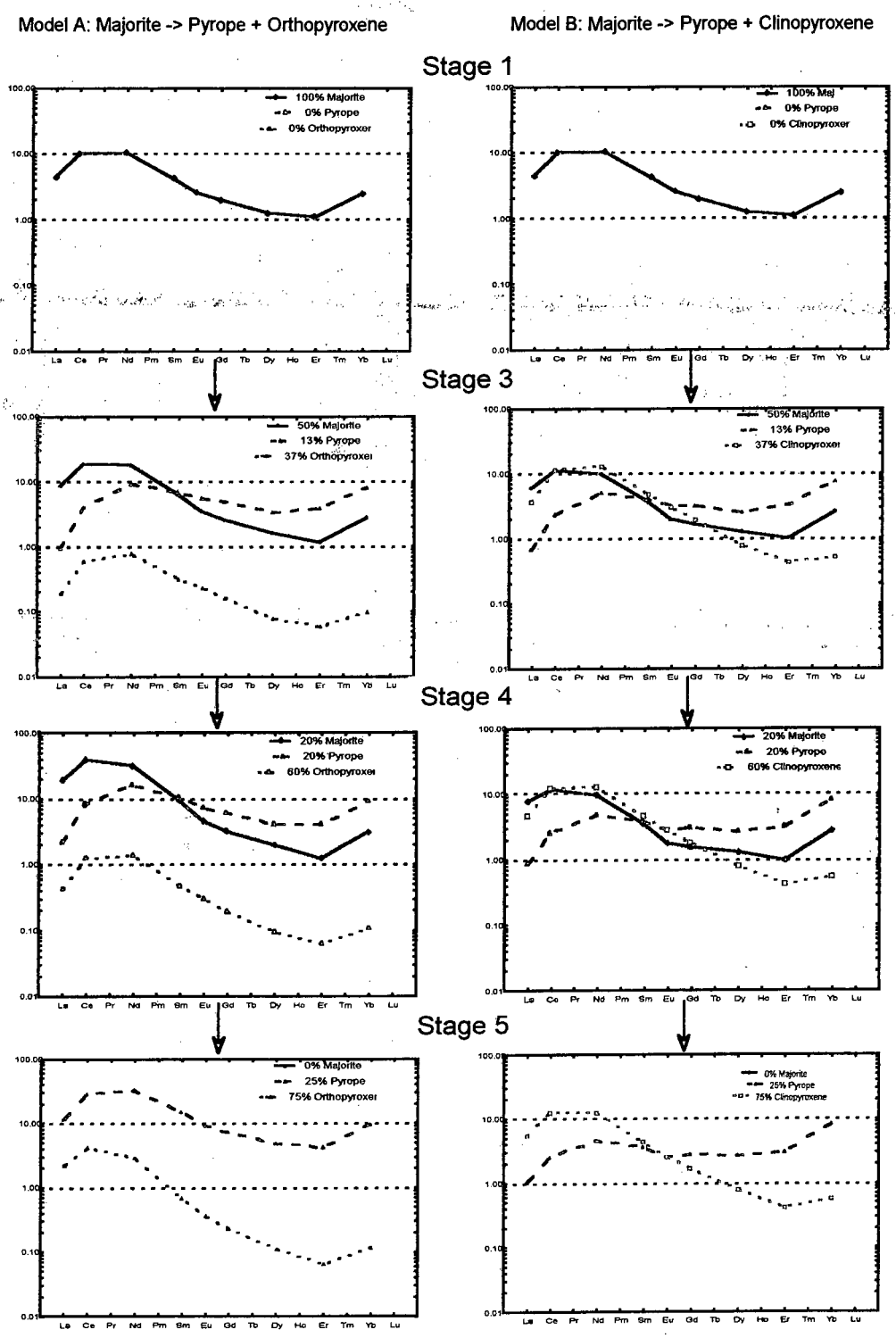

Figure 6.23 Graphical result of majorite exsolution models A and B. The chondrite normalised REE patterns are depicted for four stages of pyrope and pyroxene exsolution from majorite. The sinusoidal REE pattern is preserved by the garnet in Model A, when orthopyroxene is exsolved, whereas the pyrope forms a LREE-depleted pattern in Model B, when clinopyroxene is the exsolved pyroxene. Stages 3 and 4 show the intermediate stages in the exsolution process. The two horizontal lines provide visual reference points at: chondritic values and 10 times chondrite. All plots are chondrite normalised.

7 . GEOTHERMOBAROMETRY

7 .1. INTRODUCTION

Since Boyd (1973) proposed a geotherm for the mantle beneath Lesotho, geothermobarometric calculations have become an integral part of mantle xenolith studies. It is generally assumed that equilibrium mineral assemblages within mantle xenoliths provide a temperature with depth profile (geotherm) of the mantle in a specific location at the time of kimberlite emplacement. Helmstaedt and Harrap (1999) have however questioned the validity of this assumption. They suggest that diamonds and mantle material can be stored outside their ambient geothermal environment, in which case the constructed geotherm may not reflect the vertical section of the mantle at the time of kimberlite emplacement. This chapter is however based on the assumption that the pressures and temperatures obtained from individual xenoliths define it's ambient thermal environment at the time of kimberlite emplacement.

Lithospheric cross-sections constructed using geothermobarometry (Boyd and Gurney, 1986) support the theory of a deep keel beneath old cratonic lithosphere, and a shallower lithosphere beneath younger mobile belts. Clifford (1970) noted that primary diamond localities are almost always found within the borders of the old cratonic regions. The lithospheric component beneath the deeper keel could attain pressures and temperatures consistent with the diamond stability field (900-1300°C and 40-55 kbar, Nickel and Green, 1985). The depths from which xenoliths within kimberlite originate therefore has important implications for diamond exploration as it provides an indication of the mantle sampled and a minimum depth from which the kimberlite originated.

Geothermobarometry is based on cation exchanges between minerals *in equilibrium* using the equation: $0 = \Delta G^o + RT\ln K$. Where G^o is Gibbs Free energy, R is the gas constant, T is temperature and K is the equilibrium constant. K is a function of the activities of the phase components in the minerals, whereas $\Delta G°$ is dependant on pressure (P) and temperature (T) by the equation: $\Delta G = \Delta H - T\Delta S + (P-1)\Delta V$. Where H is enthalpy, S is entropy and V is volume (Wood and Fraser, 1976). By employing the relationship $dP/dT = \Delta S/\Delta V$, the slope of a line in P-T space is equal to $\Delta S/\Delta V$. Ideally, geobarometers have large ΔV's (shallow slope), whereas geothermometers have small ΔV's (steep slope). The point of intersection of these two arrays determines the temperature and pressure of a rock. This point varies depending on the calibration used. Cation exchange reactions are ideal geothermometers as they have a small ΔV, and large enthalpy and/or entropy, e.g. $Fe^{2+} \leftrightarrow Mg^{2+}$ ion exchange between coexisting

garnet and olivine. Mass transfer reactions, in which the cations in the reactants and products have different co-ordination numbers, are useful for barometric calculations (large ΔV).

7 .2. MAJOR ELEMENT GEOTHERMOBAROMETRY

Selection of Geothermobarometers for garnet-harzburgites

Ultramafic rocks are composed of a limited number of mineral assemblages. This means the mineral combinations available for geothermobarometric calculations are less numerous than for crustal rocks. For rocks of a harzburgitic composition (gt-opx-ol+/-chromite), the number of applicable geothermobarometers is even more limited. Geothermometers are restricted to the mineral assemblages garnet-olivine and garnet-orthopyroxene (e.g. O'Neill and Wood, 1979; O'Neill, 1980; and Harley, 1984, respectively), whereas the Al-in-orthopyroxene remains the most useful geobarometer (e.g. MacGregor, 1974; Nickel and Green, 1985; Brey and Köhler, 1990).

Geothermometer of Choice

Relative to other Fe-Mg silicates, garnet has a strong preference for iron over magnesium which has proved to be temperature dependant, with a subordinate pressure dependence (Banno, 1970; O'Neill and Wood, 1979). Within the ultramafic suite of minerals, the relatively simple structure of olivine, essentially a binary solid solution ($Fe_2SiO_4 \leftrightarrow Mg_2SiO_4$), facilitates the simplest Fe $\leftrightarrow$ Mg exchange with garnet. The exchange of the ions Al, Ca and Fe^{3+} do not complicate the ion exchange system between garnet-olivine as they might in the garnet-orthopyroxene system.

The garnet-olivine geothermometer was therefore chosen in preference to the garnet-orthopyroxene geothermometer for two reasons: Firstly, due to the simplicity of the garnet-olivine exchange reaction, which makes for an accurate geothermometer (Smith, 1999), and secondly, in order to compare the trace element geothermometry that also relies on the garnet-olivine equilibrium assemblage.

The garnet-olivine geothermometer of O'Neill and Wood (1979) makes use of the Fe $\leftrightarrow$ Mg exchange between garnet and olivine in the following reaction:

$$\underset{\text{Fe-olivine}}{3Fe_2SiO_4} + \underset{\text{Mg-garnet}}{2Mg_3Al_2Si_3O_{12}} \leftrightarrow \underset{\text{Fe-garnet}}{2Fe_3Al_2Si_3O_{12}} + \underset{\text{Mg-olivine}}{3Mg_2SiO_4}$$

Brey and Köhler (1990) found that the calibration of O'Neill and Wood (1979, and correction by O'Neill, 1980) agreed well with their experimental data. Although they did note that the scatter was larger than some of the more recent calibrations (such as Carswell and Harley, 1989), the correlation to the experimental temperatures compared better than various recent calibrations (such as Lee and

Ganguly, 1988; Carswell and Harley, 1989). The O'Neill and Wood (1979) calibration is therefore well suited for the samples of the peridotitic suite, and was used as the favoured geothermometer.

O'Neill and Wood (1979) cautioned that for garnets with high X_{Ca}^{gt} (above 0.3), their calibration was inadequate. This is not a concern in this study as all the garnets had low Ca contents, with X_{ca}^{gt} below 0.17, where X_{ca}^{gt}=Ca/(Ca+Mg+Fe). They also noted that the geothermometer is most sensitive in regions where the K_D is substantially greater than 1 [$K_D=(Fe/Mg)_{gt}/(Fe/Mg0)_{ol}$]. The K_D's calculated for the samples in this study have K_D values between 1.9 and 3.5. For such Mg-rich (peridotitic) compositions O'Neill and Wood (1979) predict that the calculated temperatures should be within 60° of the true value. Should any Fe^{3+} be present within the garnet structure, it would lead to an underestimation of the temperature (Brey and Köhler, 1990). This calibration is pressure dependant, hence an iterative process was used to obtain calculated temperatures. O'Neill and Wood (1979) note that for a fixed K_D the calculated temperature would rise between 3-6° per kbar.

For these reasons the garnet-olivine geothermometer by O'Neill and Wood (1979) is the most suitable geothermometer and has been selected for the geothermobarometric calculations.

Geobarometer of Choice

Boyd and England (1964) were among the first to demonstrate the strong pressure dependence of the Al-content in orthopyroxene coexisting with garnet in a simple system. The geobarometer is based on the solid solution of garnet in orthopyroxene, by the following reaction (Nickel and Green, 1985):

$2Mg_2Si_2O_6$	+ $MgAl_2SiO_6$	↔	$Mg_3Al_2Si_3O_{12}$
Enstatite	+ Mg-tschermak's molecule	↔	Pyrope
	in orthopyroxene solid solution		in garnet solid solution

Calibrations based on the $MgO-Al_2O_3-SiO_2$ (MAS) system (MacGregor, 1974) and the Ca-FeO-$MgO-Al_2O_3-SiO_2$ (CFMAS) system (Harley, 1984) are not suitable for this suite of rocks as the samples have a large Cr component (up to 0.02 cations per 4 oxygens in orthopyroxene and up to 0.69 cations per 12 oxygens in garnet). The Cr^{3+} in peridotitic garnets competes with Al^{3+} for position in both the garnet and orthopyroxene crystal structure. Hence the calibration used in this study needs to take the Cr content of the sample into account. The calibrations by Nickel and Green (1985) and Brey and Köhler (1990) both take the Cr^{3+} cation into consideration. They also take the Ti^{4+} and Na^{+} content into account. Brey and Köhler further take the Fe^{3+} cation into consideration. Both equations are solved iteratively with temperature.

Brey and Köhler (1990) found that the Al-in-orthopyroxene geobarometer by Nickel and Green (1985) formulated most closely to their experimental pressure, in the calibrated range (10-40 kbar). The figure

used by Brey and Köhler (1990, Figure 9.a), and the worked example in their paper however shows the calibration of Nickel and Green to be similar in the range 28 to 60 kbar, the range of interest in this project.

This study compares the results of the Brey and Köhler (1990) with those of Nickel and Green (1985). The calibration by Nickel and Green (1985) is favoured by this study for two reasons: 1) due to inconsistencies in the Fe^{3+}-related terms in the calculation of the Brey and Köhler (1990) barometer, as described in *methodology* below, and 2) the discrepancy between the Brey and Köhler (1990) results and those derived from trace element geobarometers,

Methodology

Two excel spreadsheets were constructed for the calculation of the peridotite pressures and temperatures. These were for the two pressure calibrations Nickel and Green (1985) and Brey and Köhler (1990) in conjunction with temperature determinations according to O'Neill and Wood (1979). Temperatures and pressures were obtained iteratively.

During construction of the Brey and Köhler (1990) spreadsheet discrepancies were noted associated with the addition of Fe^{3+} to the mineral formula as many of the $X_{Al,Ts}^{M1}$ terms became negative. The Fe^{3+} content in minerals cannot be directly determined using the wavelength dispersive electron microprobe at UCT, and the error associated with recalculations based on stoichiometry (e.g. Droop, 1987) for silicate minerals is large (Luth et al., 1990; Canil and O'Neill, 1996; Smith, 1999). For these reasons Fe^{3+} content in pyroxene was not used in the Brey and Köhler (1990) calibration.

The validity of the output from the constructed spreadsheets was verified using the worked example of Brey and Köhler (1990). The calibrations by Nickel and Green (1985) and O'Neill and Wood (1979) returned the correct pressure and temperature within 60°C and 3 kbar of the experimental temperature and pressure. The temperature calculated by O'Neill and Wood (1979) was further checked by using the compositional data published by Nixon and Boyd (1973), and the corresponding temperature calculations included in O'Neill and Wood's calibration. Slight deviations between calculated and published temperatures were expected as O'Neill and Wood (1979) used the pressure calculation by Wood (1974), whereas the iterative calculation in this study used the pressure calibration from Nickel and Green (1985), yet the calculated and published temperatures were within error of each other (60°, O'Neill and Wood, 1979).

Possible sources of error

Fe^{3+} in garnet is one of the major sources of error in geothermobarometric calculations. Luth et al. (1990) found that the presence of Fe^{3+} in garnet significantly influenced the temperature calculated (>200°C), and therefore indirectly affected the derived pressure. This study assumes that the Fe^{3+} content of garnet in peridotites is zero as the stoichiometric calculation of Fe^{3+} from microprobe analysis is associated with large uncertainties, particularly for Fe-poor minerals such as those found in the mantle (Luth et al., 1990). Temperatures calculated may therefore be underestimates of the actual equilibrium temperature.

Uncertainties that may have been introduced through analytical techniques were minimised by extending the counting times for elements of interest, particularly those that have low abundances. For example, the peak counting time for Al_2O_3 and Na_2O in orthopyroxene was increased from 10 seconds to 40 and 60 seconds respectively (electron microprobe analysis).

Mineral disequilibrium is another possible source of error. As geothermobarometric calibrations rely on the elemental exchange between two minerals, elemental equilibrium needs to have been attained between these minerals. Disequilibrium may be caused by a change in environmental conditions, such as in influx of heat from a plume, or due to interaction with a fluid. Major elements however re-equilibrate on relatively "short geological time scales" at mantle pressures and temperatures (Smith, 1999), hence mantle mineral assemblages have a high probability of representing equilibrium. Xenoliths not in elemental equilibrium would record events that occurred shortly prior to kimberlite emplacement (Griffin et al., 1996). The rapid eruption of the host kimberlite would ensure that the geochemical signature of the xenoliths would not have had time to re-equilibrate to shallower depths (Smith, 1999).

Results

The temperatures and pressures derived using the chosen geothermobarometer pairs are detailed in Table 7.1. A graphical representation of the results are shown in figures 7.1 a and b.

Table 7 .1 Temperature determinations by O'Neill and Wood (1979) and pressure determinations by Nickel and Green (1985) and Brey and Köhler (1990) respectively.

Kimberlite Locality	Sample No.	O'Neill & Wood gt-ol (°C)	Nickel & Green gt-opx (Kbar)	O'Neill & Wood gt-ol (°C)	Brey & Köhler gt-opx (kbar)	Rock Suite
Arnie	ARN002	969	50.9	931	42.6	Low-Ca Harzburgite
Arnie	ARN003	1006	47.4	983	42.3	High-Ca Harzburgite
Arnie	ARN004	957	51.5	945	48.5	High-Ca Harzburgite
Arnie	ARN005	970	47.1	952	42.9	High-Ca Harzburgite
Arnie	ARN006	842	43.1	823	38.9	High-Ca Harzburgite
Arnie	ARN007	1035	46.4	992	37.9	Low-Ca Harzburgite
Arnie	ARN008	738	30.1	635	13.9	Low-Ca Harzburgite
Arnie	ARN011	879	42.1	831	32.4	Low-Ca Harzburgite
Arnie	ARN013	655	28.0	592	16.5	High-Ca Harzburgite
Arnie	ARN014	891	46.5	855	38.4	High-Ca Harzburgite
Arnie	ARN017	995	46.6	950	37.4	Low-Ca Harzburgite
Arnie	ARN018	841	37.7	791	28.1	High-Ca Harzburgite
Arnie	ARN021	1043	52.5	1017	46.4	Low-Ca Harzburgite
Arnie	ARN022	884	45.1	854	38.4	High-Ca Harzburgite
Arnie	ARN025	896	40.1	840	29.4	Low-Ca Harzburgite
Arnie	ARN026	871	35.3	841	29.2	Low-Ca Harzburgite
Arnie	ARN027	916	40.0	847	27.5	Low-Ca Harzburgite
Arnie	ARN029	970	44.4	920	34.1	High-Ca Harzburgite
Misery	MIS408	917	59.5	857	45.7	Low-Ca Harzburgite
Misery	MIS413	834	47.6	Does not converge		High-Ca Harzburgite
Misery	MIS417	702	33.3	669	27.2	High-Ca Harzburgite
Misery	MIS426	735	31.2	708	26.0	Lherzolite
Misery	MIS430	768	38.5	734	31.5	High-Ca Harzburgite
Misery	MIS431	586	17.9	541	10.4	Lherzolite
Misery	MIS433	677	25.0	640	18.6	Lherzolite
Misery	MIS434	782	39.5	739	30.4	High-Ca Harzburgite
Misery	MIS463	1242	58.4	1241	58.1	Low-Ca Harzburgite
Pigeon	PGN301	688	35.0	588	16.9	Low-Ca Harzburgite
Pigeon	PGN303	1001	56.1	937	42.0	Low-Ca Harzburgite
Pigeon	PGN306	1075	48.9	1044	42.1	Lherzolite
Pigeon	PGN307	1034	49.6	1001	42.0	Lherzolite
Pigeon	PGN310	952	43.4	918	36.4	Lherzolite
Pigeon	PGN312	1045	44.1	1045	44.0	High-Ca Harzburgite
Pigeon	PGN313	842	40.6	825	36.9	High-Ca Harzburgite
Pigeon	PGN314	1039	49.9	997	40.8	Low-Ca Harzburgite
Pigeon	PGN316	1024	44.5	996	38.5	Lherzolite
Pigeon	PGN317	793	40.5	709	25.0	Low-Ca Harzburgite
Pigeon	PGN339	1039	47.3	1017	42.3	Lherzolite
Pigeon	PGN340	980	52.0	922	40.0	Low-Ca Harzburgite

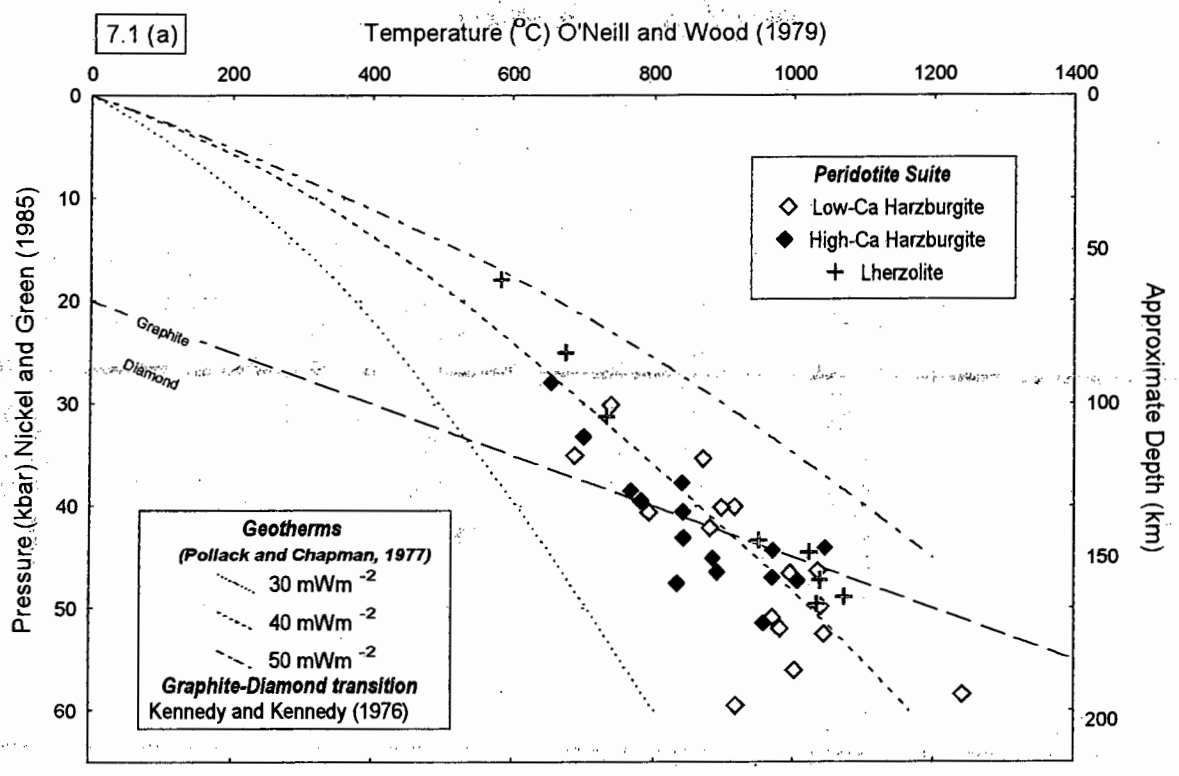

Figure 7.1 (a) Pressure (Nickel and Green, 1985) vs Temperature (O'Neill and Wood, 1979). The peridotites lie on the 40 mWm^{-2} geotherm (Pollack and Chapman, 1977). There is no systematic spatial variation between lherzolitic and harzburgitic xenoliths.

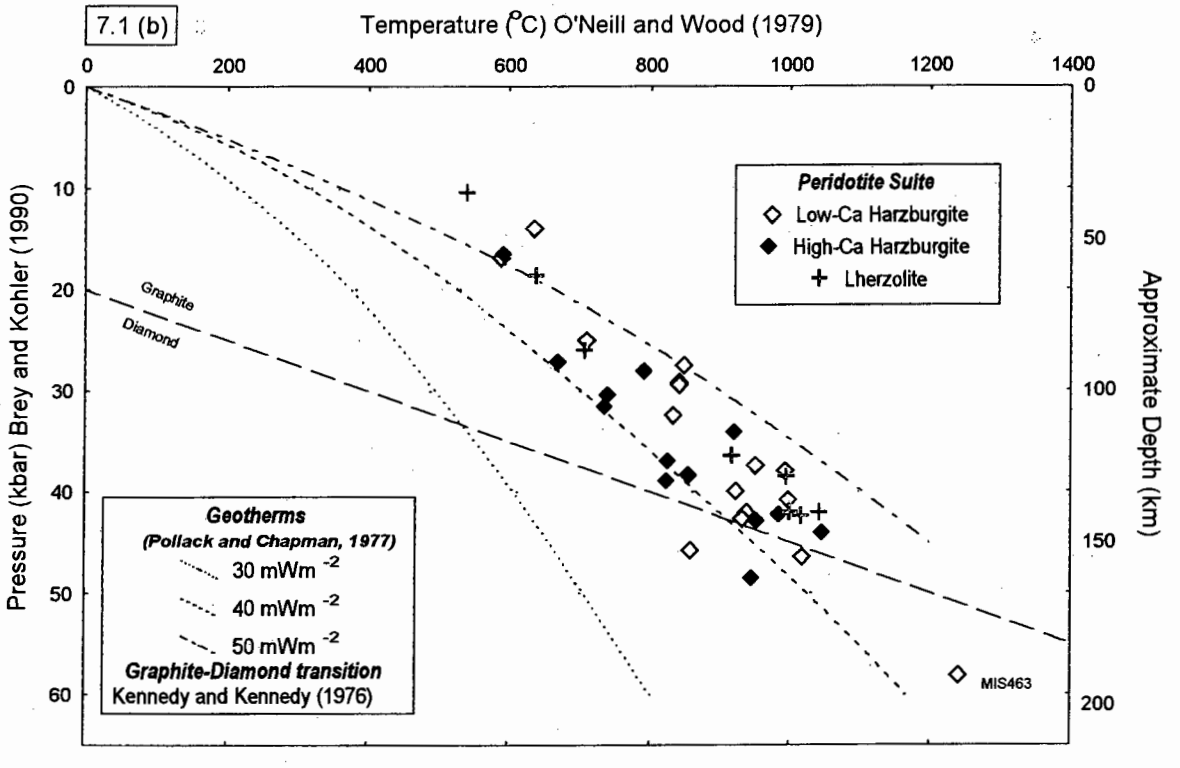

Figure 7.1 (b) Pressure (Brey and Köhler, 1990) vs Temperature (O'Neill and Wood, 1979). The peridotites define an array between the 40 and 50 mWm^{-2} geotherm (Pollack and Chapman, 1977). The lower temperature xenoliths (<640°C) lie above the 50 mWm^{-2} geotherm. There is no systematic spatial variation between lherzolitic and harzburgitic xenoliths.

Selection of Geothermobarometer for the websterites

A temperature and pressure was obtained for the two granoblastic websterites (gt-opx-cpx). Although these two rocks are not the focus of this study, the relative spatial relation within the mantle of this suite to the peridotitic rocks is of interest to stratified mantle theories (Pearson et al., 1999; Griffin et al., 1999a). Whereas the garnet-olivine geothermometer of O'Neill and Wood (1979), and the garnet-orthopyroxene geobarometer of Nickel and Green (1985) were ideal for the peridotitic rocks, they were not suitable to obtain a pressure and temperature for the pyroxenitic websterites. Hence the Brey and Köhler (1990) garnet-orthopyroxene geothermobarometer and geobarometer were used to obtain the equilibrium pressure and temperature of these two samples.

Although one should not directly compare the pressures and temperatures obtained using different geothermobarometric calibrations, the *relative* pressure and temperature of these rocks in comparison with those of the peridotite paragenesis is of interest.

Methodology

T_{BKN} (Brey and Köhler, 1990) based on the Fe $\leftrightarrow$ Mg exchange between garnet and orthopyroxene coexisting with clinopyroxene was used to determine the temperature. Pressure was calculated using the Nickel and Green spreadsheet devised for the peridotitic samples.

Results

Table 7.2 shows the temperature and pressure derived using the Brey and Köhler (1990) geothermobarometers.

Table 7 .2 Temperature and pressure of two granoblastic websterites (gt-opx-cpx) of the pyroxenite suite.

Kimberlite Locality	Sample No.	Brey & Köhler gt-opx (°C)	Brey & Köhler gt-opx (kbar)	Rock Suite
Misery	MIS438	738	17.4	Websterites
Misery	MIS439	812	17.6	Websterites

Discussion

Calculated Pressure-Temperature arrays

The calculated pressure and temperatures of the peridotitic samples are indicated in table 7.1. Whereas the absolute pressure and temperature of the Brey and Köhler (1990)- O'Neill and Wood (1979) combination is systematically lower than that of the Nickel and Green (1985) - O'Neill and Wood (1979) combination, the relative position of the samples to each other is the same.

As Figure 7.1 (a) and (b) show, the combination of O'Neill and Wood (1979) and Brey and Köhler (1990) define a xenolith geotherm between 40 and 50 mWm^{-2} (Pollack and Chapman, 1977). This is higher than other cratonic geotherms (e.g. 40 mWm^{-2} Kaapvaal, Finnerty and Boyd, 1987). That determined by the O'Neill and Wood (1979) and Nickel and Green (1985) combination define a geotherm of 40 mWm^{-2} (Pollack and Chapman, 1977). Other studies from the Slave craton also define geotherms of 40 mWm^{-2} or below. The xenoliths from the Grizzly pipe (located between Arnie and Pigeon) plot close to the 40 mWm^{-2} conductive geotherm with three samples plotting in the diamond stability field (Boyd and Canil (1997), using calibrations by O'Neill and Wood (1979) and MacGregor (1974)). A study of xenoliths from the Tli Kwi Cho kimberlite complex (south of Lac de Gras) by Pearson et al. (1999) found that the low-temperature xenoliths (<900°C) plot near the 35 mWm^{-2} geotherm of Pollack and Chapman (1977), whereas the higher temperature xenoliths (>900°C) plot along the 40 mWm^{-2} geotherm. This step was evident in most of the geothermobarometers used by Pearson et al. (1999), including the combination Nickel and Green (1985) - O'Neill and Wood (1979).

Anomalous Ps and Ts

The anomalous temperature and pressure shown by sample MIS463 may be attributed to the high degree of alteration of the garnet. The garnet in MIS463 has a large kelyphite rim (2mm) around the remaining garnet core (2mm). The lower pressures recorded by samples MIS408 and MIS413 may also be due to alteration. As in the case of MIS463, MIS408 has very large kelyphite alteration around the garnets. MIS413, on the other hand, has very small olivines (0.05mm) in comparison to the other minerals (2.5mm).

Comparison between pipes

As figure 7.2 shows, the peridotitic xenoliths from both the Arnie and Pigeon kimberlites (the two northerly kimberlite localities) have a wide range in pressure and temperature (655-1075°C and 28-56 kbar). They define a geotherm of 40 mWm^{-2} (Pollack and Chapman, 1977). The peridotitic samples from the Misery kimberlite have a similar temperature and pressure range to the other kimberlite localities (586-1242°C and 18-59.5 kbar). They do however have lower mean temperatures (804°C)

and pressures (39 kbar) than those of xenoliths from the Arnie and Pigeon kimberlites (929°C and 44 kbar), which are within error of each other (908°C and 959°C; 43 kbar and 46 kbar respectively).

Systematic variation of Cr content in garnet

There is a systematic variation of Cr_2O_3 in garnet with depth (figure 7.3). The higher the Cr-content, the closer the peridotitic xenolith to the diamond stability field (900-1300°C and 40-55 kbar, Nickel and Green, 1985). The low-Ca harzburgites that have a low Cr_2O_3 content have equilibrated at shallower depths than the diamond stability zone, whereas some lherzolites with high Cr_2O_3 content have equilibrated within the diamond stability zone (PGN339 and PGN310). In general, samples with a Cr_2O_3 content above 8 wt% have equilibrated within the diamond stability zone, those samples with Cr_2O_3 content between 6-8 wt% straddle the diamond-graphite transition line (Kennedy and Kennedy, 1976).

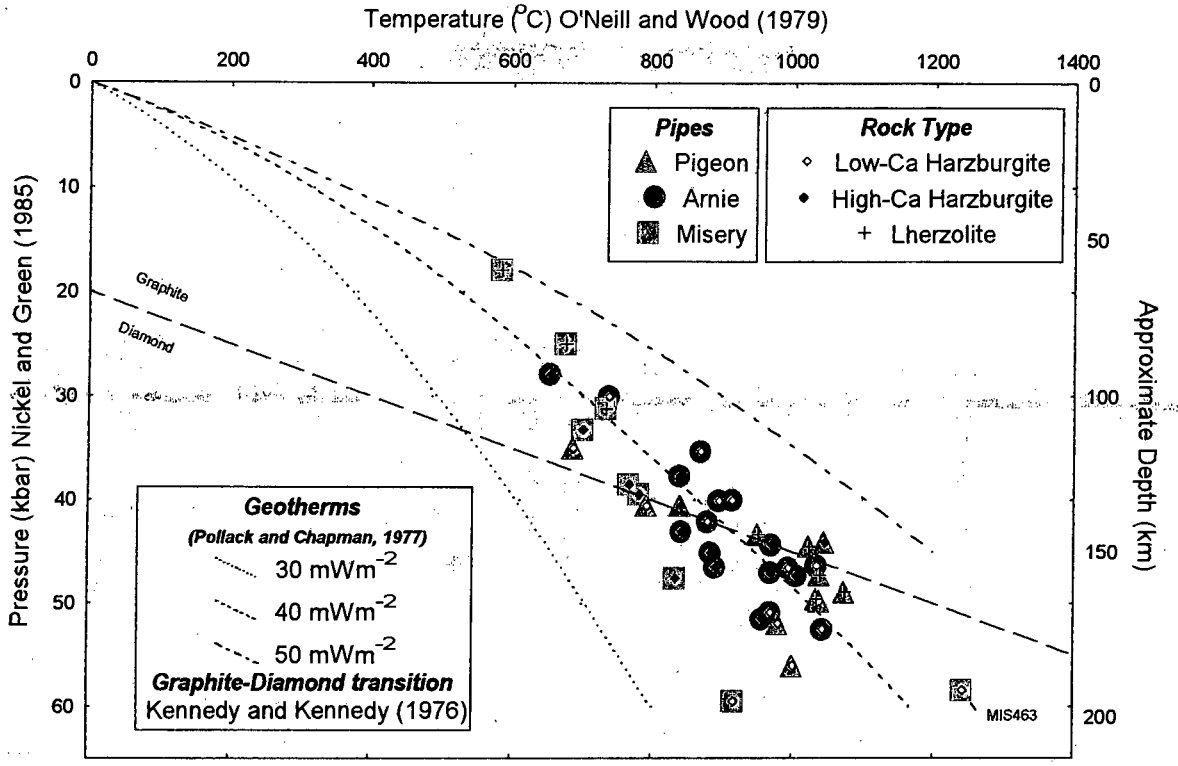

Figure 7.2 Pressure (Nickel and Green, 1985) vs Temperature (O'Neill and Wood, 1979) according to kimberlite locality. Whereas the xenoliths from the three kimberlites have similar pressure and temperature ranges (586-1242°C and 18-59.5 kbar), the xenoliths from the Misery kimberlite have lower mean temperatures (804°C) and pressures (39 kbar) than those from the Arnie and Pigeon kimberlites (929°C and 44 kbar).

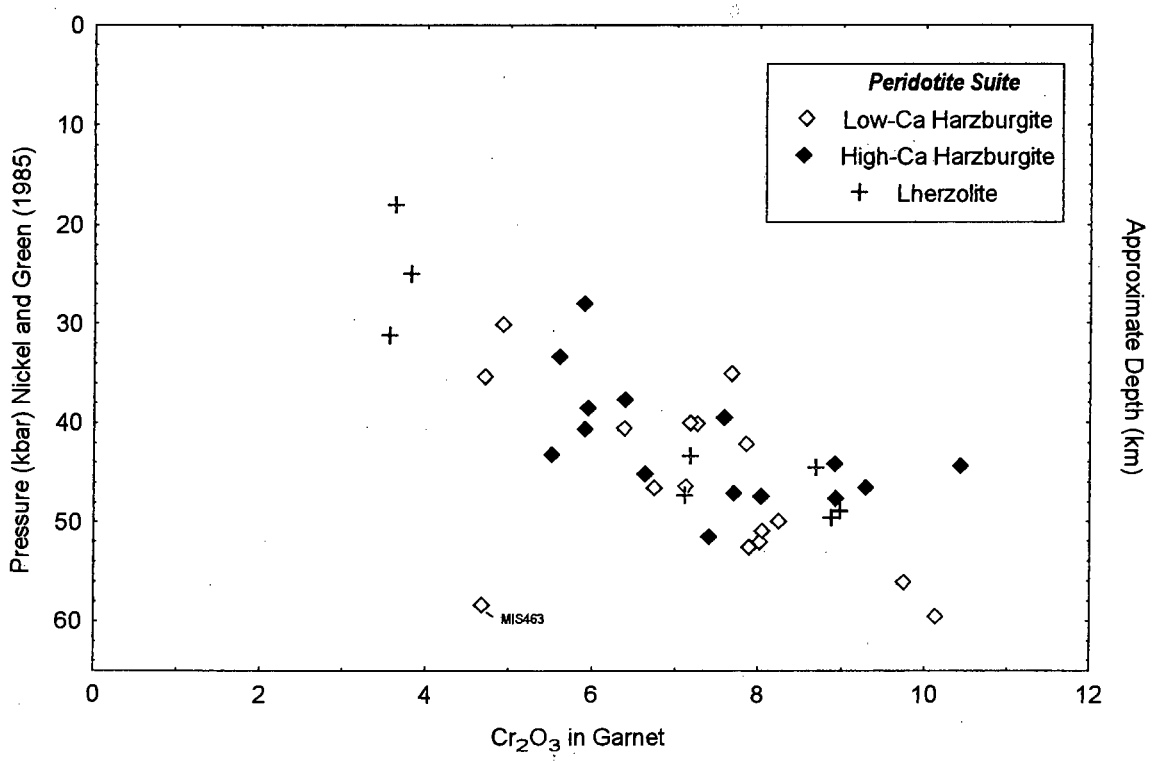

Figure 7.3 Pressure (Nickel and Green, 1985) versus Cr_2O_3 content in garnet. There is a direct relationship between Cr_2O_3 content in garnet and pressure. The high pressure xenoliths contain more Cr_2O_3. The one outlier is the altered garnet of MIS463.

7 .3. TRACE ELEMENT GEOTHERMOBAROMETRY

Several trace element geothermometers and geobarometers may be applied to peridotitic rock assemblages. Geothermometers include the Ca-in-olivine, using the Ca exchange between olivine and clinopyroxene (Köhler and Brey, 1990), Zn exchange between chromite and olivine (Ryan et al., 1996), and Ni exchange between garnet and olivine (Griffin et al., 1989; Ryan et al., 1996; Canil, 1999). The Cr content in garnet in equilibrium with chromite has been shown to be pressure dependant (Ryan et al., 1996).

This section compares the pressures and temperatures obtained using trace elements from single minerals with those obtained from the major element compositions of coexisting minerals.

Ni-in-garnet geothermometers

Only one trace element geothermometer is readily applicable to rocks of a harzburgitic composition (gt-opx-ol), namely the Ni-in-garnet geothermometer. Two Ni-in-garnet calibrations are compared in this section: the empirical calibration of Ryan et al. (1996), and the experimental calibration by Canil (1999).

The calibration of Ryan et al. (1996) is a revised calibration of Griffin et al. (1989) using a larger database and the garnet-olivine temperature calibration of O'Neill and Wood (1979) in preference to the two-pyroxene geothermometer of Finnerty and Boyd (1987) used by Griffin et al. (1989). This recalibration is more suited to rocks of a harzburgitic (clinopyroxene-free) composition. Whereas a comparison between the Ryan et al. (1996) and Griffin et al. (1989) geothermometers will not be discussed further, it was found that the calibration by Ryan et al. (1996) showed a closer correlation with the calculated xenolith geotherm described in section 7.2 than the calibration by Griffin et al. (1989).

Mechanism

There is a strong temperature dependant partitioning of Ni between olivine and garnet (Ryan et al., 1996), with garnet accepting more Ni into its structure at high temperatures (Griffin et al., 1989). The Ni content in olivine is on the order of 100 times greater than the Ni content in garnet and may therefore be seen as a buffering reservoir of Ni. Griffin et al. (1989) found the average of 76 olivine inclusions in African diamonds to be 3140+/-215 ppm. Ryan et al. (1996) also found that the measured Ni content in olivine was "essentially constant" at 2900+/360 ppm. They suggested an assumed Ni

content in olivine of 3000 ppm for Griffin et al.'s calibration (1989; equation IIb[a]). Single mineral temperature-determination may therefore be possible if the following two assumptions are valid: (1) the Ni content in olivine is uniform, and (2) that garnet was in equilibrium with olivine at the time of formation.

Methodology

An excel spreadsheet was constructed to compute the Ni-in-garnet geothermometers using the following equations:

Ryan et al. (1996) equation (1): $T\ (°C) = \{1000/[1.506 - 0.189\ln(\text{ppm } Ni_{gt})]-273\}$

Canil (1999) equation (3): $T\ (°C) = \{8772/(2.53-\ln D_{Ni}^{gt/ol}) - 273\}$ where $D_{Ni}^{gt/ol}=[Ni]_{gt}\ \text{ppm}/[Ni]_{ol}\ \text{ppm}$

Verification of Ni content in olivine

Griffin et al. (1989) and Ryan et al. (1996) proposed that the Ni content in olivine is fairly uniform (2900 +/- 360 ppm) and acts as a buffer for the Ni content in garnet. A Ni in olivine of 3000 ppm is assumed in order to facilitate the determination of temperature from a single garnet grain (Ryan et al., 1996). The applicability of the assumed average of 3000 ppm Ni in olivine to this sample suite was investigated, as was the difference in temperature determined using the assumed Ni in olivine content and actual Ni content. As Ni content determined using the electron microprobe was used for those olivines not suitable for LA-ICP-MS analysis (too fractured or too thin), a comparison between the Ni content determined using these two methods was investigated.

Both major and trace element analyses of olivine were obtained from eighteen of the twenty-two samples used in trace element geothermobarometry. The olivine in the remaining four samples was unsuitable for analysis by LA-ICP-MS due to size. The difference between the Ni content obtained from the electron microprobe, and the Ni content from the LA-ICP-MS was within the 4-sigma error range (157 ppm) for all but one sample (ARN024). Based on the accuracy of these samples, the Ni content measured by electron microprobe for the remaining four samples is assumed to be within statistical error, and are therefore used in the following discussions:

The mean Ni in olivine composition of the twenty-one of the twenty-two samples is 3085 +/-139 ppm (+/- 95% confidence level), figure 7.4. This is in error of the assumed 3000 ppm of Griffin et al. (1989). The olivine in PGN301 is small and altered, and has an anomalously low Ni content (1190 ppm) which has not been included in the mean quoted above.

---

[a] Griffin et al. (1989) equation IIb - $T\ (°C) = \{1000/[-0.435\log_{10}(Ni_{gt}/30)+0.83]\}-273$

The temperature determined using the actual Ni content in olivine is similar to that determined using the assumed Ni content of 3000 ppm (table 7.3). Generally the difference between the two temperatures is small (<35°C), and within the error associated with major element geothermometers (60°C for O'Neill and Wood, 1979). The difference in determined temperatures for four samples exceeds 35°C, three of these have higher Ni in olivine contents (>3300 ppm, with temperature differences of 53°C, 63°C and 86°C respectively). The temperature determined using the assumed Ni-in-olivine content of 3000 ppm is generally higher (16 of 21 samples), but is occasionally lower (5 of 21 samples) than the temperature determined using the actual Ni-in-olivine content. The largest difference is found in the temperature determined for PGN301 (191 °C), but this sample has an anomalously low Ni in olivine content (1190 ppm).

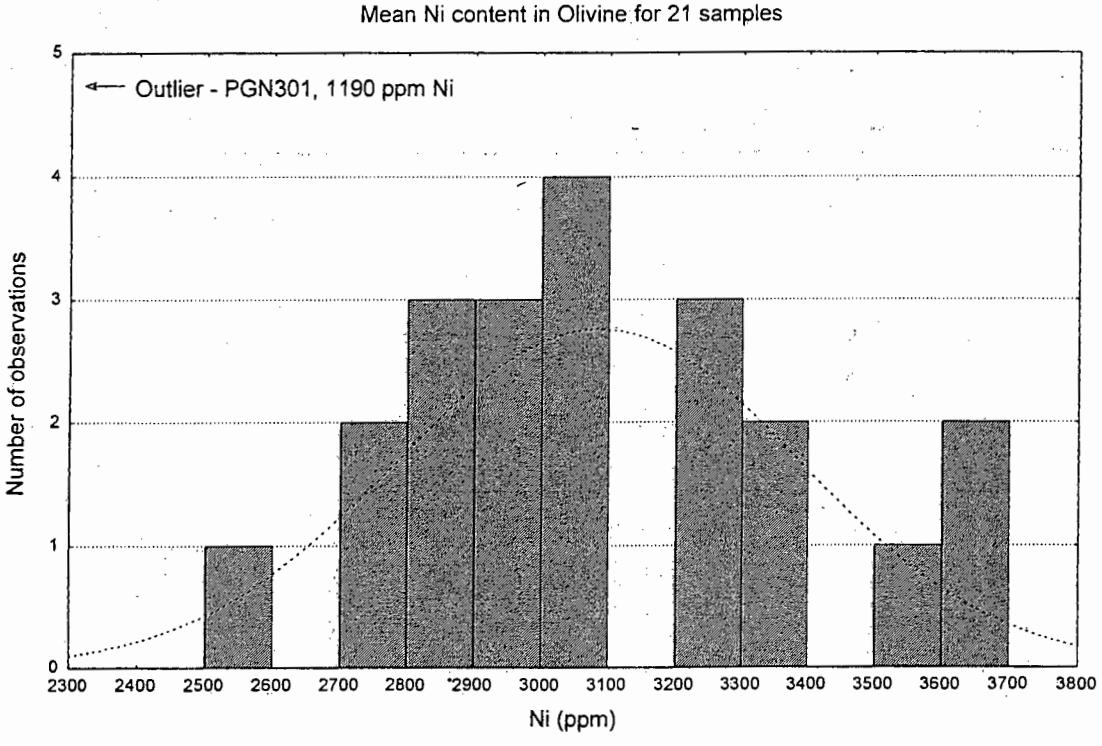

Figure 7.4 The mean concentration of Ni in olivine in the samples is similar to the assumed Ni in olivine of 3000 ppm of Griffin et al. (1989) and Ryan et al. (1996)

Table 7.3 Difference in temperature determined using actual and assumed Ni content in olivine.

Sample No	Ni Content (ppm)	T_{ni} in Gt (°C) (Griffin *et al., 1989*) Actual Ol_{Ni}	T_{ni} in Gt (°C) (Griffin *et al., 1989*) Assumed Ol_{Ni} of 3000 ppm	Difference in temperatures (°C)
ARN003	2985	926	942	16
ARN004	3300	817	848	31
ARN005	3300	786	817	31
ARN006	2985	704	709	5
ARN007	2750	990	981	10
ARN013	2829	720	715	5
ARN017	2985	972	989	18
ARN018	3536	662	696	34
ARN025	2907	1123	1134	11
ARN026	2750	722	711	11
ARN027	2907	971	986	15
MIS408	2514	859	829	30
MIS417	3300	818	852	34
PGN301	*1190*	*904*	*713*	*191*
PGN303	3615	873	936	63
PGN306	3064	1164	1200	35
PGN307	3064	1168	1199	30
PGN310	3615	1028	1114	86
PGN314	3300	1075	1129	53
PGN316	2907	1111	1122	11
PGN317	3300	704	728	24
PGN340	2828	833	832	1

Results – geothermometry

The temperatures derived using the Ni-in-garnet geothermometers are detailed in Table 7.4. A graphical representation of the results are shown in figures 7.5 a and b.

As the coexistence of garnet and olivine in the xenolith from which the temperature is being derived is one of the assumptions on which the $T_{Ni\text{-}in\text{-}garnet}$ geothermometers is based, the results have been split into two groups, namely: a) those samples with olivine present, and b) the olivine-free xenolith fragments (both pyroxenitic and lherzolitic). The trace element geothermobarometry section on page 7-21 justifies the inclusion of these olivine-free samples. (The classification of olivine-free xenoliths as lherzolitic is discussed in Section 4.2.)

Table 7 .4 Ni-Temperature determinations following Ryan et al. (1996) and Canil (1999) with O'Neill and Wood (1979) in combination with Nickel and Green (1985) for comparison.

Samples in equilibrium with olivine (used in comparison with temperatures obtained from xenoliths)

Pipe	Sample No	Major element Geothermometer	Trace element Geothermometers	
		O'Neill and Wood (1979) with Nickel and Green (1985) (°C)	Ryan et al. (1996) T_{Ni} in Garnet (°C)	Canil (1999) T_{Ni} in Garnet (°C)
Arnie	ARN003	1006	895	962
Arnie	ARN004	957	808	889
Arnie	ARN005	970	779	867
Arnie	ARN006	842	678	807
Arnie	ARN007	1035	931	1003
Arnie	ARN013	655	684	819
Arnie	ARN017	995	939	991
Arnie	ARN018	841	666	775
Arnie	ARN025	896	1071	1083
Arnie	ARN026	871	680	820
Arnie	ARN027	916	935	991
Misery	MIS408	917	790	918
Misery	MIS417	702	811	889
Pigeon	PGN301	688	681	947
Pigeon	PGN303	1001	889	927
Pigeon	PGN306	1075	1131	1106
Pigeon	PGN307	1034	1130	1109
Pigeon	PGN310	952	1053	1026
Pigeon	PGN314	1039	1067	1055
Pigeon	PGN316	1024	1060	1076
Pigeon	PGN317	793	696	807
Pigeon	PGN340	980	793	900

Pyroxenitic xenoliths and lherzolitic xenoliths with no olivine in xenolith fragment.

Pipe	Sample No	Major element Geothermometer	Trace element Geothermometers	
		Brey and Köhler (1990) gt-opx with Brey and Köhler (1990) (°C)	Ryan et al. (1996) T_{Ni} in Garnet (°C)	Canil (1999) T_{Ni} in Garnet - (°C) Assumed Ni of 3000 ppm
Misery	MIS438	738	664	795
Misery	MIS439	812	712	832
Arnie	ARN028	-	994	1028
Arnie	ARN031	-	1015	1041
Misery	MIS401	-	853	934
Misery	MIS409	-	692	817
Misery	MIS412	-	718	837
Misery	MIS419	-	1208	1156
Pigeon	PGN311	-	1305	1209
Pigeon	PGN319	-	971	1013
Pigeon	PGN320	-	824	914
Pigeon	PGN322	-	763	870
Pigeon	PGN323	-	1070	1075
Pigeon	PGN329	-	1185	1143
Pigeon	PGN337	-	1052	1064

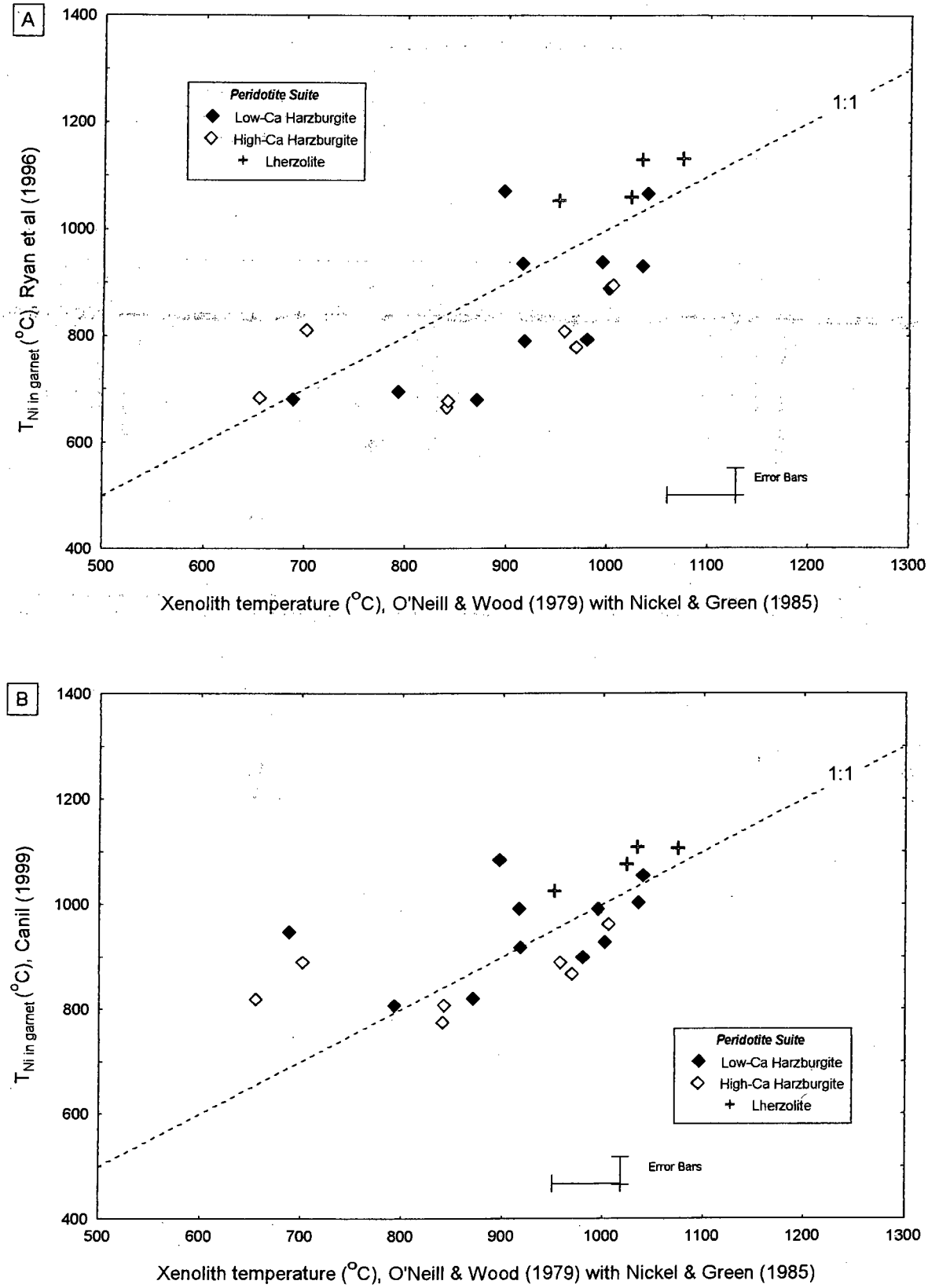

Figure 7.5 T_{Ni} temperature plotted against temperature derived from coexisting minerals (O'Neill and Wood, 1979). There is a better correlation between T_{Ni} and the xenolith temperature in the temperature range 800°C - 1100°C for T_{Ni} Canil (1999) (7.5 b) than T_{Ni} Ryan et al. (1996) (7.5 a). However, at lower temperatures (<800°C) Canil (1999) overestimates temperature, whereas T_{Ni} by Ryan et al. (1996) provides a better correlation with the xenolith temperature.

Cr-in-garnet geobarometer

Brey et al. (1991) showed that the Cr-content of chromite coexisting with garnet increases with pressure, and is insensitive to temperature. The Cr-content of the coexisting garnet is however both temperature and pressure dependant (figure 7.3., Ryan et al., 1996). Ryan et al. (1996) also noted that the Cr-content in garnet depends on the specific geotherm, and that those garnets coexisting with chromite contain maximum chrome.

The Cr-in-garnet geobarometer is based on the assumption that garnet coexisted with orthopyroxene and chromite, in which case the garnet would be in equilibrium with a Cr-saturated rock, i.e. Cr in garnet and orthopyroxene buffered by coexisting chromite. Ryan et al. (1996) noted that in cratonic areas the garnet geotherm is accurate to pressures of 60-70 kbar for depleted garnets with high Cr contents. At high pressure and temperature, Cr is absorbed into the garnet and orthopyroxene structure, and chromite no longer exists as an independent phase, and the system would therefore no longer be Cr-saturated. Cr-undersaturated rocks produce underestimates of pressure (Ryan et al., 1996).

Method

The calculation of P_{Cr} is complex. It is dependant on the composition of the garnet, the estimated orthopyroxene composition, the calculated Cr-orthopyroxene-garnet pressure, and temperature (T_{Ni}) (Ryan et al., 1996). The P_{Cr} pressures of this sample suite were calculated using a program by Ryan et al. (1996).

Since trace element geothermobarometry makes it possible to obtain pressures and temperatures from single mineral grains they can be used to determine geotherms from mineral grains in mining and exploration concentrates (Griffin and Ryan, 1995). In such cases, the coexisting mineral associations are unknown. To simulate such a situation, temperatures and pressures were obtained from all the garnets from which trace element concentrations were attained, including those with low-Cr contents. Knowing the associated minerals allows one to evaluate the operation of the geothermobarometers, as will be discussed in more detail later.

Results – barometry

The pressures derived using the Cr-in-garnet geobarometers are detailed in Table 7.5. Although the barometer is not dependant on the coexistence of olivine, for the sake of continuity the grouping used in Table 7.4 is used in Table 7.5. A graphical representation of the results are shown in figure 7.6.

Table 7 .5 Comparison of calculated P_{Cr} (Ryan et al., 1996) and Nickel and Green (1985)

Samples in equilibrium with olivine (used in comparison with temperatures obtained from xenoliths)

Pipe	Sample No	Nickel and Green (1985) (kbar)	P_{Cr} Ryan et al. (1996)	Rock Suite	Minerals
Arnie	ARN003	47.4	40.1	High-Ca Harzburgite	Chromite-bearing
Arnie	ARN004	51.5	37.4	High-Ca Harzburgite	Chromite-free
Arnie	ARN005	47.1	36.5	High-Ca Harzburgite	Chromite-free
Arnie	ARN006	43.1	31.5	High-Ca Harzburgite	Chromite-free
Arnie	ARN007	46.4	46.5	Low-Ca Harzburgite	Chromite-bearing
Arnie	ARN013	28.0	32.6	High-Ca Harzburgite	Chromite-free
Arnie	ARN017	46.6	45.1	Low-Ca Harzburgite	Chromite-bearing
Arnie	ARN018	37.7	34.3	High-Ca Harzburgite	Chromite-free
Arnie	ARN025	40.1	46.1	Low-Ca Harzburgite	Chromite-bearing
Arnie	ARN026	35.3	34.1	Low-Ca Harzburgite	Chromite-free
Arnie	ARN027	40.0	44.7	Low-Ca Harzburgite	Chromite-bearing
Misery	MIS408	59.5	44.6	Low-Ca Harzburgite	Chromite-free
Misery	MIS417	33.3	31.4	High-Ca Harzburgite	Chromite-bearing
Pigeon	PGN301	35.0	39.7	Low-Ca Harzburgite	Chromite-free
Pigeon	PGN303	56.1	47.1	Low-Ca Harzburgite	Chromite-free
Pigeon	PGN306	48.9	46.1	Lherzolite	Chromite-free
Pigeon	PGN307	49.6	47.7	Lherzolite	Chromite-free
Pigeon	PGN310	43.4	42.9	Lherzolite	Chromite-free
Pigeon	PGN314	49.9	48.1	Low-Ca Harzburgite	Chromite-free
Pigeon	PGN316	44.5	46.8	Lherzolite	Chromite-free
Pigeon	PGN317	40.5	39.1	Low-Ca Harzburgite	Chromite-free
Pigeon	PGN340	52.0	46.1	Low-Ca Harzburgite	Chromite-free

Pyroxenitic xenoliths and lherzolitic xenoliths with no olivine in xenolith fragment.

Pipe	Sample No	Nickel and Green (1985) (kbar)	P_{Cr} Ryan et al. (1996)	Rock Suite	Minerals
Arnie	ARN028	-	29.9	Clinopyroxenite	Chromite-free
Arnie	ARN031	-	22.4	Clinopyroxenite	Chromite-free
Misery	MIS401	-	51.0	Low-Ca Harzburgite	Chromite-free
Misery	MIS409	-	28.1	Lherzolite	Chromite-bearing
Misery	MIS412	-	34.9	High-Ca Harzburgite	Chromite-free
Misery	MIS419	-	39.9	Lherzolite	Chromite-free
Misery	MIS438	-	-	Websterite	Chromite-free
Misery	MIS439	-	-	Websterite	Chromite-free
Pigeon	PGN311	-	36.2	Lherzolite	Chromite-free
Pigeon	PGN319	-	8.2	Clinopyroxenite	Chromite-free
Pigeon	PGN320	-	15.1	Clinopyroxenite	Chromite-free
Pigeon	PGN322	-	12.2	Clinopyroxenite	Chromite-free
Pigeon	PGN323	-	35.3	Clinopyroxenite	Chromite-free
Pigeon	PGN329	-	37.6	Lherzolite	Chromite-free
Pigeon	PGN337	-	32.5	Lherzolite	Chromite-free

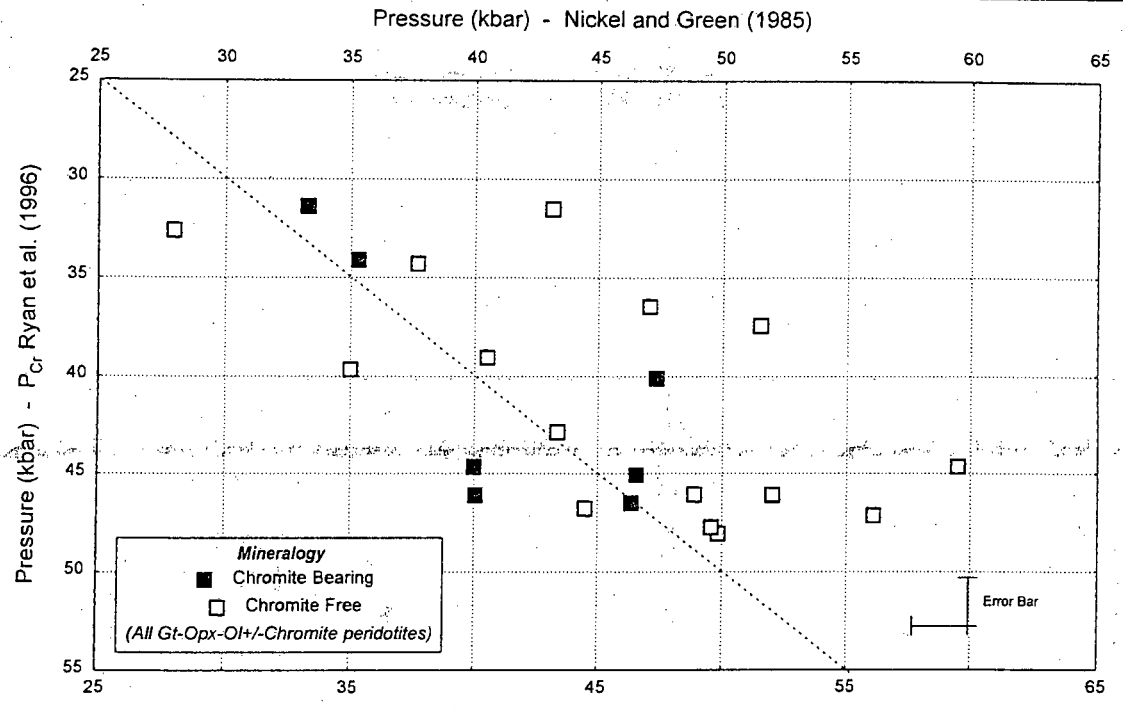

Figure 7.6 P_{Cr} plotted against pressure obtained from coexisting minerals (Nickel and Green, 1985). The correlation between the P_{Cr} and pressure derived using coexisting minerals is better for the chromite-bearing xenoliths than the chromite-free xenoliths.

Discussion

Comparison between the major and trace element geothermobarometers

Twenty-two samples have temperatures and pressures from both trace element data and major element data of coexisting garnet-olivine-orthopyroxene. A comparison was therefore made of the temperatures obtained using the trace element geothermometers (T_{Ni}) and those obtained using O'Neill and Wood (1979) in combination with Nickel and Green (1985).

The calculated Ni-in-garnet temperatures are in broad agreement with the calculated xenolith temperatures (figure 7.5). For high temperature xenoliths (>800°C) the temperatures calculated using Canil (1999) correspond more closely with the calculated xenolith temperatures than those calculated by Ryan et al. (1996). If this were the only criteria in question, then the calibration by Canil (1999) would be favoured above that by Ryan et al. (1996). However, for the low temperature samples (<800°C) the calibration by Ryan et al. (1996) corresponds more closely with the calculated xenolith temperatures, whereas those calculated by Canil (1999) deviate to higher temperatures. If one were considering only temperatures, the low temperature samples may be placed at a higher stratigraphic level than they should be using temperatures obtained by Canil (1999). Both calibrations therefore have their advantages and their disadvantages. A larger sample size would allow one to determine which of the calibrations is more true to nature.

A comparison also made between the pressures calculated using the Al-in-orthopyroxene barometer (Nickel and Green, 1985) and the P_{Cr} (Ryan et al., 1996). The chromite-bearing samples show a better correlation with the calculated xenolith geotherm (+/- 5 kbar) than the chromite-free samples (figure 7.6). The P_{Cr} geobarometer generally underestimates the pressure of the chromite-free xenoliths, a result which Ryan et al. (1996) predicted for Cr-undersaturated rocks.

Geotherms produced using trace element data

Pressures and temperatures from single mineral grains can be obtained using trace element geothermobarometry. This allows one to construct geotherms from single mineral grains from mining and exploration concentrates. The coexisting mineral associations of these grains are unknown. Temperatures and pressures were obtained from all the garnets for which trace element concentrations were attained, including those with low-Cr contents, in order to simulate such a situation.

Geotherms defined by heavy mineral concentrates show a large amount of scatter due (at least in part) to the coexistence of Cr-saturated (chromite-bearing) and Cr-undersaturated (chromite-free) xenocrysts. Ryan et al. (1996) noted that this scatter was about 3 kbar around a 35 mWm^{-2} geotherm. Due to the small number of samples, and the large scatter of determined pressure and temperatures, no distinct geotherm would have been defined using the (P_{Cr}) and (T_{Ni}) data alone for the xenoliths in this study (figure 7.7).

The advantage of knowing the associated mineral assemblage allows one to evaluate the performance of the geothermobarometer by reducing the scatter of pressures and temperatures obtained by discounting those that violate the basic assumptions of the geothermometer (needing coexisting olivine), or geobarometer (needing coexisting orthopyroxene and chromite).

This study found that the trace element geothermobarometers (P_{Cr} and T_{Ni} ; Ryan et al. 1996) compare well with the pressures and temperatures calculated from coexisting mineral pairs (O'Neill and Wood, 1979; Nickel and Green, 1985) for those samples that do not violate the basic assumptions on which the calculations are based. The majority of the peridotitic xenoliths (particularly the chromite-bearing xenoliths) plot around the 40 mWm^{-2} geotherm and in the range of the calculated pressures and temperatures using coexisting mineral pairs. Six olivine-free samples were placed in the lherzolite suite due to petrographic similarities and similar major element compositions, three of these plot off the geotherm at shallower depths, whereas three plot close to the 40 mWm^{-2} geotherm. The computed P_{Cr} and T_{Ni} the pyroxenite suite samples are unnatural, but these samples (<2 wt% Cr_2O_3 in garnet) violate one of the assumptions on which the P_{Cr} is based, namely that the garnet is in a Cr-saturated environment.

Therefore, trace element geothermobarometers (P_{Cr} and T_{Ni}) provide reliable pressures and temperatures from which to construct a geotherm from single mineral grains provided that the following basic assumptions are valid:

1. garnet coexisted with both olivine (for T_{Ni}), orthopyroxene (for P_{Cr}) and chromite (for P_{Cr});
2. olivine contained about 3000 ppm Ni;
3. garnet in equilibrium with a Cr-saturated rock, i.e. Cr in garnet and orthopyroxene buffered by coexisting chromite.

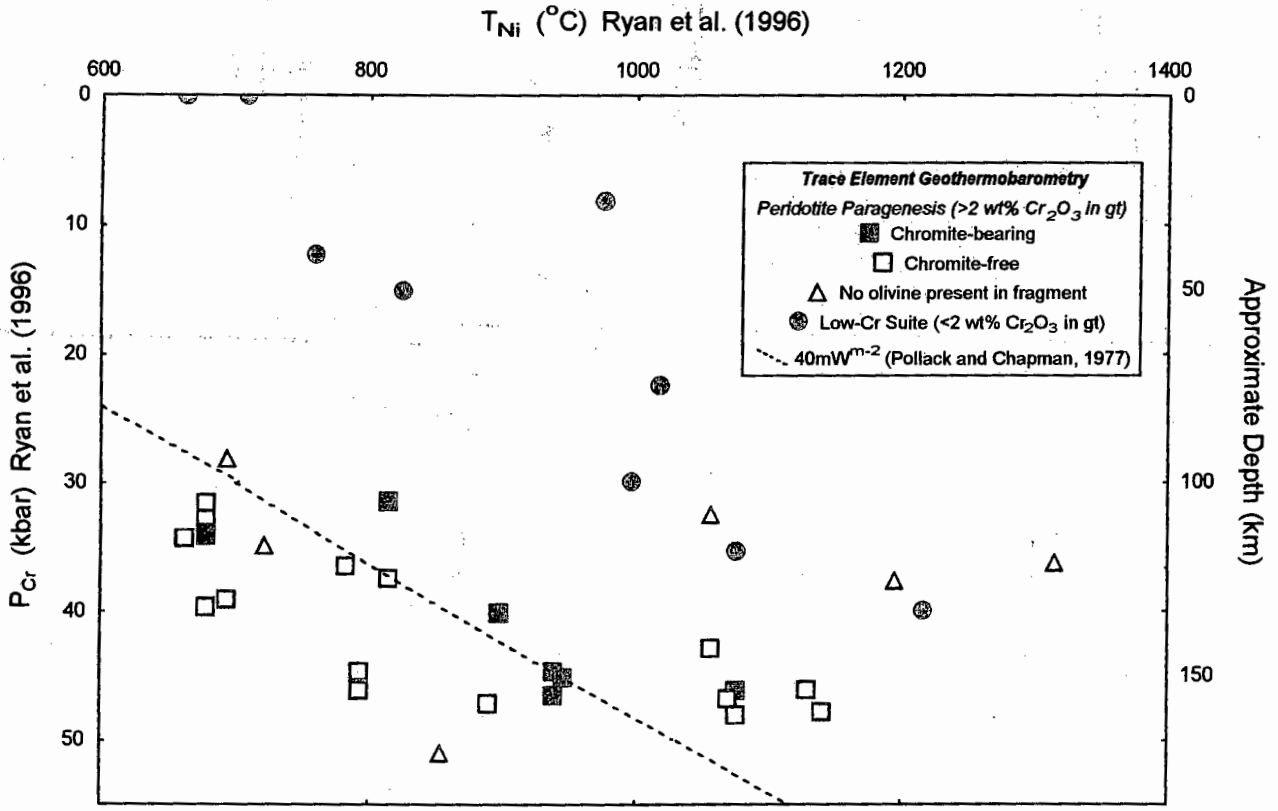

Figure 7.7 Pressures and temperatures calculated using: T_{Ni} and P_{Cr} in garnet (Ryan et al., 1996).

In order to simulate a scenario where pressures and temperatures are obtained from single minerals with unknown mineral associations (e.g. an exploration concentrate) the T_{Ni} and P_{Cr} temperatures and pressures were calculated for all garnets from which trace element concentrations were attained, including those that do not coexist with olivine and/or chromite.

The chromite-bearing peridotitic (>2 wt% Cr_2O_3 in garnet) garnets plot close to the 40 mWm^{-2} geotherm of Pollack and Chapman (1977). The chromite-free peridotitic xenoliths have a larger scatter, but also plot close to the 40 mWm^{-2} geotherm.

The P_{Cr} and T_{Ni} for the pyroxenitic (<2 wt% Cr_2O_3 in garnet) garnets and three of the olivine-free xenoliths that were presumed to be fragments of peridotitic xenoliths based on their major element chemistry are unnatural. The pressure of these xenoliths has apparently been underestimated. These xenoliths violate the basic assumptions on which the trace element geothermobarometers are based (i.e. the geothermometer needing coexisting olivine; and the geobarometer needing coexisting orthopyroxene and chromite/Cr-saturated environment).

8. DISCUSSION AND CONCLUSIONS

8. 1 INTRODUCTION

Eighty-five peridotitic and pyroxenitic mantle xenoliths from the Arnie, Misery and Pigeon kimberlites in the Lac de Gras region of the Northwest Territories were selected for this study. After a petrographic study the major element compositions of individual minerals were determined using a wavelength dispersive electron microprobe, trace element abundances were then determined using laser ablation ICP-MS. Pressures and temperatures of equilibration were then calculated using garnet-olivine, garnet-orthopyroxene and trace element geothermobarometers. The findings of these investigations are detailed at the end of their respective chapters. This chapter seeks to bring unity to these findings, and place them in context with other published work.

8. 2 MANTLE HETEROGENEITY AND DISEQUILIBRIUM FEATURES

A petrographic study of the xenoliths was undertaken using both transmitted light microscopy and binocular microscopy. It was limited by the small sample size (0.5-1.5 cm) in comparison to the large grain size (0.05-1 cm). Rock types were determined using mineral associations within the xenolith in conjunction with mineral compositions. The peridotitic suite consists of both garnet-harzburgites and garnet-lherzolites, whereas the pyroxenitic suite consists of garnet-clinopyroxenites and garnet-websterites.

Peridotitic xenoliths were dominant at all three kimberlite localities, but the Misery kimberlite entrained a higher proportion of eclogitic and websteritic xenoliths to peridotitic xenoliths than the Pigeon and Arnie kimberlites. The Misery kimberlite also had a lower proportion of low-Ca harzburgitic xenoliths to lherzolitic xenoliths than the Pigeon and Arnie kimberlites. The variation in the mantle xenoliths entrained in three kimberlites within a 40 km radius of one another may be indicative of small-scale mantle heterogeneity. Other xenoliths studies from the Slave craton have noted the large variety of xenoliths (lherzolites, harzburgites, wehrlites, eclogites, pyroxenites and megacrysts; Kopylova et al., 1999b) and lateral heterogeneity (Kopylova and Russell, 2000) of the mantle beneath the Slave province.

A large number of the pyroxenitic xenoliths (ARN028, ARN031, MIS428, MIS451, MIS454) have recrystallization and/or exsolution features. Spinel exsolution from clinopyroxene and/or orthopyroxene is also evident in lherzolitic (MIS431) and harzburgitic (ARN019) xenoliths. Similar

disequilibrium features have been noted in other kimberlite localities on the Slave craton, e.g. the Jericho kimberlite (Kopylova et al., 1999b). These transient features (Tuttle and Bowen, 1958; Field and Haggerty, 1994) are indicative of partial re-equilibration of these xenoliths from a region of high pressure and temperature to lower pressure and temperature, where the pyroxene structure can no-longer accommodate Cr^{3+} in it's structure (Ryan et al. 1996). The breakdown of garnet to kelyphite in the xenoliths from the Lac de Gras region also suggests a period of decompression and/or heating in order to return to the spinel stability field (Kempton et al., 1999). If the kelyphite rim was not caused by decompression, then a source of heat may have been provided by the intruding kimberlites. The re-equilibration of these xenoliths was arrested by entrainment in ascending kimberlites.

Such dynamic processes and small scale heterogeneity suggest a complex history for the lithosphere beneath the Slave province. A cold, brittle lithospheric keel subjected to multiple orogenies (i.e. the Thelon and Wopmay orogenies, 2.2-1.92 Ga, Doyle et al., 1999) may fracture and produce complex stratigraphic sections within the mantle. The fact that the Misery kimberlite is located less than 2 km away from the intersection of three different dyke swarms (figure 2.5) suggests that it is a region of structural weakness within the continental lithosphere. This weakness may be related to faulting as the dykes and the Misery kimberlite may preferentially have used the faults as a conduits. Helmstaedt and Harrap (1999) suggest that fault movements within the lithosphere, or isostatic rebound of Archean lithosphere due to erosion of overlying strata may trap and store diamonds and mantle rocks outside their stability fields. Although their theory cannot be validated without more information about the internal structure of the continental lithosphere, it may explain the small scale heterogeneities in the mantle sampled by kimberlites in close proximity to one another.

8. 3 COMPOSITION AND MODE OF FORMATION

The harzburgitic xenoliths were subdivided into two groups based on the CaO and Cr_2O_3 content in garnet using the 85% line of Gurney (1984). The major element mineral composition of the high-Ca harzburgitic xenoliths is similar to that of the lherzolitic xenoliths, whereas the trace element mineral composition of the garnets are characteristic of the low-Ca harzburgitic garnets in this study and other studies (Shimizu, 1975; Nixon et al., 1987; Hoal et al., 1994; Shimizu and Sobolev, 1995; Stachel et al., 1999; Stiefenhofer et al., 1999).

The minerals of the low-Ca harzburgitic xenoliths tended to be more Mg rich and Ca poor than those of the lherzolitic xenoliths. In a discussion about different mechanisms for the formation of the low-Ca harzburgites Boyd et al. (1993) also noted that in general low-Ca harzburgites are slightly more

depleted in Si, Ca, Al and Fe, and have higher Mg and Ni contents in comparison to lherzolitic xenoliths.

The compositional differences between the lherzolitic xenoliths and the harzburgitic xenoliths would suggest that they either had a different mode of formation, or that they have undergone different processes since formation. Several theories have been suggested in literature for the formation of low-Ca garnet harzburgites, namely:

1. subduction and partial melting of oceanic lithosphere (Kesson and Ringwood, 1989; Boyd et al., 1993)
2. depletion due to multiple melt extraction (Boyd et al., 1993);
3. extraction of Ca from garnet into crystalline carbonate (Boyd and Gurney, 1982) or carbonate melt (Luth, 1999)

The low-Ca harzburgitic minerals are geochemically similar to peridotitic mineral inclusions in diamond, which suggests a genetic link (Gurney and Switzer, 1973; Gurney, 1984; Richardson et al., 1984; Meyer, 1987). In addition to providing a mechanism for the formation of the low-Ca harzburgites, the third mechanism (Boyd and Gurney, 1982; Luth, 1999) would provide a source of carbon for diamond formation, and compliment the theory of Griffin et al. (1999b) for the formation of the MREE-enriched pattern in low-Ca harzburgitic garnets. Griffin et al. (1999b) suggest that due to size similarities the LREE's which normally substitute for Ca have fewer sites available for substitution in the Ca-poor harzburgitic garnets than in the Ca-rich lherzolitic garnets. A carbonate-rich fluid would both strip the rock of Ca (Luth, 1999), and may provide a source for the LREE's. Whereas these processes may be contemporaneous, they need not be. A carbonate-rich fluid may strip the host rock of carbonate in one process, and LREE enrichment may occur at a later time from a second carbonate-rich fluid, or metasomatic fluid or proto-kimberlitic fluids. Coexistence of harzburgitic xenoliths with a carbonate may also explain the apparent rarity of these rocks in comparison to lherzolitic rocks. The explosive decomposition and reaction of the carbonate during assent of the kimberlite would result in the disaggregation of the harzburgitic xenolith (Boyd and Gurney, 1982).

8.4 REE MODELLING

This study, and numerous other studies (Shimizu, 1975; Nixon et al., 1987; Hoal et al., 1994; Shimizu and Sobolev, 1995; Stachel et al., 1999; Stiefenhofer et al., 1999) have noted two REE patterns that commonly occur in harzburgitic garnets (both high- and low-Ca) and garnet inclusions in diamond, but not in lherzolites, namely a MREE enriched pattern (Sm-peak) and a sinusoidal pattern (Ce, Nd-peak).

Whereas the MREE-enriched pattern may be explained by melt interaction (Hoal et al., 1994; Griffin et al., 1999b), no model was found to explain the formation of the sinusoidal REE patterns.

In order to suggest an explanation for the sinusoidal REE pattern in low-Ca harzburgitic garnets this study investigated the partitioning of REE's between phases during processes of exsolution from a mineral with a chondrite normalised sinusoidal REE pattern. Majorite was selected as the starting material as it may have a sinusoidal REE pattern as it has similar partitioning coefficients to clinopyroxene. In addition, the lithospheric mantle beneath the Slave craton has a majoritic component. Majoritic inclusions in diamond have been found in the Lac de Gras region (Davies et al., 1999; Pokhilenko et al., 2001).

Whereas the absolute abundance's of the resultant phases from exsolution processes are dependant on the initial concentration, the model shows that the sinusoidal REE pattern from a majoritic starting material could be preserved in the exsolved pyrope if the exsolution products are pyrope and orthopyroxene (i.e. a harzburgitic composition; Model A). However, if the starting majoritic component was more Ca-rich and the exsolution products were clinopyroxene and pyrope then the exsolved pyrope would have a LREE-depleted pattern (Model B), as seen in the lherzolitic garnets.

8. 5 GEOTHERMS AND P-T-COMPOSITION RELATIONSHIP

Geothermobarometric calculations indicate that the xenoliths from the Arnie, Misery and Pigeon kimberlites define a cratonic geotherm of 40 $mW.m^{-2}$. The pressures and temperatures determined using trace element geothermobarometry were similar to those determined using coexisting mineral pairs for those xenoliths for which the assumptions on which the geothermobarometers were based were true. The geotherm determined using the trace element geothermobarometers was therefore similar to that calculated using coexisting minerals.

Geothermobarometry has shown that although there is a geochemical similarity between low-Ca harzburgitic garnets and peridotitic garnets included in diamond, not all low-Ca harzburgitic xenoliths have pressures and temperatures of equilibration within the diamond stability field (900-1300°C and 40-55 kbar, Nickel and Green, 1985). The low-Ca harzburgites that have a low Cr_2O_3 content (<6 wt%) have equilibrated at shallower depths than the diamond stability zone (ARN008, ARN013, MIS417), whereas some lherzolites with high Cr_2O_3 content (>8 wt%) have equilibrated within the diamond stability zone (PGN339 and PGN310). In general, those samples with Cr_2O_3 content between 6-8 wt% straddle the diamond-graphite transition line of Kennedy and Kennedy (1976).

8. 6 LAYERED MANTLE BENEATH THE SLAVE PROVINCE?

Numerous mantle studies from kimberlite localities within the NWT recognise a layered lithosphere beneath the Slave craton (Griffin et al., 1999a; Pearson et al., 1999; Kopylova and Russell, 2000).

A plot of Y and Ti versus temperature (T_{Ni}) would suggest that the lherzolitic garnets have higher temperatures of equilibration and are more enriched in Y and Ti than the harzburgitic garnets (figures 8.1 and 8.2). These findings would correlate well with the layered mantle theory proposed by Griffin et al. (1999a) and Pearson et al. (1999). The two layers mapped out by Griffin et al. (1999a) are based on the major and trace element concentrations of single garnet and chromite grains from numerous kimberlites over an area of 9000 km^2. They recognise an ultra-depleted layer above a less depleted layer that contains eclogite, with the contact at 150 +/-10 km beneath Lac de Gras. This ultra-depleted layer is restricted to the northern part of the Contwyoto terrane (Griffin et al., 1999a). The garnets in peridotites derived from the ultra-depleted layer have low median values of Y (1.5 ppm), Zr (5 ppm), Ti (380 ppm) and Ga (4 ppm) in comparison to those from the deeper layer having median values of Y (8 ppm), Zr (33 ppm); Ti (1800 ppm) and Ga (8 ppm).

The compositional boundary of Griffin et al. (1999a) at 150 +/-10 km coincides with a step in a geotherm calculated for the xenoliths from the Tli Kwi Cho kimberlite complex south of Lac de Gras (kimberlite pipes DO-18, DO-27 and A154S; Pearson et al., 1999). The numerous geothermobarometers used (including O'Neill and Wood, 1979; and Nickel and Green, 1985) concur that below 900°C the xenoliths lie on the 35 mWm^{-2} geotherm, whereas between 900°C and 1250°C they lie on the 40 mWm^{-2} geotherm of Pollack and Chapman (1977).

However, a larger number of pressures and temperatures have been determined for the peridotitic population using coexisting garnet-olivine and garnet-orthopyroxene geothermobarometry in this study than trace element techniques. This major element geothermobarometry does not support two distinct layers within the lithospheric mantle beneath the central Slave craton. Figure 8.3 shows that harzburgites and lherzolites are inter-layered throughout the mantle beneath the Slave craton.

Only a small number of xenoliths were selected for trace element analysis in this study. A more extensive study of the trace element composition and geothermobarometric state of xenoliths in comparison to single grain geothermobarometry from the Lac de Gras region would be necessary to decide if the layering beneath the Lac de Gras region is real or not. Such a large-scale trace element study is beyond the scope of this project.

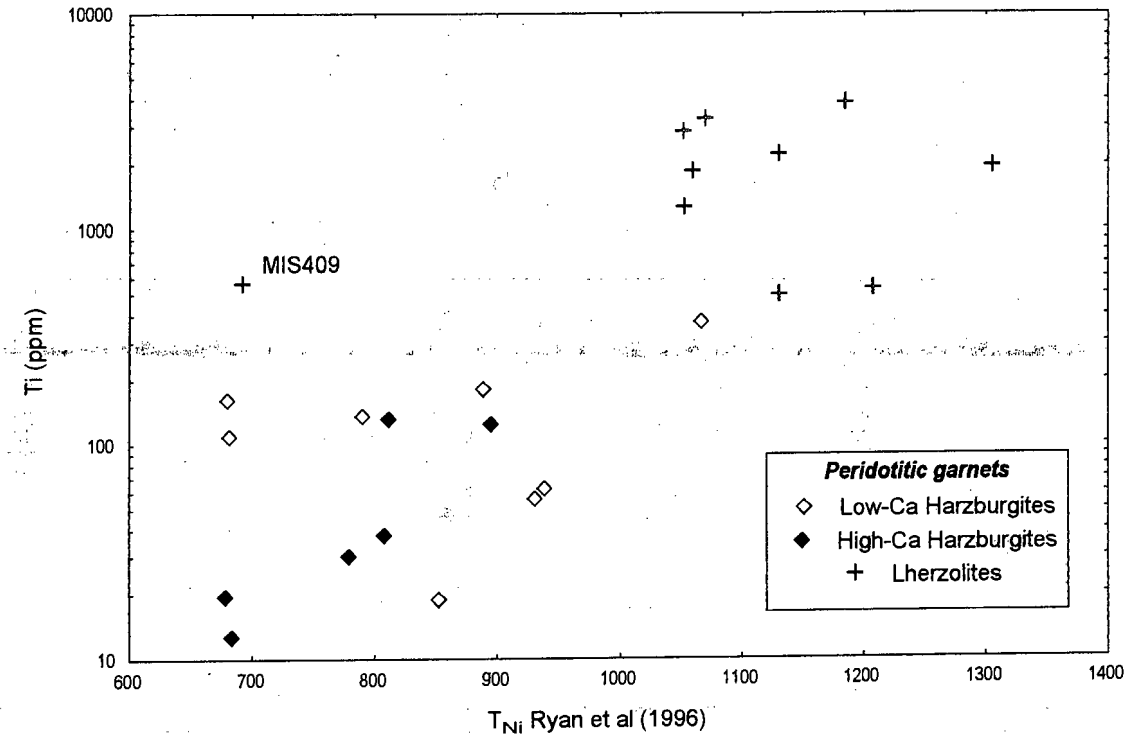

Figure 8.1 Ti in garnet vs T_{Ni} . Based on single grain trace element geothermobarometry it appears that the there are two distinct layers within the lithospheric mantle beneath the Slave craton. The lherzolitic garnets are more enriched in Ti, and have higher temperatures of equilibrium than the harzburgitic garnets.

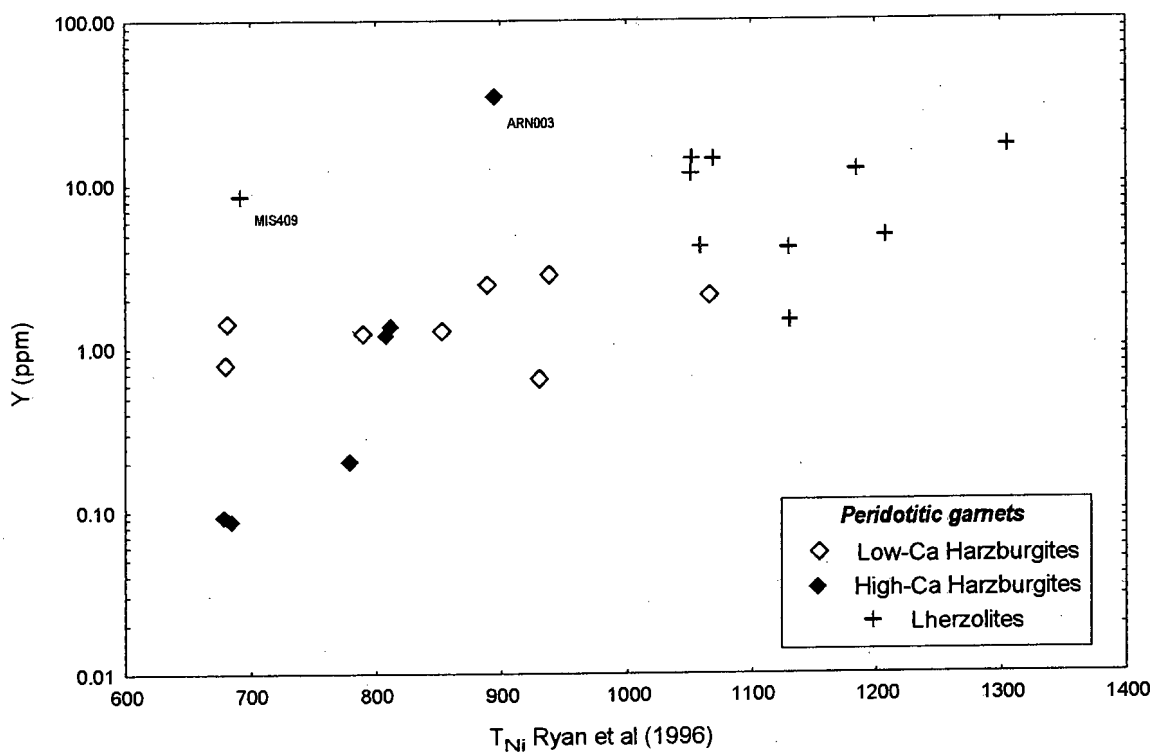

Figure 8.2 T in garnet vs T_{Ni} . This plot also shows two distinct layers defined by the lherzolitic and harzburgitic garnets. According to single mineral trace element geothermobarometry the lherzolitic garnets are more enriched in Y, and have higher temperatures of equilibrium than the harzburgitic garnets.

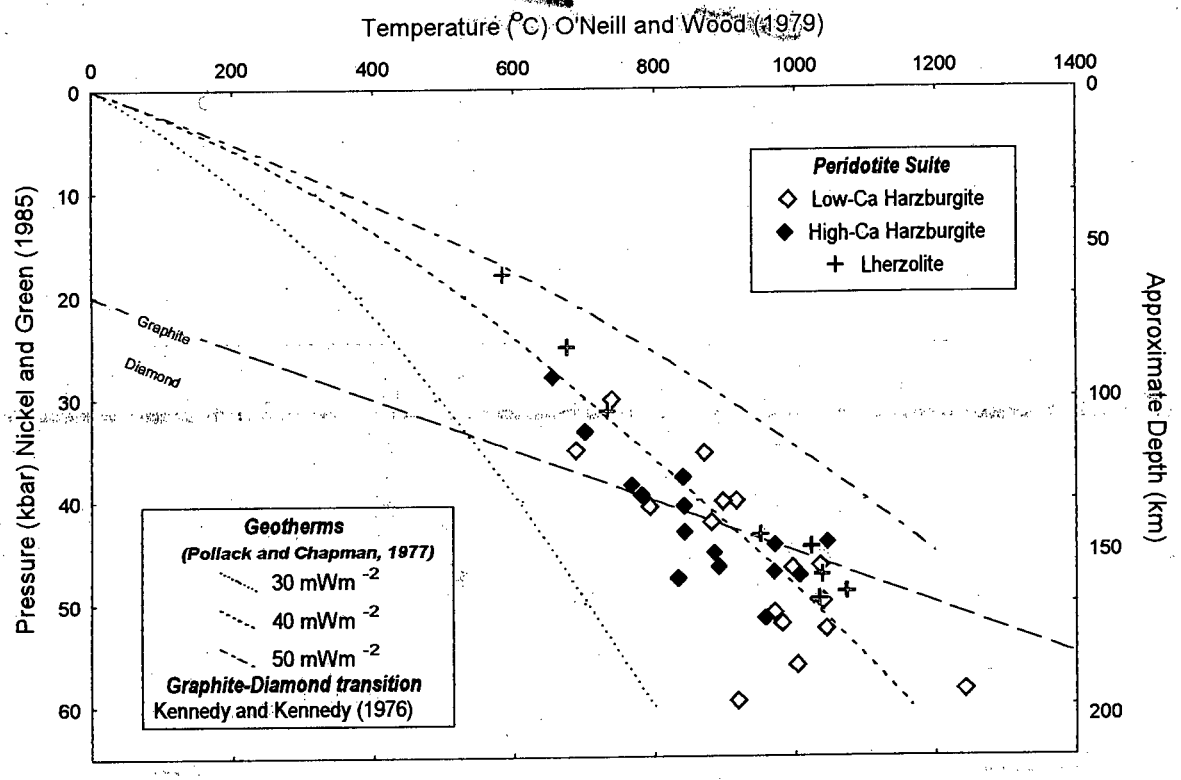

Figure 8.3 In contrast to the T_{Ni}-Composition plots (fig 8.1 and 8.2), pressures and temperatures determined using coexisting mineral pairs indicate that harzburgitic xenoliths are abundant at depth (110-180 km), and that although there is a higher concentration of lherzolites at greater depth (140-170 km), they are inter-layered with harzburgites over a large depth interval (80-170 km).

8. 7 CONCLUSIONS

- A large variety of mantle xenoliths were entrained by the Arnie, Misery and Pigeon kimberlites, namely lherzolites, harzburgites, clinopyroxenites and websterites. Eclogites and megacrysts were noted during sample selection, but were not selected for study as they form part of an independent study.

- Spinel exsolution from clinopyroxene and orthopyroxene has been observed in both the peridotitic and pyroxenitic xenoliths. Garnet exsolution from clinopyroxene is apparent in one clinopyroxenite from the Misery kimberlite. A greater number of xenoliths with exsolution features were noted from the Misery kimberlite than the Arnie and Pigeon kimberlites. These exsolution textures attest to dynamic processes in operation within the lithospheric mantle beneath the Slave craton. The variety and different proportions of xenolith types sampled by individual kimberlites also suggests small scale mantle heterogeneity.

- Major and trace element studies highlight the compositional differences between the pyroxenitic and peridotitic xenoliths, and subtle differences between the lherzolitic and harzburgitic xenoliths:
    - The minerals of the pyroxenitic xenoliths are more Fe-rich and Cr-poor than those of the peridotitic minerals. The minerals of the harzburgitic xenoliths are generally more Mg-rich than those of the lherzolitic xenoliths.
    - Trace element abundances in garnet differ between different suites. The elements (Ti, Y, Nd and Zr) in garnet discriminate well between the harzburgitic, lherzolitic and pyroxenitic suites. The majority of the harzburgitic garnets (both low-Ca and high-Ca) are LREE-enriched with respect to the lherzolitic garnets, as reflected in their higher Nd content. In contrast, the lherzolitic garnets are more enriched in Ti and Y than the harzburgitic garnets. The abundance of Zr in garnet discriminates well between the lherzolitic and pyroxenitic garnets. The lherzolites have higher Zr contents than the pyroxenites (figure 6.1).

- The distribution of REE's between phases during exsolution processes were modelled using mineral/mineral partition coefficients. Based on the assumption that majorite has a sinusoidal REE pattern, the models show that the sinusoidal REE pattern can be preserved in the exsolved pyrope if pyrope and orthopyroxene are the exsolution products. However, the exsolved pyrope has a LREE-depleted pattern if pyrope and clinopyroxene are the exsolution products.

- Geothermobarometry using the calibrations by Nickel and Green (1985) and O'Neill and Wood (1979) show that the xenoliths from the Arnie, Misery and Pigeon kimberlites define a cratonic geotherm of 40 $mW.m^{-2}$.

- The pressure and temperature determined using trace element geothermobarometry (P_{Cr} and T_{Ni}) is similar to that determined using major element geothermobarometry (Fe and Mg exchange between garnet and olivine; and Al in orthopyroxene).
  - The deviation of T_{Ni} from the major element temperature (O'Neill and Wood, 1979) is smaller for the T_{Ni} (Canil, 1999) than the T_{Ni} (Ryan et al., 1996) for xenoliths with temperatures above 800°C. However, the calibration by Canil (1999) overestimates the temperature of xenoliths that equilibrated at temperatures below 800°C according to major element geothermobarometry. The calibration of Ryan et al. (1996) provides a better temperature estimate for those xenoliths with equilibration temperatures below 800°C. *Future study required:* A larger data set would be required to determine which of these calibrations provide a better reflection of the true pressure and temperature.
  - The P_{Cr} determined using Ryan et al. (1996) compares favourably with the pressure determined using major element geothermobarometry for those samples that coexist with chromite, and garnets with high Cr_2O_3 contents, i.e. those samples that did not violate the assumptions on which the geobarometer is based.

- Trace element compositions and geothermobarometry appear to support a two-layered lithospheric mantle model (Griffin et al., 1999; Pearson et al., 1999). However, major element geothermobarometry does not support the two-layer model, but shows that harzburgites and lherzolites are inter-layered with depth throughout the lithospheric mantle. *Future study required:* Further investigations using coexisting mineral (major element) geothermobarometry and trace element compositions would be required to determine if a two-layered lithospheric mantle exists beneath this region of the central Slave craton.

9. REFERENCES

Anders E. and Grevesse N. (1989) Abundances of the elements; meteoritic and solar. *Geochimica Cosmochimica Acta*, **53**, p 197-214

Banno S. (1970) Classifications of eclogite in terms of physical conditions of their origin. *Phys. Earth Planet. Inter.*. **3** p 405-421

Barrell J. (1914) The strength of the earth's crust: Part VI. Relations of isostatic movements to a sphere of weakness - the Asthenosphere. *J of Geology*, **22**, p 655-683

Basu A.R. (1977) Textures, microfractures and deformation of ultramafic xenoliths from San Quintin, Baja California. *Tectonophysics*, **43**, p213-246

Baumgartner M. (1994) The xenoliths from the Okenyenya volcanic breccia. *MSc thesis, University of Cape Town, RSA*

Bergman S.C. (1987) Historical Review. *In: Mantle Xenoliths Ed:* Nixon P.H. John Wiley & Sons Ltd. p 33-40

Bilal A. and Touret J.L.R. (2001) Translated Title: Mantle Xenoliths in Recent volcanism from the Syrian Rift. *Bulletin de la Societe Geologique de France.* **172, 1.** p 3-16

Boyd F.R. (1973) A pyroxene geotherm. *Geochimica Cosmochimica Acta*, **37**, p2533-2546

Boyd F.R. (1989) Compositional distinction between oceanic and cratonic lithosphere. *Earth and Planetary Science letters*, **96**, p 15-26.

Boyd F.R. and Canil D. (1997) Peridotite Xenoliths from the Slave Craton, North West Territories. *Seventh Annual V.M. Goldschmidt Conference. LPI Contribution No. 921 Lunar and Planetary Institute, Housten,* p 34-45.

Boyd F.R. and England J.L. (1964) The system enstatite-pyrope. *Carnigie Inst. Washington Yearbook.* **63** p 157-161

Boyd F.R. and Gurney J.J. (1982) Low-Ca garnets: Keys to craton structure and diamond crystallization. *Carnegie Institution of Washington Yearbook,* **71**, p 261-267

Boyd F.R. and Gurney J.J. (1986) Diamonds and the African lithosphere. *Science*, **232**, p 472-477

Boyd F.R. and Nixon P.H. (1972) Ultramafic nodules from the Thaba Putsoa kimberlite pipe. *Carnegie Inst. Year Book 81*, p 362-373

Boyd F.R., Pearson D.G. and Mertzman S.A. (1999) Spinel-facies peridoties from the Kaapvaal root. *In: Proceedings of the Seventh International Kimberlite conference, Cape Town. Eds.: Gurney J.J., Gurney J.L., Pascoe M.D. and Richardson S.H.* p 40-48

Boyd F.R., Pearson D.G., Nixon P.H. and Mertzman S.A. (1993) Low-Ca garnet harzburgites from southern Africa: their relations to craton structure and diamond crystallization. *Contributions to Mineralogy and Petrology*, **113**, p 352-366

Brey G.P. and Köhler T. (1990) Geothermobarometry in four-phase lherzolites II. New thermobarometers, and practical assessment of existing thermobarometers. *J of Petrology,* **31 (6)**, p 1353-1378

Brey G.P., Doroshev A. and Kogarko L. (1991) The join pyrope-knorringite: Experimental constraints for a new geothermometer for coexisting garnet and spinel. *In: 5th International Kimberlite Conference, CPRM Special Publication, 2/9. Companhai de Pesquisa de Recursos Mineralais, Brazilia,* p 26-28

Burgess S.R. and Harte B. (1999) Tracing lithospheric evolution through the analysis of heterogeneous G9/G19 garnets in peridotite xenoliths, I: major element chemistry. *In: Proceedings of the seventh international kimberlite conference, Cape Town. Eds.: Gurney J.J., Gurney J.L., Pascoe M.D. and Richardson S.H.* p 66-80

Canil D. (1999) The Ni-in-garnet geothermometer: calibration at natural abundances. *Contributions to Mineralogy and Petrology*, **136**, p 240-246

Canil D. and O'Neill H. St. C. (1996) Distribution of ferric iron in some upper mantle assemblages. *J of Petrology*, 37, p 609-635

Carlson J.A., Kirkley M.B., Thomas E.M. and Hillier W.D. (1999) Recent Canadian Kimberlite Discoveries. *In: Proceedings of the seventh international kimberlite conference, Cape Town. Eds.: Gurney J.J., Gurney J.L., Pascoe M.D. and Richardson S.H.* p 81-89

Carswell D.A. (1990) Eclogites and eclogite facies: definitions and classification. *In: Eclogite facies Rocks Ed: Careswell D.A,* Blackie, p 1-13

Carswell D.A. and Harley S.L. (1989) Mineral barometry and thermometry. *In: Eclogite facies rocks. Ed:* Careswell D.A. *Glasgow: Blackie, p 83-110*

Chen X., Wang X. Chen Z. and Zhang Q. (1996) The P-T path of formation and evolution of Mengxhong Eclogite, Donghai, Jiangsu. *J of Geomatics.* **2,4.** p 49-54.

Clement C.R., Skinner E.M.W. and Scott Smith B.H. (1984) Kimberlite redefined. *J of Geology,* **92 (2)**, p 223-228

Clifford T.N. (1970) The structural framework of Africa. *In: African magmatism and tectonics. Eds: Clifford and Gass* , Hafner Publ. Co., Darien, Conn. p 1-26.

Clowes R.M., ed. (1997) LITHOPROBE V Proposal - evolution of a continent revealed. Published by the LITHOPROBE Secretariat. The University of British Columbia, Vancouver, BC, p 292

Daly R.A. (1914) *Igneous rocks and their origin.* McGraw-Hill, New York, pp 563

Davies R.M., Griffin W.L., Pearson N.J., Andrew A.S., Doyle B.J. and O'Reilly S.Y. (1999) Diamonds from the deep: Pipe DO-27, Slave Craton, Canada. *In: Proceedings of the seventh international kimberlite conference, Cape Town. Eds.: Gurney J.J., Gurney J.L., Pascoe M.D. and Richardson S.H.* p 148-155

Davis W.J. and Kjarsgaard B.A. (1997) A Rb-Sr isochron age for a kimberlite from the recently discovered Lac de Gras field, Slave Province, Northwest Canada. *J of Geology.* **105**, p 503-509

Dawson J.B. (1981) The nature of the upper mantle. Hallimond Lecture to the mineralogical society of Great Britain and Ireland, 1980. *Mineralogical Magazine,* **44**, p 1-18

Mounting the samples in epoxy has a few disadvantages, as distinguishing between strained and unstrained minerals is difficult, and exsolution textures are difficult to detect.

The advantages however out-weigh the disadvantages:

1) The colours of minerals are vivid and can be clearly noted (figure 3.1). Previous studies have noted a correlation between garnet colour and mineral chemistry (Sobolev et al., 1973; Dawson and Stephens, 1975). Garnet colour is a useful aid for the classification of samples into different rock types, and has application for diamond exploration programs.
2) The 3-dimensional nature of the samples is readily apparent. This is particularly noticeable during textural analysis based on a 2-dimensional textural scheme (figure 4.4).
3) The samples are thick enough to easily obtain full trace element analyses using laser ablation techniques without ablating through the mineral.

Samples from the Arnie kimberlite

Scale bar: 2cm. Plane-polarised light.

Samples from the Pigeon kimberlite

Scale bar: 2cm. Plane-polarised light.

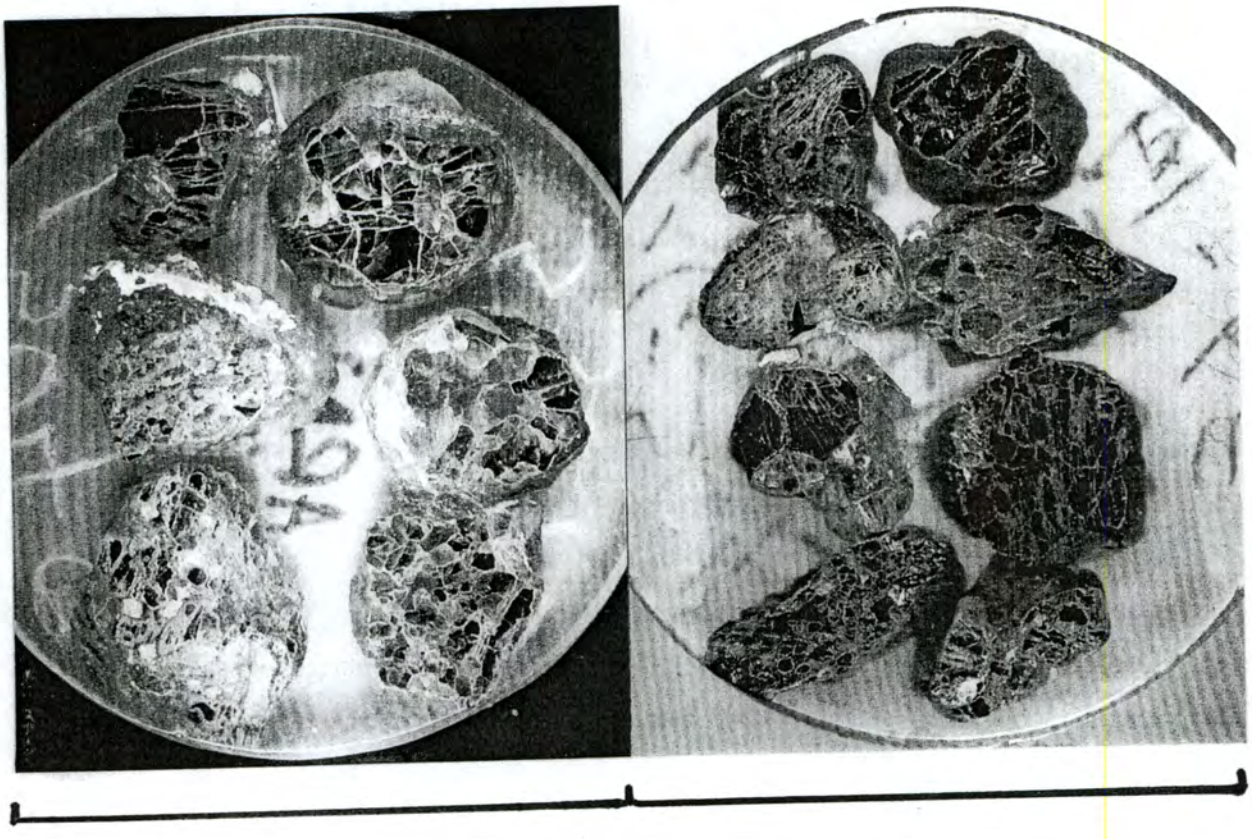

Figure 3.1 Samples mounted in epoxy show vivid colours. The xenoliths from the Arnie kimberlite are chromite-rich, whereas those from the Pigeon kimberlite have a higher proportion of clinopyroxene.

Dawson J.B. and Stephens W.E. (1975) Statistical classification of garnets from kimberlite and associated xenoliths. *J of Geology*, **83**, p589-607.

Deer W.A., Howie R.A. and Zussman J. (1995) *An introduction to the rock-forming minerals, 2nd edition.* Longman Group Ltd, England, pp 696

Dia Met Annual Reports (1997-1998), (1998-1999), (1999-2000)

Doyle B.J., Kivi K. and Scott Smith B.H. (1999) The Tli Kwi Cho (DO27 and DO18) diamondiferous kimberlite complex, Northwest Territories, Canada. *In: Proceedings of the seventh international kimberlite conference, Cape Town. Eds.: Gurney J.J., Gurney J.L., Pascoe M.D. and Richardson S.H.* p 194-204

Droop G.T.R. (1987) A general equation for estimating Fe^{3+} concentrations in ferromagnesian silicates and oxides from microprobe analyses, using stoichiometric criteria. *Mineralogical Magazine*, **51**, p 431-435

Earnest R.E. and Baragar W.R.A. (1992) Evidence from magmatic fabric for the flow pattern of magma in the Makenzie giant radiating dyke swarm. *Nature*, **356.** p 511-513

Fahrig W.F. (1987) The tectonic setting of continental dyke swarms: Failed arm and early passive margins. *In: Mafic dyke swarms Eds: Halls H.C. and Fahrig W.F. Geological Society of Canada Special Paper*, **34**, p 331-348

Field S.W. and Haggerty S.E. (1994) Symplectites in upper mantle peridotites: development and implications for the growth of subsolidus garnet, pyroxene and spinel. *Contributions to Mineralogy and Petrology*, **118**, p 138-156

Finnerty A.A. and Boyd F.R. (1987) Thermobarometry for garnet peridotites: basis for the compositional structure of the upper mantle. *In: Mantle Xenoliths Ed: Nixon P.H.* Wiley, London, p 381-402

Fipke C.E., Gurney J.J. and Moore R.O. (1995) Diamond exploration techniques emphasising indicator mineral geochemistry and Canadian examples. *Geological Survey of Canada Bulletin 423*, p 1-86

Francis D.M. (1978) The Implications of the Compositional Dependence of Texture in Spinel Lherzolite Xenoliths. *J of Geology*, **86**, p 473-485

Gallahan W.E. and Nielsen R.L. (1992) The partitioning of Sc, Y and the rare earth elements between high-Ca pyroxene and natural mafic to intermediate lavas at 1 atmosphere. Geochimica Cosmochimica Acta., **56**, p 2387-2404

Geikie A. (1897) *The founders of geology*. Macmillan, pp 486

Grégoire M., Bell D.R. and le Roex A.P. (2001) Garnet lherzolites from the Kaapvaal Craton (South Africa): trace element evidence for a metasomatic history. *Preprint.*

Griffin W.L. and Ryan C.G. (1995) Trace elements in indicator minerals: area selection and target evaluation in diamond exploration. *J of Geochemical Exploration*, **53**, p 311-337

Griffin W.L., Cousens D.R., Ryan C.G., Sie S.H. and Suter G.F. (1989) Ni in chrome pyrope garnets: a new geothermometer. *Contributions to Mineralogy and Petrology.*, **103**, p 199-202

Griffin W.L., Doyle B.J., Ryan C.G., Pearson N.J., O'Reilly S.Y., Natapov L., Kivi K., Kretschmar U. and Ward J. (1999a) Lithospheric Structure and mantle terranes: Slave craton, Canada. *In: Proceedings of the seventh international kimberlite conference, Cape Town. Eds. Gurney J.J., Gurney J.L., Pascoe M.D. and Richardson S.H.* p 644-658

Griffin W.L., Shee S.R., Ryan C.G., Win T.T. and Wyatt B.A. (1999b) Harzburgite to lherzolite and back again: metasomatic processes in ultramafic xenoliths from the Wesselton kimberlite, Kimberley, South Africa. *Contributions to Mineralogy and Petrology*, **134**, p 232-250

Griffin W.L., Smith D. Ryan C.G., O'Reilly S.Y. and Win T-T. (1996) Trace element zoning in mantle minerals: Metasomatism and thermal events in the upper mantle. *The Canadian Mineralogist*, **34**, p 1179-1193

Grütter H.S., Apter D.B. and Kong J. (1999) Crust-Mantle coupling: Evidence from mantel-derived xenolcrystic garnets. *In: Proceedings of the seventh international kimberlite conference, Cape Town. Eds. Gurney J.J., Gurney J.L., Pascoe M.D. and Richardson S.H.* p 307-313

Gurney J.J. (1984) A correlation between garnets and diamonds in kimberlites. *In: Kimberlites occurrence and origin; a basis for conceptual models in exploration. Eds: Glover J.E. and Harris P.G.* Univ. West Australia, Geology Dept. and Extension Service. Perth, West Australia, p 143-166

Gurney J.J. and Switzer G.S. (1973) The discovery of garnets closely related to diamonds in the Finsch Pipe, South Africa. *Contributions to Mineralogy and Petrology*, **39**, p 103-116

Gurney J.J., Jacob W.R.O. and Dawson J.B. (1979) Megacrysts from the Monastery kimberlite pipe, South Africa. *In: The Mantle Sample: Inclusions in Kimberlites and Other Volcanics, Eds: Boyd F.R. and Meyer H.O.A.* p. 227-243, A.G.U. Washington.

Haggerty S.E. (1995) Petrochemistry of ultradeep (>300km) and transition zone xenoliths. *Extended abstracts of 6th International Kimberlite Conference, United Institute of Geology, Geophysics and Mineralogy, Siberian branch of Russian Academy of Sciences,* p 214-216

Harley S.L. (1984) The solubility of Alumina in Orthopyroxene coexisting with garnet in FeO-MgO-Al_2O_3-SiO_2 and Ca-FeO-MgO-Al_2O_3-SiO_2. *J of Petrology,* **25**,3. p 665-696

Harte B. (1977) Rock nomenclature with particular relation to deformation and recrystallization textures in olivine-bearing xenoliths. *J of Geology*, **85**, p279-288

Harte B. (1987) Metasomatic events recorded in mantle xenoliths: an overview. *In: Mantle Xenoliths Ed: Nixon P.H.* Wiley, London, p 625-640

Harte B. and Gurney J.J. (1975) Evolution of clinopyroxene and garnet in an eclogite nodule from the Roberts Victor kimberlite pipe, South Africa. *Phys. Chem. Earth,* **9.** p 367-387

Harte B., Gurney J.J. and Harris J.W. (1980) The formation of peridotite suite inclusions in diamond. *Contributions to Mineralogy and Petrology,* **72**, p 181-190

Hatton C.J. (1978) Geochemistry and origin of xenoliths from the Roberts Victor mine. *Ph.D. Thesis, Univ. Cape Town* (unpublished).

Helmstaedt H. and Gurney J.J. (1992) Geotectonic controls on the formation of diamonds and their kimberlitic and lamproitic host rocks: applications to diamond exploration. *Proceedings of the 5th International kimberlite conference*, Brazil, p 236-250

Helmstaedt H.H. and Harrap R.M. (1999) Tectonic aspects of the diamond-kimberlite connection: Testing for explanatory coherence in upper mantle models. *In: Proceedings of the seventh international kimberlite conference, Cape Town. Eds.: Gurney J.J., Gurney J.L., Pascoe M.D. and Richardson S.H.* p 361-371

Hoal K.E.O., Hoal B.G., Erlank A.J. and Shimizu N. (1994) Metasomatism of the mantle lithosphere recorded by rare earth elements in garnets. *Earth and Planetary Science Letters*, **126**, p 303-313

Jerade E.A., Taylor L. A., Crozaz G. and Sobolev N.V. (1993) Exsolution of garnet within clinopyroxene of mantle eclogites: major and trace element chemistry. *Contributions to Mineralogy and Petrology*, **144**. p 148-159

Kempton P.D., Lopez-Escobar L., Hawkesworth, C.J., Pearson D.G. Wright D.W. and Ware A.J. (1999) Spinel-Garnet lherzolite xenoliths from Pali Aike, Part 1: Petrography, mineral chemistry and geothermobarometry. *In: Proceedings of the seventh international kimberlite conference, Cape Town. Eds. Gurney J.J., Gurney J.L., Pascoe M.D. and Richardson S.H.* p 403-414

Kennedy C.S. and Kennedy G.C. (1976) The equilibrium boundary between graphite and diamond. *J Geophysical Research*, **73**, p 2467-2470

Kesson S.E. and Ringwood A.E. (1989) Slab-mantle interactions 2: the formation of diamonds. *Chemical Geology*, **78**, p 97-118

King J. and Helmstaedt H. (1997) The Slave Province, North West Territories, Canada. *In: Greenstone Belts. Eds:* De Wit M. and Ashwal L.D. Clarendon Press, Oxford. p459-479.

Kjarsgaard B. Jacob, Z.J. and Sparks R.S. (1999) Preliminary geology, Esker Lake, NWT. Geological Survey of Canada. *Open File 3702*. Scale 1:50 000

Kjarsgaard B.A. (1996) Kimberlites. *In: Searching for diamonds in Canada Eds: LeCeminant A.N., Richardson D.G., DiLarioo R.N. and Richardson K.A. Geological Survey of Canada, Open File 3228,* p29-37

Kjarsgaard B.A. and Wyllie R.J.S. (1993) Geology of the Paul Lake area, Lac de Gras, NWT (76 D/9) Geological Survey of Canada. *Open File 2966*. Scale 1:50 000

Kjarsgaard B.A., Spark R.N. and Jacob Z.J. (1994) Preliminary Geology, Koala, NWT (76 D/10) Geological Survey of Canada. *Open File 2739*. Scale 1:50 000

Kopylova M.G. and Russell J.K. (2000) Chemical stratification of cratonic lithosphere: constraints from the Northern Slave craton, Canada. *Earth and Planetary Science Letters*, **181**, p 71-87

Kopylova M.G., Russel J.K. and Cookenboo H. (1999a) Mapping the lithosphere beneath the North Central Slave Craton. *In: Proceedings of the seventh international kimberlite conference, Cape Town. Eds.: Gurney J.J., Gurney J.L., Pascoe M.D. and Richardson S.H.* p 468-479

Nickel and Green (1985) Empirical geothermobarometry for garnet peridotites and implications for the nature of the lithosphere, kimberlites and diamonds. *Earth and Planetary Science Letters*, **73**, p 158-170

Nielson Pike J.E. and Schwarzman E.C. (1977) Classification of Textures in Ultramafic Xenoliths. *J of Geology*, **85**, p49-61

Nixon P.H. and Boyd F.R. (1973) Petrogenesis of the Granular and Sheared ultrabasic nodule suite in kimberlites. *In: Lesotho Kimberlites Ed:* Nixon P.H. Lesotho National Development Composition. p 48-56.

Nixon P.H. and Davies E.R. (1987) Mantle xenolith perspectives. *In: Mantle Xenoliths Ed:* Nixon P.H. John Wiley & Sons Ltd. p 741-756

Nixon, P.H., van Clasteren, P.W.C., Boyd F.R. and Hawkesworth C.J. (1987) Harzburgites with garnets of diamond facies from southern African kimberlites. *In: Mantle Xenoliths Ed: Nixon, P.H.* John Wiley and Sons Ltd., Chichester, p 523-533

Northern Miner (1993) BHP-DiaMet age date kimberlites. *Northern Miner*. **v79 #29**. p 1

O'Neill H. St.C. (1980) An experimental Study of the Fe-Mg partitioning between garnet and olivine and its calibration as a geothermometer: corrections. *Contributions to Mineralogy and Petrology.* **72** p 337

O'Neill H. St.C. and Wood B.J. (1979) An experimental study of the Fe-Mg partitioning between garnet and olivine and its calibration as a geothermometer. *Contributions to Mineralogy and Petrology.* **70** p 59-70 *With corrections (O'Neill, 1980)*

Pearson N.J., Griffin W.L., Doyle B.J., O'Reilly S.Y., Van Achterbergh E. and Kivi K. (1999) Xenoliths from the kimberlite pipes from the Lac de Gras Area, Slave Craton, Canada. *In: Proceedings of the seventh international kimberlite conference, Cape Town. Eds.: Gurney J.J., Gurney J.L., Pascoe M.D. and Richardson S.H.* p 644-658

Pearson N.J., O'Reilly S.Y. and Griffin W.L. (1995) The crust-mantle boundary beneath cratons and craton margins: a transect across the south-west margin of the Kaapvaal craton. *Lithos*, **36**. p 257-287.

Perkins W.T., Pearce N.J.G.; Westgate J.A. (1997) The development of laser ablation ICP-MS and calibration strategies; examples from the analysis of trace elements in volcanic glass shards and sulfide minerals. *Geostandards Newsletter*, **21** (2) p 175-190

Pokhilenko N.P., McDonanld J.A., Hall A.E. and Sobolev N.V. (2001) Abnormally thick Cambrian lithosphere of the Southeast Slave craton: evidence from crystalline inclusions in diamonds and pyrope compositions in Snap Lake kimberlites. *The Slave-Kaapvaal Workshop-2001*, Ontario.

Pokhilenko N.P., Sobolev N.V., Kuligin S.S. and Shimizu N. (1999) Particularities of distribution of pyroxene paragenesis garnets in Yakutian Kimberlites and some aspects of the evolution of the Siberian craton lithospheric mantle. *In: Proceedings of the seventh international kimberlite conference, Cape Town. Eds.: Gurney J.J., Gurney J.L., Pascoe M.D. and Richardson S.H.* p 689-698

Pollack H.K. and Chapman D.S. (1977) The flow of heat from the earth's interior. *Scientific American*, **237 (2)**, p 60-68, 73-76

Richardson S.H., Gurney J.J., Erlank A.J. and Harris J.W. (1984) Origin of diamonds in old enriched mantle. *Nature*, **310**, p 198-202

Ringwood A.E., Kesson S.E., Hibberson W. and Ware N. (1992) Origin of kimberlites and related magmas. *Earth and Planetary Science Letters*, **113**, p 521-538

Ryan C.G., Griffin W.L. and Pearson N.J. (1996) Garnet geotherms: Pressure-temperature data from Cr-pyrope garnet xenocrysts in volcanic rocks. *J of Geophysical Research,* **101**, p 5611-5625

Sautter V. and Harte B. (1988) Diffusion Gradients in an eclogite xenolith from the Roberts Victor kimberlite Pipe: 1. Mechanism and evolution of garnet exsolution in Al_2O_3-rich clinopyroxene. *J of Petrology,* **29,6**. p 1325-1352

Sen G. (1987) Xenoliths associated with the Hawaiian Hot Spot *In: Mantle Xenoliths Ed: Nixon P.H.* John Wiley & Sons Ltd, Chichester. p 359-375.

Shimizu N. (1975) Rare earth elements in garnets and clinopyroxenes from garnet lherzolite inclusions in kimberlites. *Earth and Planetary Science Letters*, **25**, p 26-32

Shimizu N. and Kushiro I. (1975) The partitioning of rare earth elements between garnet and liquid at high pressures: preliminary experiments. *Geophysical Research Letters*, **2 (10)**, p 413-416

Shimizu N. and Richardson S.H. (1987) Trace element abundance patterns of garnet inclusions in peridotite-suite diamonds. *Geochimica et Cosmochimica Acta*, **51**, p 755-758

Shimizu N. and Sobolev N.V. (1995) Young peridotitic diamonds from the Mir kimberlite pipe. *Nature*, **375**, p 394-397

Smith D. (1999) Temperatures and Pressures of Mineral Equilibration in Peridotite Xenoliths: Review, Discussion, and Implications. *In: Mantle Petrology: Field Observations and high Pressure Experimentation: A Tribute to Francis R. (Joe) Boyd. Eds. Fei, Bertka, Mysen.* Geochemical Society Special Publication No. 6.

Sobolev N.V. (1977) Deep-seated inclusions in kimberlites and the problem of the composition of the upper mantle. *American Geophysical Union, Washington.*

Sobolev N.V., Lavrent'ev Y.G., Pokhilenko N.P. and Usova V. (1973) Chrome-rich garnets from the kimberlites of Yakutia and their parageneses. *Contributions to Mineralogy and Petrology*, **40**, p 39-52

Stachel T., Harris J.W. and Brey G.P. (1999) REE patterns of peridotitic and eclogitic inclusions in diamonds from Mwadui (Tanzania). *In: Proceedings of the seventh international kimberlite conference, Cape Town. Eds. Gurney J.J., Gurney J.L., Pascoe M.D. and Richardson S.H.* p 829-835

Steifenhofer J., Viljoen K.S., Tainton K.M., Dobbe R. and Hannweg G.W. (1999) The petrology of a mantle xenolith suite from Venetia, South Africa. *In: Proceedings of the seventh international kimberlite conference, Cape Town. Eds. Gurney J.J., Gurney J.L., Pascoe M.D. and Richardson S.H.* p 836-845

Stott G.M. (1997) The Superior province, Canada. *In: Greenstone Belts. Eds:* De Wit M. and Ashwal L.D. Clarendon Press, Oxford. p 480-481

Streckeisen A. (1976) To each plutonic rock its proper name. *Earth Science Reviews*, **12**, 1-33.

Streckeisen A.(1980) Classification and nomenclature of volcanic rocks, lamprophyres, carbonatites and melilitic rocks; IUGS Subcommission on the Systematics of Igneous Rocks, recommendations and suggestions. *Geologische Rundschau.* **69**; 1, p 194-207

Suzuki T., Akaogi M and Nakamura E. (2000) Partitioning of major elements between garnet-structured minerals and silicate melt at pressure of 3-15 GPa. *Physics of the Earth and Planetary Interiors,* **120**, p 79-92

Tuttle O.F. and Bowen N.L. (1958) Origin of granite in the light of experimental studies in the system $NaAlSi_3O_8$-$KAlSi_3O_8$-SiO_2-H_2O. Geological Society of America Mem, **74**.

van Achterbergh E., Griffin W.L., She S.R., Wyatt B.A. and Sharma A.L. (1998) Natural trace element distribution for garnet, clino- and orthopyroxene: variations with temperature and pressure. 7th International Kimberlite Conference, Cape Town, Extended abstracts, p 934-936

van Achterbergh E., Griffin W.L. and Stienhofer J. (2001) Metasomatism in mantle xenoliths from the Letlekane kimberlites: estimation of element fluxes. *Contributions to Mineralogy and Petrology*, **141**, p 397-414

Villeneuve M.E. and Relf C. (1998) Tectonic setting of 2.6 Ga carbonatites in the Slave province, NW Canada. J of Petrology, 39, p 1975-1986

Wang W. and Gasparik T. (2001) Metasomatic clinopyroxene inclusions in diamonds from the Liaoning province, China. *Geochimica et Cosmochimia*, **65 (4)**, p 611-620

White W.M. (1997) *Geochemistry* "An on-line textbook, eventually to be published by John-Hopkins University Press".

Whittaker E.J.W. and Muntus R. (1970) Ionic radii for use in geochemistry. *Geochimica Cosmochimica Acta*, **34**, p 945-956

Wood B.J. (1974) Solubility of Alumina in orthopyroxene coexisting with garnet. *Contrib. Mineralogy and Petrology*. **46** p 1-15

Wood B.J. and Fraser D.G. (1976) *Elementary thermodynamics for geologists.* Oxford University Press, Oxford, England. p 1-303.

Xie Q., Campbell McCuaig T. and Kerrich R. (1995) Secular trends in the melting depths of mantle plumes: evidence from HFSE/REE systematics of Archean high-Mg lavas and modern oceanic basalts. *Chemical Geology*, **126**, p 29-42

Zhang R.Y. and Liou J.G. (1999) Exsolution lamellae in minerals from ultrahigh-pressure rocks. *International Geology Review.* 41; 11: Winston and Son. Silver Spring MD, USA. p 981-993

References from which major element compositions were obtained for Kaapvaal peridotites

Bell D.R. (1981) Ultramafic xenoliths from the Koffiefontein kimberlite pipe, RSA. *Honours thesis, University of Cape Town.*

Boyd F.R. and Nixon P.H. (1978) Ultramafic nodules from the Kimberley pipes, South Africa. *Geochimica et Cosmochimica Acta.* 42; 9, p 1367-1382.

Boyd J. (1974) Ultramafic nodules from the Frank Smith kimberlite pipe, South Africa. *Carnegie Inst Year Book,* **73**, p 285-294

Hatton C.J. (1978) The geochemistry and origin of xenoliths from the Roberts Victor mine. *PhD thesis, University of Cape Town*

Kimberlite Research Group Database, University of Cape Town.

Lawless P.J. (1978) Some aspects of the mineral chemistry of the peridotite xenolith suite from the Bultfontein Diamond mine Kimberley, South Africa. *PhD thesis, University of Cape Town.*

McCandless T.E. and Gurney J.J. (1986) Internal report 10, University of Cape Town.

Mofokeng S.W. (1995) Some aspects of the geochemistry of the Frank Smith kimberlite pipe mantle nodules. *Honours thesis, University of Cape Town.*

Moore R.O. (1986) A study of the kimberlites, diamonds and associated rocks and minerals from the Monastery mine, South Africa. *PhD thesis, University of Cape Town.*

Muusha M. (1997) A geochemical study of the River Ranch kimberlite pipe and associated diamonds and mantle minerals: Limpopo Mobile Belt, Zimbabwe. *MSc thesis, University of Cape Town.*

Robinson D.N.; Gurney J.J. and Shee S.R. (1984) Diamond eclogite and graphite eclogite xenoliths from Orapa, Botswana. *In: Kimberlites; II, The mantle and crust-mantle relationships. Ed:* Kornprobst J. Elsevier Sci. Publ. Amsterdam, Netherlands. p 11-24

Shee S. R. (1978) The mineral chemistry of xenoliths from the Orapa kimberlite pipe, Botswana. *MSc thesis, University of Cape Town.*

Shee S.R. (1985) The petrogenesis of the Wesselton mine kimberlites Kimberley, Cape Province, RSA. *PhD thesis, University of Cape Town.*

Skinner C.P. (1986) A study of the peridotite nodule suite from the Finsch kimberlite, South Africa. *Honours thesis, University of Cape Town.*

Smith M.R. (1981) Structural, petrological and geochemical studies of ultramafic nodules from kimberlite. *PhD thesis, University of Oxford.*

Waters F.G. (1987) The geochemical study of metasomatised peridotite and marid nodules from the Kimberley pipes, South Africa. *PhD thesis, University of Cape Town.*

Winterburn P.A. (1987) Geochemical studies of peridotite xenoliths from the Southern African kimberlites. *PhD thesis, University of Edinburgh.*

Appendix 1

Petrographic Descriptions

- Xenoliths from the Arnie Kimberlite
- Xenoliths from the Misery Kimberlite
- Xenoliths from the Pigeon Kimberlite

Tabulated Summary of Petrographic Descriptions

PETROGRAPHIC DESCRIPTIONS

Modal proportions quoted herein are visual approximations of the modal proportion of the minerals in the sample. Not much weight should be placed in the modal proportions of these samples. The sample size is small, and the modal proportions may not reflect the true modal proportion of the larger rock body. This is particularly relevant for poikilitic samples.

XENOLITHS FROM THE ARNIE KIMBERLITE

ARN002 - Low-Ca Harzburgite

This sample has a coarse equant texture (Harte, 1977), and consists of ~50% garnet, 23% orthopyroxene and 22% olivine. The 5% primary chromite is in close spatial relation to the orthopyroxene grains. The garnet rims have been altered into kelyphite (1 mm), and small (<0.5 mm) small (<0.5 mm) spinels are abundant in these altered zones. The sample is 0.5 by 0.75 cm in size.

ARN003 - High-Ca Harzburgite

This coarse equant textured xenolith consists of about 45% garnet, 5% orthopyroxene, 45% olivine and 5% primary chromite. The garnet grains are surrounded by a kelyphite rim. It is 0.6 by 1.0 cm in size.

ARN004 - High-Ca Harzburgite

This 0.7 by 0.8 cm xenolith has a poikilitic texture. It consists of 80% garnet, 10% olivine and 10% orthopyroxene (~1 by 1 mm in size). Both the orthopyroxene and olivine have been altered. The olivine is cloudy, and the altered orthopyroxene is brown.

ARN005 - High-Ca Harzburgite

This sample has a coarse equant texture, with curvy-linear grain boundaries and 120° grain intersections. It is 0.7 by 0.75 cm in size, and consists of about 30% garnet, 40% orthopyroxene and 30% olivine.

ARN006 - High-Ca Harzburgite

This 0.6 by 0.6 cm xenolith has a granoblastic texture (Harte, 1977). It consists of about 40% garnet, 38% orthopyroxene, 20% olivine and 2% primary chromite. The grains have straight grain boundaries and 120° grain intersections.

ARN007 - Low-Ca Harzburgite

This sample consists predominantly of garnet (80%). It contains about 5% orthopyroxene in one very small sub-rounded grain, and about 10% olivine. The garnet is fractured, and has been altered along the fractures. Small grains (<0.5mm) of spinel can be found in the altered region. One grain of primary chromite is sub-rounded and enclosed on three sides by garnet. The chromite is not spatially related to the orthopyroxene.

ARN008 - Low-Ca Harzburgite

This 0.5 by 0.5 cm sample has a poikilitic texture. It consists predominantly of garnet (95%), but includes rounded <0.5 by 0.5 mm orthopyroxene (1%) and olivine (4%) grains. The garnet has a lilac colour, and a thick kelyphite rim (1 mm).

ARN009 - High-Ca Harzburgite

This poikilitic textured sample consists predominantly of garnet (75%). Smaller (1 by 2 mm) grains of orthopyroxene are sub-oval in shape. Primary chromite (5%) is present. One chromite grain has an orthopyroxene core. Portions of the xenolith are highly altered, and tiny spinel grains are common within this alteration.

ARN010 - Low-Ca Harzburgite

This poikilitic sample is dominantly garnet, and is similar in many respects to ARN008. It has a large kelyphite rim, and is lilac in colour. It encloses one 1 by 1 mm orthopyroxene grain.

ARN011 - Low-Ca Harzburgite

This granuloblastic textured xenolith is 0.5 by 0.5 cm in size. It consists of 70% garnet, 24% orthopyroxene, 2% olivine and 4% chromite. The chromite is spatially related to the orthopyroxene.

ARN012 - Low-Ca Harzburgite

This 0.5 by 0.5 cm poikilitic textured sample is dominantly composed of garnet (70%). The garnet encloses a subhedral hexagonal orthopyroxene grain (1.5 by 1.5 mm). Orthopyroxene composes 25% of the sample, and chromite about 5%. The chromite is spatially related to the orthopyroxene.

ARN013 - High-Ca Harzburgite

This granoblastic 0.5 by 0.7 cm sample has 120° grain intersections. It consists of about 50% garnet, 27% orthopyroxene, and 23% olivine.

ARN014 - High-Ca Harzburgite

This granoblastic 0.5 by 0.8 cm sample has 120° grain intersections. It consists of about 50% garnet, 25% orthopyroxene, and 25% olivine. There has been kelyphite formation around the garnets, with associated small (<0.5 mm) spinel in the alteration rim.

ARN017 - Low-Ca Harzburgite

This 1.0 by 0.7 cm poikilitic xenolith consists predominantly of garnet (83%). A thick kelyphite rim surrounds the garnet (1 mm). The garnet completely encloses numerous (5%) rounded chromite grains (1 by 1 mm) and smaller (<0.05 mm) orthopyroxene (2%) grains. The olivine grains (7%) occur both within the poikilitic garnet, and breach the kelyphite rim. The olivine breaching the rim has undergone alteration and is cloudy. The larger olivine grains on the periphery of the poikilitic garnet suggest that the poikilitic texture is a small scale texture within a larger textural feature.

ARN018 - High-Ca Harzburgite

This granuloblastic sample has 120° grain intersections and straight grain boundaries. It consists predominantly of garnet (50%) and orthopyroxene (40%), and to a lesser degree olivine (10%). It is 0.7 by 0.75 cm in size.

ARN019 - Low-Ca Harzburgite

This poikilitic textured sample consists predominantly of garnet (58%). The garnet encloses 1 by 1mm, and 2 by 2mm sub-rounded orthopyroxene grains that compose about 40% of the sample. Macroscopic chromite needles have exsolved from the orthopyroxene. Small (<0.05 mm) chromite grains border the orthopyroxene grains. This is evidence of chromite exsolution from orthopyroxene. This sample is 0.6 by 0.75 cm in size.

ARN021 - Low-Ca Harzburgite

This sample consists predominantly of garnet (78%). The garnet in this granuloblastic sample has undergone a high degree of alteration, and consequently has a high proportion of small spinel grains within the altered portions. The majority of the olivine and orthopyroxene grains are also highly altered. Olivine comprises about 5% of the sample, and orthopyroxene about 15%. This sample is 0.6 by 0.9 cm in size.

ARN022 - High-Ca Harzburgite

This coarse equant sample has undergone very little alteration. The grains are subhedral, with 120° grain intersections. The orthopyroxene grains are slightly smaller in size than the garnet and olivine grains. Garnet is dominant (55%), with 35% olivine and 10% orthopyroxene. This sample is 0.6 by 0.8 cm in size.

ARN023 - Lherzolite

This 0.5 by 0.7 cm sample consists of portions of two grains: a red garnet (10%) and cloudy olivine (90%). The garnet has a rounded grain boundary.

ARN024 - Lherzolite

This 0.5 by 0.6 cm sample also consists of only two grains. Cloudy olivine completely encloses a rounded purple garnet grain (>2 by 2 mm in size). A small (0.5 by 0.5 mm) rounded olivine grain is completely enclosed by the garnet grain.

ARN025 - Low-Ca Harzburgite

This coarse equant textured sample consists predominantly of garnet (50%) and olivine (35%). Orthopyroxene (10%) and chromite (5%) also form part of the mineral assemblage. Chromite is spatially related to orthopyroxene. The grains have straight grain boundaries and 120° grain intersections. And some of the orthopyroxenes have subhedral shapes. As for ARN017, large olivine grains breach the kelyphite rim surrounding the xenolith.

ARN026 - Low-Ca Harzburgite

This 0.9 by 0.9 cm sample has a coarse equant texture and consists of about 50% garnet, 25% olivine and 25% orthopyroxene. The minerals are all extremely fresh, with no kelyphite formation around the garnet. The grain boundaries are curvy-linear and have 120° grain intersections.

ARN027 - Low-Ca Harzburgite

This sample is remarkably similar in texture to ARN025. It has a coarse equant texture, with straight grain boundaries and 120° grain intersections. It has however undergone more alteration than ARN025, and the xenolith is surrounded by a thick kelyphite rim (1 mm). It consists predominantly of garnet (55%) and olivine (28%). Orthopyroxene (10%) and chromite (7%) also form part of the mineral assemblage.

ARN028 - Clinopyroxenite

This 0.6 by 0.75 sample has small red garnets (1 by 1 mm) within a cloudy clinopyroxene groundmass. The garnets are located at the grain intersections between adjacent clinopyroxene grains. The clinopyroxenes have straight grain boundaries, and the grain intersections approximate 120°. The sample consists of 15% garnet and 85% clinopyroxene.

ARN029 - High-Ca Harzburgite

This sample is predominantly garnet (93%), with a poikilitic texture. The garnet encloses sub-rounded grains of orthopyroxene (1 by 1 mm) and olivine (0.5 by 0.5 mm). The sample is 0.6 by 0.75 cm in size.

ARN030 - Lherzolite

This 0.4 by 0.45 cm sample is dominantly garnet (95%). It contains a portion of an olivine grain on one side (0.5 by 0.5 mm in size). The garnet is fractured and altered along the fractures.

ARN031 - Clinopyroxenite

This sample is dominantly clinopyroxene (85%), containing about 15% garnet. The garnets are small (1 by 1 mm) in size, and as for ARN028, they are located at the intersection of clinopyroxene grains. The clinopyroxene is very milky. It has straight grain boundaries and 120° grain intersections. The sample is 0.75 by 1.4 cm in size.

ARN032 - Lherzolite

This sample contains no garnet. It is 0.7 by 1.4 cm in size. It is dominantly olivine (80%). It contains small (1 by 3 mm) grains of clinopyroxene (15%), and an altered mineral, presumably orthopyroxene (5%). A trace amount of chromite was noted within the clinopyroxene grain (<0.5 mm in size).

ARN033 - Lherzolite

This sample consists of olivine (65%), with one grain of clinopyroxene (35%). The olivine is cloudy. The sample is 0.6 by 0.8 cm in size.

ARN034 - Lherzolite

This sample contains no garnet. It consists predominantly of olivine (95%) and one grain of clinopyroxene (5%). The olivine is cloudy. The sample is 0.7 by 0.8 cm in size.

ARN035 - Lherzolite

This sample consists predominantly of olivine (90%) and one grain of clinopyroxene (10%). It contains no garnet, and the olivine is cloudy. The sample is 0.7 by 0.8 cm in size.

ARN036 - Lherzolite

This sample contains no garnet. It consists predominantly of olivine (90%) and one grain of clinopyroxene (10%). The olivine is cloudy. The sample is 0.7 by 0.9 cm in size.

ARN037 - Lherzolite

This sample consists predominantly of olivine (88%) and one grain of clinopyroxene (2%), and one grain of orthopyroxene (10%). It contains no garnet, and the olivine is highly fractured and cloudy. The orthopyroxene is sub-oval in shape (worm-like). The sample is 0.7 by 0.8 cm in size.

XENOLITHS FROM THE MISERY KIMBERLITE

MIS401 - Low-Ca Harzburgite

This poikilitic textured sample consists predominantly of garnet (90%), enclosing small (0.5 by 0.5 mm) rounded orthopyroxenes (10%). The garnet is lilac in colour, and is highly fractured. Tiny spinel grains are located within the altered zones. The sample is 0.4 by 0.7 cm in size.

MIS408 - Low-Ca Harzburgite

This 0.75 by 0.9 cm sample has a coarse equant texture. It consists predominantly (50%) of highly fractured garnet. The garnet has been highly altered along these fractures, and tiny spinels are found within the fractures. The olivine is also highly fractured, and has also undergone alteration. Olivine comprises about 48% of the rock. The orthopyroxene grain appears very similar to the olivine grains, and could only be determined using the electron microprobe. Orthopyroxene comprises about 2% of the sample.

MIS409 - Lherzolite

This poikilitic textured sample is 0.35 by 0.45 cm in size. It consists predominantly of garnet (67%), with enclosed grains of clinopyroxene (10%), orthopyroxene (3%) and Cr-spinel (10%). It is one of the few lherzolitic samples that contain primary Cr-spinel. Two rounded spinel grains occur in spatial relation to orthopyroxene and clinopyroxene, whereas the third grain is completely surrounded by garnet. The major element chemistry of these grains differ (as explained in chapter 5). A kelyphite rim surrounds the garnet, but clinopyroxene grains breach the rim and occur on the outer limits of the kelyphite rim. This may be an indication that the poikilitic texture is part of a larger textural body.

MIS411 - Low-Ca Harzburgite

This sample has a poikilitic texture. Garnet encloses rounded to oval orthopyroxene and olivine grains (1 by 1 mm in size). The olivine has been highly altered. Garnet comprises about 50% of the sample, orthopyroxene about 30%, and olivine about 20%. It is 0.4 by 0.5 cm in size.

MIS412 - High-Ca Harzburgite

This sample has a very similar texture to MIS411. It has a garnet hosted poikilitic texture and consists of about 50% garnet and 50% orthopyroxene (1 by 1 mm in size). The garnet is highly fractured.

MIS413 - High-Ca Harzburgite

This sample is granuloblastic. It is 0.8 by 0.9 cm in size. Orthopyroxene is the most abundant mineral (67%), followed by garnet, which comprises about 30% of the sample. Olivine comprises about 3% of the sample. The olivine appears very similar to the orthopyroxene grains, and could only be

determined using the electron microprobe. The garnet grains are rounded and have thick kelyphite rims (0.5 mm), with a small fresh core (<0.25 to 1 mm in size). Tiny spinel grains occur within the alteration rim.

MIS417 - High-Ca Harzburgite

This garnet-poikilitic sample is 0.4 by 0.7 cm in size. It dominantly consists of garnet (65%), with 20% orthopyroxene, 10% olivine and 5% chromite. The olivine and orthopyroxene grains are oval (1 by 1 mm). Spinel exsolution is evident in the orthopyroxene, and small (<0.5 mm) spinel grains are located along the orthopyroxene grain boundaries.

MIS419 - Lherzolite

This 0.4 by 0.7 cm granuloblastic equant sample consists of garnet (25%), clinopyroxene (30%) and orthopyroxene (45%). The grain boundaries are straight, and have 120° grain intersections. The garnet rims have been altered into kelyphite. One garnet grain completely encloses a rounded clinopyroxene grain.

MIS420 - High-Ca Harzburgite

This coarse equant textured sample is highly altered. The garnet, comprising about 60% of the sample has almost completely been altered, as has the orthopyroxene, which composes 40% of the sample. Many tiny spinel grains occur within the altered zones.

MIS426 - Lherzolite

This 0.4 by 0.5 cm sample has a garnet hosted poikilitic texture. The garnet encloses rounded to oblong clinopyroxene, orthopyroxene, olivine and chromite. The garnet is fractured and surrounded by a kelyphite rim. One large clinopyroxene grain, and one olivine grain lie on the outer perimeter of the garnet grain, indicating that the poikilitic texture may be a small-scale textural feature within a larger textural association. The garnet comprises about 70% of the sample, clinopyroxene (8%), orthopyroxene (7%), olivine (7%) and chromite (8%).

MIS428 - Pyroxenite

This sample has unique characteristics within this sample selection. Clinopyroxene is the dominant mineral, and has a coarse equant texture (Harte, 1977). Both spinel and garnet exsolution have occurred within the clinopyroxene grains. The spinel and garnet lamellae are parallel to one-another, presumably having exsolved along the same crystallographic face. The individual garnet lamellae taper toward the terminating ends. Rounded and oblong small (0.5 by 0.5 mm) garnet and orthopyroxene grains lie along the clinopyroxene grain boundaries forming a necklace texture. These grains are concentrated within the area of the inferred triple junction between the primary clinopyroxene grains.

The garnet and orthopyroxene both appear to have exsolved from the primary clinopyroxene grains and recrystallized along the grain boundaries. The sample consists of clinopyroxene (75%), garnet (15%) and orthopyroxene (10%). And the sample is 0.4 by 0.6 cm in size.

MIS430 - High-Ca Harzburgite

This coarse equant textured sample is dominantly garnet (55%). The olivine (15%) is highly serpentinised, and the orthopyroxene highly fractured. The grain boundaries are straight and have 120° grain intersections. The sample is 0.6 by 0.75 cm in size.

MIS431 - Lherzolite

This coarse equant textured sample is 0.6 by 0.9 cm in size. It consists of about 8% garnet, 40% clinopyroxene, 45% orthopyroxene, 2% olivine and 5% chromite. The garnet has almost completely been altered into kelyphite, and the olivine into serpentine. Spinel exsolution is evident within the clinopyroxene grains. The sample is coarse grained, with straight grain boundaries and 120° grain intersections.

MIS433 - Lherzolite

This sample consists of about 30% garnet, 20% clinopyroxene, 35% orthopyroxene, 10% olivine and 5% chromite. The olivine has been completely serpentinised, but the surrounding minerals are fresh. It has a coarse equant texture and the grains have straight grain boundaries and 120° grain intersections. The sample is 0.4 by 0.6 cm in size.

MIS434 - High-Ca Harzburgite

This 0.5 by 0.5 cm sample has a coarse equant texture. It consists of about 50% garnet, about 40% orthopyroxene and 10% olivine. The olivine has almost completely altered into serpentine. The majority of the grains have straight grain boundaries and 120° grain intersections, but some of the orthopyroxene has curved grain boundaries, one grain in particular is "worm-like" in form.

MIS438 - Websterite

This granoblastic textured sample consists of garnet (40%), orthopyroxene (30%) and clinopyroxene (30%). The grain boundaries are straight, and have 120° grain intersections. Microscopic needles are abundant within the garnet grains. These needles are orientated in three directions, presumably along crystallographic axes. The sample is 0.5 by 0.6 cm in size.

MIS439 - Websterite

This sample in many ways is identical to MIS438. It has a granoblastic texture, straight grain boundaries and 120° grain intersections. It consists of about 40% garnet, 30% orthopyroxene and 30% clinopyroxene. It is 0.4 by 0.6 cm in size. .

MIS451 - Clinopyroxenite

This 0.6 by 0.65 cm sample is dominantly clinopyroxene (90%). A large amount of spinel exsolution has occurred within this sample. The continuous nature of the spinel exsolution, its orientation, and lack of grain boundaries suggest that the whole sample consists of a single clinopyroxene grain surrounding two garnet grains (1 by 1 mm in size), which comprise about 10% of the sample.

MIS454 - Clinopyroxenite

This sample is bimineralic. It is composed of about 45% garnet and 55% clinopyroxene. It has a coarse equant texture with straight to curvy-linear grain boundaries, and 120° grain intersections. Spinel exsolution has occurred within the clinopyroxene grains, and microscopic needles have exsolved from the garnet. This sample is 0.4 by 0.55 cm in size.

MIS463 - Low-Ca Harzburgite

This sample is 0.4 by 0.75 cm in size. It consists predominantly of orthopyroxene (50%). The orthopyroxene completely encloses rounded olivine and garnet grains. The olivine grains have undergone serpentinisation, and comprise about 10% of the sample. The single garnet grain has almost completely been altered: only a 0.5 by 1 mm core remains from a 2.5 by 3.5 mm grain. The olivine and garnet are not in contact with each other. This fact, and the large degree of alteration of the garnet have unfavourable implications for geothermobarometric calculations.

XENOLITHS FROM THE PIGEON KIMBERLITE

PGN301 - Low-Ca Harzburgite

This coarse equant textured, 0.8 by 0.3 cm xenolith consists of 85% garnet, 8% orthopyroxene and 7% olivine in three independent grains. The garnet is fractured, and small (<0.5 mm) oxides reside in the alteration zone in the fractures.

PGN303 - Low-Ca Harzburgite

This 0.9 by 0.5 cm poikilitic textured xenolith consists predominantly of garnet. The xenolith is highly fractured. Small (<0.5 mm) oxides reside in the large fracture zones. Small grains (<0.5 mm) of oval shaped olivine and orthopyroxene are completely enclosed by the garnet. A trace amount of oxide is located next to the oxide. Modal percentage: 95% garnet, 3% olivine, 2% orthopyroxene.

PGN306 - Lherzolite

This 0.5 by 0.5 garnet-poikilitic xenolith consists of highly fractured garnet that encloses sub-rounded grains of orthopyroxene and olivine. The olivine grains are 1.5 by 1 mm in size, whereas the orthopyroxene grain is even smaller. Small (<0.5 mm) oxides reside in the fractures in the garnet. Modal percentages: 80% garnet, 15% olivine, 5% orthopyroxene.

PGN307 - Lherzolite

This porphyroclastic xenolith is 0.75 by 0.6 cm in size. About 70% of the sample consists of olivine, of which a small amount (<5%) of the olivine has been recrystallized. The garnet (20%) is rounded and fractured, with a 0.5 mm kelyphite rim. About 10% of the sample is orthopyroxene.

PGN308 - Lherzolite

This 0.8 by 0.5 cm xenolith has an orthopyroxene hosted poikilitic texture. Small (0.5 by 0.5 mm) grains of sub-rounded and slightly larger (1 by 1 mm) subhedral garnet grains are completely enclosed in orthopyroxene, which comprises 85% of the sample. Garnet comprises 15% of the sample.

PGN309 - Lherzolite

This 0.8 by 0.6 cm xenolith has an orthopyroxene hosted poikilitic texture. Three small (1 by 1 mm and 0.5 by 0.5 mm) grains of sub-rounded garnet are completely enclosed by an orthopyroxene grain, which comprises 85% of the sample. Garnet comprises 15% of the sample.

PGN310 - Lherzolite

This 0.75 by 0.6 cm coarse equant textured xenolith is dominantly olivine (75%). A sub-rounded grain of garnet (0.25 by 0.2 cm) lies adjacent a smaller clinopyroxene grain. This clinopyroxene is fairly, but

a second clinopyroxene grain appears to be fresh, being a bright, clear green. The grain boundaries are straight, with grain boundaries approximately 120°.

PGN311 - Lherzolite

This 0.75 by 0.4 cm xenolith has an orthopyroxene hosted poikilitic texture. Two small (1 by 1 mm) grains of sub-rounded garnet are completely enclosed in orthopyroxene, which comprises 85% of the sample. Garnet comprises 15% of the sample. One garnet grain encloses two circular grains, but these have been completely altered and therefore cannot be classified.

PGN312 - High-Ca Harzburgite

This coarse equant textured 1 by 0.6 cm xenolith consists of one rounded grain of garnet which comprises 25% of the sample. 75 % of the sample consists of an equal amount of olivine and orthopyroxene. A small amount (<5%) of the olivine has been recrystallized and become fine grained. Both the garnet and the other silicates appear to be fairly altered.

PGN313 - High-Ca Harzburgite

This coarse equant textured 0.6 by 0.5 cm xenolith consists of equal proportions of garnet, orthopyroxene and olivine. The orthopyroxene and olivine have been highly altered, and a small portion of the olivine has been recrystallized. The garnet however is very fresh.

PGN314 - Low-Ca Harzburgite

This coarse equant textured 0.5 by 0.5 cm. xenolith consists of one sub-rounded grain on garnet comprising 85%, and equal amounts of olivine and orthopyroxene on the garnet's perimeter.

PGN315 - High-Ca Harzburgite

This garnet hosted poikilitic xenolith is 0.5 by 0.5 cm in size. The garnet completely encloses an oblong, rounded olivine grain 0.25 by 0.1 cm in size. The garnet is reddish and highly fractured, and comprises 90% of the sample, whereas the orthopyroxene comprises 10%.

PGN316 - Lherzolite

This porphyroclastic 0.8 by 0.3 cm xenolith consists of two rounded grains of garnet which comprises 35% of the sample. 65 % of the sample consists of an equal amount of olivine and orthopyroxene. A small amount (<10%) of the olivine has been recrystallized and become fine grained. One of the garnet grains is completely altered, whereas the second is just fractured.

PGN317 - Low-Ca Harzburgite

This 0.75 by 0.5 garnet hosted poikilitic textured xenolith consists of 75% garnet, 15% orthopyroxene and 10% olivine. The garnet encloses grains of orthopyroxene and olivine. The olivine grains are 1 by 1 mm in size, whereas the orthopyroxene grains are both similar and smaller in size.

PGN318 - Low-Ca Harzburgite

This 0.6 by 0.4 poikilitic textured xenolith has garnet enclosing two sub-oval orthopyroxene grains (<1 by 1 mm). The garnet is highly fractured and comprises 90% of the sample.

PGN319 - Clinopyroxenite

This 0.75 by 0.6 cm poikilitic xenolith consists predominantly (75%) fresh dark green and milky clinopyroxene. It completely encloses rounded ovals of 0.25 by 1.5 cm and smaller orange garnet (25%).

PGN320 - Pyroxenite

This 0.5 by 0.5 cm granoblastic xenolith consists of equal amounts of orange garnet and bright green clinopyroxene. The grain boundaries are straight with 120° intersections. The clinopyroxene is fresh, but the majority of the garnet has been altered. Grain sizes approximate 1 by 2 cm.

PGN321 - Lherzolite

This is an extremely small sample. It is 0.3 by 0.3 cm, and consists of a single garnet grain and a single milky clinopyroxene grain in equal proportions.

PGN322 - Pyroxenite

This 1 by 0.6 cm coarse equant textured xenolith consists of equal amounts of garnet and bright green clinopyroxene. The grain boundaries are near straight with 120° intersections. The clinopyroxene is fresh, but the majority of the garnet has been altered.

PGN323 - Lherzolite

This 0.7 by 0.5 cm xenolith has a garnet hosted poikilitic texture. The garnet is highly fractured. The orange-red garnet completely encloses bright green clinopyroxene, which comprises 25% of the sample, whereas the garnet comprises 75% of the sample.

PGN324 - Lherzolite

This 0.75 by 0.7 cm "porphyroclastic" xenolith comprises 60% of fine grained (<1 by 1 mm) matrix of olivine and clinopyroxene, with two larger (>2 by 2 mm) grains of garnet.

PGN325 - Lherzolite

This coarse equant textured 0.3 by 0.3 cm xenolith consists of equal proportions of garnet, clinopyroxene and orthopyroxene. The grains intersect at 120°.

PGN329 - Lherzolite

This 0.7 by 0.6 cm coarse equant textured xenolith consists of garnet (48%), orthopyroxene (48%), clinopyroxene (4%). The majority of the grains are greater than 2 by 2 mm and have straight grain boundaries with 120° intersections. The one rounded clinopyroxene grain is small (<0.5 mm) in size and is completely enclosed by orthopyroxene.

PGN333 - Lherzolite

This 0.7 by 0.6 poikilitic textured xenolith is dominantly composed of garnet (90%). Small grains of olivine, clinopyroxene and oxide lie on the margin of the massive garnet area. These grains are 1 by 0.5 mm (or smaller) in size.

PGN336 - Lherzolite

This sample has a poikilitic texture, and is dominantly composed of clinopyroxene (70%). It is 0.8 by 0.3 cm in size. The clinopyroxene completely encloses small (<1 by 1 mm) grains of garnet (25%), and olivine (5%).

PGN337 - Lherzolite

This coarse equant textured, 0.7 by 0.6 cm sample consists of equal proportions of garnet, orthopyroxene and clinopyroxene. The grain boundaries are all straight, with 120° intersections. The orthopyroxene has been highly altered, whereas the clinopyroxene and garnet have only been fractured and altered along the fractures.

PGN338 - Lherzolite

This coarse equant textured, 0.7 by 0.4 cm xenolith consists of highly fractured and altered garnet (65%), highly fractured and altered orthopyroxene (25%), bright green clinopyroxene (5%) and phlogopite (5%). Small (<0.5 mm) oxides may be found along fractures in the garnet and along the perimeter of the garnet grains. The grain boundaries are all near straight, and have 120° intersections.

PGN339 - Lherzolite

This 0.6 by 0.4 coarse equant textured xenolith consists of one highly fractured garnet grain (60%), which is bound on two sides by clinopyroxene (20%) and by olivine (20%). A small portion of the olivine grain has recrystallized to form smaller grains.

PGN340 - Low-Ca Harzburgite

This 1.1 by 0.75 cm coarse equant textured xenolith contains about 40% garnet, 40% olivine and 20% orthopyroxene. They are generally equigranular. The orthopyroxene is almost completely altered, whereas the olivine and garnet are not. The orthopyroxene completely surrounded by garnet is not as altered as those free-standing grains in the mineral matrix.

PGN341 - Low-Ca Harzburgite

This 1 by 1 cm poikilitic textured xenolith comprises about 80% garnet, which completely encloses rounded orthopyroxene and olivine grains. These grains are 1 by 1 mm in size or smaller. The orthopyroxene grains are fresh, but the olivine grains are completely altered. The garnet is fractured, and small (<0.5 mm) oxides can be found along the fractures.

PGN342 - Low-Ca Harzburgite

This 0.8 by 0.6 cm poikilitic textured xenolith consists predominantly of garnet (80%), enclosing smaller (<1 by 1 mm) grains of olivine (20%). The garnet is highly fractured, and small (<0.5 mm) oxides can be found along these fractured zones.

PGN343 - Low-Ca Harzburgite

This 0.75 by 0.5 cm poikilitic textured xenolith comprises about 80% garnet, which completely encloses rounded orthopyroxene and olivine grains. These grains are 1 by 1 mm (or smaller) in size. The orthopyroxene grains are fresh, but the olivine grains are completely altered. The garnet is fractured, and small (<0.5 mm) oxides can be found along the fractures.

Sumary of Petrographic Descriptions

Kimberlite Locality	Sample_No	Rock Type	Mineral Assemblage	% Gt	% Cpx	% Opx	% Ol	% Phlogopite	% Primary Spinel	Secondary Spinel	Primary / Exsolved Spinel Grains	Other Exsolution Features	Texture
Arnie	ARN002	Harzburgite (Low-Ca)	gt-opx-ol-spinel	50		23	22		5	Present	Primary		Coarse equant
Arnie	ARN003	Harzburgite (High-Ca)	gt-opx-ol-spinel	45		5	45		5	Present	Primary		Coarse equant
Arnie	ARN004	Harzburgite (High-Ca)	gt-opx-ol	80		10	10						Poikilitic (gt)
Arnie	ARN005	Harzburgite (High-Ca)	gt-opx-ol	30		40	30						Coarse equant
Arnie	ARN006	Harzburgite (High-Ca)	gt-opx-ol-spinel	40		30	28		2	Present	Exsolved		Granuloblastic
Arnie	ARN007	Harzburgite (Low-Ca)	gt-opx-ol-spinel	80		5	10		5	Present	Primary		Poikilitic (gt)
Arnie	ARN008	Harzburgite (Low-Ca)	gt-opx-ol	95		1	4						Poikilitic (gt)
Arnie	ARN009	Harzburgite (High-Ca)	gt-opx-spinel	75		20			5	Present	Primary		Poikilitic (gt)
Arnie	ARN010	Harzburgite (Low-Ca)	gt-opx	75		25							Poikilitic (gt)
Arnie	ARN011	Harzburgite (Low-Ca)	gt-opx-ol-spinel	70		24	2		4	Present	Exsolved		Granuloblastic
Arnie	ARN012	Harzburgite (Low-Ca)	gt-opx-spinel	70		25			5	Present	Exsolved		Poikilitic (gt)
Arnie	ARN013	Harzburgite (High-Ca)	gt-opx-ol	50		27	23						Granuloblastic
Arnie	ARN014	Harzburgite (High-Ca)	gt-opx-ol	50		25	25			Present			Granuloblastic
Arnie	ARN017	Harzburgite (Low-Ca)	gt-opx-ol-spinel	83		2	7		7	Present	Primary		Poikilitic (gt)
Arnie	ARN018	Harzburgite (High-Ca)	gt-opx-ol	50		40	10						Granuloblastic
Arnie	ARN019	Harzburgite (Low-Ca)	gt-opx-spinel	58		40			2	Present	Exsolved	Spinel exsolution in pyx	Poikilitic (gt)
Arnie	ARN021	Harzburgite (Low-Ca)	gt-opx-ol	78		15	5			Present			Granuloblastic
Arnie	ARN022	Harzburgite (High-Ca)	gt-opx-ol	55		10	35			Present			Coarse equant
Arnie	ARN023	Lherzolite	gt-ol	10			90						Poikilitic (ol)
Arnie	ARN024	Lherzolite	gt-ol	45			55						Poikilitic (ol)
Arnie	ARN025	Harzburgite (Low-Ca)	gt-opx-ol-spinel	50		10	35		5	Present	Primary		Coarse equant
Arnie	ARN026	Harzburgite (Low-Ca)	gt-opx-ol	50		25	25						Coarse equant
Arnie	ARN027	Harzburgite (Low-Ca)	gt-opx-ol-spinel	55		28	10		7	Present	Primary		Coarse equant
Arnie	ARN028	Clinopyroxenite	gt-cpx	15	85								Coarse equant
Arnie	ARN029	Harzburgite (High-Ca)	gt-opx-ol	93		5	2						Poikilitic (gt)
Arnie	ARN030	Lherzolite	gt-ol	95			5						Poikilitic (gt)
Arnie	ARN031	Clinopyroxenite	gt-cpx	15	85								Coarse equant
Arnie	ARN032	Lherzolite	gt-opx-cpx-ol		15	5	80			Present			Poikilitic (ol)
Arnie	ARN033	Lherzolite	cpx-ol-phlogopite		35		65	Trace					Poikilitic (ol)
Arnie	ARN034	Lherzolite	cpx-ol		5		95						Poikilitic (ol)
Arnie	ARN035	Lherzolite	cpx-ol		10		90						Poikilitic (ol)
Arnie	ARN036	Lherzolite	cpx-ol		10		90						Poikilitic (ol)
Arnie	ARN037	Lherzolite	opx-cpx-ol		2	10	88						Poikilitic (ol)

Key: Poikilitic (host mineral)

Sumary of Petrographic Descriptions

Kimberlite Locality	Sample_No	Rock Type	Mineral Assemblage	% Gt	% Cpx	% Opx	% Ol	% Phlogopite	% Primary Spinel	Secondary Spinel	Primary / Exsolved Spinel Grains	Other Exsolution Features	Texture
Misery	MIS401	Harzburgite (Low-Ca)	gt-opx	90		10				Present			Poikilitic (gt)
Misery	MIS408	Harzburgite (Low-Ca)	gt-opx-ol	50		2	48			Present			Coarse equant
Misery	MIS409	Lherzolite	gt-opx-cpx-spinel	67	10	3			10	Present	Primary		Poikilitic (gt)
Misery	MIS411	Harzburgite (Low-Ca)	gt-opx-ol	50		30	20			Present			Poikilitic (gt)
Misery	MIS412	Harzburgite (High-Ca)	gt-opx	50		50				Present			Poikilitic (gt)
Misery	MIS413	Harzburgite (High-Ca)	gt-opx-ol	30		67	3			Present			Granuloblastic
Misery	MIS417	Harzburgite (High-Ca)	gt-opx-ol-spinel	65		20	10		5	Present	Exsolved	Spinel exsolution in pyx	Poikilitic (gt)
Misery	MIS419	Lherzolite	gt-opx-cpx	25	30	45				Present			Granuloblastic
Misery	MIS420	Harzburgite (High-Ca)	gt-opx	60		40				Present			Coarse equant
Misery	MIS426	Lherzolite	gt-opx-cpx-ol-spinel	70	8	7	7		8	Present	Primary		Coarse equant (near poikilitic)
Misery	MIS428	Clinopyroxenite	gt-opx-cpx	15	75	10						Spinel exsolution in pyx, Garnet	Coarse equant with necklace
Misery	MIS430	Harzburgite (High-Ca)	gt-opx-ol	55		30	15			Present			Coarse equant
Misery	MIS431	Lherzolite	gt-opx-cpx-ol-spinel	8	45	40	2		5	Present	Primary	Spinel exsolution in pyx	Coarse equant
Misery	MIS433	Lherzolite	gt-opx-cpx-ol-spinel	30	20	35	10		5	Present	Primary		Coarse equant
Misery	MIS434	Harzburgite (High-Ca)	gt-opx-ol	50		40	10			Present			Coarse equant
Misery	MIS438	Websterite	gt-opx-cpx	40	30	30						Needles in garnet	Granuloblastic
Misery	MIS439	Websterite	gt-opx-cpx	40	30	30							Granuloblastic
Misery	MIS451	Clinopyroxenite	gt-cpx	10	90					Present		Spinel exsolution in pyx	Poikilitic (cpx)
Misery	MIS454	Clinopyroxenite	gt-cpx	45	55					Present		Spinel exsolution in pyx, Needles in garnet	Coarse equant
Misery	MIS463	Harzburgite (Low-Ca)	gt-opx-ol	40		50	10						Poikilitic (opx)

Sumary of Petrographic Descriptions

Kimberlite Locality	Sample_No	Rock Type	Mineral Assemblage	% Gt	% Cpx	% Opx	% Ol	% Phlogopite	% Primary Spinel	Secondary Spinel	Primary / Exsolved Spinel Grains	Other Exsolution Features	Texture
Pigeon	PGN301	Harzburgite (Low-Ca)	gt-opx-ol	75		15	10						Coarse equant
Pigeon	PGN303	Harzburgite (Low-Ca)	gt-opx-ol	95		2	3		Trace	Present			Poikilitic (gt)
Pigeon	PGN306	Lherzolite	gt-opx-ol	75		5	20			Present			Poikilitic (gt)
Pigeon	PGN307	Lherzolite	gt-opx-ol	15		25	60						Porphyroclastic
Pigeon	PGN308	Lherzolite	gt-opx	15		85							Poikilitic (opx)
Pigeon	PGN309	Lherzolite	gt-opx	15		85							Poikilitic (opx)
Pigeon	PGN310	Lherzolite	gt-opx-cpx-ol	20	20	10	50						Coarse equant
Pigeon	PGN311	Lherzolite	gt-opx	15		85							Poikilitic (opx)
Pigeon	PGN312	Harzburgite (High-Ca)	gt-opx-ol	25		40	35						Coarse equant
Pigeon	PGN313	Harzburgite (High-Ca)	gt-opx-ol	35		30	35						Coarse equant
Pigeon	PGN314	Harzburgite (Low-Ca)	gt-opx-ol	70		15	15			Present			Coarse equant
Pigeon	PGN315	Harzburgite (High-Ca)	gt-ol	80			20						Poikilitic (gt)
Pigeon	PGN316	Lherzolite	gt-opx-ol	40		30	30						Porphyroclastic
Pigeon	PGN317	Harzburgite (Low-Ca)	gt-opx-ol	75		20	5						Poikilitic (gt)
Pigeon	PGN318	Harzburgite (Low-Ca)	gt-opx	85		15							Poikilitic (gt)
Pigeon	PGN319	Clinopyroxenite	gt-cpx	20	80								Poikilitic (cpx)
Pigeon	PGN320	Clinopyroxenite	gt-cpx	50	50								Coarse equant
Pigeon	PGN321	Lherzolite	gt-cpx	45	55								Coarse equant
Pigeon	PGN322	Clinopyroxenite	gt-cpx	50	50								Coarse equant
Pigeon	PGN323	Lherzolite	gt-cpx	55	45								Poikilitic (gt)
Pigeon	PGN324	Lherzolite	Gt-cpx-ol	45	30		25						Porphyroblastic
Pigeon	PGN325	Lherzolite	gt-opx-cpx	35	30	35							Coarse equant
Pigeon	PGN329	Lherzolite	gt-opx-cpx	50	2	48				Present			Coarse equant
Pigeon	PGN333	Lherzolite	Gt-cpx-ol-spinel	88	3		7		2	Present	Exsolved		Poikilitic (gt)
Pigeon	PGN336	Lherzolite	Gt-cpx-ol	40	50		10			Present			Poikilitic (cpx)
Pigeon	PGN337	Lherzolite	gt-opx-cpx	50	25	25				Present			Coarse equant
Pigeon	PGN338	Lherzolite	gt-opx-cpx-phlogopite	55	10	30		5		Present			Coarse equant
Pigeon	PGN339	Lherzolite	Gt-cpx-ol	55	20	Trace	25			Present			Coarse equant
Pigeon	PGN340	Harzburgite (Low-Ca)	gt-opx-ol-spinel	35		20	45		1	Present	Exsolved		Coarse equant
Pigeon	PGN341	Harzburgite (Low-Ca)	gt-opx-ol	80		10	10			Present			Poikilitic (gt)
Pigeon	PGN342	Harzburgite (Low-Ca)	gt-ol	70			30						Poikilitic (gt)
Pigeon	PGN343	Harzburgite (Low-Ca)	gt-opx-ol-spinel	85		10	4		1	Present	Exsolved		Poikilitic (gt)

Appendix 2

Major Element Analysis

- Operating conditions
- Lower limits of detection
- Standard deviation

Major Element Analyses

- Garnet
- Clinopyroxene
- Orthopyroxene
- Olivine
- Chromite

MAJOR ELEMENT ANALYSIS

Operating conditions for the Electron Microprobe

Accelerating Potential	15 kV	
Beam Current	40 nA	
Beam Size	1-2 μm	
Analysing Crystals	1) TLAP	Mg, Na
	2) TLAP	Si, Al
	3) LIF	Fe, Mn, Ni
	4) PET	Ca, Ti, Cr
Peak Count Times	Orthopyroxene - Al_2O_3	40 seconds
	Orthopyroxene - Na_2O	60 seconds
	All other oxides	10 seconds

Lower Limit of Detection (wt%) ♦

Oxide	Olivine	Pyroxene	Garnet	Mica	Chromite
SiO_2	0.04	0.04	0.04	0.04	0.04
TiO_2	0.04	0.04	0.04	0.04	0.05
Al_2O_3	0.03	0.01	0.05	0.05	0.04
Cr_2O_3	0.04	0.04	0.06	0.04	0.05
FeO	0.08	0.08	0.08	0.08	0.08
MnO	0.06	0.06	0.09	0.05	0.07
MgO	0.04	0.04	0.04	0.04	0.04
CaO	0.03	0.05	0.09	0.03	0.02
Na_2O	-	0.01	0.01	0.03	-
K_2O	-	-	-	0.03	-
NiO	0.10	-	-	-	-

Standard Deviation (wt%) ♦

Oxide	Olivine	Pyroxene	Garnet	Mica	Chromite
SiO_2	0.28	0.28	0.27	0.28	0.04
TiO_2	0.04	0.04	0.04	0.10	0.34
Al_2O_3	0.03	0.02	0.19	0.14	0.04
Cr_2O_3	0.05	0.08	0.09	0.05	0.08
FeO	0.35	0.21	0.31	0.20	0.46
MnO	0.06	0.07	0.12	0.06	0.09
MgO	0.25	0.14	0.15	0.16	0.16
CaO	0.06	0.18	0.12	0.02	0.03
Na_2O	-	0.01	0.02	0.03	-
K_2O	-	-	0.03	0.13	-
NiO	0.08	-	-	-	-

♦ Lower limits of detection and standard deviations adapted from Baumgartner (1994).

Major element Analyses - Garnet

Sample No.	ARN002	ARN003	ARN004	ARN005	ARN006	ARN007	ARN008	ARN009	ARN010	ARN011	ARN012	ARN013	ARN014
SiO_2	41.10	40.93	40.98	40.64	41.20	41.36	42.18	40.88	42.33	41.31	40.88	40.78	40.91
TiO_2	<0.04	<0.04	<0.04	<0.04	<0.04	<0.04	<0.04	0.07	<0.04	<0.04	0.07	<0.04	<0.04
Al_2O_3	17.84	17.94	18.39	18.13	19.70	18.20	20.11	16.85	20.16	18.00	17.68	19.57	16.35
Cr_2O_3	8.04	8.02	7.40	7.70	5.50	7.12	4.91	8.60	4.92	7.85	7.47	5.89	9.28
FeO	6.91	7.06	7.21	7.38	8.22	6.99	7.78	7.45	7.85	7.21	7.24	8.43	7.37
MnO	0.43	0.48	0.41	0.42	0.58	0.42	0.43	0.45	0.47	0.43	0.42	0.61	0.47
MgO	19.88	19.19	18.88	18.27	18.92	22.63	22.47	19.34	22.77	20.17	21.04	18.41	18.05
CaO	4.86	6.60	6.51	6.89	5.92	2.96	1.35	6.09	1.64	4.63	4.45	5.55	7.25
Na_2O	0.03	0.04	0.02	0.02	0.04	0.04	0.03	0.04	0.03	0.02	0.04	nd	0.02
Total	**99.10**	**100.27**	**99.78**	**99.45**	**100.09**	**99.73**	**99.27**	**99.78**	**100.16**	**99.64**	**99.27**	**99.33**	**99.71**
Atomic Pro													
Si	3.002	2.975	2.985	2.981	2.983	2.981	3.020	2.994	3.009	3.000	2.982	2.980	3.011
Ti	0.000	0.000	0.000	0.000	0.000	0.001	0.000	0.004	0.000	0.001	0.004	0.000	0.001
Al	1.536	1.536	1.578	1.567	1.681	1.546	1.697	1.454	1.689	1.541	1.519	1.686	1.419
Cr	0.465	0.461	0.426	0.446	0.315	0.406	0.278	0.498	0.277	0.451	0.431	0.340	0.540
Fe	0.422	0.429	0.439	0.453	0.498	0.421	0.466	0.457	0.466	0.438	0.441	0.515	0.454
Mn	0.026	0.030	0.025	0.026	0.035	0.026	0.026	0.028	0.028	0.026	0.026	0.038	0.029
Mg	2.165	2.079	2.050	1.997	2.043	2.432	2.399	2.111	2.413	2.184	2.287	2.006	1.981
Ca	0.380	0.514	0.508	0.541	0.460	0.228	0.103	0.478	0.125	0.361	0.348	0.435	0.572
Na	0.004	0.008	0.001	0.003	0.006	0.005	0.005	0.005	0.004	0.003	0.005	0.013	0.003
Total	**8.000**	**8.031**	**8.013**	**8.014**	**8.021**	**8.045**	**7.994**	**8.029**	**8.010**	**8.005**	**8.042**	**8.013**	**8.010**
Mg#	83.68	82.90	82.36	81.53	80.41	85.23	83.74	82.21	83.80	83.30	83.83	79.54	81.37
Al/Cr ratio	3.31	3.33	3.70	3.51	5.34	3.81	6.10	2.92	6.11	3.42	3.53	4.95	2.63
# Analyses	6	4	5	5	5	7	9	12	5	13	4	6	5
Suite	Low-Ca Harzburgite	High-Ca Harzburgite	High-Ca Harzburgite	High-Ca Harzburgite	High-Ca Harzburgite	Low-Ca Harzburgite	Low-Ca Harzburgite	High-Ca Harzburgite	Low-Ca Harzburgite	Low-Ca Harzburgite	Low-Ca Harzburgite	High-Ca Harzburgite	High-Ca Harzburgite

Major element Analyses - Garnet

Sample No.	ARN017	ARN018	ARN019	ARN021	ARN022	ARN023	ARN024	ARN025	ARN026	ARN027	ARN028	ARN029	ARN030
SiO_2	42.04	41.50	42.33	40.80	40.77	42.10	41.31	41.59	42.28	42.11	40.59	40.37	41.93
TiO_2	<0.04	<0.04	0.07	<0.04	<0.04	0.43	0.30	<0.04	0.04	<0.04	0.11	0.13	0.13
Al_2O_3	19.05	19.24	19.63	17.81	18.94	20.13	17.23	18.97	20.96	18.65	19.67	15.83	21.81
Cr_2O_3	6.74	6.38	5.86	7.89	6.62	3.86	8.10	7.26	4.70	7.17	4.17	10.42	2.83
FeO	7.00	7.84	7.72	7.06	8.39	7.84	6.87	7.07	7.36	7.34	12.66	7.43	8.14
MnO	0.44	0.45	0.44	0.46	0.53	0.31	0.35	0.42	0.40	0.43	0.48	0.43	0.40
MgO	21.28	18.75	20.23	20.03	19.16	20.00	19.30	20.95	20.49	21.33	16.38	18.84	19.96
CaO	2.86	5.29	3.28	5.45	6.11	5.16	5.87	3.49	3.96	3.50	6.09	6.14	5.05
Na_2O	nd	nd	nd	0.02	0.02	0.07	0.07	0.04	0.02	0.04	0.02	0.05	0.04
Total	**99.57**	**99.54**	**99.72**	**99.53**	**100.54**	**99.88**	**99.40**	**99.79**	**100.21**	**100.57**	**100.18**	**99.63**	**100.28**
Atomic Pro													
Si	3.022	3.014	3.040	2.977	2.956	3.021	3.017	2.996	3.010	3.012	2.988	2.980	2.989
Ti	0.000	0.000	0.004	0.001	0.000	0.023	0.017	0.000	0.002	0.000	0.006	0.007	0.007
Al	1.614	1.647	1.662	1.532	1.619	1.702	1.483	1.610	1.759	1.572	1.706	1.377	1.833
Cr	0.383	0.366	0.333	0.455	0.380	0.219	0.467	0.413	0.265	0.405	0.243	0.608	0.159
Fe	0.421	0.476	0.463	0.431	0.509	0.470	0.420	0.426	0.438	0.439	0.779	0.458	0.485
Mn	0.027	0.028	0.027	0.029	0.033	0.019	0.022	0.026	0.024	0.026	0.030	0.027	0.024
Mg	2.280	2.030	2.167	2.178	2.071	2.139	2.101	2.250	2.175	2.274	1.798	2.073	2.122
Ca	0.221	0.411	0.252	0.426	0.474	0.397	0.460	0.269	0.302	0.268	0.481	0.485	0.386
Na	0.021	0.014	0.022	0.002	0.003	0.009	0.010	0.006	0.003	0.005	0.002	0.007	0.005
Total	**7.990**	**7.986**	**7.969**	**8.030**	**8.045**	**8.000**	**7.996**	**7.995**	**7.977**	**8.002**	**8.033**	**8.023**	**8.011**
Mg#	84.41	80.99	82.38	83.49	80.27	81.98	83.35	84.09	83.22	83.82	69.76	81.89	81.39
Al/Cr ratio	4.21	4.49	4.99	3.36	4.26	7.78	3.17	3.90	6.65	3.88	7.03	2.26	11.49
# Analyses	5	6	4	3	2	5	6	11	5	4	8	9	4
Suite	Low-Ca Harzburgite	High-Ca Harzburgite	Low-Ca Harzburgite	Low-Ca Harzburgite	High-Ca Harzburgite	Lherzolite	Lherzolite	Low-Ca Harzburgite	Low-Ca Harzburgite	Low-Ca Harzburgite	Clino-pyroxenite	High-Ca Harzburgite	High-Ca Harzburgite

Major element Analyses - Garnet

Sample No.	ARN031	MIS401	MIS408	MIS409	MIS411	MIS412	MIS413	MIS417	MIS419	MIS420	MIS426	MIS428	MIS430
SiO_2	41.56	41.27	40.34	41.68	41.42	40.46	39.74	41.02	41.52	39.67	41.58	40.46	40.48
TiO_2	0.05	<0.04	<0.04	<0.04	<0.04	<0.04	<0.04	<0.04	<0.04	<0.04	0.09	0.05	<0.04
Al_2O_3	22.21	18.11	16.90	21.24	20.25	18.57	16.67	19.52	19.39	15.93	21.23	21.02	19.24
Cr_2O_3	1.72	8.21	10.13	3.64	5.02	6.46	8.92	5.59	5.35	10.28	3.56	2.04	5.93
FeO	10.04	7.42	7.57	8.16	7.89	7.69	11.83	8.42	6.79	8.58	8.49	16.58	8.79
MnO	0.41	0.50	0.47	0.41	0.45	0.45	0.71	0.52	0.30	0.61	0.40	0.78	0.58
MgO	19.30	22.91	20.06	19.36	20.32	17.88	15.79	17.87	20.65	15.70	19.77	13.70	17.85
CaO	4.84	1.10	4.66	5.17	4.30	7.66	6.13	6.97	5.96	9.56	4.94	6.00	6.62
Na_2O	0.02	0.04	0.02	0.02	0.02	0.02	0.02	0.02	0.03	0.03	0.03	0.02	0.02
Total	**100.16**	**99.56**	**100.17**	**99.68**	**99.67**	**99.19**	**99.80**	**99.93**	**100.00**	**100.36**	**100.10**	**100.64**	**99.54**
Atomic Pro													
Si	2.982	2.978	2.947	2.998	2.986	2.977	2.978	2.987	2.987	2.955	2.983	2.998	2.969
Ti	0.003	0.000	0.002	0.000	0.000	0.000	0.000	0.000	0.000	0.000	0.005	0.003	0.001
Al	1.878	1.540	1.455	1.801	1.720	1.610	1.472	1.675	1.644	1.399	1.795	1.835	1.663
Cr	0.098	0.468	0.585	0.207	0.286	0.376	0.528	0.322	0.304	0.606	0.202	0.120	0.344
Fe	0.603	0.448	0.463	0.491	0.476	0.473	0.741	0.513	0.409	0.535	0.509	1.027	0.539
Mn	0.025	0.031	0.029	0.025	0.028	0.028	0.045	0.032	0.019	0.039	0.024	0.049	0.036
Mg	2.065	2.464	2.185	2.077	2.183	1.961	1.764	1.940	2.215	1.744	2.114	1.513	1.951
Ca	0.372	0.085	0.365	0.399	0.332	0.604	0.492	0.544	0.459	0.763	0.380	0.476	0.520
Na	0.002	0.006	0.000	0.003	0.002	0.002	0.003	0.003	0.004	0.005	0.004	0.002	0.003
Total	**8.028**	**8.020**	**8.031**	**7.999**	**8.013**	**8.031**	**8.023**	**8.016**	**8.041**	**8.045**	**8.016**	**8.023**	**8.027**
Mg#	77.40	84.62	82.52	80.89	82.11	80.55	70.42	79.08	84.42	76.54	80.59	59.57	78.35
Al/Cr ratio	19.22	3.29	2.49	8.70	6.02	4.28	2.79	5.20	5.40	2.31	8.88	15.32	4.83
# Analyses	7	4	4	5	4	7	9	12	4	5	5	4	7
Suite	Clino-pyroxenite	Low-Ca Harzburgite	Low-Ca Harzburgite	Lherzolite	Low-Ca Harzburgite	High-Ca Harzburgite	High-Ca Harzburgite	High-Ca Harzburgite	Lherzolite	High-Ca Harzburgite	Lherzolite	Clino-pyroxenite	High-Ca Harzburgite

Major element Analyses - Garnet

Sample No.	MIS431	MIS433	MIS434	MIS438	MIS439	MIS451	MIS454	MIS456	MIS463	PGN301	PGN303	PGN306	PGN307
SiO_2	41.29	41.32	41.00	38.91	39.30	41.09	42.15	41.26	42.26	40.45	40.55	39.54	41.06
TiO_2	0.10	0.12	<0.04	0.08	0.06	0.15	0.13	0.17	0.10	<0.04	<0.04	<0.04	0.49
Al_2O_3	21.30	21.76	18.23	22.26	22.44	23.05	22.35	22.89	20.71	18.80	17.31	17.42	16.88
Cr_2O_3	3.63	3.82	7.58	0.44	0.27	0.48	2.03	0.45	4.67	7.67	9.74	8.98	8.88
FeO	8.79	8.40	8.39	22.03	18.73	14.11	9.15	14.69	6.51	7.71	8.16	8.26	6.58
MnO	0.42	0.41	0.52	0.51	0.50	0.41	0.41	0.33	0.32	0.45	0.47	0.35	0.32
MgO	18.60	18.96	16.68	10.25	12.67	16.04	19.05	16.06	20.95	20.24	20.17	18.77	20.12
CaO	5.09	5.12	7.22	5.66	5.39	4.45	4.68	4.70	4.37	4.06	3.55	5.82	5.82
Na_2O	0.02	0.02	0.02	0.02	0.02	0.02	0.03	0.01	0.02	0.04	0.03	0.02	0.05
Total	**99.23**	**99.92**	**99.64**	**100.14**	**99.38**	**99.80**	**99.98**	**100.57**	**99.91**	**99.44**	**99.98**	**99.17**	**100.20**
Atomic Pro													
Si	2.992	2.970	3.013	2.955	2.958	2.996	3.014	2.995	3.010	2.949	2.960	2.929	2.981
Ti	0.006	0.007	0.001	0.004	0.003	0.008	0.007	0.009	0.005	0.001	0.000	0.000	0.027
Al	1.819	1.843	1.578	1.992	1.990	1.980	1.883	1.958	1.739	1.615	1.489	1.521	1.444
Cr	0.208	0.217	0.440	0.026	0.016	0.028	0.115	0.026	0.263	0.442	0.562	0.526	0.510
Fe	0.533	0.505	0.516	1.399	1.179	0.861	0.547	0.891	0.388	0.470	0.498	0.512	0.400
Mn	0.026	0.025	0.032	0.033	0.032	0.026	0.025	0.020	0.019	0.028	0.029	0.022	0.020
Mg	2.009	2.031	1.827	1.161	1.421	1.744	2.030	1.738	2.225	2.199	2.196	2.073	2.177
Ca	0.395	0.394	0.568	0.460	0.435	0.348	0.358	0.366	0.333	0.317	0.278	0.462	0.453
Na	0.000	0.001	0.000	0.000	0.004	0.001	0.004	0.002	0.002	0.006	0.004	0.002	0.007
Total	**7.989**	**7.994**	**7.977**	**8.031**	**8.038**	**7.992**	**7.983**	**8.005**	**7.985**	**8.025**	**8.016**	**8.048**	**8.018**
Mg#	79.04	80.09	77.99	45.35	54.67	66.95	78.77	66.10	85.15	82.40	81.51	80.20	84.49
Al/Cr ratio	8.76	8.48	3.59	75.84	122.24	70.91	16.41	76.37	6.61	3.65	2.65	2.89	2.83
# Analyses	8	6	3	3	4	4	3	3	4	4	7	3	5
Suite	Lherzolite	Lherzolite	High-Ca Harzburgite	Websterite	Websterite	Clino-pyroxenite	Clino-pyroxenite	Clino-pyroxenite	Low-Ca Harzburgite	Low-Ca Harzburgite	Low-Ca Harzburgite	Lherzolite	Lherzolite

Major element Analyses - Garnet

Sample No.	PGN308	PGN309	PGN310	PGN311	PGN312	PGN313	PGN314	PGN315	PGN316	PGN317	PGN318	PGN319	PGN320	PGN321
SiO_2	41.15	42.30	41.19	41.77	40.81	40.58	41.41	39.75	41.06	40.66	40.18	39.95	41.10	41.52
TiO_2	0.05	<0.04	0.11	<0.04	<0.04	<0.04	<0.04	<0.04	<0.04	<0.04	<0.04	<0.04	<0.04	0.32
Al_2O_3	16.61	20.83	18.26	20.43	17.25	19.63	18.11	15.27	16.89	19.86	17.38	22.34	22.77	21.47
Cr_2O_3	8.99	3.18	7.19	3.79	8.91	5.90	8.24	11.50	8.69	6.37	9.09	0.65	2.29	3.81
FeO	7.55	7.79	7.26	7.65	6.51	7.95	6.75	6.52	6.47	8.12	7.64	18.26	6.82	7.37
MnO	0.36	0.29	0.39	0.30	0.36	0.47	0.33	0.38	0.28	0.47	0.46	0.36	0.10	0.30
MgO	18.76	20.39	19.41	20.12	19.77	18.70	21.37	19.47	20.04	20.63	19.59	14.53	16.37	20.08
CaO	6.66	4.97	5.56	5.16	5.77	5.81	3.69	6.30	5.68	3.29	5.29	4.29	10.06	5.21
Na_2O	0.04	0.03	nd	0.04	0.03	0.02	0.03	0.06	0.03	0.02	0.02	0.03	0.02	0.07
Total	**100.17**	**99.79**	**99.49**	**99.26**	**99.42**	**99.03**	**99.95**	**99.26**	**99.13**	**99.42**	**99.66**	**100.42**	**99.53**	**100.14**
Atomic Pro														
Si	3.008	3.027	3.000	3.013	2.984	2.969	2.986	2.949	3.006	2.949	2.948	2.959	2.968	2.966
Ti	0.003	0.000	0.006	0.000	0.000	0.000	0.001	0.001	0.000	0.000	0.000	0.000	0.000	0.017
Al	1.430	1.756	1.567	1.736	1.486	1.692	1.539	1.335	1.457	1.697	1.503	1.950	1.938	1.808
Cr	0.520	0.180	0.414	0.216	0.515	0.341	0.469	0.674	0.503	0.365	0.527	0.038	0.131	0.215
Fe	0.462	0.466	0.442	0.462	0.398	0.487	0.407	0.405	0.396	0.492	0.469	1.131	0.412	0.440
Mn	0.022	0.018	0.024	0.018	0.023	0.029	0.020	0.024	0.017	0.029	0.029	0.023	0.006	0.018
Mg	2.044	2.175	2.108	2.164	2.154	2.040	2.297	2.154	2.187	2.231	2.143	1.604	1.762	2.138
Ca	0.522	0.381	0.434	0.399	0.452	0.455	0.285	0.500	0.445	0.256	0.416	0.340	0.778	0.399
Na	0.005	0.005	0.017	0.005	0.004	0.001	0.004	0.008	0.004	0.003	0.003	0.005	0.003	0.010
Total	**8.016**	**8.007**	**8.012**	**8.013**	**8.017**	**8.014**	**8.010**	**8.049**	**8.016**	**8.021**	**8.038**	**8.050**	**7.999**	**8.010**
Mg#	81.57	82.35	82.65	82.42	84.40	80.73	84.94	84.18	84.67	81.91	82.05	58.65	81.05	82.94
Al/Cr ratio	2.75	9.76	3.79	8.02	2.88	4.96	3.28	1.98	2.90	4.65	2.85	51.52	14.82	8.40
# Analyses	10	7	7	7	4	4	6	7	4	5	12	5	4	4
Suite	High-Ca Harzburgite	High-Ca Harzburgite	Lherzolite	High-Ca Harzburgite	High-Ca Harzburgite	High-Ca Harzburgite	Low-Ca Harzburgite	High-Ca Harzburgite	Lherzolite	Low-Ca Harzburgite	Low-Ca Harzburgite	Clino-pyroxenite	Clino-pyroxenite	Lherzolite

Major element Analyses - Garnet

Sample No.	PGN322	PGN323	PGN324	PGN325	PGN329	PGN333	PGN336	PGN337	PGN338	PGN339	PGN340	PGN341	PGN342	PGN343
SiO_2	40.94	41.50	40.83	40.99	41.49	40.90	40.84	42.28	41.01	41.68	41.83	41.14	40.84	41.23
TiO_2	<0.04	0.28	<0.04	<0.04	0.86	0.04	0.17	0.62	0.04	0.35	<0.04	<0.04	<0.04	<0.04
Al_2O_3	22.96	20.06	17.60	18.60	19.52	18.07	16.75	20.77	15.17	18.65	18.44	17.68	16.30	17.88
Cr_2O_3	2.13	5.06	8.02	7.30	4.45	7.85	8.99	3.39	11.73	7.12	8.01	8.78	10.18	8.31
FeO	8.39	7.85	7.59	8.11	8.10	7.92	7.54	8.50	6.80	7.58	7.31	7.48	7.73	7.88
MnO	0.14	0.34	0.36	0.50	0.38	0.56	0.38	0.35	0.42	0.45	0.47	0.46	0.50	0.47
MgO	16.14	19.19	18.83	18.76	19.70	17.69	18.10	19.47	17.28	18.77	21.28	18.99	19.03	19.71
CaO	10.00	6.46	6.34	5.89	5.33	6.16	6.92	4.92	7.10	5.54	2.36	5.30	5.01	4.10
Na_2O	0.02	0.03	0.05	0.02	0.05	nd	nd	nd	nd	nd	nd	nd	nd	nd
Total	**100.70**	**100.77**	**99.62**	**100.16**	**99.87**	**99.35**	**99.82**	**100.48**	**99.68**	**100.34**	**99.83**	**99.97**	**99.76**	**99.74**
Atomic Pro														
Si	2.944	2.977	2.990	2.981	2.994	3.005	3.000	3.018	3.032	3.011	3.012	2.997	3.000	3.001
Ti	0.000	0.015	0.000	0.000	0.047	0.002	0.009	0.033	0.002	0.019	0.000	0.000	0.001	0.000
Al	1.945	1.696	1.519	1.594	1.660	1.564	1.450	1.747	1.321	1.588	1.565	1.518	1.411	1.534
Cr	0.121	0.287	0.464	0.420	0.254	0.456	0.522	0.191	0.685	0.407	0.456	0.506	0.591	0.478
Fe	0.504	0.471	0.465	0.493	0.489	0.487	0.463	0.507	0.421	0.458	0.440	0.456	0.475	0.480
Mn	0.008	0.020	0.022	0.031	0.023	0.035	0.023	0.021	0.026	0.028	0.029	0.028	0.031	0.029
Mg	1.730	2.052	2.056	2.034	2.119	1.938	1.982	2.072	1.904	2.022	2.284	2.062	2.083	2.139
Ca	0.770	0.496	0.498	0.459	0.412	0.485	0.544	0.377	0.562	0.429	0.182	0.414	0.394	0.320
Na	0.001	0.005	0.007	0.002	0.007	0.022	0.021	0.025	0.019	0.027	0.018	0.021	0.021	0.021
Total	**8.024**	**8.019**	**8.021**	**8.014**	**8.005**	**7.993**	**8.015**	**7.992**	**7.973**	**7.987**	**7.987**	**8.001**	**8.008**	**8.002**
Mg#	77.42	81.34	81.55	80.47	81.25	79.92	81.06	80.33	81.90	81.54	83.84	81.89	81.45	81.68
Al/Cr ratio	16.08	5.91	3.27	3.80	6.53	3.43	2.78	9.14	1.93	3.91	3.43	3.00	2.39	3.21
# Analyses	4	5	5	9	5	9	4	4	4	4	4	8	4	4
Suite	Clino-pyroxenite	Lherzolite	Lherzolite	Lherzolite	Lherzolite	Lherzolite	Lherzolite	Lherzolite	Lherzolite	Lherzolite	Low-Ca Harzburgite	Low-Ca Harzburgite	Low-Ca Harzburgite	Low-Ca Harzburgite

Major Element Analyses - Clinopyroxene

Sample No	ARN028	ARN031	ARN032	ARN033	ARN034	ARN035	ARN036	MIS409	MIS419	MIS426	MIS428	MIS431	MIS433	MIS438
SiO_2	53.81	54.19	54.81	54.45	54.41	54.81	54.22	54.14	54.48	54.17	53.92	54.63	55.03	52.16
TiO_2	<0.04	<0.04	<0.04	0.17	0.09	0.24	0.21	<0.04	0.05	0.15	0.07	0.17	0.20	0.60
Al_2O_3	0.44	0.64	2.16	1.35	2.44	1.62	1.92	3.42	1.22	3.80	1.21	3.86	3.72	4.41
Cr_2O_3	0.24	0.17	2.52	2.19	3.75	3.43	3.30	2.26	0.96	2.32	0.38	2.37	2.32	0.30
FeO	3.74	2.80	2.20	2.30	2.28	2.35	2.24	1.57	2.71	1.67	2.63	1.62	1.66	5.10
MnO	0.11	0.12	0.08	0.10	0.05	0.08	0.09	0.06	0.12	0.06	0.05	<0.04	0.07	0.07
MgO	18.26	18.95	15.19	16.48	15.60	15.58	15.92	15.40	19.59	14.65	16.60	14.44	14.38	14.48
CaO	22.01	22.22	20.71	21.27	18.37	19.46	19.37	20.83	19.48	20.17	23.75	20.13	20.27	22.19
Na_2O	0.49	0.39	2.46	1.72	2.92	2.41	2.55	2.35	0.95	2.69	0.49	2.77	2.68	1.21
Total	**99.17**	**99.53**	**100.12**	**100.09**	**99.93**	**100.01**	**99.85**	**100.03**	**99.56**	**99.70**	**99.10**	**100.03**	**100.33**	**100.50**
Atomic Prop														
Si	1.978	1.975	1.986	1.978	1.974	1.989	1.972	1.958	1.973	1.963	1.979	1.971	1.979	1.905
Ti	0.001	0.000	0.000	0.005	0.003	0.006	0.006	0.000	0.001	0.004	0.002	0.004	0.005	0.016
Al	0.019	0.027	0.092	0.058	0.104	0.069	0.082	0.146	0.052	0.162	0.053	0.164	0.158	0.190
Cr	0.007	0.005	0.072	0.063	0.107	0.098	0.095	0.064	0.028	0.066	0.011	0.068	0.066	0.009
Fe	0.115	0.085	0.067	0.070	0.069	0.071	0.068	0.047	0.082	0.051	0.081	0.049	0.050	0.156
Mn	0.003	0.004	0.002	0.003	0.002	0.002	0.003	0.002	0.004	0.002	0.002	0.001	0.002	0.002
Mg	1.001	1.030	0.821	0.892	0.843	0.843	0.863	0.830	1.057	0.792	0.908	0.777	0.771	0.788
Ca	0.867	0.868	0.804	0.828	0.714	0.756	0.755	0.807	0.756	0.783	0.934	0.778	0.781	0.869
Na	0.035	0.028	0.173	0.121	0.205	0.170	0.180	0.164	0.066	0.189	0.035	0.194	0.187	0.086
Total	**4.026**	**4.022**	**4.017**	**4.018**	**4.021**	**4.006**	**4.024**	**4.019**	**4.019**	**4.013**	**4.004**	**4.005**	**3.998**	**4.022**
# Analyses	5	5	2	2	2	2	2	6	6	2	3	2	2	3
Mg#	89.70	92.35	92.49	92.74	92.42	92.19	92.68	94.61	92.80	93.99	91.85	94.09	93.92	83.49
Ca#	46.41	45.73	49.49	48.12	45.84	47.29	46.65	49.29	41.68	49.73	50.70	50.04	50.33	52.42
Suite	Clino-pyroxenite	Clino-pyroxenite	Lherzolite (no garnet)	Lherzolite (no garnet)	Lherzolite (no garnet)	Lherzolite (no garnet)	Lherzolite (no garnet)	Lherzolite (no garnet)	Lherzolite	Lherzolite	Clino-pyroxenite	Lherzolite	Lherzolite	Websterite
En, wo, fs	0.981	0.979	0.839	0.886	0.801	0.833	0.832	0.821	0.935	0.796	0.952	0.790	0.793	0.867
Wo	0.423	0.422	0.395	0.405	0.345	0.376	0.366	0.382	0.365	0.375	0.458	0.377	0.382	0.395
En	0.500	0.515	0.410	0.446	0.422	0.421	0.432	0.415	0.529	0.396	0.454	0.388	0.385	0.394
Fs	0.057	0.043	0.033	0.035	0.035	0.036	0.034	0.024	0.041	0.025	0.040	0.024	0.025	0.078
Acm	0.051	0.044	0.035	0.035	0.042	0.011	0.047	0.038	0.038	0.026	0.009	0.011	0.000	0.043
CaTs	0.021	0.024	0.013	0.017	0.024	0.005	0.022	0.042	0.026	0.033	0.019	0.025	0.016	0.078
Jd	0.000	0.000	0.138	0.086	0.164	0.158	0.132	0.126	0.028	0.164	0.026	0.183	0.191	0.042

Major Element Analyses - Clinopyroxene

Sample No	MIS439	MIS451	MIS454	PGN310	PGN319	PGN320	PGN321	PGN322	PGN323	PGN324	PGN325	PGN329	PGN333	PGN336
SiO_2	53.07	54.30	54.36	54.50	53.58	53.04	53.87	52.99	53.85	54.41	54.00	54.67	54.94	55.07
TiO_2	0.56	0.11	0.28	0.10	0.10	0.12	0.21	0.12	0.17	0.43	<0.04	0.25	<0.04	<0.04
Al_2O_3	5.14	2.90	3.35	1.89	3.02	3.83	1.66	4.32	1.32	1.29	1.96	1.70	2.19	1.04
Cr_2O_3	0.25	0.29	1.42	2.23	0.21	1.22	0.86	1.26	1.11	1.12	3.00	1.00	2.87	1.34
FeO	4.30	2.17	2.04	2.36	5.67	1.69	3.19	1.75	2.79	2.84	1.78	3.26	1.78	2.66
MnO	0.04	0.05	0.05	0.08	0.07	<0.04	0.12	<0.04	0.08	0.11	0.06	0.09	0.05	0.09
MgO	14.01	16.22	15.00	16.87	15.88	16.05	19.29	15.84	18.89	18.56	16.22	18.12	15.14	18.50
CaO	21.03	22.20	20.91	19.31	19.33	22.06	19.68	22.27	21.11	20.37	19.97	19.00	20.04	20.42
Na_2O	1.83	1.68	2.40	2.11	2.26	2.17	1.38	2.38	1.19	1.34	2.61	1.44	2.41	0.96
Total	**100.23**	**99.94**	**99.82**	**99.56**	**100.15**	**100.20**	**100.28**	**100.90**	**100.57**	**100.48**	**99.60**	**99.58**	**99.45**	**100.19**
Atomic Prop														
Si	1.928	1.966	1.970	1.981	1.957	1.922	1.948	1.909	1.947	1.963	1.967	1.982	1.997	1.987
Ti	0.015	0.003	0.008	0.003	0.003	0.003	0.006	0.003	0.005	0.012	0.000	0.007	0.001	0.001
Al	0.220	0.124	0.143	0.081	0.130	0.164	0.071	0.184	0.056	0.055	0.084	0.073	0.094	0.044
Cr	0.007	0.008	0.041	0.064	0.006	0.035	0.025	0.036	0.032	0.032	0.086	0.029	0.082	0.038
Fe	0.131	0.066	0.062	0.072	0.173	0.051	0.096	0.053	0.084	0.086	0.054	0.099	0.054	0.080
Mn	0.001	0.002	0.002	0.002	0.002	0.000	0.004	0.000	0.002	0.003	0.002	0.003	0.002	0.003
Mg	0.758	0.876	0.810	0.914	0.865	0.867	1.040	0.851	1.018	0.998	0.881	0.980	0.820	0.995
Ca	0.818	0.861	0.812	0.752	0.757	0.856	0.762	0.860	0.818	0.787	0.780	0.738	0.780	0.789
Na	0.129	0.118	0.169	0.149	0.160	0.153	0.096	0.166	0.083	0.094	0.184	0.101	0.170	0.067
Total	**4.008**	**4.024**	**4.015**	**4.018**	**4.052**	**4.052**	**4.047**	**4.061**	**4.046**	**4.029**	**4.039**	**4.011**	**3.999**	**4.005**
# Analyses	3	3	2	5	2	3	3	2	2	3	4	2	3	4
Mg#	85.31	93.01	92.92	92.72	83.33	94.42	91.52	94.17	92.35	92.10	94.21	90.83	93.81	92.52
Ca#	51.90	49.58	50.05	45.13	46.67	49.69	42.30	50.26	44.54	44.10	46.94	42.97	48.75	44.24
Suite	Websterite	Clino-pyroxenite	Clino-pyroxenite	Lherzolite	Clino-pyroxenite	Clino-pyroxenite	Lherzolite	Clino-pyroxenite	Lherzolite	Lherzolite	Lherzolite	Lherzolite	Lherzolite	Lherzolite
En, wo, fs	0.825	0.886	0.830	0.861	0.877	0.850	0.926	0.838	0.936	0.923	0.841	0.903	0.826	0.926
Wo	0.381	0.415	0.395	0.368	0.358	0.391	0.358	0.386	0.385	0.381	0.374	0.364	0.389	0.388
En	0.379	0.438	0.405	0.457	0.432	0.434	0.520	0.425	0.509	0.499	0.441	0.490	0.410	0.498
Fs	0.065	0.033	0.031	0.036	0.087	0.026	0.048	0.026	0.042	0.043	0.027	0.049	0.027	0.040
Acm	0.016	0.048	0.030	0.036	0.104	0.103	0.094	0.122	0.092	0.058	0.079	0.022	0.000	0.009
CaTs	0.057	0.031	0.023	0.016	0.040	0.075	0.046	0.088	0.048	0.026	0.033	0.011	0.002	0.012
Jd	0.113	0.071	0.138	0.113	0.056	0.049	0.002	0.044	0.000	0.036	0.105	0.079	0.171	0.058

Major Element Analyses - Clinopyroxene

Sample No	PGN337	PGN338	PGN339
SiO_2	55.35	55.17	55.43
TiO_2	0.22	<0.04	0.19
Al_2O_3	1.77	1.35	1.90
Cr_2O_3	0.91	2.93	2.30
FeO	3.20	1.92	2.12
MnO	0.15	0.09	0.08
MgO	17.59	16.29	15.79
CaO	19.29	19.98	19.61
Na_2O	1.42	1.76	2.05
Total	**99.93**	**99.56**	**99.50**
Atomic Prop			
Si	1.997	2.002	2.008
Ti	0.006	0.001	0.005
Al	0.075	0.058	0.081
Cr	0.026	0.084	0.066
Fe	0.096	0.058	0.064
Mn	0.004	0.003	0.002
Mg	0.946	0.882	0.853
Ca	0.745	0.777	0.761
Na	0.099	0.124	0.144
Total	**3.996**	**3.988**	**3.985**
# Analyses	2	2	2
Mg#	90.75	93.80	92.99
Ca#	44.08	46.85	47.15
Suite	Lherzolite	Lherzolite	Lherzolite
En, wo, fs	0.895	0.860	0.846
Wo	0.374	0.390	0.387
En	0.473	0.441	0.427
Fs	0.048	0.029	0.032
Acm	0.000	0.000	0.000
CaTs	0.000	0.000	0.000
Jd	0.108	0.148	0.173

Phlogopite Analysis

Sample No	PGN338
SiO_2	43.82
TiO_2	0.07
Al_2O_3	13.49
FeO	2.96
MnO	<0.05
MgO	24.63
CaO	0.00
Na_2O	<0.03
K_2O	9.46
Total	**94.50**
Atomic Proportions based on 24(O, OH, F)	
Si	6.703
Ti	0.008
Al	2.433
Fe	0.379
Mn	0.005
Mg	5.618
Ca	0.001
Na	0.005
K	1.846
Total	**16.998**

Major Element Analyses - Orthopyroxene

Sample No	ARN002	ARN003	ARN004	ARN005	ARN006	ARN007	ARN008	ARN009	ARN010	ARN011	ARN012	ARN013	ARN014
SiO_2	58.15	57.63	57.94	57.58	57.81	57.22	57.78	57.37	58.10	57.41	57.39	57.88	58.53
TiO_2	<0.04	<0.04	<0.04	<0.04	<0.04	<0.04	<0.04	<0.04	<0.04	<0.04	<0.04	<0.04	<0.04
Al_2O_3	0.47	0.66	0.42	0.60	0.58	0.62	0.61	0.53	0.54	0.53	0.62	0.65	0.42
Cr_2O_3	0.32	0.49	0.24	0.34	0.47	0.43	0.28	0.40	0.24	0.33	0.45	0.32	0.26
FeO	4.31	4.63	4.76	4.47	4.63	4.35	4.18	4.70	4.19	4.37	4.52	4.51	4.58
MnO	0.10	0.14	0.15	0.12	0.12	0.13	0.10	0.12	0.09	0.12	0.11	0.11	0.13
MgO	36.46	35.11	36.20	35.48	36.13	36.29	36.83	36.94	36.22	36.95	36.64	36.73	35.79
CaO	0.26	0.41	0.36	0.33	0.20	0.20	0.12	0.35	0.11	0.27	0.30	0.22	0.35
Na_2O	0.03	0.09	0.02	0.03	0.04	0.15	0.09	0.12	0.09	0.08	0.19	0.07	0.08
Total	**100.11**	**99.31**	**100.09**	**99.16**	**99.98**	**99.42**	**100.25**	**100.57**	**99.60**	**100.09**	**100.26**	**100.54**	**100.18**
Atomic Pro													
Si	1.984	1.988	1.982	1.987	1.979	1.970	1.972	1.958	1.989	1.964	1.963	1.971	1.997
Ti	0.000	0.000	0.000	0.000	0.000	0.000	0.000	0.000	0.000	0.000	0.000	0.000	0.000
Al	0.019	0.027	0.017	0.024	0.023	0.025	0.025	0.021	0.022	0.021	0.025	0.026	0.017
Cr	0.009	0.014	0.007	0.009	0.013	0.012	0.007	0.011	0.007	0.009	0.012	0.009	0.007
Fe	0.123	0.134	0.136	0.129	0.132	0.125	0.119	0.134	0.120	0.125	0.129	0.128	0.131
Mn	0.003	0.004	0.004	0.003	0.003	0.004	0.003	0.004	0.003	0.003	0.003	0.003	0.004
Mg	1.854	1.806	1.846	1.825	1.844	1.863	1.874	1.880	1.849	1.885	1.868	1.864	1.820
Ca	0.009	0.015	0.013	0.012	0.007	0.007	0.004	0.013	0.004	0.010	0.011	0.008	0.013
Na	0.002	0.006	0.001	0.002	0.002	0.010	0.006	0.008	0.006	0.005	0.013	0.005	0.005
Total	**4.003**	**3.994**	**4.007**	**4.001**	**4.004**	**4.016**	**4.021**	**4.030**	**3.999**	**4.023**	**4.025**	**4.014**	**3.994**
Mg#	93.78	93.09	93.14	93.40	93.30	93.70	94.01	93.33	93.91	93.78	93.52	93.55	93.30
Ca#	0.51	0.85	0.72	0.67	0.39	0.39	0.23	0.68	0.21	0.53	0.58	0.43	0.70
# Analyses	2	4	2	5	2	5	4	7	4	12	5	7	6
Suite	Low-Ca Harzburgite	High-Ca Harzburgite	High-Ca Harzburgite	High-Ca Harzburgite	High-Ca Harzburgite	Low-Ca Harzburgite	Low-Ca Harzburgite	High-Ca Harzburgite	Low-Ca Harzburgite	Low-Ca Harzburgite	Low-Ca Harzburgite	High-Ca Harzburgite	High-Ca Harzburgite
CaTs	0.02	0.01	0.02	0.01	0.02	0.03	0.03	0.04	0.01	0.04	0.04	0.03	0.00
Jd	0.00	0.02	-0.01	0.01	-0.01	-0.02	-0.02	-0.05	0.01	-0.04	-0.04	-0.02	0.02
Acm	0.01	-0.01	0.01	0.00	0.01	0.03	0.04	0.06	0.00	0.05	0.05	0.03	-0.01
Wo	0.00	0.00	0.00	0.00	-0.01	-0.01	-0.01	-0.01	0.00	-0.01	-0.01	-0.01	0.00
En	0.93	0.90	0.92	0.91	0.92	0.93	0.94	0.94	0.92	0.94	0.93	0.93	0.91
Fs	0.06	0.07	0.07	0.06	0.07	0.06	0.06	0.07	0.06	0.06	0.06	0.06	0.07

Major Element Analyses - Orthopyroxene

Sample No	ARN017	ARN018	ARN019	ARN021	ARN022	ARN025	ARN026	ARN027	ARN029	ARN037	MIS401	MIS408	MIS409
SiO_2	57.96	57.92	58.37	58.11	57.86	57.52	57.47	57.68	56.98	57.71	58.67	58.38	57.47
TiO_2	<0.04	<0.04	<0.04	<0.04	<0.04	<0.04	<0.04	<0.04	<0.04	0.08	<0.04	<0.04	<0.04
Al_2O_3	0.61	0.70	0.53	0.48	0.46	0.59	0.92	0.60	0.55	0.56	0.48	0.27	0.88
Cr_2O_3	0.52	0.36	0.26	0.36	0.22	0.40	0.43	0.41	0.43	0.39	0.34	0.23	0.30
FeO	4.26	4.65	4.14	4.35	4.69	4.34	4.36	4.44	4.77	4.74	4.36	4.56	4.43
MnO	0.13	0.13	0.10	0.13	0.14	0.12	0.11	0.14	0.14	0.10	0.13	0.12	0.09
MgO	36.29	35.90	36.52	35.80	35.53	36.94	36.06	36.01	36.18	35.93	36.22	35.68	36.36
CaO	0.21	0.30	0.17	0.32	0.20	0.24	0.30	0.23	0.40	0.46	0.07	0.26	0.14
Na_2O	0.14	0.03	0.08	0.08	0.02	0.13	0.04	0.14	0.18	0.17	0.07	0.01	0.03
Total	**100.12**	**100.00**	**100.20**	**99.63**	**99.11**	**100.30**	**99.72**	**99.67**	**99.68**	**100.14**	**100.36**	**99.53**	**99.80**
Atomic Pro													
Si	1.979	1.981	1.987	1.992	1.995	1.964	1.971	1.980	1.963	1.976	1.994	2.003	1.970
Ti	0.000	0.000	0.001	0.000	0.000	0.000	0.000	0.000	0.001	0.002	0.000	0.000	0.000
Al	0.024	0.028	0.021	0.019	0.019	0.024	0.037	0.024	0.023	0.023	0.019	0.011	0.036
Cr	0.014	0.010	0.007	0.010	0.006	0.011	0.012	0.011	0.012	0.011	0.009	0.006	0.008
Fe	0.122	0.133	0.118	0.125	0.135	0.124	0.125	0.127	0.137	0.136	0.124	0.131	0.127
Mn	0.004	0.004	0.003	0.004	0.004	0.003	0.003	0.004	0.004	0.003	0.004	0.003	0.003
Mg	1.847	1.831	1.853	1.829	1.826	1.880	1.844	1.843	1.858	1.834	1.835	1.825	1.858
Ca	0.008	0.011	0.006	0.012	0.007	0.009	0.011	0.009	0.015	0.017	0.003	0.009	0.005
Na	0.009	0.002	0.005	0.006	0.001	0.008	0.003	0.010	0.012	0.011	0.005	0.001	0.002
Total	**4.007**	**4.001**	**4.001**	**3.996**	**3.993**	**4.023**	**4.006**	**4.007**	**4.025**	**4.011**	**3.993**	**3.989**	**4.009**
Mg#	93.82	93.22	94.02	93.62	93.11	93.81	93.66	93.54	93.11	93.11	93.68	93.31	93.61
Ca#	0.42	0.60	0.33	0.64	0.40	0.46	0.60	0.46	0.80	0.90	0.15	0.51	0.27
# Analyses	2	2	2	3	3	4	4	5	5	2	4	2	7
Suite	Low-Ca Harzburgite	High-Ca Harzburgite	Low-Ca Harzburgite	Low-Ca Harzburgite	High-Ca Harzburgite	Low-Ca Harzburgite	Low-Ca Harzburgite	Low-Ca Harzburgite	High-Ca Harzburgite	High-Ca Harzburgite	Low-Ca Harzburgite	Low-Ca Harzburgite	Lherzolite
CaTs	0.02	0.02	0.01	0.01	0.00	0.04	0.03	0.02	0.04	0.02	0.01	0.00	0.03
Jd	0.00	0.00	0.00	0.01	0.01	-0.04	-0.01	-0.01	-0.04	-0.01	0.02	0.02	-0.02
Acm	0.01	0.00	0.00	-0.01	-0.01	0.05	0.01	0.01	0.05	0.02	-0.01	-0.02	0.02
Wo	-0.01	0.00	0.00	0.00	0.00	-0.01	-0.01	-0.01	-0.01	0.00	0.00	0.01	-0.01
En	0.92	0.92	0.93	0.91	0.91	0.94	0.92	0.92	0.93	0.92	0.92	0.91	0.93
Fs	0.06	0.07	0.06	0.06	0.07	0.06	0.06	0.06	0.07	0.07	0.06	0.07	0.06

Major Element Analyses - Orthopyroxene

Sample No	MIS411	MIS412	MIS413	MIS417	MIS419	MIS420	MIS426	MIS428	MIS430	MIS431	MIS433	MIS434	MIS438	MIS439
SiO_2	56.96	57.01	56.85	57.52	56.89	56.96	58.61	57.27	58.33	57.52	57.88	58.34	54.46	55.54
TiO_2	<0.04	<0.04	<0.04	<0.04	<0.04	<0.04	0.05	0.06	<0.04	0.05	0.05	<0.04	0.21	0.05
Al_2O_3	0.73	0.60	0.28	0.43	0.63	0.41	0.74	0.56	0.43	1.16	0.92	0.47	1.71	2.02
Cr_2O_3	0.25	0.35	0.16	0.10	0.15	0.21	0.30	0.15	0.15	0.48	0.36	0.21	0.13	0.09
FeO	4.27	4.63	7.23	4.57	4.82	5.32	4.47	9.64	4.49	4.47	4.37	4.70	16.48	12.62
MnO	0.12	0.10	0.19	0.12	0.11	0.13	0.07	0.13	0.09	0.11	0.09	0.15	0.15	0.13
MgO	37.17	37.21	34.88	36.55	36.34	36.51	35.52	32.65	36.93	36.07	36.27	36.24	27.10	30.22
CaO	<0.05	<0.05	0.05	<0.05	0.37	<0.05	0.19	0.25	0.14	0.27	0.22	0.19	0.35	0.20
Na_2O	0.06	0.04	0.04	0.03	0.13	0.05	0.02	0.01	0.02	0.06	0.05	0.04	0.02	0.03
Total	**99.77**	**100.13**	**99.84**	**99.52**	**99.55**	**99.73**	**100.00**	**100.74**	**100.59**	**100.19**	**100.22**	**100.34**	**100.62**	**100.89**
Atomic Pro														
Si	1.957	1.955	1.975	1.979	1.963	1.965	1.999	1.987	1.981	1.965	1.973	1.988	1.955	1.951
Ti	0.000	0.000	0.000	0.000	0.000	0.000	0.001	0.002	0.000	0.001	0.001	0.000	0.006	0.001
Al	0.030	0.024	0.011	0.017	0.026	0.017	0.030	0.023	0.017	0.047	0.037	0.019	0.072	0.084
Cr	0.007	0.009	0.004	0.003	0.004	0.006	0.008	0.004	0.004	0.013	0.010	0.006	0.004	0.002
Fe	0.123	0.133	0.210	0.132	0.139	0.154	0.128	0.280	0.128	0.128	0.124	0.134	0.495	0.371
Mn	0.004	0.003	0.005	0.003	0.003	0.004	0.002	0.004	0.003	0.003	0.003	0.004	0.004	0.004
Mg	1.904	1.902	1.807	1.875	1.869	1.878	1.806	1.689	1.870	1.836	1.844	1.841	1.451	1.583
Ca	0.000	0.000	0.002	0.000	0.014	0.000	0.007	0.009	0.005	0.010	0.008	0.007	0.014	0.008
Na	0.004	0.003	0.003	0.002	0.009	0.003	0.001	0.000	0.001	0.004	0.003	0.003	0.002	0.002
Total	**4.027**	**4.029**	**4.018**	**4.012**	**4.027**	**4.025**	**3.982**	**3.998**	**4.009**	**4.006**	**4.004**	**4.001**	**4.002**	**4.006**
Mg#	93.94	93.47	89.58	93.44	93.08	92.44	93.40	85.79	93.62	93.51	93.68	93.22	74.56	81.02
Ca#	0.00	0.00	0.10	0.00	0.73	0.00	0.38	0.54	0.27	0.53	0.44	0.37	0.93	0.48
# Analyses	2	4	4	4	5	4	2	3	2	2	3	2	3	2
Suite	Low-Ca Harzburgite	High-Ca Harzburgite	High-Ca Harzburgite	High-Ca Harzburgite	Lherzolite	High-Ca Harzburgite	Lherzolite	Clino-pyroxenite	High-Ca Harzburgite	Lherzolite	Lherzolite	High-Ca Harzburgite	Websterite	Websterite
CaTs	0.04	0.04	0.02	0.02	0.04	0.04	0.00	0.01	0.02	0.03	0.03	0.01	0.04	0.05
Jd	-0.05	-0.06	-0.03	-0.02	-0.04	-0.05	0.04	0.00	-0.02	-0.01	0.00	0.00	0.00	-0.01
Acm	0.05	0.06	0.04	0.02	0.05	0.05	-0.04	0.00	0.02	0.01	0.01	0.00	0.00	0.01
Wo	-0.02	-0.02	-0.01	-0.01	-0.01	-0.02	0.00	0.00	-0.01	-0.01	-0.01	0.00	-0.01	-0.02
En	0.95	0.95	0.90	0.94	0.93	0.94	0.90	0.84	0.94	0.92	0.92	0.92	0.73	0.79
Fs	0.06	0.07	0.11	0.07	0.07	0.08	0.06	0.14	0.06	0.06	0.06	0.07	0.25	0.19

Major Element Analyses - Orthopyroxene

Sample No	MIS463	PGN301	PGN303	PGN306	PGN307	PGN308	PGN309	PGN310	PGN311	PGN312	PGN313	PGN314	PGN316	PGN317
SiO_2	57.86	57.94	58.48	57.13	59.00	57.37	57.06	57.95	56.75	58.76	58.17	58.02	57.87	58.20
TiO_2	0.05	<0.04	<0.04	<0.04	0.04	0.04	0.06	0.05	<0.04	<0.04	<0.04	<0.04	<0.04	<0.04
Al_2O_3	0.59	0.38	0.39	0.56	0.54	0.56	0.62	0.57	0.63	0.54	0.38	0.54	0.56	0.41
Cr_2O_3	0.26	0.21	0.36	0.39	0.38	0.45	0.19	0.32	0.18	0.08	0.14	0.35	0.32	0.24
FeO	4.48	4.39	4.84	5.75	4.46	5.22	5.70	4.71	5.55	4.63	4.58	4.48	4.35	4.55
MnO	0.10	0.13	0.12	0.09	0.10	0.12	0.12	0.10	0.12	0.10	0.14	0.11	0.09	0.11
MgO	35.58	36.56	36.45	34.84	34.61	35.79	35.39	35.77	35.08	36.17	36.58	36.51	35.94	36.55
CaO	0.63	0.22	0.19	0.72	0.73	0.81	0.94	0.52	0.93	<0.05	<0.05	<0.05	<0.05	<0.05
Na_2O	0.13	0.04	0.06	0.16	0.13	0.14	0.14	0.14	0.13	0.10	0.07	0.07	0.15	0.03
Total	**99.71**	**99.88**	**100.91**	**99.68**	**100.01**	**100.51**	**100.23**	**100.14**	**99.38**	**100.57**	**100.23**	**100.22**	**99.47**	**100.28**
Atomic Pro														
Si	1.986	1.983	1.984	1.975	2.014	1.965	1.964	1.982	1.968	1.997	1.986	1.980	1.989	1.986
Ti	0.001	0.000	0.000	0.001	0.001	0.001	0.002	0.001	0.000	0.000	0.000	0.000	0.000	0.000
Al	0.024	0.015	0.015	0.023	0.022	0.022	0.025	0.023	0.026	0.022	0.015	0.022	0.023	0.017
Cr	0.007	0.006	0.010	0.011	0.010	0.012	0.005	0.009	0.005	0.002	0.004	0.009	0.009	0.006
Fe	0.129	0.125	0.137	0.166	0.127	0.150	0.164	0.135	0.161	0.131	0.131	0.128	0.125	0.130
Mn	0.003	0.004	0.003	0.003	0.003	0.003	0.003	0.003	0.003	0.003	0.004	0.003	0.003	0.003
Mg	1.820	1.865	1.844	1.796	1.761	1.828	1.816	1.824	1.814	1.833	1.862	1.858	1.842	1.859
Ca	0.023	0.008	0.007	0.027	0.027	0.030	0.035	0.019	0.034	0.000	0.000	0.001	0.000	0.000
Na	0.009	0.003	0.004	0.011	0.009	0.009	0.009	0.009	0.009	0.006	0.004	0.005	0.010	0.002
Total	**4.002**	**4.008**	**4.005**	**4.012**	**3.973**	**4.021**	**4.024**	**4.005**	**4.021**	**3.994**	**4.006**	**4.007**	**4.000**	**4.003**
Mg#	93.40	93.69	93.07	91.53	93.26	92.43	91.71	93.12	91.86	93.31	93.43	93.56	93.64	93.47
Ca#	1.26	0.44	0.38	1.46	1.49	1.61	1.87	1.03	1.86	0.00	0.00	0.08	0.00	0.00
# Analyses	4	3	2	2	3	5	5	3	4	2	2	5	5	3
Suite	Low-Ca Harzburgite	Low-Ca Harzburgite	Low-Ca Harzburgite	Lherzolite	Lherzolite	High-Ca Harzburgite	High-Ca Harzburgite	Lherzolite	High-Ca Harzburgite	High-Ca Harzburgite	High-Ca Harzburgite	Low-Ca Harzburgite	Lherzolite	Low-Ca Harzburgite
CaTs	0.01	0.02	0.02	0.02	-0.01	0.03	0.03	0.02	0.03	0.00	0.01	0.02	0.01	0.01
Jd	0.01	-0.01	-0.01	-0.01	0.06	-0.03	-0.04	0.00	-0.03	0.02	-0.01	-0.01	0.01	0.00
Acm	0.00	0.02	0.01	0.02	-0.05	0.04	0.05	0.01	0.04	-0.01	0.01	0.01	0.00	0.01
Wo	0.01	0.00	0.00	0.00	0.02	0.00	0.00	0.00	0.00	0.00	-0.01	-0.01	-0.01	-0.01
En	0.91	0.93	0.92	0.90	0.88	0.91	0.91	0.91	0.91	0.92	0.93	0.93	0.92	0.93
Fs	0.06	0.06	0.07	0.08	0.06	0.07	0.08	0.07	0.08	0.07	0.07	0.06	0.06	0.06

Major Element Analyses - Orthopyroxene

Sample No	PGN318	PGN325	PGN329	PGN337	PGN338	PGN339	PGN340	PGN341	PGN343
SiO_2	58.03	57.19	57.37	57.66	58.73	57.48	57.91	59.05	58.20
TiO_2	<0.04	0.13	0.13	0.12	<0.04	0.11	<0.04	<0.04	<0.04
Al_2O_3	0.48	0.44	0.63	0.58	0.44	0.95	0.45	0.39	0.40
Cr_2O_3	0.24	0.22	0.21	0.20	0.41	0.74	0.24	0.24	0.28
FeO	4.55	4.89	5.77	5.87	4.46	5.08	4.24	4.18	4.37
MnO	0.16	0.12	0.12	0.15	0.11	0.14	0.11	0.07	0.10
MgO	35.85	36.69	35.09	34.48	35.86	34.71	36.98	36.49	35.59
CaO	0.08	0.29	0.85	0.79	0.50	0.97	0.15	0.24	0.22
Na_2O	0.12	0.09	0.15	0.14	0.11	0.15	0.01	0.02	0.05
Total	**99.62**	**100.10**	**100.34**	**99.98**	**100.64**	**100.34**	**100.11**	**100.68**	**99.34**
Atomic Pro									
Si	1.992	1.962	1.972	1.986	1.995	1.971	1.976	1.998	2.001
Ti	0.000	0.003	0.003	0.003	0.000	0.003	0.000	0.000	0.000
Al	0.019	0.018	0.025	0.024	0.018	0.038	0.018	0.015	0.016
Cr	0.007	0.006	0.006	0.005	0.011	0.020	0.007	0.006	0.007
Fe	0.131	0.140	0.166	0.169	0.127	0.146	0.121	0.118	0.126
Mn	0.005	0.004	0.004	0.004	0.003	0.004	0.003	0.002	0.003
Mg	1.835	1.877	1.798	1.771	1.816	1.775	1.881	1.841	1.824
Ca	0.003	0.011	0.031	0.029	0.018	0.036	0.005	0.009	0.008
Na	0.008	0.006	0.010	0.009	0.007	0.010	0.000	0.002	0.003
Total	**3.999**	**4.026**	**4.015**	**4.001**	**3.995**	**4.002**	**4.012**	**3.992**	**3.989**
Mg#	93.36	93.05	91.56	91.29	93.48	92.41	93.95	93.96	93.55
Ca#	0.16	0.57	1.71	1.61	0.99	1.97	0.29	0.47	0.44
# Analyses	4	5	2	2	2	1	4	2	2
Suite	Low-Ca Harzburgite	Lherzolite	Lherzolite	Lherzolite	Lherzolite	Lherzolite	Low-Ca Harzburgite	Low-Ca Harzburgite	Low-Ca Harzburgite
CaTs	0.01	0.03	0.03	0.01	0.01	0.03	0.02	0.00	0.00
Jd	0.01	-0.05	-0.02	0.01	0.02	0.01	-0.02	0.02	0.03
Acm	0.00	0.05	0.03	0.00	-0.01	0.00	0.02	-0.02	-0.02
Wo	0.00	-0.01	0.00	0.01	0.01	0.00	-0.01	0.00	0.00
En	0.92	0.94	0.90	0.89	0.91	0.89	0.94	0.92	0.91
Fs	0.07	0.07	0.08	0.08	0.06	0.07	0.06	0.06	0.06

Major Element Analyses - Olivine

Sample No	ARN002	ARN003	ARN004	ARN005	ARN006	ARN007	ARN008	ARN011	ARN013	ARN014	ARN017	ARN018	ARN021
SiO_2	42.03	40.55	41.23	41.40	41.28	40.51	41.18	41.03	41.14	40.52	41.34	40.84	41.12
TiO_2	<0.04	<0.04	<0.04	<0.04	<0.04	<0.04	<0.04	<0.04	<0.04	<0.04	<0.04	<0.04	<0.04
Al_2O_3	<0.03	<0.03	0.03	<0.03	0.03	0.03	0.04	0.03	<0.03	<0.03	<0.03	<0.03	<0.03
Cr_2O_3	<0.04	0.04	0.04	0.05	<0.04	0.05	0.06	<0.04	<0.04	<0.04	0.04	0.04	0.06
FeO	7.19	7.54	7.27	7.91	7.69	7.38	6.93	7.09	7.07	7.43	7.61	7.81	7.66
MnO	0.08	0.12	0.08	0.09	0.11	0.11	0.11	0.08	0.11	0.11	0.13	0.10	0.12
MgO	51.10	50.10	50.18	50.20	50.34	50.79	51.07	51.54	52.03	52.03	51.09	50.57	50.43
CaO	0.06	<0.03	<0.03	<0.03	<0.03	<0.03	<0.03	0.03	<0.03	0.03	<0.03	<0.03	<0.03
NiO	0.41	0.38	0.42	0.42	0.38	0.35	0.42	0.37	0.36	0.40	0.38	0.45	0.39
Total	**100.90**	**98.76**	**99.26**	**100.11**	**99.86**	**99.23**	**99.83**	**100.20**	**100.76**	**100.57**	**100.63**	**99.84**	**99.80**
Atomic Prop													
Si	1.008	0.998	1.006	1.005	1.004	0.992	0.999	0.993	0.990	0.980	0.998	0.995	1.001
Ti	0.000	0.000	0.000	0.000	0.000	0.000	0.000	0.000	0.000	0.000	0.000	0.000	0.000
Al	0.000	0.001	0.001	0.000	0.001	0.001	0.001	0.001	0.000	0.001	0.001	0.001	0.000
Cr	0.000	0.001	0.001	0.001	0.000	0.001	0.001	0.000	0.000	0.001	0.001	0.001	0.001
Fe	0.144	0.155	0.148	0.161	0.156	0.151	0.141	0.144	0.142	0.150	0.154	0.159	0.156
Mn	0.002	0.002	0.002	0.002	0.002	0.002	0.002	0.002	0.002	0.002	0.003	0.002	0.003
Mg	1.827	1.837	1.826	1.817	1.825	1.853	1.847	1.859	1.867	1.876	1.838	1.837	1.830
Ca	0.002	0.000	0.000	0.000	0.000	0.001	0.000	0.001	0.001	0.001	0.000	0.000	0.000
Ni	0.008	0.008	0.008	0.008	0.007	0.007	0.008	0.007	0.007	0.008	0.007	0.009	0.008
Total	**2.991**	**3.002**	**2.993**	**2.994**	**2.996**	**3.007**	**3.000**	**3.006**	**3.010**	**3.019**	**3.001**	**3.004**	**2.998**
Mg#	92.69	92.22	92.48	91.88	92.11	92.47	92.93	92.83	92.92	92.59	92.29	92.03	92.15
Fo	92.69	92.22	92.48	91.88	92.11	92.47	92.93	92.83	92.92	92.59	92.29	92.03	92.15
Fa	7.31	7.78	7.52	8.12	7.89	7.53	7.07	7.17	7.08	7.41	7.71	7.97	7.85
# Analyses	2	3	2	2	2	3	3	2	5	3	2	2	2
Suite	Low-Ca Harzburgite	High-Ca Harzburgite	High-Ca Harzburgite	High-Ca Harzburgite	High-Ca Harzburgite	Low-Ca Harzburgite	Low-Ca Harzburgite	Low-Ca Harzburgite	High-Ca Harzburgite	High-Ca Harzburgite	Low-Ca Harzburgite	High-Ca Harzburgite	Low-Ca Harzburgite

Major Element Analyses - Olivine

Sample No	ARN022	ARN023	ARN024	ARN025	ARN026	ARN027	ARN029	ARN030	ARN032	ARN033	ARN034	ARN035	ARN036	ARN037
SiO_2	41.28	39.27	39.87	40.29	40.98	40.88	40.21	40.81	41.11	39.99	40.24	40.49	40.18	39.89
TiO_2	<0.04	<0.04	<0.04	<0.04	<0.04	<0.04	<0.04	<0.04	<0.04	<0.04	<0.04	<0.04	<0.04	<0.04
Al_2O_3	<0.03	<0.03	<0.03	<0.03	<0.03	<0.03	0.03	0.03	<0.03	<0.03	<0.03	<0.03	<0.03	<0.03
Cr_2O_3	0.04	<0.04	0.05	<0.04	<0.04	<0.04	0.04	<0.04	<0.04	<0.04	<0.04	0.04	0.04	0.05
FeO	8.10	8.91	7.42	7.15	7.34	7.45	8.00	5.68	8.03	8.81	7.70	8.43	7.54	7.76
MnO	0.15	0.11	0.11	0.11	0.07	0.11	0.13	0.06	0.11	0.12	0.10	0.07	0.09	0.13
MgO	50.35	49.97	51.61	51.38	50.36	51.20	50.16	51.93	51.34	51.55	51.95	51.06	51.03	51.96
CaO	<0.03	0.06	0.04	<0.03	<0.03	<0.03	0.03	<0.03	<0.03	0.03	<0.03	0.03	<0.03	0.03
NiO	0.51	0.39	0.42	0.37	0.35	0.38	0.38	0.35	0.31	0.30	0.31	0.28	0.36	0.39
Total	**100.44**	**98.76**	**99.53**	**99.37**	**99.12**	**100.09**	**98.98**	**98.90**	**100.98**	**100.84**	**100.38**	**100.45**	**99.30**	**100.25**
Atomic Prop														
Si	1.001	0.976	0.976	0.985	1.002	0.992	0.990	0.994	0.991	0.972	0.977	0.984	0.985	0.971
Ti	0.000	0.000	0.000	0.000	0.000	0.000	0.000	0.000	0.000	0.000	0.000	0.001	0.001	0.000
Al	0.000	0.000	0.000	0.000	0.000	0.000	0.001	0.001	0.000	0.000	0.000	0.001	0.000	0.000
Cr	0.001	0.001	0.001	0.001	0.000	0.001	0.001	0.000	0.001	0.000	0.001	0.001	0.001	0.001
Fe	0.164	0.185	0.152	0.146	0.150	0.151	0.165	0.116	0.162	0.179	0.156	0.171	0.155	0.158
Mn	0.003	0.002	0.002	0.002	0.001	0.002	0.003	0.001	0.002	0.002	0.002	0.002	0.002	0.003
Mg	1.820	1.850	1.883	1.873	1.836	1.853	1.841	1.886	1.845	1.867	1.880	1.850	1.864	1.886
Ca	0.000	0.002	0.001	0.001	0.000	0.001	0.001	0.000	0.000	0.001	0.000	0.001	0.001	0.001
Ni	0.010	0.008	0.008	0.007	0.007	0.007	0.008	0.007	0.006	0.006	0.006	0.006	0.007	0.008
Total	**2.999**	**3.024**	**3.024**	**3.015**	**2.998**	**3.007**	**3.009**	**3.005**	**3.008**	**3.028**	**3.023**	**3.015**	**3.014**	**3.028**
Mg#	91.72	90.91	92.54	92.76	92.44	92.45	91.79	94.22	91.93	91.25	92.32	91.52	92.34	92.28
Fo	91.72	90.91	92.54	92.76	92.44	92.45	91.79	94.22	91.93	91.25	92.32	91.52	92.34	92.28
Fa	8.28	9.09	7.46	7.24	7.56	7.55	8.21	5.78	8.07	8.75	7.68	8.48	7.66	7.72
# Analyses	2	4	6	5	3	6	1	2	1	2	2	2	2	2
Suite	High-Ca Harzburgite	Lherzolite	Lherzolite	Low-Ca Harzburgite	Low-Ca Harzburgite	Low-Ca Harzburgite	High-Ca Harzburgite	High-Ca Harzburgite	Lherzolite	Lherzolite	Lherzolite	Lherzolite	Lherzolite	Lherzolite

Major Element Analyses - Olivine

Sample No	MIS408	MIS413	MIS417	MIS426	MIS430	MIS431	MIS433	MIS434	MIS463	PGN301	PGN303	PGN306	PGN307	PGN310
SiO_2	40.56	40.17	40.98	41.35	41.46	41.39	40.86	41.03	40.69	41.15	40.74	40.57	40.88	39.48
TiO_2	<0.04	<0.04	<0.04	<0.04	<0.04	<0.04	<0.04	<0.04	<0.04	<0.04	<0.04	<0.04	<0.04	<0.04
Al_2O_3	<0.03	0.03	<0.03	<0.03	0.03	0.03	0.03	<0.03	<0.03	<0.03	<0.03	<0.03	<0.03	<0.03
Cr_2O_3	0.04	<0.04	<0.04	<0.04	0.04	<0.04	0.04	<0.04	0.05	0.31	0.05	0.11	<0.04	0.13
FeO	7.12	11.98	6.97	7.38	7.82	7.22	7.30	7.95	8.08	6.22	8.59	9.58	7.15	7.72
MnO	0.10	0.15	0.08	0.07	0.11	0.09	0.09	0.10	0.11	0.18	0.13	0.09	0.09	0.09
MgO	51.46	46.52	50.78	50.55	49.96	51.62	50.96	50.54	50.04	52.14	49.46	48.28	51.20	50.98
CaO	<0.03	0.04	0.06	<0.03	<0.03	<0.03	<0.03	<0.03	<0.03	0.10	<0.03	0.10	<0.03	0.03
NiO	0.32	0.30	0.42	0.27	0.44	0.27	0.40	0.37	0.50	<0.21	0.46	0.39	0.39	0.46
Total	**99.65**	**99.21**	**99.32**	**99.67**	**99.86**	**100.64**	**99.69**	**100.04**	**99.54**	**100.31**	**99.45**	**99.13**	**99.75**	**98.90**
Atomic Prop														
Si	0.988	1.003	0.999	1.005	1.008	0.997	0.995	0.998	0.996	0.991	1.000	1.003	0.994	0.975
Ti	0.000	0.000	0.000	0.000	0.000	0.000	0.000	0.000	0.000	0.000	0.000	0.000	0.000	0.000
Al	0.001	0.001	0.000	0.000	0.001	0.001	0.001	0.000	0.001	0.001	0.001	0.000	0.000	0.000
Cr	0.001	0.000	0.000	0.001	0.001	0.000	0.001	0.001	0.001	0.006	0.001	0.002	0.000	0.003
Fe	0.145	0.250	0.142	0.150	0.159	0.145	0.149	0.162	0.165	0.125	0.176	0.198	0.145	0.159
Mn	0.002	0.003	0.002	0.001	0.002	0.002	0.002	0.002	0.002	0.004	0.003	0.002	0.002	0.002
Mg	1.868	1.732	1.846	1.832	1.811	1.853	1.849	1.832	1.826	1.872	1.810	1.780	1.856	1.876
Ca	0.001	0.001	0.002	0.000	0.000	0.000	0.000	0.000	0.001	0.003	0.000	0.003	0.001	0.001
Ni	0.006	0.006	0.008	0.005	0.009	0.005	0.008	0.007	0.010	0.003	0.009	0.008	0.008	0.009
Total	**3.011**	**2.996**	**3.000**	**2.994**	**2.991**	**3.003**	**3.004**	**3.002**	**3.003**	**3.005**	**2.999**	**2.996**	**3.006**	**3.024**
Mg#	92.80	87.38	92.85	92.43	91.93	92.73	92.56	91.89	91.70	93.73	91.12	89.99	92.74	92.17
Fo	92.80	87.38	92.85	92.43	91.93	92.73	92.56	91.89	91.70	93.73	91.12	89.99	92.74	92.17
Fa	7.20	12.62	7.15	7.57	8.07	7.27	7.44	8.11	8.30	6.27	8.88	10.01	7.26	7.83
# Analyses	2	2	5	2	2	2	2	2	3	1	2	3	4	3
Suite	Low-Ca Harzburgite	High-Ca Harzburgite	High-Ca Harzburgite	Lherzolite	High-Ca Harzburgite	Lherzolite	Lherzolite	High-Ca Harzburgite	Low-Ca Harzburgite	Low-Ca Harzburgite	Low-Ca Harzburgite	Lherzolite	Lherzolite	Lherzolite

Major Element Analyses - Olivine

Sample No	PGN312	PGN313	PGN314	PGN315	PGN316	PGN317	PGN324	PGN333	PGN336	PGN339	PGN340	PGN342
SiO_2	40.44	40.48	40.29	40.10	40.25	40.30	40.21	40.79	40.81	41.35	41.46	40.85
TiO_2	<0.04	<0.04	<0.04	<0.04	<0.04	<0.04	<0.04	<0.04	<0.04	<0.04	<0.04	<0.04
Al_2O_3	<0.03	<0.03	<0.03	<0.03	<0.03	<0.03	<0.03	<0.03	0.03	<0.03	<0.03	<0.03
Cr_2O_3	<0.04	<0.04	<0.04	<0.04	<0.04	<0.04	<0.04	0.05	0.07	0.05	0.05	0.05
FeO	7.43	7.76	7.34	7.02	7.16	7.31	9.15	7.94	9.39	8.74	7.75	8.02
MnO	0.11	0.09	0.10	0.08	0.08	0.09	0.11	0.12	0.15	0.14	0.13	0.13
MgO	51.03	51.07	51.18	52.17	51.31	50.98	49.26	50.08	49.93	49.49	51.15	50.57
CaO	0.04	<0.03	<0.03	<0.03	<0.03	<0.03	0.07	<0.03	0.04	<0.03	<0.03	<0.03
NiO	0.37	0.39	0.42	0.41	0.37	0.42	0.39	0.47	0.41	0.44	0.36	0.39
Total	**99.45**	**99.83**	**99.35**	**99.80**	**99.20**	**99.14**	**99.24**	**99.49**	**100.85**	**100.28**	**100.92**	**100.05**
Atomic Prop												
Si	0.988	0.987	0.986	0.976	0.985	0.988	0.993	0.998	0.992	1.006	0.998	0.994
Ti	0.000	0.000	0.000	0.000	0.000	0.000	0.000	0.000	0.000	0.001	0.000	0.000
Al	0.001	0.000	0.000	0.000	0.001	0.000	0.001	0.001	0.001	0.001	0.001	0.000
Cr	0.000	0.000	0.000	0.000	0.000	0.000	0.000	0.001	0.001	0.001	0.001	0.001
Fe	0.152	0.158	0.150	0.143	0.147	0.150	0.189	0.162	0.191	0.178	0.156	0.163
Mn	0.002	0.002	0.002	0.002	0.002	0.002	0.002	0.003	0.003	0.003	0.003	0.003
Mg	1.860	1.857	1.867	1.894	1.873	1.863	1.813	1.827	1.809	1.795	1.836	1.835
Ca	0.001	0.000	0.000	0.000	0.000	0.000	0.002	0.000	0.001	0.000	0.000	0.000
Ni	0.007	0.008	0.008	0.008	0.007	0.008	0.008	0.009	0.008	0.009	0.007	0.008
Total	**3.011**	**3.012**	**3.014**	**3.023**	**3.014**	**3.012**	**3.007**	**3.001**	**3.007**	**2.993**	**3.001**	**3.005**
Mg#	92.45	92.15	92.55	92.99	92.74	92.55	90.56	91.84	90.46	90.99	92.17	91.83
Fo	92.45	92.15	92.55	92.99	92.74	92.55	90.56	91.84	90.46	90.99	92.17	91.83
Fa	7.55	7.85	7.45	7.01	7.26	7.45	9.44	8.16	9.54	9.01	7.83	8.17
# Analyses	3	4	6	3	4	3	2	3	2	2	2	2
Suite	High-Ca Harzburgite	High-Ca Harzburgite	Low-Ca Harzburgite	High-Ca Harzburgite	Lherzolite	Low-Ca Harzburgite	Lherzolite	Lherzolite	Lherzolite	Lherzolite	Low-Ca Harzburgite	Low-Ca Harzburgite

Major Element Analyses - Chromite

Sample No	ARN002	ARN002	ARN002	ARN002	ARN002	ARN003	ARN003	ARN006	ARN006	ARN006	ARN006	ARN007	ARN007	ARN009
SiO_2	<0.04	0.09	0.07	<0.04	0.07	0.09	0.10	<0.04	<0.04	<0.04	<0.04	<0.04	0.05	0.06
TiO_2	<0.05	<0.05	0.60	<0.05	1.19	0.96	0.82	<0.05	<0.05	<0.05	<0.05	0.07	0.06	0.23
Al_2O_3	6.82	7.16	13.71	6.66	8.93	9.74	9.12	10.55	10.41	10.25	10.43	8.20	8.17	6.27
Cr_2O_3	62.69	63.41	51.82	61.99	56.08	54.45	57.86	58.93	59.11	59.09	59.52	61.87	60.84	60.86
FeO	13.76	13.86	14.13	13.45	14.36	13.81	13.81	14.97	15.09	14.54	15.52	12.73	12.67	13.16
Fe_2O_3	3.80	2.97	6.16	3.76	6.09	6.08	5.45	3.14	3.49	3.38	2.93	3.17	4.79	5.33
MnO	0.23	0.28	0.31	0.30	0.31	0.37	0.33	0.40	0.34	0.34	0.34	0.29	0.19	0.29
MgO	12.50	12.59	13.38	12.32	12.95	13.04	13.40	12.02	12.04	12.26	11.68	13.28	13.52	12.79
CaO	<0.02	<0.02	0.02	0.03	0.19	<0.02	0.02	<0.02	<0.02	<0.02	0.12	<0.02	<0.02	<0.02
Total	**99.83**	**100.37**	**100.19**	**98.52**	**100.17**	**98.52**	**100.90**	**100.02**	**100.48**	**99.86**	**100.55**	**99.65**	**100.31**	**98.99**
Atomic Proportions based on 4 Oxygens														
Si	0.001	0.003	0.002	0.000	0.002	0.003	0.003	0.001	0.000	0.000	0.000	0.001	0.002	0.002
Ti	0.000	0.000	0.015	0.000	0.030	0.024	0.020	0.000	0.000	0.000	0.000	0.002	0.001	0.006
Al	0.269	0.279	0.524	0.266	0.349	0.385	0.352	0.409	0.402	0.398	0.403	0.319	0.318	0.250
Cr	1.657	1.659	1.328	1.661	1.471	1.444	1.499	1.531	1.532	1.538	1.542	1.615	1.586	1.630
Fe^{2+}	0.385	0.384	0.383	0.381	0.398	0.387	0.378	0.411	0.414	0.400	0.425	0.352	0.349	0.373
Fe^{3+}	0.096	0.074	0.150	0.096	0.152	0.153	0.134	0.078	0.086	0.084	0.072	0.079	0.119	0.136
Mn	0.006	0.008	0.009	0.009	0.009	0.010	0.009	0.011	0.010	0.009	0.009	0.008	0.005	0.008
Mg	0.623	0.621	0.647	0.622	0.640	0.652	0.654	0.589	0.589	0.602	0.571	0.654	0.665	0.646
Ca	0.000	0.000	0.001	0.001	0.007	0.000	0.001	0.000	0.000	0.000	0.004	0.000	0.000	0.000
Total	**3.036**	**3.028**	**3.057**	**3.036**	**3.058**	**3.059**	**3.051**	**3.029**	**3.033**	**3.032**	**3.027**	**3.030**	**3.045**	**3.052**
Mg#	56.48	57.59	54.80	56.61	53.78	54.67	56.06	54.64	54.08	55.43	53.41	60.31	58.68	55.95
Cr#	86.04	85.58	71.72	86.19	80.81	78.95	80.98	78.94	79.20	79.45	79.28	83.50	83.32	86.68
# Analyses	1	1	1	1	1	1	1	1	1	1	1	1	1	1
Type	Exsolved	Exsolved	Secondary	Exsolved	Secondary	Secondary	Secondary	Exsolved	Exsolved	Exsolved	Exsolved	Primary	Primary	Primary
Suite	Low-Ca Harzburgite	Low-Ca Harzburgite	Low-Ca Harzburgite	Low-Ca Harzburgite	Low-Ca Harzburgite	High-Ca Harzburgite	High-Ca Harzburgite	High-Ca Harzburgite	High-Ca Harzburgite	High-Ca Harzburgite	High-Ca Harzburgite	Low-Ca Harzburgite	Low-Ca Harzburgite	High-Ca Harzburgite

Major Element Analyses - Chromite

Sample No	ARN009	ARN009	ARN009	ARN009	ARN011	ARN011	ARN011	ARN012	ARN012	ARN012	ARN012	ARN017	ARN017	ARN017
SiO_2	0.06	0.08	0.06	0.08	0.05	0.06	0.09	0.09	0.07	0.07	0.08	0.06	0.07	0.08
TiO_2	0.25	0.25	0.27	0.26	<0.05	<0.05	0.06	0.34	0.27	0.29	0.26	<0.05	0.07	0.13
Al_2O_3	6.41	6.54	6.25	6.25	6.91	6.76	7.12	7.02	6.80	6.92	7.07	7.40	7.50	7.68
Cr_2O_3	61.10	61.50	61.56	61.85	60.65	62.00	61.55	60.72	61.03	60.98	61.41	61.67	61.77	61.86
FeO	13.68	13.70	13.64	13.80	13.57	14.43	14.21	14.01	13.79	13.92	14.17	13.78	13.67	14.43
Fe_2O_3	5.10	5.05	4.94	4.81	6.14	4.80	5.06	4.36	3.99	4.48	4.29	3.41	3.42	3.31
MnO	0.33	0.27	0.30	0.30	0.27	0.29	0.27	0.28	0.28	0.25	0.29	0.24	0.27	0.35
MgO	12.55	12.74	12.63	12.59	12.78	12.24	12.52	12.48	12.39	12.52	12.46	12.41	12.58	12.24
CaO	<0.02	<0.02	<0.02	0.02	<0.02	<0.02	<0.02	<0.02	<0.02	<0.02	<0.02	<0.02	<0.02	<0.02
Total	**99.48**	**100.13**	**99.65**	**99.97**	**100.39**	**100.62**	**100.87**	**99.30**	**98.63**	**99.44**	**100.04**	**99.01**	**99.35**	**100.06**
Atomic Proportions based on 4 Oxygens														
Si	0.002	0.003	0.002	0.003	0.002	0.002	0.003	0.003	0.003	0.002	0.003	0.002	0.002	0.003
Ti	0.006	0.006	0.007	0.007	0.001	0.001	0.001	0.009	0.007	0.007	0.007	0.001	0.002	0.003
Al	0.255	0.258	0.248	0.247	0.272	0.266	0.279	0.278	0.271	0.274	0.278	0.293	0.295	0.301
Cr	1.630	1.627	1.639	1.641	1.605	1.636	1.616	1.614	1.633	1.620	1.621	1.636	1.631	1.625
Fe^{2+}	0.386	0.383	0.384	0.387	0.380	0.403	0.395	0.394	0.390	0.391	0.396	0.387	0.382	0.401
Fe^{3+}	0.129	0.127	0.125	0.122	0.155	0.121	0.126	0.110	0.101	0.113	0.108	0.086	0.086	0.083
Mn	0.009	0.008	0.008	0.008	0.008	0.008	0.008	0.008	0.008	0.007	0.008	0.007	0.008	0.010
Mg	0.632	0.636	0.634	0.630	0.638	0.609	0.620	0.626	0.625	0.627	0.620	0.621	0.626	0.606
Ca	0.000	0.000	0.000	0.001	0.000	0.000	0.000	0.000	0.000	0.000	0.000	0.000	0.000	0.000
Total	**3.049**	**3.048**	**3.048**	**3.046**	**3.059**	**3.046**	**3.048**	**3.042**	**3.039**	**3.043**	**3.041**	**3.033**	**3.033**	**3.031**
Mg#	55.06	55.47	55.46	55.31	54.40	53.78	54.33	55.38	55.97	55.42	55.20	56.78	57.24	55.63
Cr#	86.48	86.32	86.85	86.91	85.49	86.02	85.29	85.29	85.76	85.53	85.35	84.82	84.68	84.38
# Analyses	1	1	1	1	1	1	1	1	1	1	1	1	1	1
Type	Primary	Primary	Primary	Primary	Primary	Primary	Primary	Primary	Primary	Primary	Primary	Primary	Primary	Primary
Suite	High-Ca Harzburgite	High-Ca Harzburgite	High-Ca Harzburgite	High-Ca Harzburgite	Low-Ca Harzburgite	Low-Ca Harzburgite	Low-Ca Harzburgite	Low-Ca Harzburgite	Low-Ca Harzburgite	Low-Ca Harzburgite	Low-Ca Harzburgite	Low-Ca Harzburgite	Low-Ca Harzburgite	Low-Ca Harzburgite

Major Element Analyses - Chromite

Sample No	ARN019	ARN019	ARN019	ARN021	ARN022	ARN022	ARN025	ARN025	ARN025	ARN025	ARN025	ARN025	ARN025	ARN025
SiO_2	<0.04	<0.04	<0.04	0.08	0.04	<0.04	0.09	0.07	0.04	0.09	0.07	0.08	<0.04	0.04
TiO_2	0.62	0.55	0.62	0.60	<0.05	<0.05	0.18	<0.05	<0.05	<0.05	<0.05	<0.05	<0.05	<0.05
Al_2O_3	9.96	10.03	10.21	13.72	9.99	9.95	5.85	7.41	7.64	7.45	7.15	7.30	7.54	7.33
Cr_2O_3	58.95	57.88	59.11	52.56	59.20	59.10	61.87	61.22	60.68	60.28	61.33	61.25	62.17	61.23
FeO	15.22	14.77	14.84	13.14	14.50	15.29	15.23	13.79	13.28	12.85	13.73	13.87	13.71	13.52
Fe_2O_3	2.46	3.19	2.77	6.22	4.10	3.60	5.11	4.15	4.78	5.17	3.88	4.23	4.18	4.29
MnO	0.30	0.21	0.26	0.37	0.31	0.28	0.34	0.28	0.34	0.34	0.25	0.24	0.28	0.33
MgO	12.13	12.30	12.58	14.13	12.47	11.87	11.63	12.47	12.79	13.03	12.35	12.42	12.78	12.53
CaO	<0.02	<0.02	<0.02	0.02	<0.02	<0.02	<0.02	<0.02	<0.02	<0.02	<0.02	<0.02	<0.02	0.02
Total	**99.65**	**98.93**	**100.40**	**100.83**	**100.63**	**100.17**	**100.29**	**99.41**	**99.55**	**99.22**	**98.76**	**99.39**	**100.72**	**99.30**
Atomic Prop														
Si	0.000	0.000	0.000	0.002	0.001	0.001	0.003	0.003	0.001	0.003	0.002	0.003	0.001	0.001
Ti	0.015	0.014	0.015	0.014	0.000	0.001	0.004	0.000	0.000	0.000	0.000	0.000	0.001	0.000
Al	0.387	0.392	0.393	0.519	0.386	0.387	0.233	0.293	0.301	0.294	0.284	0.289	0.294	0.290
Cr	1.536	1.519	1.525	1.333	1.534	1.542	1.653	1.622	1.604	1.599	1.636	1.625	1.624	1.625
Fe^{2+}	0.419	0.410	0.405	0.352	0.398	0.422	0.430	0.387	0.371	0.360	0.387	0.389	0.379	0.379
Fe^{3+}	0.061	0.080	0.068	0.150	0.101	0.089	0.130	0.105	0.120	0.131	0.099	0.107	0.104	0.108
Mn	0.008	0.006	0.007	0.010	0.009	0.008	0.010	0.008	0.010	0.010	0.007	0.007	0.008	0.010
Mg	0.596	0.609	0.612	0.676	0.609	0.584	0.586	0.623	0.638	0.652	0.621	0.621	0.629	0.627
Ca	0.000	0.000	0.000	0.001	0.000	0.000	0.000	0.000	0.000	0.000	0.000	0.000	0.000	0.001
Total	**3.023**	**3.030**	**3.026**	**3.057**	**3.038**	**3.034**	**3.050**	**3.040**	**3.046**	**3.050**	**3.037**	**3.041**	**3.040**	**3.041**
Mg#	55.36	55.42	56.41	57.36	55.00	53.31	51.12	55.92	56.46	57.04	56.12	55.61	56.59	56.24
Cr#	79.88	79.47	79.52	71.99	79.90	79.93	87.65	84.72	84.21	84.45	85.20	84.92	84.69	84.85
# Analyses	1	1	1	1	1	1	1	1	1	1	1	1	1	1
Type	Exsolved	Exsolved	Exsolved	Secondary	Secondary	Secondary	Exsolved	Exsolved	Exsolved	Exsolved	Exsolved	Exsolved	Exsolved	Exsolved
Suite	Low-Ca Harzburgite	Low-Ca Harzburgite	Low-Ca Harzburgite	Low-Ca Harzburgite	High-Ca Harzburgite	High-Ca Harzburgite	Low-Ca Harzburgite	Low-Ca Harzburgite	Low-Ca Harzburgite	Low-Ca Harzburgite	Low-Ca Harzburgite	Low-Ca Harzburgite	Low-Ca Harzburgite	Low-Ca Harzburgite

Major Element Analyses - Chromite

Sample No	ARN027	ARN027	ARN027	ARN027	ARN032	ARN032	ARN033	ARN033	MIS401	MIS401	MIS409	MIS409	MIS409	MIS409
SiO_2	0.06	<0.04	0.04	<0.04	<0.04	<0.04	0.09	0.07	<0.04	0.07	<0.04	<0.04	0.04	<0.04
TiO_2	<0.05	<0.05	<0.05	<0.05	0.15	0.17	1.52	1.49	0.05	<0.05	0.12	0.29	0.37	0.20
Al_2O_3	7.39	7.47	7.41	7.33	6.16	6.34	6.26	6.52	7.26	7.28	21.35	21.29	24.42	24.54
Cr_2O_3	61.16	61.67	60.90	60.68	59.18	58.93	58.03	57.65	61.67	61.54	45.39	45.17	42.03	42.13
FeO	13.38	13.55	13.33	12.95	17.33	17.40	14.43	14.57	13.70	13.30	14.18	14.09	13.31	13.14
Fe_2O_3	4.74	4.48	4.89	5.43	6.74	6.77	6.45	6.13	3.90	3.95	3.97	3.93	3.77	3.86
MnO	0.34	0.26	0.28	0.32	0.41	0.36	0.29	0.28	0.34	0.35	0.17	0.17	0.19	0.13
MgO	12.77	12.78	12.79	13.02	10.12	10.18	12.97	12.71	12.44	12.67	13.58	13.74	14.64	14.64
CaO	<0.02	<0.02	<0.02	<0.02	0.02	0.02	0.02	0.07	<0.02	<0.02	<0.02	<0.02	<0.02	<0.02
Total	**99.83**	**100.24**	**99.64**	**99.76**	**100.11**	**100.19**	**100.05**	**99.50**	**99.38**	**99.18**	**98.77**	**98.69**	**98.77**	**98.66**
Atomic Prop														
Si	0.002	0.001	0.001	0.001	0.000	0.001	0.003	0.002	0.001	0.002	0.000	0.001	0.001	0.000
Ti	0.000	0.000	0.000	0.000	0.004	0.004	0.038	0.038	0.001	0.000	0.003	0.007	0.009	0.005
Al	0.291	0.293	0.292	0.289	0.249	0.256	0.248	0.260	0.287	0.288	0.793	0.790	0.888	0.893
Cr	1.614	1.620	1.611	1.605	1.609	1.599	1.544	1.541	1.635	1.631	1.130	1.124	1.025	1.029
Fe^{2+}	0.374	0.376	0.373	0.362	0.499	0.499	0.406	0.412	0.384	0.373	0.374	0.371	0.343	0.339
Fe^{3+}	0.119	0.112	0.123	0.137	0.174	0.175	0.163	0.156	0.098	0.100	0.094	0.093	0.087	0.090
Mn	0.009	0.007	0.008	0.009	0.012	0.010	0.008	0.008	0.010	0.010	0.005	0.004	0.005	0.003
Mg	0.636	0.633	0.638	0.649	0.519	0.521	0.651	0.641	0.622	0.633	0.638	0.645	0.673	0.674
Ca	0.000	0.000	0.000	0.000	0.001	0.001	0.001	0.003	0.000	0.000	0.000	0.000	0.000	0.000
Total	**3.045**	**3.043**	**3.047**	**3.052**	**3.067**	**3.067**	**3.063**	**3.060**	**3.037**	**3.038**	**3.036**	**3.035**	**3.033**	**3.034**
Mg#	56.35	56.45	56.27	56.55	43.54	43.59	53.32	53.02	56.31	57.27	57.70	58.14	60.98	61.11
Cr#	84.74	84.70	84.65	84.74	86.58	86.18	86.15	85.58	85.06	85.01	58.78	58.74	53.58	53.52
# Analyses	1	1	1	1	1	1	1	1	1	1	1	1	1	1
Type	Exsolved	Exsolved	Exsolved	Exsolved	Exsolved	Exsolved	Exsolved	Exsolved	Exsolved	Exsolved	Primary	Primary	Primary	Primary
Suite	Low-Ca Harzburgite	Low-Ca Harzburgite	Low-Ca Harzburgite	Low-Ca Harzburgite	Lherzolite	Lherzolite	Lherzolite	Lherzolite	Low-Ca Harzburgite	Low-Ca Harzburgite	Lherzolite	Lherzolite	Lherzolite	Lherzolite

Major Element Analyses - Chromite

Sample No	MIS409	MIS409	MIS411	MIS411	MIS413	MIS413	MIS413	MIS417	MIS417	MIS426	MIS426	MIS430	MIS430	MIS431
SiO_2	<0.04	0.06	0.06	0.06	0.09	0.08	0.05	<0.04	<0.04	0.04	<0.04	0.06	<0.04	<0.04
TiO_2	0.27	<0.05	<0.05	<0.05	1.02	0.47	1.22	<0.05	0.05	0.56	0.54	0.08	0.06	0.54
Al_2O_3	24.30	20.74	19.30	22.14	10.41	15.96	11.50	11.31	11.68	15.77	17.00	11.96	11.81	15.76
Cr_2O_3	42.05	45.73	48.00	46.32	52.50	48.47	51.95	56.84	57.10	50.28	49.75	56.63	56.83	50.46
FeO	12.75	13.12	12.98	12.64	15.97	15.29	14.40	15.94	14.95	16.19	17.00	16.54	15.62	16.53
Fe_2O_3	4.73	4.79	4.74	3.40	6.86	6.96	6.24	3.20	3.99	5.35	4.28	3.10	3.13	4.42
MnO	0.13	0.21	0.30	0.32	0.38	0.50	0.35	0.35	0.39	0.26	0.22	0.28	0.35	0.17
MgO	15.08	14.14	14.23	14.74	11.85	12.68	12.94	11.25	12.25	12.37	11.90	11.27	11.64	11.94
CaO	<0.02	0.08	<0.02	<0.02	<0.02	0.08	0.10	<0.02	<0.02	<0.02	0.02	<0.02	<0.02	<0.02
Total	**99.35**	**98.86**	**99.61**	**99.63**	**99.08**	**100.49**	**98.76**	**98.91**	**100.42**	**100.82**	**100.71**	**99.91**	**99.45**	**99.82**
Atomic Prop														
Si	0.001	0.002	0.002	0.002	0.003	0.002	0.002	0.001	0.000	0.001	0.000	0.002	0.000	0.000
Ti	0.006	0.000	0.000	0.000	0.026	0.011	0.031	0.000	0.001	0.014	0.013	0.002	0.001	0.013
Al	0.881	0.770	0.716	0.806	0.413	0.607	0.451	0.443	0.449	0.597	0.640	0.463	0.458	0.601
Cr	1.022	1.139	1.195	1.131	1.396	1.236	1.365	1.495	1.474	1.275	1.256	1.471	1.480	1.291
Fe^{2+}	0.328	0.346	0.342	0.326	0.449	0.412	0.400	0.444	0.408	0.434	0.454	0.455	0.430	0.447
Fe^{3+}	0.109	0.113	0.112	0.079	0.174	0.169	0.156	0.080	0.098	0.129	0.103	0.077	0.078	0.108
Mn	0.003	0.006	0.008	0.008	0.011	0.014	0.010	0.010	0.011	0.007	0.006	0.008	0.010	0.005
Mg	0.691	0.664	0.668	0.678	0.595	0.610	0.642	0.558	0.596	0.592	0.567	0.552	0.572	0.576
Ca	0.000	0.003	0.000	0.000	0.000	0.003	0.003	0.000	0.000	0.000	0.001	0.000	0.000	0.000
Total	**3.042**	**3.043**	**3.043**	**3.030**	**3.067**	**3.065**	**3.060**	**3.030**	**3.037**	**3.049**	**3.039**	**3.029**	**3.029**	**3.041**
Mg#	61.25	59.12	59.53	62.59	48.84	51.20	53.55	51.59	54.08	51.23	50.43	50.97	52.95	50.94
Cr#	53.72	59.66	62.52	58.39	77.19	67.07	75.18	77.12	76.63	68.13	66.25	76.06	76.35	68.23
# Analyses	1	1	1	1	1	1	1	1	1	1	1	1	1	1
Type	Primary	Primary	Secondary	Secondary	Secondary	Secondary	Secondary	Exsolved	Exsolved	Primary	Primary	Secondary	Secondary	Primary
Suite	Lherzolite	Lherzolite	Low-Ca Harzburgite	Low-Ca Harzburgite	High-Ca Harzburgite	High-Ca Harzburgite	High-Ca Harzburgite	High-Ca Harzburgite	High-Ca Harzburgite	Lherzolite	Lherzolite	High-Ca Harzburgite	High-Ca Harzburgite	Lherzolite

Major Element Analyses - Chromite

Sample No	MIS431	MIS433	MIS433	PGN303	PGN303	PGN333	PGN340	PGN341	PGN341	PGN343
SiO_2	<0.04	<0.04	0.05	0.09	0.08	0.07	0.07	0.06	0.07	0.04
TiO_2	0.58	0.62	0.54	0.15	0.15	0.25	<0.05	<0.05	0.05	0.21
Al_2O_3	16.46	16.24	15.67	6.58	6.78	7.68	7.91	7.54	7.82	10.94
Cr_2O_3	49.51	50.26	50.37	61.06	60.44	60.17	62.13	60.65	60.93	56.03
FeO	16.93	16.90	15.41	15.16	15.14	15.00	13.83	14.42	14.17	15.70
Fe_2O_3	4.50	4.16	5.18	4.22	4.40	5.03	3.68	4.27	4.00	4.98
MnO	0.23	0.20	0.29	0.33	0.29	0.31	0.33	0.31	0.24	0.42
MgO	11.81	11.91	12.72	11.45	11.43	12.05	12.69	12.03	12.34	11.68
CaO	<0.02	<0.02	<0.02	0.02	0.04	0.02	<0.02	<0.02	<0.02	0.03
Total	**100.06**	**100.31**	**100.23**	**99.05**	**98.75**	**100.58**	**100.65**	**99.30**	**99.61**	**100.02**
Atomic Prop										
Si	0.001	0.001	0.002	0.003	0.003	0.002	0.002	0.002	0.002	0.001
Ti	0.014	0.015	0.013	0.004	0.004	0.006	0.000	0.001	0.001	0.005
Al	0.625	0.615	0.594	0.264	0.272	0.302	0.307	0.299	0.308	0.427
Cr	1.262	1.277	1.281	1.641	1.629	1.585	1.619	1.613	1.609	1.466
Fe^{2+}	0.456	0.454	0.415	0.431	0.432	0.418	0.381	0.406	0.396	0.434
Fe^{3+}	0.109	0.101	0.126	0.108	0.113	0.126	0.091	0.108	0.100	0.124
Mn	0.006	0.005	0.008	0.010	0.008	0.009	0.009	0.009	0.007	0.012
Mg	0.568	0.570	0.610	0.580	0.581	0.599	0.624	0.603	0.615	0.576
Ca	0.000	0.000	0.000	0.001	0.002	0.001	0.000	0.000	0.000	0.001
Total	**3.042**	**3.038**	**3.048**	**3.041**	**3.043**	**3.048**	**3.035**	**3.041**	**3.038**	**3.047**
Mg#	50.10	50.70	53.04	51.86	51.62	52.37	56.89	54.00	55.32	50.80
Cr#	66.86	67.49	68.32	86.16	85.67	84.02	84.05	84.37	83.95	77.46
# Analyses	1	1	1	1	1	1	1	1	1	1
Type	Primary	Primary	Primary	Exsolved	Exsolved	Primary	Secondary	Secondary	Secondary	Secondary
Suite	Lherzolite	Lherzolite	Lherzolite	Low-Ca Harzburgite	Low-Ca Harzburgite	Lherzolite	Low-Ca Harzburgite	Low-Ca Harzburgite	Low-Ca Harzburgite	Low-Ca Harzburgite

Appendix 3

Trace Element Analysis

- Operating conditions
- Operating conditions on different days

Reference Tables

- Lower limits of detection (LLD)
- Primitive Mantle and Chondrite compositions

Trace Element Analyses

- Garnet
- Clinopyroxene
- Orthopyroxene
- Olivine

TRACE ELEMENT ANALYSIS BY LA-ICP-MS

Trace element compositions for individual minerals were obtained using the Perkin Elmer Elan 6000 Inductively Coupled Plasma-Mass Spectrometer (ICP-MS), coupled to a CETAC LSX-200 UV Laser. This equipment is housed in the Department of Geological Sciences, UCT.

Operating conditions for the LA-ICP-MS

Laser power	5.0 mJ per pulse
Pulse repetition rate	4 Hz
Diameter of laser beam	Spot 4: +/- 100 μm
	Spot 5: +/- 200 μm

Operating conditions on different days

To ensure that the standardisation was correct, and that operating conditions were the same between analytical runs on different days, two reference standards were used. MON-32 and MON-34 were used as the reference standard for garnet and JJG1424 for pyroxene. The following plots show that the operating conditions and standardisation were similar on different days.

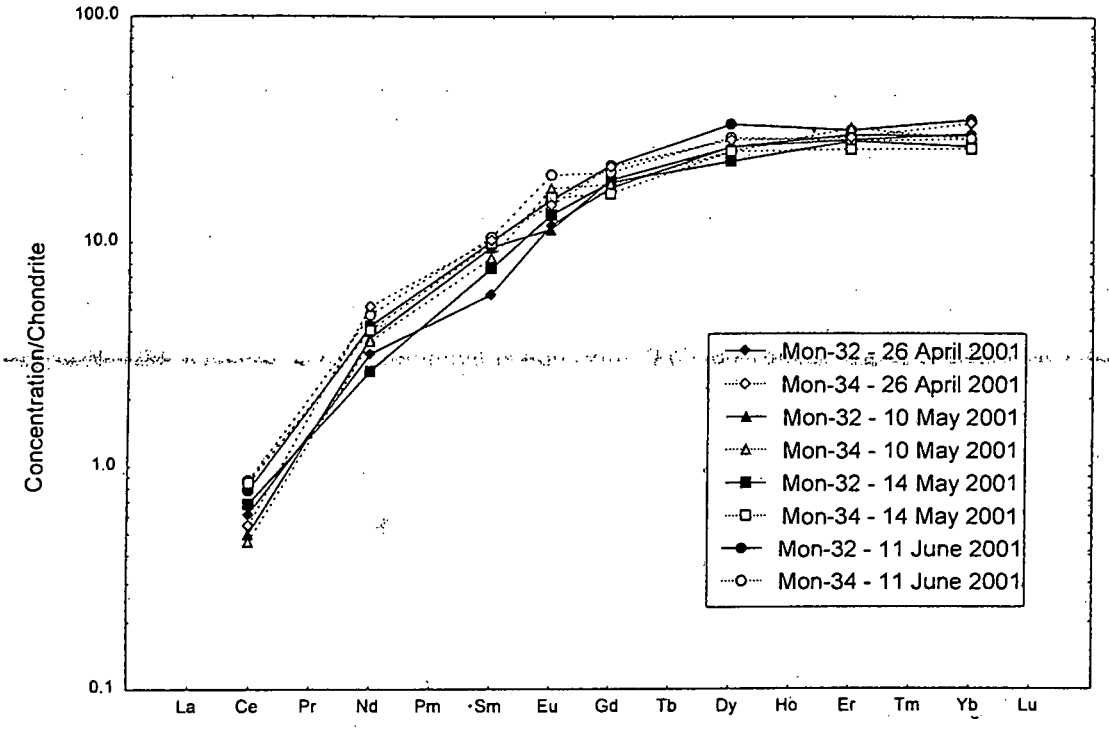

Figure A3.1 Similar analyses of the natural garnet standards MON-32 and MON-34 on different analytical days shows homogeneity between operating conditions and standardisation on different analytical days.

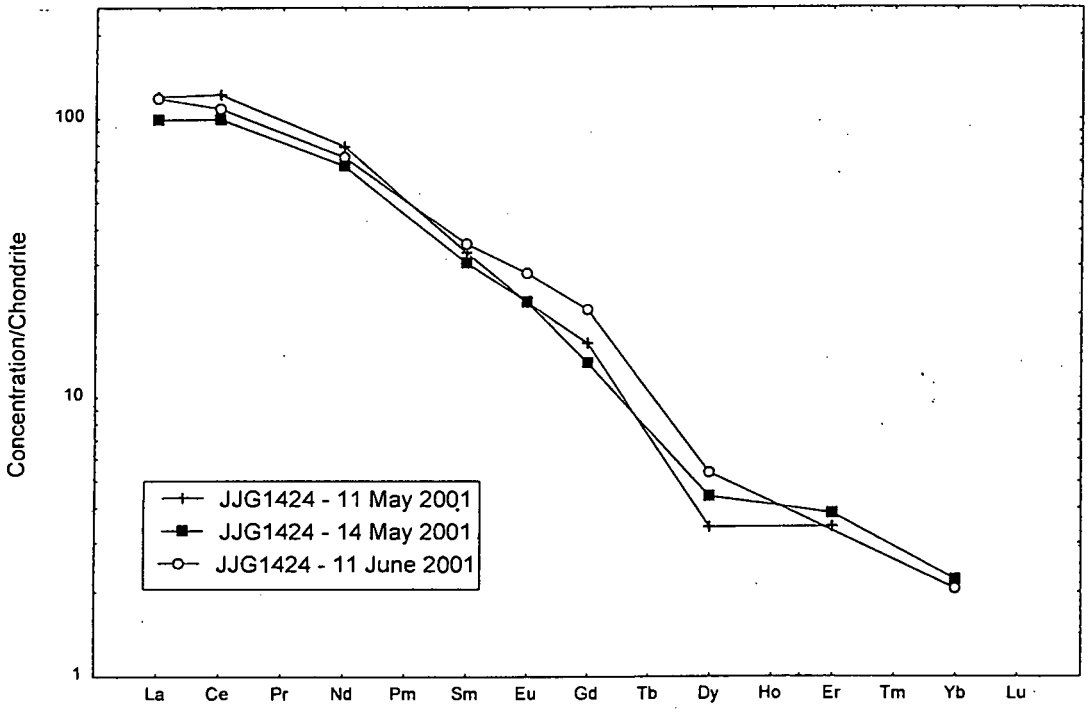

Figure A3.2 Similar analyses of the natural clinopyroxene standard JJG1424 on different analytical days shows homogeneity between operating conditions and standardisation on different analytical days.

Standards

Mineralogy	Cpx	Cpx	Cpx	Gt	Gt	Gt	Gt	Gt	Gt	Gt	Gt
Date	11-May-01	14-May-01	11-Jun-01	26-Apr-01	10-May-01	14-May-01	11-Jun-01	26-Apr-01	10-May-01	14-May-01	11-Jun-01
Standard	**JJG1424**	**JJG1424**	**JJG1424**	**Mon-32**	**Mon-32**	**Mon-32**	**Mon-32**	**Mon-34**	**Mon-34**	**Mon-34**	**Mon-34**
Sc	33	32	36	74	72	75	86	77	70	67	75
Ti	1466	1628	1869	5736	5875	5930	6861	6305	6036	5929	6322
V	549	553	597	247	233	234	266	250	223	222	246
Co	14	15	14	54	58	53	56	54	53	51	55
Ni	192	214	229	59	65	56	71	127	125	113	141
Rb	<0.737	<0.737	<0.737	<0.737	<0.737	<0.737	<0.737	<0.737	<0.737	<0.737	1.0
Sr	362	327	328	0.51	0.57	0.50	0.54	0.60	0.59	0.66	1.0
Y	3.8	3.0	3.3	36	37	36	44	38	36	36	40
Zr	51	57	64	104	104	104	126	111	100	97	108
Nb	<0.224	1.2	0.46	<0.224	0.27	0.34	<0.224	0.23	1.1	0.27	0.60
Ba	3.7	5.5	7.8	<1.611	<1.611	<1.611	<1.611	<1.611	<1.611	<1.611	<1.611
La	28	23	28	<0.433	<0.433	<0.433	<0.433	<0.433	<0.433	<0.433	<0.433
Ce	74	60	65	0.37	0.30	0.41	0.47	0.33	0.28	0.51	0.52
Nd	36	31	33	1.4	1.7	1.2	1.9	2.3	1.6	1.8	2.1
Sm	4.9	4.5	5.2	0.85	1.4	1.1	1.5	1.5	1.2	1.4	1.5
Eu	1.2	1.2	1.6	0.67	0.64	0.74	0.86	0.82	0.97	0.88	1.1
Gd	3.1	2.6	4.1	3.4	3.7	3.7	4.3	4.3	3.6	3.2	4.0
Dy	0.83	1.1	1.3	6.5	6.4	5.6	8.1	6.9	6.2	6.2	7.1
Er	0.54	0.61	<0.474	4.5	4.8	4.5	5.0	4.6	5.1	4.1	4.5
Yb	<0.261	0.36	0.33	4.9	4.9	4.3	5.7	5.5	4.7	4.2	4.7
Hf	2.5	2.7	3.5	2.4	2.8	2.7	3.4	2.8	2.9	2.6	2.8
Ta	<0.045	0.051	0.090	0.052	0.10	0.12	0.069	<0.045	0.071	0.051	0.14
Th	1.9	1.8	2.2	<0.288	<0.288	<0.288	<0.288	<0.288	<0.288	<0.288	<0.288
U	0.21	<0.169	<0.169	<0.169	<0.169	<0.169	<0.169	<0.169	<0.169	<0.169	<0.169

Lower limits of detection (LLD) for the trace elements analysed based on counting statistics.

LLD - Spot size 4	
Element	LLD (ppm)
Sc	3.766
Ti	25.624
V	32.071
Co	1.809
Ni	3.289
Rb	0.737
Sr	0.367
Y	0.714
Zr	0.214
Nb	0.224
Ba	1.611
La	0.433
Ce	0.132
Nd	0.211
Sm	0.261
Eu	0.539
Gd	0.414
Dy	0.496
Er	0.474
Yb	0.261
Hf	0.474
Ta	0.045
Th	0.288
U	0.169

LLD - Spot size 5	
Element	LLD (ppm)
Sc	0.325
Ti	1.842
V	2.697
Co	0.161
Ni	0.865
Rb	0.055
Sr	0.031
Y	0.064
Zr	0.020
Nb	0.022
Ba	0.142
La	0.044
Ce	0.012
Nd	0.021
Sm	0.027
Eu	0.051
Gd	0.048
Dy	0.056
Er	0.054
Yb	0.029
Hf	0.052
Ta	0.005
Th	0.029
U	0.013

Primitive Mantle and Chondrite compositions used for normalising the trace element composition of minerals for primitive mantle and REE plots.

Element	Composition of Primitive Mantle from McDonough and Sun (1995) (ppm)	Composition of Chondrite from Anders and Grevesse (1989) (ppm)
Sc	16.2	
Ti	1205	
V	82.0	
Co	105	
Ni	1960	
Rb	0.600	
Sr	19.9	
Y	4.30	
Zr	10.5	
Nb	0.658	
Ba	6.60	
La	0.648	0.235
Ce	1.675	0.603
Nd	1.250	0.452
Sm	0.406	0.147
Eu	0.154	0.056
Gd	0.544	0.197
Dy	0.674	0.243
Er	0.438	0.159
Yb	0.441	0.163
Hf	0.283	
Ta	0.037	
Th	0.0795	
U	0.0203	

Trace element chemistry - Garnet

Sample No	ARN003	ARN004	ARN005	ARN006	ARN007	ARN013	ARN017	ARN018	ARN025	ARN026	ARN027	ARN028	ARN031
Sc	448	286	198	233	270	202	276	227	495	193	333	227	222
Ti	125	38	30	20	56	13	63	<25	<25	163	<25	537	263
V	288	297	296	197	176	167	209	315	319	155	220	538	438
Co	43	39	37	40	44	36	48	50	70	34	46	50	50
Ni	31	22	19	11	36	11	37	10	56	11	36	44	47
Rb	<0.055	<0.055	0.14	<0.055	0.14	0.06	<0.737	<0.737	<0.737	<0.055	<0.737	<0.737	1.1
Sr	1.8	1.8	3.3	0.29	1.2	0.18	0.92	<0.367	1.8	6.7	1.04	<0.367	<0.367
Y	35	1.2	0.20	0.093	0.65	0.09	2.8	<0.714	<0.714	0.80	<0.714	9.6	4.9
Zr	107	3.3	1.0	0.42	32	0.70	46	<0.214	53	64	36	1.9	0.43
Nb	1.3	0.090	0.12	0.057	0.33	0.057	<0.224	<0.224	0.50	0.13	0.30	0.77	0.64
Ba	0.44	1.1	0.38	1.4	0.50	0.30	<1.61	1.9	2.78	<0.142	<1.61	<1.61	<1.61
La	0.25	0.67	1.4	0.076	0.13	0.15	<0.433	<0.433	0.92	1.52	<0.433	<0.433	<0.433
Ce	2.0	5.4	4.2	0.25	1.3	0.32	1.0	0.29	2.3	8.2	1.4	0.27	<0.132
Nd	7.7	6.2	2.6	0.32	5.2	0.47	4.8	0.60	9.4	5.5	6.1	0.54	0.37
Sm	5.5	0.92	0.23	0.17	3.4	0.17	2.4	<0.261	5.1	0.78	3.5	<0.261	<0.261
Eu	2.4	0.25	0.075	<0.051	0.94	<0.051	1.1	<0.539	1.3	0.13	1.3	<0.539	<0.539
Gd	10.2	0.49	0.12	0.078	2.2	0.17	2.8	<0.414	3.6	0.46	2.6	<0.414	<0.414
Dy	8.8	0.16	0.06	<0.056	0.39	0.11	0.95	<0.496	0.68	0.19	<0.496	1.7	0.66
Er	3.2	0.15	<0.054	<0.054	<0.054	<0.054	<0.474	<0.474	0.66	<0.054	<0.474	1.3	1.00
Yb	2.2	0.26	0.14	0.07	0.16	0.05	0.82	0.74	0.30	0.22	<0.261	1.3	0.99
Hf	1.7	0.082	<0.052	<0.052	0.63	<0.052	0.80	<0.474	1.0	2.1	0.93	<0.474	<0.474
Ta	0.13	0.025	0.018	0.028	0.026	<0.005	<0.045	<0.045	0.11	0.013	0.053	0.13	0.15
Th	0.037	0.11	0.12	<0.029	<0.029	<0.029	<0.288	<0.288	0.45	<0.029	<0.288	<0.288	<0.288
U	0.11	0.067	0.087	0.021	0.046	0.03	<0.169	<0.169	0.21	0.05	<0.169	<0.169	<0.169
Y/Nd	4.6	0.20	0.077	0.29	0.13	0.19	0.59			0.15		18	13
Ti/Nd	16	6.2	11	61	11	27	13			30		991	705
Spot Size	5	5	5	5	5	5	4	4	4	5	4	4	4
Suite	High-Ca Harzburgite	High-Ca Harzburgite	High-Ca Harzburgite	High-Ca Harzburgite	Low-Ca Harzburgite	High-Ca Harzburgite	Low-Ca Harzburgite	High-Ca Harzburgite	Low-Ca Harzburgite	Low-Ca Harzburgite	Low-Ca Harzburgite	Clino-pyroxenite	Clino-pyroxenite

Trace element chemistry - Garnet

Sample No	MIS401	MIS408	MIS409	MIS412	MIS417	MIS419	MIS438	MIS439	PGN301	PGN303	PGN306	PGN307	PGN310	PGN311
Sc	424	307	129	144	231	122	64	65	223	222	127	103	148	125
Ti	19	137	567	<25	133	532	921	371	110	182	500	2241	1270	1968
V	153	266	106	240	233	285	132	123	235	297	414	355	344	397
Co	37	34	31	33	33	37	60	70	38	45	47	37	48	54
Ni	26	20	12	14	22	81	10.2	13	11	30	65	67	53	101
Rb	0.13	0.13	0.24	<0.737	0.079	0.83	<0.737	<0.737	1.2	1.5	0.97	<0.737	<0.737	<0.737
Sr	2.3	5.5	0.22	1.8	0.71	0.77	<0.367	<0.367	3.2	0.75	<0.367	0.87	0.82	0.54
Y	1.3	1.2	8.6	<0.714	1.4	4.9	47	20	1.4	2.4	1.5	4.1	14	17
Zr	5.7	3.7	4.7	<0.214	4.2	12	26	2.8	6.4	27	5.8	15	54	16
Nb	0.19	0.039	0.34	1.0	0.10	0.72	<0.224	<0.224	<0.224	0.84	1.1	0.50	0.39	0.58
Ba	0.23	0.18	0.19	<1.61	0.42	<1.61	<1.61	<1.61	<1.61	2.86	<1.61	<1.61	1.6	<1.61
La	0.73	3.1	0.05	0.47	0.33	<0.433	<0.433	<0.433	0.93	0.52	<0.433	<0.433	<0.433	<0.433
Ce	5.5	6.1	0.15	1.7	2.6	0.58	0.69	<0.132	3.6	2.85	0.49	0.78	0.66	0.52
Nd	5.4	3.5	0.27	1.2	6.0	1.5	1.1	0.43	2.4	3.32	1.6	2.19	2.44	1.18
Sm	0.63	0.51	0.36	<0.261	1.3	0.83	1.3	<0.261	0.44	0.98	0.41	0.77	2.1	<0.261
Eu	0.15	0.14	0.24	<0.539	0.30	<0.539	0.9	<0.539	<0.539	<0.539	<0.539	<0.539	1.1	<0.539
Gd	0.42	0.28	1.2	<0.414	0.62	1.2	4.8	1.6	<0.414	0.67	0.50	0.96	3.2	1.2
Dy	0.39	0.34	1.8	<0.496	0.32	<0.496	8.0	3.2	<0.496	1.2	0.53	0.93	3.0	2.4
Er	0.13	0.21	1.2	<0.474	0.20	<0.474	5.2	2.4	<0.474	<0.474	<0.474	0.65	1.3	2.4
Yb	0.46	0.52	1.3	<0.261	0.71	0.33	5.7	2.8	0.84	0.88	0.91	<0.261	1.3	3.2
Hf	0.084	0.10	0.24	0.78	0.11	<0.474	0.64	<0.474	<0.474	0.78	<0.474	0.75	0.78	0.67
Ta	0.037	0.014	0.11	0.30	0.057	0.17	<0.045	0.062	0.057	<0.045	<0.045	0.094	0.076	<0.045
Th	0.13	0.20	<0.029	<0.288	0.12	<0.288	<0.288	<0.288	<0.288	<0.288	<0.288	<0.288	<0.288	<0.288
U	0.21	0.06	0.076	<0.169	0.05	<0.169	<0.169	<0.169	0.23	0.35	0.22	<0.169	<0.169	<0.169
Y/Nd	0.24	0.35	32		0.23	3.2	42	46	0.61	0.74	0.91	1.9	5.9	14
Ti/Nd	3.5	39	2100		22	347	818	863	47	55	311	1022	520	1663
Spot Size	5	5	5	4	5	4	4	4	4	4	4	4	4	4
Suite	Low-Ca Harzburgite	Low-Ca Harzburgite	Lherzolite	High-Ca Harzburgite	High-Ca Harzburgite	Lherzolite	Websterite	Websterite	Low-Ca Harzburgite	Low-Ca Harzburgite	Lherzolite	Lherzolite	Lherzolite	Lherzolite

Trace element chemistry - Garnet

Sample No	PGN314	PGN316	PGN317	PGN319	PGN320	PGN322	PGN323	PGN329	PGN337	PGN340
Sc	117	97	190	70	21	22	142	100	100	265
Ti	371	1881	<25	541	385	369	3273	3878	2850	<25
V	269	346	187	52	67	45	348	310	290	168
Co	39	38	38	101	53	52	42	41	39	40
Ni	56	55	12	41	23	17	56	77	53	20
Rb	<0.737	0.82	<0.737	<0.737	1.1	1.3	0.88	<0.737	<0.737	7.5
Sr	0.57	0.64	0.39	0.77	0.42	0.37	0.72	0.61	0.54	2.8
Y	2.1	4.2	<0.714	9.6	2.3	2.5	14	12	12	<0.714
Zr	29	14	0.88	3.0	1.2	0.69	48	39	27	1.1
Nb	<0.224	0.96	0.30	<0.224	0.31	<0.224	0.34	0.28	0.44	<0.224
Ba	<1.61	<1.61	<1.61	<1.61	<1.61	<1.61	<1.61	<1.61	<1.61	11
La	0.44	<0.433	<0.433	<0.433	<0.433	<0.433	<0.433	<0.433	<0.433	0.89
Ce	0.44	0.65	1.0	<0.132	0.21	0.26	0.41	0.29	0.16	4.7
Nd	1.4	1.4	1.5	0.86	0.87	0.85	1.5	1.8	0.75	4.4
Sm	0.50	0.95	0.62	0.29	<0.261	<0.261	0.72	0.62	0.54	0.53
Eu	0.58	<0.539	<0.539	<0.539	<0.539	<0.539	0.71	<0.539	<0.539	<0.539
Gd	0.85	0.61	<0.414	1.4	0.57	0.56	2.1	1.5	1.3	<0.414
Dy	0.79	0.83	<0.496	2.0	0.80	0.57	2.3	2.1	2.1	0.11
Er	0.57	1.0	0.90	1.1	0.53	0.50	1.6	1.7	1.4	<0.474
Yb	0.56	0.87	<0.261	1.7	0.48	1.06	1.5	1.5	1.6	<0.261
Hf	0.66	0.86	<0.474	<0.474	<0.474	<0.474	1.6	1.4	0.86	<0.474
Ta	<0.045	0.27	0.13	0.088	0.11	0.12	0.049	<0.045	<0.045	<0.045
Th	<0.288	<0.288	<0.288	<0.288	<0.288	<0.288	<0.288	<0.288	<0.288	<0.288
U	<0.169	<0.169	<0.169	<0.169	<0.169	<0.169	<0.169	<0.169	<0.169	<0.169
Y/Nd	1.5	2.9		11	2.7	2.9	9.5	6.9	16	
Ti/Nd	272	1322		627	444	432	2183	2178	3798	
Spot Size	4	4	4	4	4	4	4	4	4	4
Suite	Low-Ca Harzburgite	Lherzolite	Low-Ca Harzburgite	Clino-pyroxenite	Clino-pyroxenite	Clino-pyroxenite	Lherzolite	Lherzolite	Lherzolite	Low-Ca Harzburgite

Trace element chemistry - Clinopyroxene

Sample No	ARN028	ARN031	ARN032	ARN033	MIS409	MIS419	MIS438	MIS439	PGN310	PGN319	PGN320	PGN322	PGN323	PGN329	PGN337
Sc	4.9	9.6	102	25	31	10.0	36	38	18	27	4.6	<3.77	16	9.6	12
Ti	74	74	97	1017	941	95	5219	2659	402	550	647	727	778	1180	1075
V	93	158	223	210	271	128	438	578	328	212	145	139	217	215	254
Co	32	27	12	16	10.4	23	40	45	19	50	16	17	24	26	25
Ni	430	412	188	299	197	443	318	573	315	558	442	474	380	382	350
Rb	<0.737	0.46	3.5	2.0	1.0	<0.737	<0.737	1.6	<0.737	<0.737	<0.737	<0.737	<0.737	0.98	<0.737
Sr	8.2	23	1803	222	109	120	29	49	332	368	195	198	150	125	132
Y	<0.714	0.36	8.6	1.3	<0.714	<0.714	4.1	1.8	1.7	1.4	<0.714	<0.714	0.95	1.4	1.6
Zr	0.90	0.49	58	5.6	4.0	0.56	54	6.8	9.7	5.8	1.1	0.93	2.6	3.5	3.3
Nb	0.49	0.66	1.4	0.41	0.56	0.54	<0.224	0.85	1.00	<0.224	0.72	0.93	0.22	0.81	0.42
Ba	9.4	10.3	2.8	13	2.6	<1.61	<1.61	5.9	4.6	<1.61	2.9	<1.61	<1.61	2.6	6.0
La	2.4	5.9	59	3.2	1.2	2.1	4.7	0.94	4.0	8.3	2.0	2.0	2.0	2.0	2.4
Ce	3.7	9.5	170	10.1	2.3	6.8	18	2.1	15	24	4.7	4.8	7.0	7.0	8.4
Nd	1.0	2.7	90	7.6	1.5	5.2	19	2.2	13	19	1.9	1.7	5.2	4.7	5.7
Sm	0.36	0.33	11	1.5	0.41	0.67	5.3	0.94	2.4	2.4	<0.261	<0.261	0.82	1.1	1.1
Eu	<0.539	0.076	2.7	<0.539	<0.539	<0.539	1.3	<0.539	0.63	0.75	<0.539	<0.539	<0.539	<0.539	<0.539
Gd	<0.414	0.22	5.9	0.57	0.59	0.56	3.9	1.2	1.4	1.5	<0.414	<0.414	0.52	0.90	0.71
Dy	<0.496	0.32	2.8	<0.496	<0.496	<0.496	1.8	0.76	<0.496	0.57	<0.496	<0.496	<0.496	<0.496	0.55
Er	<0.474	<0.054	0.82	<0.474	<0.474	<0.474	<0.474	<0.474	<0.474	<0.474	<0.474	<0.474	<0.474	<0.474	<0.474
Yb	<0.261	0.56	0.66	0.37	<0.261	<0.261	0.36	<0.261	<0.261	0.32	<0.261	0.28	<0.261	0.41	0.53
Hf	<0.474	<0.052	2.0	0.59	<0.474	<0.474	2.5	0.53	0.63	0.51	<0.474	<0.474	<0.474	<0.474	<0.474
Ta	0.082	0.090	0.15	0.066	<0.045	0.059	<0.045	<0.045	0.054	<0.045	0.19	0.091	0.066	<0.045	<0.045
Th	<0.288	0.34	0.79	<0.288	<0.288	<0.288	<0.288	<0.288	<0.288	<0.288	<0.288	<0.288	<0.288	<0.288	<0.288
U	<0.169	0.032	0.35	<0.169	<0.169	<0.169	<0.169	<0.169	0.24	0.42	<0.169	<0.169	<0.169	<0.169	<0.169
Spot Size	4	5	4	4	4	4	4	4	4	4	4	4	4	4	4
Suite	Clino-pyroxenite	Clino-pyroxenite	Lherzolite	Lherzolite	Lherzolite	Lherzolite	Websterite	Websterite	Lherzolite	Clino-pyroxenite	Clino-pyroxenite	Clino-pyroxenite	Lherzolite	Lherzolite	Lherzolite

Trace element chemistry - Orthopyroxene

Sample No	ARN003	ARN004	ARN005	ARN006	ARN007	ARN013	ARN018	ARN025	ARN026	ARN027	MIS409	MIS412	MIS417
Sc	<3.77	<3.77	<3.77	17	<3.77	<3.77	<3.77	<3.77	<3.77	<3.77	<3.77	2.3	<3.77
Ti	<25	<25	<25	<25	<25	<25	<25	<25	83	<25	280	3.3	29
V	<32	<32	<32	35	<32	<32	37	<32	39	<32	<32	34	47
Co	42	44	42	41	47	43	42	43	39	45	29	38	34
Ni	653	559	579	515	647	585	504	600	481	652	444	481	435
Rb	1.8	<0.737	1.1	2.7	0.99	1.4	1.0	1.7	1.8	1.9	1.1	<0.055	<0.737
Sr	1.7	0.93	1.4	3.3	0.63	1.0	1.3	1.7	4.2	1.7	<0.367	1.5	<0.367
Y	<0.714	<0.714	<0.714	1.4	<0.714	<0.714	<0.714	<0.714	<0.714	<0.714	<0.714	<0.064	<0.714
Zr	0.55	0.27	0.44	0.72	0.60	0.37	0.25	<0.214	0.82	0.41	0.37	0.08	<0.214
Nb	1.4	<0.224	<0.224	0.56	0.45	0.40	0.28	0.77	0.78	0.80	0.43	0.25	0.55
Ba	4.1	2.2	2.5	3.8	<1.61	<1.61	<1.61	4.3	<1.61	3.2	<1.61	0.39	<1.61
La	0.67	<0.433	<0.433	<0.433	0.79	0.61	0.96	0.78	1.2	0.83	<0.433	0.16	<0.433
Ce	0.54	<0.132	0.36	0.36	0.35	0.21	0.39	0.38	0.23	0.22	<0.132	0.29	0.30
Nd	0.98	0.54	0.35	0.52	<0.211	0.43	0.64	<0.211	<0.211	0.69	0.36	0.068	0.28
Sm	0.74	0.70	0.33	0.31	<0.261	0.44	0.51	0.58	0.34	0.51	<0.261	<0.027	<0.261
Eu	<0.539	<0.539	<0.539	<0.539	<0.539	<0.539	<0.539	<0.539	<0.539	0.59	<0.539	<0.051	<0.539
Gd	<0.414	0.62	0.57	<0.414	<0.414	<0.414	<0.414	0.52	0.58	0.54	<0.414	0.19	<0.414
Dy	0.65	<0.496	<0.496	<0.496	<0.496	0.56	0.63	<0.496	0.76	0.56	<0.496	0.14	<0.496
Er	<0.474	<0.474	<0.474	<0.474	0.50	<0.474	0.59	<0.474	0.99	0.51	<0.474	<0.054	<0.474
Yb	0.42	0.30	<0.261	0.74	0.35	0.77	0.63	0.42	0.97	0.70	<0.261	0.057	<0.261
Hf	<0.474	<0.474	<0.474	0.59	<0.474	<0.474	<0.474	<0.474	<0.474	0.56	<0.474	<0.052	<0.474
Ta	0.19	<0.045	0.078	0.10	0.065	0.094	0.25	0.12	0.19	0.11	<0.045	0.069	0.088
Th	<0.288	<0.288	<0.288	<0.288	<0.288	<0.288	<0.288	<0.288	<0.288	<0.288	<0.288	0.055	<0.288
U	<0.169	<0.169	<0.169	<0.169	<0.169	<0.169	<0.169	<0.169	<0.169	<0.169	<0.169	0.020	<0.169
Spot Size	4	4	4	4	4	4	4	4	4	4	4	5	4
Suite	High-Ca Harzburgite	High-Ca Harzburgite	High-Ca Harzburgite	High-Ca Harzburgite	Low-Ca Harzburgite	High-Ca Harzburgite	High-Ca Harzburgite	Low-Ca Harzburgite	Low-Ca Harzburgite	Low-Ca Harzburgite	Lherzolite	High-Ca Harzburgite	High-Ca Harzburgite

Trace element chemistry - Orthopyroxene

Sample No	MIS419	MIS438	MIS439	PGN301	PGN306	PGN310	PGN311	PGN314	PGN316	PGN317	PGN329	PGN337
Sc	<3.77	4.51	<3.77	<3.77	<3.77	<3.77	<3.77	<3.77	<3.77	<3.77	5.0	4.6
Ti	69	1174	377	<25	265	177	202	60	176	<25	653	593
V	<32	97	103	<32	40	35	33	<32	<32	<32	40	44
Co	50	99	105	44	50	46	51	48	47	38	52	52
Ni	800	517	1080	589	693	685	720	797	751	552	699	620
Rb	1.0	<0.737	1.0	1.3	3.8	0.83	<0.737	<0.737	0.99	0.46	<0.737	0.87
Sr	0.87	0.38	3.9	1.0	4.9	3.5	0.39	2.9	1.2	0.55	1.9	2.5
Y	<0.714	<0.714	<0.714	<0.714	<0.714	<0.714	<0.714	<0.714	<0.714	<0.714	<0.714	<0.714
Zr	<0.214	3.8	0.35	<0.214	0.24	<0.214	<0.214	<0.214	<0.214	<0.214	<0.214	<0.214
Nb	0.50	<0.224	0.35	0.37	0.67	0.34	<0.224	0.55	0.35	0.25	0.76	0.68
Ba	<1.61	<1.61	4.3	<1.61	9.0	3.7	<1.61	3.8	<1.61	<1.61	8.2	5.9
La	<0.433	<0.433	<0.433	0.64	<0.433	<0.433	<0.433	0.97	0.62	<0.433	<0.433	0.53
Ce	<0.132	0.61	0.43	0.23	0.18	0.27	<0.132	0.61	<0.132	0.25	0.59	0.49
Nd	0.30	0.46	0.25	<0.211	<0.211	<0.211	0.24	0.28	<0.211	<0.211	0.38	0.37
Sm	<0.261	<0.261	<0.261	<0.261	<0.261	<0.261	<0.261	<0.261	<0.261	<0.261	0.52	0.42
Eu	<0.539	<0.539	<0.539	<0.539	<0.539	<0.539	<0.539	<0.539	<0.539	<0.539	<0.539	<0.539
Gd	<0.414	<0.414	<0.414	<0.414	<0.414	<0.414	<0.414	<0.414	<0.414	<0.414	0.77	<0.414
Dy	<0.496	<0.496	<0.496	<0.496	<0.496	<0.496	<0.496	<0.496	<0.496	<0.496	<0.496	<0.496
Er	<0.474	<0.474	<0.474	<0.474	<0.474	<0.474	<0.474	<0.474	<0.474	<0.474	<0.474	<0.474
Yb	<0.261	0.43	<0.261	<0.261	0.36	1.1	0.85	<0.261	0.69	<0.261	0.60	0.59
Hf	<0.474	<0.474	<0.474	<0.474	<0.474	<0.474	<0.474	<0.474	<0.474	<0.474	<0.474	<0.474
Ta	0.093	<0.045	0.049	0.11	<0.045	0.05	<0.045	0.10	0.13	0.23	0.057	0.16
Th	<0.288	<0.288	<0.288	<0.288	<0.288	<0.288	<0.288	<0.288	<0.288	<0.288	<0.288	<0.288
U	<0.169	<0.169	<0.169	<0.169	<0.169	<0.169	<0.169	<0.169	<0.169	<0.169	<0.169	<0.169
Spot Size	4	4	4	4	4	4	4	4	4	4	4	4
Suite	Lherzolite	Websterite	Websterite	Low-Ca Harzburgite	Lherzolite	Lherzolite	Lherzolite	Low-Ca Harzburgite	Lherzolite	Low-Ca Harzburgite	Lherzolite	Lherzolite

Trace element chemistry - Olivine

Sample No	ARN003	ARN005	ARN006	ARN013	ARN018	ARN025	ARN026	ARN027	ARN032	ARN033	MIS417	PGN306	PGN310
Sc	<3.77	<3.77	<3.77	<3.77	<3.77	<3.77	<3.77	<3.77	2.3	<3.77	<3.77	<3.77	<3.77
Ti	<25	<25	<25	<25	<25	<25	<25	<25	16	70	<25	<25	49
V	<32	<32	<32	<32	<32	<32	<32	<32	5.0	<32	<32	<32	<32
Co	114	127	114	120	112	108	111	108	117	119	109	120	107
Ni	2521	2881	2758	2868	2530	2298	2264	2460	2061	2370	2547	2340	2414
Rb	2.4	0.80	0.86	0.76	<0.737	0.90	<0.737	1.9	0.11	<0.737	<0.737	1.0	<0.737
Sr	<0.367	<0.367	<0.367	<0.367	0.90	0.41	1.3	0.95	1.2	2.7	<0.367	0.59	<0.367
Y	<0.714	<0.714	<0.714	<0.714	<0.714	0.077	<0.714	0.24	<0.064	<0.714	<0.714	<0.714	<0.714
Zr	0.34	0.51	0.51	0.58	<0.214	<0.214	0.65	0.47	0.44	0.37	0.33	0.59	<0.214
Nb	3.5	<0.224	0.65	0.69	0.76	1.5	<0.224	1.9	5.9	0.31	0.39	1.1	0.31
Ba	<1.61	2.1	<1.61	<1.61	2.9	<1.61	2.6	<1.61	1.6	<1.61	<1.61	<1.61	<1.61
La	<0.433	<0.433	<0.433	0.74	1.3	0.80	1.2	1.0	0.50	<0.433	<0.433	<0.433	<0.433
Ce	0.23	0.16	<0.132	0.24	0.40	0.20	0.22	<0.132	0.38	0.21	<0.132	0.23	0.28
Nd	0.43	0.34	<0.211	0.61	0.25	<0.211	0.31	<0.211	0.27	0.26	0.24	<0.211	0.30
Sm	0.60	1.01	<0.261	1.0	0.47	0.77	0.99	1.0	0.081	<0.261	<0.261	<0.261	<0.261
Eu	<0.539	<0.539	<0.539	<0.539	<0.539	<0.539	0.89	<0.539	<0.051	<0.539	<0.539	<0.539	<0.539
Gd	0.44	0.58	<0.414	0.79	<0.414	0.70	<0.414	<0.414	0.078	<0.414	<0.414	<0.414	<0.414
Dy	0.79	0.76	0.54	1.3	<0.496	<0.496	0.70	0.63	<0.056	<0.496	<0.496	<0.496	<0.496
Er	<0.474	1.1	<0.474	<0.474	<0.474	0.48	0.59	0.70	<0.054	0.70	<0.474	<0.474	<0.474
Yb	1.3	0.70	0.82	0.89	0.61	0.31	0.41	<0.261	0.34	0.58	<0.261	<0.261	<0.261
Hf	<0.474	<0.474	<0.474	<0.474	0.67	<0.474	<0.474	<0.474	<0.052	<0.474	<0.474	<0.474	<0.474
Ta	0.32	0.17	0.10	0.25	0.084	0.13	0.068	<0.045	0.31	0.21	0.10	0.10	0.066
Th	<0.288	<0.288	<0.288	<0.288	<0.288	<0.288	<0.288	<0.288	<0.029	<0.288	<0.288	<0.288	<0.288
U	<0.169	<0.169	<0.169	<0.169	<0.169	<0.169	<0.169	<0.169	<0.013	<0.169	<0.169	<0.169	0.20
Spot Size	4	4	4	4	4	4	4	4	5	4	4	4	4
Suite	High-Ca Harzburgite	High-Ca Harzburgite	High-Ca Harzburgite	High-Ca Harzburgite	High-Ca Harzburgite	Low-Ca Harzburgite	Low-Ca Harzburgite	Low-Ca Harzburgite	Lherzolite	Lherzolite	High-Ca Harzburgite	Lherzolite	Lherzolite

Trace element chemistry - Olivine

Sample No	PGN314	PGN316	PGN317
Sc	<3.77	<3.77	<3.77
Ti	<25	38	<25
V	<32	<32	<32
Co	110	116	115
Ni	2510	2552	2496
Rb	2.2	1.2	<0.737
Sr	2.0	0.44	<0.367
Y	<0.714	<0.714	<0.714
Zr	<0.214	0.63	0.44
Nb	0.77	<0.224	0.50
Ba	11	<1.61	<1.61
La	<0.433	0.75	<0.433
Ce	0.84	<0.132	0.15
Nd	0.61	0.32	<0.211
Sm	<0.261	<0.261	0.65
Eu	<0.539	0.54	<0.539
Gd	<0.414	<0.414	<0.414
Dy	<0.496	<0.496	<0.496
Er	<0.474	0.71	<0.474
Yb	<0.261	0.63	0.66
Hf	<0.474	<0.474	<0.474
Ta	0.088	0.16	0.065
Th	<0.288	<0.288	<0.288
U	0.17	<0.169	<0.169
Spot Size	4	4	4
Suite	Low-Ca Harzburgite	Lherzolite	Low-Ca Harzburgite